KUVEMPU UNIVERSITY

Department of PG Studies and Research in Chemistry, Jnanasahydri,
Kuvempu University, Shankaraghtta-577451

A Thesis submitted to the Faculty of Science, Kuvempu University

For the award of the degree of

DOCTOR OF PHILOSOPHY
in
CHEMISTRY

"SYNTHESIS, CHARACTERIZATION AND APPLICATIONS OF SOME NOVEL NITROGEN HETEROCYCLIC COMPOUNDS"

-: Submitted By: -

Mr. K. Upendranath M.Sc.
Research Scholar
Dept. of P.G. Studies and Research in Chemistry
Kuvempu University, Jnanasahyadri
Shankaraghatta-577451

-: Research Supervisor: -

Dr. Talavara Venkatesh M.Sc., Ph.D.
Assistant Professor
Dept. of P.G. Studies and Research in Chemistry
Kuvempu University, Jnanasahyadri
Shankaraghatta-577451

2022-23

KUVEMPU UNIVERSITY

Department of PG Studies and Research in Chemistry, Jnanasahydri,
Kuvempu University, Shankaraghtta-577451

A Thesis submitted to the Faculty of Science, Kuvempu University

For the award of the degree of

DOCTOR OF PHILOSOPHY
in
CHEMISTRY

"SYNTHESIS, CHARACTERIZATION AND APPLICATIONS OF SOME NOVEL NITROGEN HETEROCYCLIC COMPOUNDS"

-: Submitted By: -

Mr. K. Upendranath M.Sc.
Research Scholar
Dept. of P.G. Studies and Research in Chemistry
Kuvempu University, Jnanasahyadri
Shankaraghatta-577451

-: Research Supervisor: -

Dr. Talavara Venkatesh M.Sc., Ph.D.
Assistant Professor
Dept. of P.G. Studies and Research in Chemistry
Kuvempu University, Jnanasahyadri
Shankaraghatta-577451

2022-23

Mr. K. Upendranath M.Sc.,
Research Scholar
Dept. of P G Studies and Research in
Chemistry, Jnanasahyadri Shankaraghtta,
Shivamogga (D)-577451, Karnataka.
E-mail: upendrarwl@gmail.com

DECLARATION

I hereby declare that the research work presented in this thesis entitled **"SYNTHESIS, CHARACTERIZATION AND APPLICATIONS OF SOME NOVEL NITROGEN HETEROCYCLIC COMPOUNDS"** is submitted to the Department of PG Studies and Research in Chemistry, Kuvempu University for the award of the degree of **Doctor of Philosophy in Chemistry** is bonafide work of the research work carried out by me under the supervision of **Dr. Talavara Venkatesh,** Assistant Professor, Department of P.G. Studies and Research in Chemistry, Kuvempu University, Jnanasahyadri, Shankaragatta.

I further declare that the contents presented in the thesis or any part, therefore, has not been submitted elsewhere for any other degree, diploma or similar title in any other universities.

Date: 13/01/2023

Place: **Shankaragatta.**

Mr. K. Upendranath

KUVEMPU UNIVERSITY

Dr. TALAVARA VENKATESH M.Sc., Ph.D.
Assistant Professor

Department of P.G. Studies and
Research in Chemistry, Jnanasahyadri,
Kuvempu University,
Shankaraghatta-577451
Shivamogga (Dist), Karnataka, India
Mobile No: +917259417026
Email: venkateshatalwar@gmail.com

Certificate

This is to certify that the work reported in this thesis entitled **"SYNTHESIS, CHARACTERIZATION AND APPLICATIONS OF SOME NOVEL NITROGEN HETEROCYCLIC COMPOUNDS"** submitted by **Mr. K. Upendranath,** to the Faculty of Science, Kuvempu University, for the award of **Doctor of Philosophy in Chemistry** is a record of the bonafide and original research work carried out by him under my guidance and direct supervision. The work reported in this thesis has formed the basis for the award of any degree or diploma or any other similar title in any other institution or university.

Date: 13/01/2023
Place: Shankaraghtta.

Dr. Talavara Venkatesh

(Research Supervisor)

Dedicated To

My Father

Who had vision

And

My Family

Acknowledgements

Major research work like this is never the work of anyone alone. The contribution of many different people in their different ways has made thispossible. It gives me immense pleasure to acknowledge all the persons who came in contact directly or indirectly in the way with helping hands, during my research tenure. I wouldlike to extend my appreciation, especially to the following.

Foremost, I a m very much thankful and express sincere gratitude to my research supervisor **Dr. Talavara Venkatesh**, Assistant Professor, Dept. of P.G. Studies and Research in Chemistry, Kuvempu University, for the continuous support of my Ph.D., study and research work, for his patience, motivation, enthusiasm, and immense knowledge. His guidance helped me in all the time of my research work. I could not have imagined having a better advisor and mentor for my Ph.D., study.

I am immensely thankful to **Prof. Y. Arthoba Nayaka** Professor and Chairman, **Prof. Yadav. D. Bodke** and **Prof. J. Keshvayya**, Department of P.G. Studies and Research Chemistry, Kuvempu University for their valuable constructive suggestions, friendly approach, and encouragement during the Ph.D., research work.

It will be worthless to me, if I tried to express my deep feeling of love and affection through words to the backbone of my life, who encouraged me to do research and kept faith in me, my beloved parents **Mrs. Renuka L**. and father **Shri. K.M Kantharaj,** I express my special thanks to my grandparents **Shri. L.F Hanagi** and **Mrs. Kamala Hanagi**. who guided me since my childhood and supported me morally in every situation. Special loveable thanks to my aunties **Mrs. Manjula Hanagi.** and **Mrs. Usha,** uncles **Shri B.S. Hanagi,** and **Shri. L. Bsavaraju.**

I express my lovely thanks to my biggest strength and supporter beloved brother **K. Lohith.**

My little brothers **Rajendra Hanagi**, **Koushik Hanagi,** and my cousin **Harsha raj, Megha B** and other family members who have been the source of encouragement throughout my educational career.

I express my loveable gratitude to my life partner **Ms. Pooja Hanagi**, for her encouragement and love towards me and my research work.

I am very thankful to my friend **Iranna Udachayan** Ph.D scholar, aerial university, Israel for his encouragement and his support during my research work.

I place on record my sincere thanks to **SC/ST cell**, Kuvempu University for financial support to carry out the research work.

I am very grateful to my research colleagues **Sukanya S.H, Priya rani R.S, Surendra naik, Megha G.V, Dr. O. Nagaraj, Dr. Kirthan B.R** and other research scholars, Department of Chemistry and my friends **Sandeep Dongre**, **Raviteja**, **Vinay G.P** and **Prakash J,** Kuvempu University, for his kind co-operation and moral support during my research work.

I express my special thanks to my Guest Faculty and Non-teaching staff at, the Department of Chemistry, Kuvempu University, for their kind cooperation and support.

I would like many thanks to **Dr. G. Nagaraju** and **Dr. M. Shashank**, SIT Tumkur for their spectral characterization and collaboration work during my research work.

I am very much honorable to SAIF, Karnataka University, Mysore University, and Mangalore University, for providing the instrumental facility, I am also thankful to the Department of Microbiology, Maratha Mandala, NGH Institute of Dental Science & Research Centre, Belgaum, Karnataka, and LAYA Workstation, Haveri.

Last but not the least, I am truly grateful for the many hands and hearts that helped me to my research work.

Great thanks to all my well-wishers.....

K. Upendra .....

Ouriginal by Turnitin

Document Information

Analyzed document	KU-TH-CHE-UPENDRANATH-K-22.pdf (D154940167)
Submitted	2023-01-05 10:52:00
Submitted by	Walmiki R H
Submitter email	walmiki_rh@rediffmail.com
Similarity	1%
Analysis address	walmiki_rh.kuvempu@analysis.urkund.com

Sources included in the report

SA	**Arulaabranranam-PhD-Physics-JM-AAA Cheyyar.pdf** Document Arulaabranranam-PhD-Physics-JM-AAA Cheyyar.pdf (D110579685)	1
SA	**SP04-Senthil.doc** Document SP04-Senthil.doc (D20652076)	1
SA	**D. PARTHASARATHI - Chemistry - Final Thesis.pdf** Document D. PARTHASARATHI - Chemistry - Final Thesis.pdf (D116977469)	3
SA	**thesis-1.pdf** Document thesis-1.pdf (D133423545)	1
SA	**Abstract and Chapters (1).docx** Document Abstract and Chapters (1).docx (D128637526)	1
SA	**Amul B-Ph.D-Phy-AAA Clge.docx** Document Amul B-Ph.D-Phy-AAA Clge.docx (D136034631)	2
SA	**DANIEL AZHARI_2019378111.pdf** Document DANIEL AZHARI_2019378111.pdf (D127449730)	1
SA	**A.G.Anitha SRC Thesis.docx** Document A.G.Anitha SRC Thesis.docx (D46260411)	1
W	URL: http://www.jmchemsci.com/article_145013.html Fetched: 2022 03-31 10:39:25	1

Entire Document

LIST OF ABBREVIATIONS

λ_{max}	Absorption maxima
ADME-T	Absorption, distribution, metabolism, excretion and toxicity
A-549	Adenocarcinomic human alveolar basal epithelial cells
pKa	Acid dissociation constant
AR	Acid Red
Å	Angstrom
K_b	Binding constant
^{13}C-NMR	Carbon Nuclear Magnetic Resonance
CT_{50}	Cytotoxicity 50 percent
η	Chemical hardness
σ	Chemical softness
μ	Chemical potential
J	Coupling constant
COSMO- RS	Conductor like Screening Model for Real Solvents
°C	Degree celsius
DFT	Density functional theory
$CDCl_3$	Deuterated chloroform
DMSO-d_6	Deuterated Dimethyl sulfoxide
DPPH	2, 2-diphenyl-1-picrylhydrazyl.
D	doublet
DMF	Dimethyl formamide
eV	Electron volt
A	Electron affinity
χ	Electronegativity
ω	Electrophilicity index
FMOs	Frontier molecular orbitals
FT-IR	Fourier Transform Infrared
(ΔG)	Gibbs free energy change
HOMO	Highest Occupied Molecular Orbital
HRMS	High-Resolution Mass Spectrometry
HSQC	Heteronuclear Single Quantum Coherence or Correlation
IE	Ionization Energy
Kcal	Kilocalorie
kD	Kilo Dalton
LD_{50}	Lothal Dose 50 percent
LUMO	Lowest unoccupied molecular orbital
µL	Microlitre
MCF-7	Michigan Cancer Foundation-7
µg	Microgram
mg	Milligram
mL	Millilitre
mm	Millimetre
mmol	Mill mole
µmol L^{-1}	Micromole per litre
MHz	Megahertz

ε	Molar extinction coefficient
MCR's	Multicomponent reactions
MIC	Minimum inhibitory concentration
MMP	Matrix metalloproteinase
MP	Melting point
MTT	3-(4,5-dimethylthiazol-2-yl)-5-(3-carboxymethoxyphenyl)-2-(4-sulfophenyl)-2Htetrazolium
MCR's	Multicomponent reactions
m	multiplet
MG	Malachite Green
nm	Nanometre
DMPD	N, N-dimethylp-phenylenediamine
Viz.	Namely
PL	Photoluminescence
ppm	Parts per million
2D	Two dimentonal
3D	Three dimentonal
p-TSA	*para*-Toluenesulfonic acid
^{1}H-NMR	Proton Nuclear Magnetic Resonance
RT	Room Temperature
s	Singlet
TLC	Thin-Layer Chromatography
TMS	Tetramethylsilane
TOF MS	Time-of-Flight Mass Spectrometry
TPSA	Topological Polar Surface Area
UV-Vis	Ultraviolet-Visible

CONTENTS

Chapter-1

Introduction

1. Introduction

Chemistry is a branch of science that deals with the study of any transformation that takes place within the structure and composition of matter. Synthesized compounds have greatly influenced modern life, not only changing our lifestyle but also standardizing the quality of life, and man-made products used in daily life are made up of many composition chemicals [1-2].

In that, many types of research have been carried out from past decades to the present in designing and developing new heterocyclic compounds from synthetic organic chemistry to meet up all kinds of interest in pharmacology, optoelectronics, material sciences, and so on [3-5]. Synthetic organic chemistry plays a vital role in the synthesis of novel heterocyclic derivatives which can be used in the field of medicinal chemistry, molecular biology, materials science, and electronics by synthesizing specific compounds for scientific and technological investigations [6-8]. Designing synthetic routes and strategies for the synthesis of new organic compounds is known as the heart of organic synthesis [9]. Synthesis of new organic compounds will have several advantages in researching to unravel the intrinsic and extrinsic chemical behavior of small molecules and the development of new methods for synthesis. Similarly, the characterization of compounds by spectral means would create benchmarks for the characterization of similar molecules.

Heterocyclic chemistry is a branch of chemistry, that is studied interestingly in the organic chemistry. Organic compounds are the heterocyclic compounds which contains at least one hetero atom in the benzene ring [10, 11]. The heterocyclic term has been derived from the Greek word, which means different, and a cyclic ring must have a at least one hetero atom, such as nitrogen, oxygen and sulphur are the most

common heteroatoms [12]. The position of the heteroatom in the benzene ring will influence the physicochemical properties of the molecule, and heterocyclic compounds are broadly classified into two types aliphatic and aromatic [13]. Aliphatic heterocyclic compounds are known as small molecules and the position of heteroatoms of cyclic in the ring will understands their properties. While aromatic heterocyclic compounds make up a significant class of organic compounds which displays aromatic behavior and follows Huckel's (4n+2) rule [14, 15].

Synthesis of heterocyclic compounds has evolved as a powerful tool for producing new derivatives for biological and material science applications, where compounds play a vital role in both the applications because of their structural properties [16]. Major research has been carried to the synthesis of biologically active compounds and further, it was evaluated for optical and electrochemical studies to use in energy conversion devices. According to the literature, compounds containing nitrogen and oxygen atoms in the benzene ring have given much attention to the design and synthesis of new heterocyclic compounds [17]. Oxygen-containing heterocyclic compounds have been synthesized rapidly till now due to their natural abundance and diverse application in both photophysical and biological areas. Other than oxygen, nitrogen-containing heterocyclic compounds have been concentrated for the last few years in synthetic organic chemistry based on the chemical and structural properties to be used in the various felid of chemistry [18, 19].

Nitrogen-bearing heterocyclic compounds are an important and unique class in heterocyclic chemistry, a remarkable research work has been carried out till now on the development of new molecules and compositions [20]. In synthetic organic chemistry, nitrogen-containing heterocyclic compounds play a key role and it is not only important because of their abundance but also their biological and photophysical

significance. Most of the pharmacological drugs were derived from these heterocyclic compounds [21].

N-heterocyclic compounds such as pyrimidine, pyridine, imidazole, indole and carbazole etc., are possessed broadly in medicinal and materials science applications as promising compounds [22]. In general, these compounds have electron rich center which may accept or donate the electrons and also have some molecular interactions like hydrogen bonding formation, dipole-dipole interactions, hydrophobic effects, van-der waals forces and π-stacking interaction nitrogen. From these intermolecular force helps to the nitrogen to bind the variety of enzymes and receptors in biological target with high binding affinity [23-25].

Till date, there are numerous nitrogen-substituted heterocyclic compounds well-known in medicinal chemistry as, anti-bacterial, anti-fungal, anti-inflammatory, anti-cancer, anti-diabetic, anti-TB, anti-malaria and other bio-active agents [26, 27]. Similarly, they have also proved their stability in OLEDs, sensors, forensic science, photovoltaic cells, corrosion inhibitors and other optoelectronic applications [28, 29].

Role of multicomponent reactions (MCRs) in the synthesis of nitrogen-contain heterocyclic compounds

Multi-component reactions (MCRs) are one of the new synthetic strategies in modern organic chemistry so that novel compounds are easily synthesized in a one-step reaction. It defines the reaction process by which more than two reactants are assembled into a structure with functional diversity and complexity in a one-pot synthesis. There is no addition of any reactants or changing conditions during the whole reaction process to afford new molecules. It has many advantages while performing the reaction in regard atom economy, simple reaction, efficiency,

selectivity and convergence. Further, the reaction process did not need an organic solvent so it can also perform in water as a solvent. In these cases, the products could precipitate out from the reaction mixture, which enables purification simply by filtration and washing without chromatography or recrystallization [30]. They are upstanding as a tool for synthesizing polyfunctional molecules with high competence in multistep synthesis. Globally, it has been explored as an efficient tool for synthesizing new heterocyclic compounds to use in various filed of chemistry [31].

Nitrogen-containing heterocyclic compounds:

1.1 Pyrimidines.

Pyrimidines or pyrimidinones are the most important member of all the diazines (1,3 diazine **Fig. 1**) which are similar to pyridine and benzene ring by having nitrogen atoms at 1st and 3rd position [32]. It was first isolated by Gabriel and Colman in 1899, only one nitrogen atom of pyrimidine can be alkylated by the alkylating agent and are less basic in nature compared to pyridine [33]. It is colorless compound, having less π-electron density develops less energy; therefore, nucleophilic substitution easier than electrophilic substitution [34].

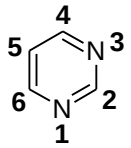

Fig. 1. Pyrimidine

Pyrimidines got much interest to organic researcher because of their chemical and biological properties. It is commonly found Vitamins like thiamine and riboflavin and folic acid (**Fig. 2**) [35] and they have been found well-known biologically active species as anti-analgesic, anti-microbial, anti-inflammatory and anti-cancer agents because of the building-blocking site and electron-rich moieties on the nitrogen atoms

[36, 37]. Pyrimidine moieties are considered as photonic materials, due to their better photophysical properties by having high electron affinity and π-acceptor character [38, 39]. Majorly, it exhibits higher fluorescent properties with anchoring (electron-withdrawing and donating) groups [40, 41] and themselves act as an electron-withdrawing group due to π-deficient nature which increases color sensitivity, luminous properties and solvatochromic behavior. Similarly, pyrimidine ring makes easier the oxidative addition of palladium to a chlorine-carbon bond in positions 2nd, 4th and 6th [42, 43].

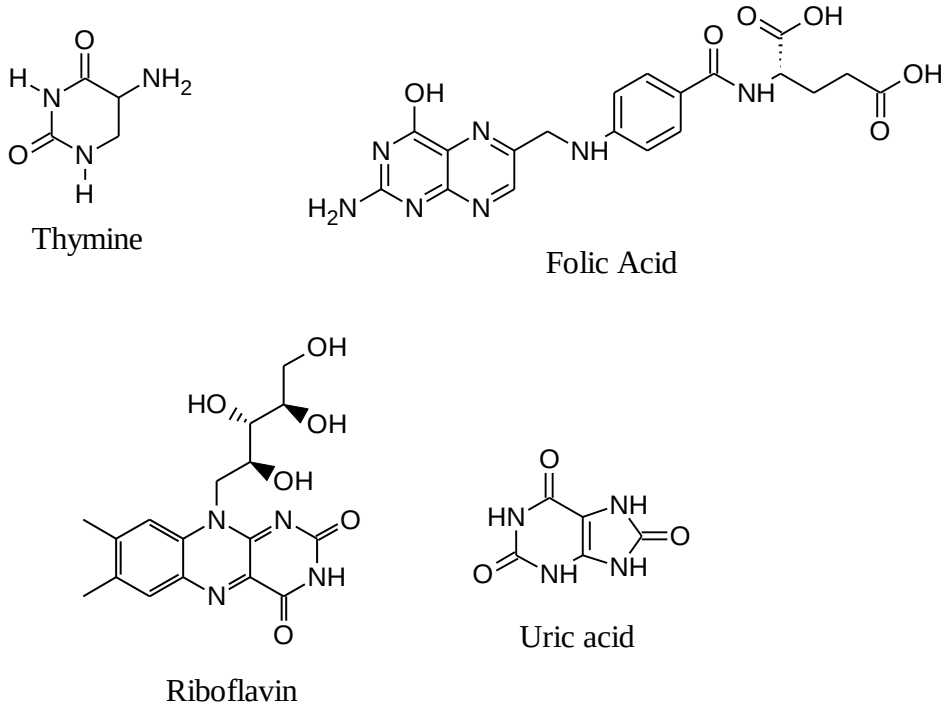

Fig. 2. Naturally occurring Pyrimidines

1.2 Pyridine.

Pyridine is another nitrogen containing heterocyclic compound, which was derived from the Greek word and is the combination of two words "pyr" which means fire and "idine" refer to aromatic bases. It is a planer six-membered ring with the presence of nitrogen atom at 1st position. The first pyridine base was isolated in 1846 by Anderson, picoline (**Fig. 3**). After quite a long time its structure was determined

by Wilhelm Körner in 1869 and James Dewar in 1871 [44], and it was suggested that the structure of pyridine might be analogous to quinoline and naphthalene. Mainly it was produced from coal tar and is a colorless organic compound, but older or impure samples can appear yellow in color so that the benzene ring occurs in many important compounds [45]. It has been found in many applications in various felid of chemistry including agrochemicals, pharmaceuticals, and Vitamins. Monopyridines, bipyridines or tripyridines were used as chelate metallic ions as nitrogen donor ligands to the efficient organometallic catalyst in coordination chemistry. Further, it is also involved in supramolecular structures, materials and surfaces, organocatalysts and polymers [46]. A large number of heterocyclic compounds containing pyridine rings are associated with diverse pharmacological properties such as anti-microbial, anti-cancer, anti-convulsant, anti-viral, anti-HIV and anti-fungal agents [47-53].

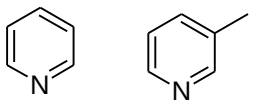

Pyridine Picoline

Fig. 3.

1.2.1 Naturally occurring pyridine compounds.

Pyridine derivatives are often present in many plant-based alkaloids as a partial structure such as Nicotine and Anabasine are found in tobacco, whereas Ricinine is present in castor oil and Acroline betelnut (**Fig. 4**). Nicotinamide adenine dinucleotide phosphate (NADP) is a cofactor used in anabolic reactions and nucleic acid syntheses which is used by all forms of cellular life [54]. Two essential Vitamins, Niacin (vitamin B_3) and Pyridoxine (vitamin B_6) contain the pyridine ring (**Fig. 5**) [55].

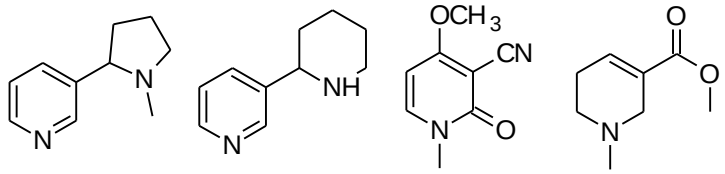

Nicotine Anabasine Ricinine Arecoline

Fig. 4. Naturally occurring pyridine compounds.

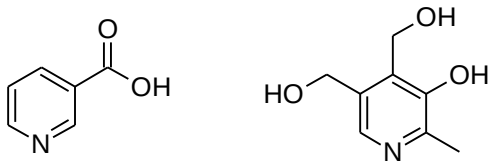

Niacin Pyridoxine

Fig. 5. Pyridines found in vitamins B_3 and B_6

1.3 Schiff base compounds.

The reaction between primary amine and carbonyl compounds leads to the formation of an imine or azomethine group, and the reaction is carried out in different solvents at different conditions. The Schiff base reaction was first introduced by the German scientist, Hugo Schiff in 1864 [56], it is a chemical bond containing a carbon-nitrogen bond as a functional group and the general formula is $RR^1C=N-R^2$, where R^1 and R^2 (**Fig. 6**) are the substituted aromatic or heterocyclic, alkyl and aryl groups, and R may be a hydrogen or methyl group [57].

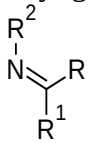

Fig. 6. General structure of Schiff base compounds

Schiff base have been investigated in relation to a wide range of contexts in the field of pharmacological fields as well as in the electrochemical and material science applications. They have also been considered for the inhibition of amyloid-β aggregation and are common enzymatic intermediates where an amine, such as the

terminal group of a lysine residue, reversibly reacts with aldehyde or ketone of cofactor or substrate [58]. Some of the common Schiff base compounds are displayed in **Fig. 7.**

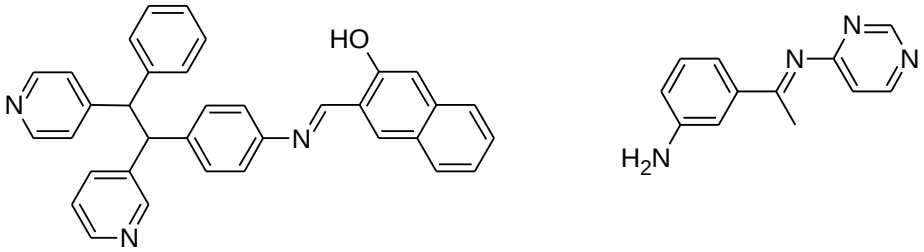

Fig. 7. Some of the organic Schiff base compounds

1.4 UV-Visible spectrophotometer.

Absorption of light in a specific region gives qualitative and quantitative information from overlapping bands of the analytes and interferences [59] with a measurement of wavelength from around 200 nm to 800 nm under the computer-controlled instrument. It is a cost-effective, simple, versatile, non-destructive method as a function of wavelength and a normal spectrum by mathematical transformation of spectral curve into a derivative. This technique usually improves resolution bands, eliminates the influence of background or matrix and provides more defined fingerprints than traditional ordinary or direct absorbance spectra. When the interaction between incident radiation and the electron cloud in a chromophore results in an electronic transition involving the promotion of one or more of the outer shell or the bonding electrons from a ground state into a higher energy state. The absorption bands can also be measured for different materials such as films, powders, monolithic solids and liquid materials [60-62].

Generally, UV and visible spectrophotometry are used for the identification of a number of conjugations in organic compounds. Moreover, aromatic conjugation and involvement of electronic transitions will cause the different shifts. Each organic

compound will process different electronic transitions based on aromatic conjugation and with substituted chromophores. The conduction and valance band has been determined using the energy gap equation (1) with help of the maximum absorption peak. Further, it was widely used as a tool for quantitative analysis, characterization, and quality control in the agricultural, pharmaceutical, and biomedical fields [63].

$$Eg = 1240/\lambda_{onset}\,\text{eV} \qquad \text{— (1)}$$

1.5 Photoluminescence (PL).

Absorption of photons in the visible regions exciting one of its electrons to a higher electronic excited state, and then radiates a photon as the electron returns to a lower energy state is termed as photoluminescence (PL). In general, it is divided into three types: fluorescence, phosphorescence and chemiluminescence. The radiation transition causes fluorescence to occur without a change in the spin multiplicity in a molecule, and a change in the spin multiplicity leads to phosphorescence and further, chemiluminescence will glow by the chemical reaction [64].

It is an optical phenomenon that has got much interest in materials science applications to understand the photophysical properties of the compounds under solvent media or solid media or at the gaseous phase. Emission bands were recorded based on the excitation values which were noted by using a UV-visible spectrophotometer at molar concentrations at room temperature [65]. Excited bands appeared at a longer wavelength in the red or blue regions whereas metal complex bands appear in the red region similarly the heterocyclic compounds appeared in blue regions. The presence of chromophores such as electron-donating and electron-withdrawing groups will influence the emission bands towards longer wavelength. Further, using PL bands stokes shift have been calculated. Stokes shift is termed as the difference between absorption and emission band, a larger difference is said to be

an anti-stokes shift, and a smaller difference is called stokes shift. In addition, with help of the PL study, the quantum efficiency will be calculated which informs the number of protons absorbed under the medium and also helps the synthesized compounds to use in the OLEDs, electroluminescent, DSSCs, and other material science applications [66].

1.6 C.V. analysis.

Cyclic voltammogram is a useful electrochemical technique to measure the redox peak currents through the electrochemical cell, it was first reported and described theoretically by Randle's in the year of 1938 [67]. CV is also invaluable to study electron transfer-initiated chemical reactions, which include catalysis and is used for the initial characterization of an electrochemically active system. The power of cyclic voltammetry results from its ability to rapidly provide considerable information on the thermodynamics of redox processes, the kinetics of heterogeneous electron-transfer reactions, and on coupled chemical reactions or adsorption processes. It is also known as the potential sweep technique, which involves sweeping the electrode potential between potential limits called E_1 and E_2 as a known sweep rate (scan rate). On reaching limit E_2 the sweep is reversed to E_1 to get a complete cyclic scan. A graph scanning is plotted current versus potential and indicates the potential at which the redox process occurs. The potential axis is referred to as a time axis that is related to scan rates. CV is a signal for a linear potential scan with a triangular waveform and a triangular potential excitation signal sweeps the potential of an electrode between two values, at times called switching potential [68, 69].

The electrochemical cell is made up of three electrode systems, a working electrode, a counter electrode and a reference electrode, where a potentiostat controls the potential. The current of the working electrode is recorded as a function of its potential measured against the reference electrode, but the voltage is applied between them and the current passes between the working and auxiliary electrodes. Thus, the current-voltage curve is not disturbed by an appreciable solution resistance which causes an IR (voltage) drop between the working and auxiliary electrodes. Ohm's law states that (V=IR) voltage (V), is equal to the product of current (I) and resistance (R), when current flows the recorded potential is distorted (shifted by an amount equal to I x R). If appreciable, it causes the current-potential curve to be distorted and draws out over a large potential range, with a three-electrode system, recorded potential is that between the working and reference electrode, with essentially no flow of current.

The highest occupied molecular orbital (HOMO) and Lowest unoccupied molecular orbitals have been calculated experimentally by the estimation of redox onset potentials. Redox onset potentials have been estimated from the CV graph where values can calculate using equations (2 and 3). HOMO-LUMO values inform that intrinsic and extrinsic properties of compounds which can be studied have been carried out in various fields [70, 71].

$$E_{(\mathrm{HOMO})} = -\,[E_{(\mathrm{ox\text{-}onset})} + 4.4]\ \mathrm{eV} \qquad \text{— (2)}$$

$$E_{(\mathrm{LUMO})} = -\,[E_{(\mathrm{red\text{-}onset})} + 4.4]\ \mathrm{eV} \qquad \text{— (3)}$$

1.7 Density Functional Theory.

Density functional theory (DFT), is one of the most widely used methods of quantum chemical approaches in physics and chemistry to calculate the structure of atoms, molecules, crystals, surfaces, and their interactions [72, 73]. The theoretical

investigations involve a popular code, a standard basis, and a functional approximation for organic and inorganic chemistry molecules. It has been very prevalent in computational studies in the 1970s, however, it was not until the 1990s that improvements made it acceptably accurate for quantum-chemical applications. This theory was developed on based Thomas-Fermi's theory on the approximate method for finding the electronic structure of atoms using one-electron ground state density. In 1950s, Slater eagerly combined this idea with Hartree's orbital method in the Xα scheme [74]. Later, the Hohenberg-Kohn (HK) theorem proved that an exact method based on ρ(r) exists in principle [75]. The modern version in use today is Kohn-Sham (KS) DFT, which defines self-consistent equations that must be solved for a set of orbitals whose density, ρ(r) is defined to be exactly that of the real system [76, 77].

Computational studies can be directly related to experimental values to the understandable quantities, energies, structures, and spectroscopic assets because the theory and experiment can collaborate successfully to complement each other. Vibrational, magnetic resonance and electronic spectroscopies were calculated theoretically at solvent method as well as the gaseous method with help of bias set parameters. Owing to the ready applicability to ever larger and more realistic systems, DFT is constantly pushing the scope of questions, be they fundamental or applied, that can be addressed in such a concerted manner [80, 81].

The Frontier molecular orbitals (FMOs) are the important parameters in the theoretical studies, both the parameter details the acceptor or donor characteristics of electrons and it is said to highest occupied molecular orbitals (HOMO) and lowest unoccupied molecular orbitals (LUMO). Similarly, there are other important parameters, calculated by the Koopmans theorem such as chemical hardness, softness

electronegativity, electrophilicity and chemical potential using reported formulaes [82]. The calculated quantum parameters reveal the intrinsic and extrinsic properties of organic and inorganic compounds [83, 84].

The Kohn-Sham eigen values do not represent excitation energies and there is no DFT analogue of Koopmans' theorem. Fortunately, there are extensions to conventional DFT that allow the calculation of excited-state properties. One such method, time-dependent DFT (TDDFT) has become very popular for calculations of excited states. Going beyond the Born-Oppenheimer approximation is also required in certain cases where the decoupling between the nuclear and electronic motions does not hold anymore, corresponding to non-adiabatic coupling(s). There are also theoretical challenges to be faced in this domain, and the DFT representation is at the forefront of new developments in synthetic organic chemistry [85].

1.8 Photocatalytic activity.

Purification of water is one of the most challenging and crucial tasks faced nowadays, which was caused by the textile, dyes, leather, pulp, paper and other industries [86]. There are several methods were used for the purification of water namely absorption, photocatalysis, sedimentation, filtration, chemical and membrane technologies, chlorination and advanced oxidation processes (AOPs). Photocatalysis is the acceleration of a photoreaction in the presence of a catalyst and is also called photocatalytic degradation (PCD). Presently PCD is one of the purification methods gaining importance by having the advantage of complete mineralization, no waste disposal, low-cost, and ambient temperature and pressure. Photocatalysts are inorganic semiconductor materials whose energy level structure is well described by the quantum theory of solids and catalyzed photolysis, light is absorbed by an

adsorbed substrate. In photogenerated catalysis, the photocatalytic activity (PCA) depends on the ability of the catalyst to create electron-hole pairs, which generate free radicals (e.g. hydroxyl radicals: $^{\bullet}OH$) able to undergo secondary reactions. There are numerous nano metal oxides were used as catalysts [87, 88].

Dyes are the leading environmental pollutants in the aquatic region, the discoloration slows biological degradation, and the high COD nature of the dyes becomes toxic and hazardous to many organisms. The decontamination of wastewater was extremely done by photocatalysts and their heterostructures under light irradiation [89]. Over the last several years, a series number of studies were adopted for the removal of hazardous dyes in the pollutants are reverse osmosis, ultrafiltration, activated carbon, chlorination, biodegradation, COD, and photodegradation. Nowadays, photocatalysis is the emerging technique to overawe the environment and water pollution. CuO, TiO_2, ZnO, Fe_2O_3, and some other metal oxides were extremely used for photocatalytic applications. Due to the insolubility of metal oxide nanoparticles and the formation of by-products in the water molecule, researchers are interested to design and develop simple metal-free organic light-absorbing and emission compounds as photocatalysts [90].

1.9 Latent Fingerprint.

Fingerprints have been extensively studied because of their uniqueness in identifying individuals based on whorl, arch and loop shape patterns [91]. Fingerprints have several minutiae such as ridge flow, core, delta, bifurcation and sweat pore which are different for each individual and independent of age [92]. Therefore, fingerprints have been used as an effective technique for identifying individual information in criminal investigations [93]. For identification, fingerprints

need to develop on hard and soft surfaces, and visualization has been taken using different techniques. Two types of fingerprints named patent fingerprints which are visible to the eyes and latent fingerprints are hard to visible, hence LFPs are required to develop and visualize using different techniques and powders [94].

There were three different types of latent fingerprint powders; regular, metallic and luminescent. Regular fingerprint powder consists of a resinous polymer and a colorant. It was hard to develop on challenging surfaces. The use of metallic compounds was harmful to user health because of metallic powder containing meshed metals with lead, gold and silver. They were effective in the development of LFPs except for the problems of low resolution, less sensitive, low contrast and high background noise, Low resolution was due to the non-fluorescence nature of the samples [95]. To provide a better solution to these problems, the development of luminescent materials was in demand for replacing metal and magnetic powders [96]. The need for current science and innovation in novel materials with explicit properties builds the interest of the worldwide scientific community. In recent years, an enormous number of victories and logical information in nanotechnology permit the formation of nanomaterials with the required underlying, physical and chemical properties. The capacity to control the design of nanomaterials can prompt the advancement of new advances in different areas of science. As of now, nanomaterials with numerous capacities can be utilized for different applications [97]. Among them, the rare earth ions activated inorganic phosphors have been paid much attention due to their outstanding structural, high color purity, long decay times, strong brightness, chemical and thermal stability and widespread applications in various fields, namely solar cell, bio-imaging, forensic science, white light-emitting diodes, optical heater, sensors, displays devices etc., [98].

1.10 *in* Silico molecular docking studies.

Molecular docking studies are one of the methods which were approached theoretically to understand and predict molecular recognition, structurally, finding binding modes and binding affinities. It is also called protein-ligand docking is widely used in the computational tool, where the interaction between a given protein target and small molecule ligand gives a favourable structure to the compound. It has a wide variety of uses and applications in drug discovery, including structure-activity studies, lead optimizations, finding potential leads by virtual screening, providing binding hypotheses to facilitate prediction for mutagenesis studies, assisting X-ray crystallography in the fitting of substance and inhibitors to electron density, chemical mechanism studies and combinatorial library design [99].

Molecular docking studies were carried out in Auto Dock Vina 4, Schrödinger and some other software packages as a standard tool with particular docking protocols in quite different time scales. There is a choice of two local search methods (Solis and Wets and Pattern Search; two global search methods, Monte-Carlo (MC) simulated annealing (SA), and the genetic algorithm (GA); and one hybrid global-local search method.

Virtual screening based on the molecular descriptor and physicochemical properties of active or inactive ligands has great usefulness in finding the binding score. However, molecular docking when used as the final stage in virtual screening helps to provide a three-dimensional structural hypothesis of how small molecules or ligand interacts with a given or targeted protein [100-102].

1.11 Some of the recently reported nitrogen-containing heterocyclic compounds and their applications have been discussed as follows:

1.11.1 Luminescence properties:

Pyrimidine derivatives are used in the field of energy conversion devices and light-emitting diodes from past decades. Arylpyrimidines (**1a-c**) and arylethynylpyrimidines (**2a-e**) have been reported by Sylvain Achelle *et. al.*, These compounds have highly π-deficient aromatic heterocycles, and exhibit strong blue fluorescence in THF solution (λ_{emi} = 345 nm to 436 nm, ΦF up to 0.6, therefore, they can be used as an electron-withdrawing part in push-pull structures for ICT [103].

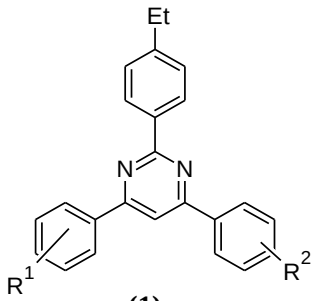

(1)

1a: R^1 = 3,5-Cl ; R^2 = OH,
1b: R^1 = 4-OEt ; R^2 = OCH_3
1c: R^1 = 3-Ph ; R^2 = F

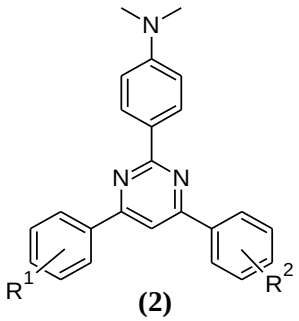

(2)

2a: R^1= 3,5-Cl ; R^2 = OH
2b: R^1 = 4-OEt ; R^2 = OCH_3
2c: R^1 = 4-Ph ; R^2 = Cl
2d: R^1 = 2-(4-napthyl)
2e: R^1 = 4-(9-cabazolyl)

Similarly, extended conjugation with pyrimidine derivatives bearing piro-fluorene substituents (**3a-e**) was synthesized by Shi *et al.* These compounds exhibit intense blue light emission in dichloromethane solution (λ_{emi} = 399-406 nm, ΦF = 0.37-0.63) and as solid (λ_{emi} = 416 nm to 443 nm) [104].

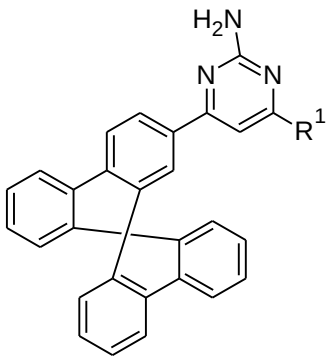

(3)

3a: R^1=Ph
3b: R^1=1-Napthyl
3c: R^1=C_6H_4Cl
3d: R^1=C_6H_4OMe
3e: R^1=2-Thienyl

Achelle S. *et al.*, reported a new carbazole pyrimidine derivatives (**4** and **5**) by Suzuki cross-coupling reaction and obtained good yield. These synthesized compounds have been studied for photophysical properties at low concentration, where compounds absorbed at 282 nm to 388 nm and emitted at 382 nm to 486 nm. Further, based on PL study, quantum yield has been calculated and gives 0.01 to 0.65 Φ_F [105].

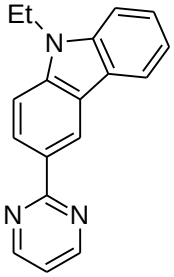

(4)

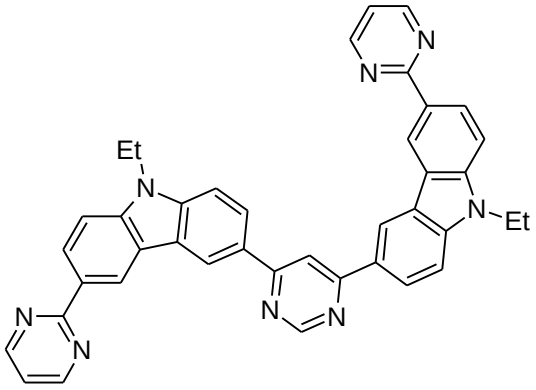

(5)

1.11.2 Fluorescence properties:

Suryawanshi *et al.*, reported a cyano and amine groups substituted pyrimidine derivatives (**6**) [29] and Bolduc *et al.*, reported a thiophene substituted pyrimidine derivatives (**7**) as fluorescence materials [106].

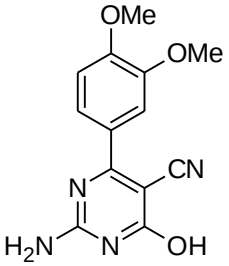

(6)

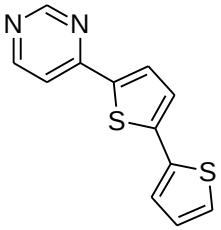

(7)

Verbitskiy and co-workers synthesized a series of 4 and 5-thiophenyl substituted pyrimidine compounds (**8** and **9**) exhibit blue fluorescence (λ_{emi} = 394 nm to 472 nm). The quantum yield observed are much higher for 4-substituted pyrimidine (**8)** (Φ_F = 0.82-1.00) than for 5-substituted pyrimidine (**9**) (Φ_F = 0.06-0.11) and potentially used for DSSCs application [107].

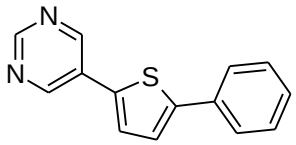

(8)

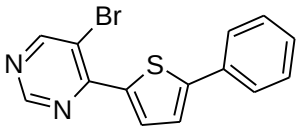

(9)

Wang *et al.*, reported a carbazole containing 4-monosubstituted pyrimidine derivatives (**10**) and (**11**) exhibit bright fluorescence with excellent quantum yields (ΦF = 0.53-0.93) in the blue region in DCM solvent (λ_{emi} = 397 nm to 472 nm) as well as in solid film (λ_{emi} = 423 nm to 473 nm). Similarly, triphenylamine pyrimidine derivative (**12-15**) exbibits a strong emission in $CHCl_3$ solution from the anthracenyl group (λ_{emi} = 410 nm, ΦF = 0.39) [108]

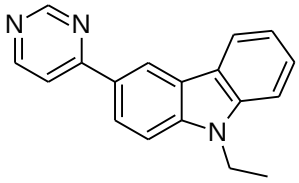

(10)

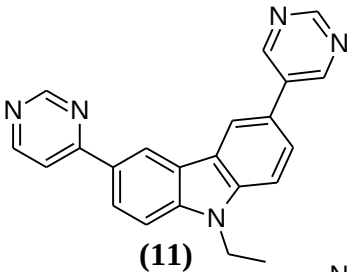

(11)

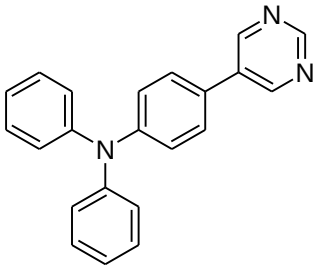

(12)

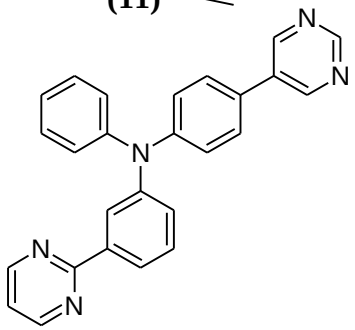

(13)

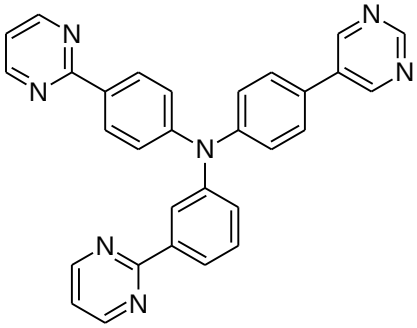

(14)

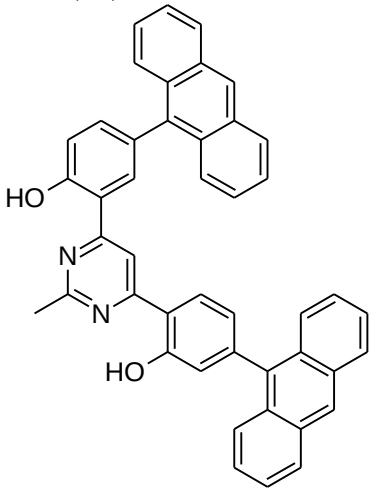

(15)

1.11.3 Anti-cancer agents:

H.T. Abdel-Mohsen *et al.*, reported a new series of imidazole substituted pyrimidine derivatives (**16** and **17**) and studied their potent antitumor activities different cancer cell lines (A-459, MCF-7 and BT-474). Obtained compounds shows better anticancer activity with all the cancer cell lines by exhibiting higher LD_{50} values of 70.3 and 53.65 µg/mL respectively [109].

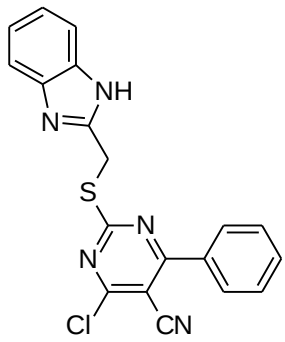

(16)

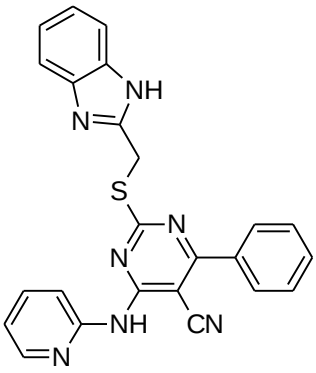

(17)

A.A. Abd Elhameed *et al.*, reported a new thiazolo[4,5-d]pyrimidine and dithiazolo[3,2-a:5′,4′-e]pyrimidinone derivatives (**18** and **19**) and studied their antitumor activities against three different cancer cell lines (ovary, breast, lung). The synthesized compounds have shown better invitro cytotoxicity effect against three cell lines by exhibiting least IC_{50} (89.76 ± 4.3 46.24 ± 2.5 and 31.83 ± 2.2) values [110].

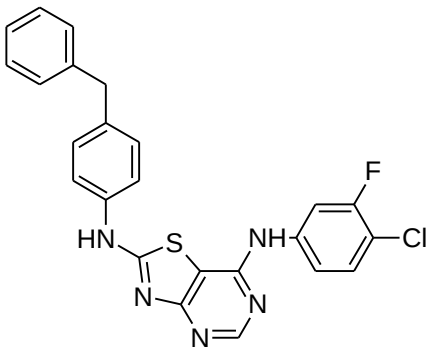

(18)

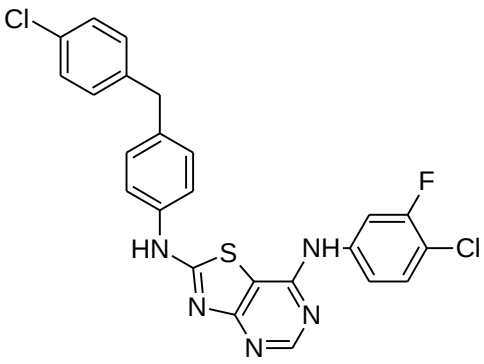

(19)

K. Mohammed *et al.,* reported a novel pyridine derivatives as anti-cancer agents in the year 2018. These compounds show better anti-tumor activity against HL-60, MCF-7 and HCT-116 cell lines by exhibiting least IC_{50} values 0.19±0.02, 0.13±0.012 and 3.97±0.38 respectively [111].

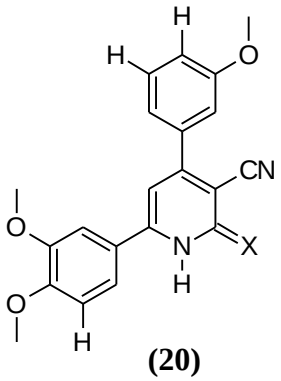

(20)

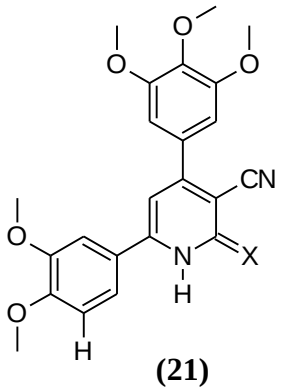

(21)

1.11.4 Aggregation Induce Emission behavior:

Trupthi *et al.,* reports a five cyano substituted pyridine compounds (**22-26**) and has been analyzed absorption and emission properties with electrochemical behavior [112]. Obtained compounds shows fine redox behavior in aqueous electrolyte and compounds emitted in blue regions at 456 nm to 587 nm further compounds exhibits better solvatochromic behavior in solvent media under UV-radiation.

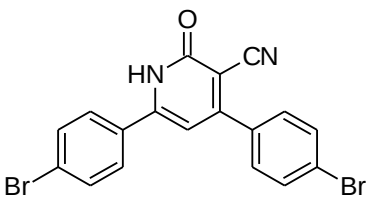

(22)

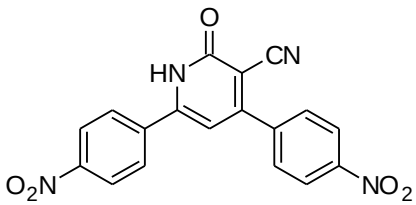

(23)

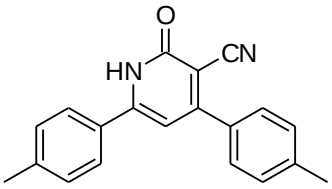

(24)

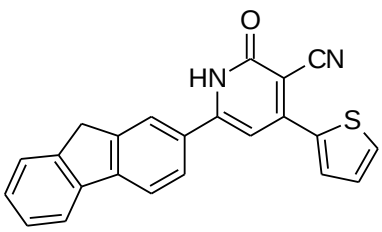

(25)

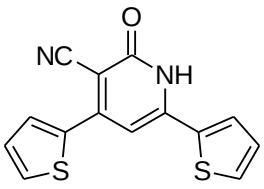

(26)

In 2022, M. Yu and his co-workers synthesized a new cayno substituted bipyridine derivatives (**27a-d**) in solvent media using Iodine as a catalyst and fine aggregate induced emission behavior in solvent media and all the compounds shows fluorescence property at 565 nm to 582 nm at very low concentration [113].

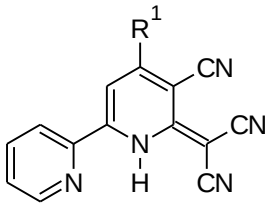

27a: R^1 = Ph
27b: R^1 = 4-$MeOC_6H_4$
27c: R^1 = 4-$Me2NC_6H_4$
27d: R^1 = 4-$Ph_2NC_6H_4$

(27)

In 2018, A.S. Ananda *et al.,* reported a new diphenylamine-pyridyl acetonitrile (**28 a-b**)) compound and exhibits better absorption property in solvent media at 284 nm to 422 nm and AIE studies have been carried out in non-polar to polar solvent, and found high emission fluorescence behavior in different solvents when irradiated with UV light [114].

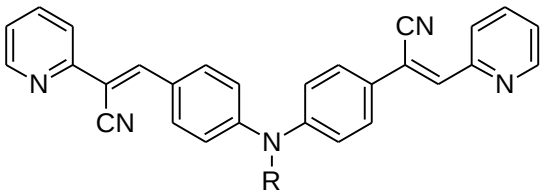

28a: R = C_6H_{13}
28b: R = $C_{12}H_{25}$

(28)

1.11.5 Current-voltage materials:

Basavarajappa *et al.,* reported an optoelectronic and current-voltage Schiff base hydroxy substituted coumarin (**29-31**) Schiff base derivatives under solvent medium using acid catalyst. These compounds have better optical characteristics by the observing absorption band at 407 nm of visible region, and found better photocurrent response under light medium [115-117].

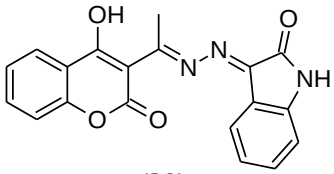

(29)

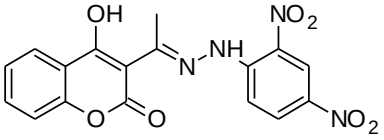

(30)

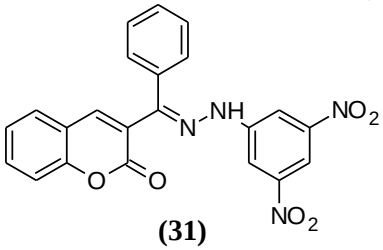

(31)

Hemavathi *et al.,* reported a electrochemical and DSSCs studies of pyridine derivatives (**32, 33**) in the year 2018. Both the derivatives show better redox behavior in presence of solvent as electrolyte and gives 3.34% of solar efficiency under sunlight [118].

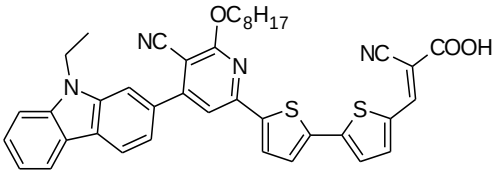

(32)

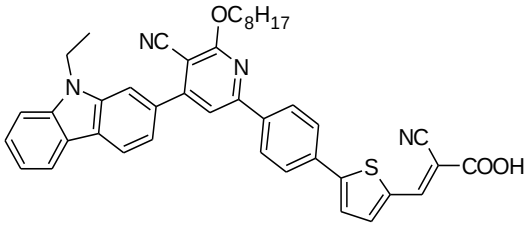

(33)

Abdeslam *et al.,* reported a photovoltaic property of novel quinoxaline- 2,3-dione derivatives (**34-37**). All the synthesized compounds show better electric conversion properties of open circuit voltage at 2.16 eV, 3.391 eV, 3.097 eV, and 2.025 eV respectively [119].

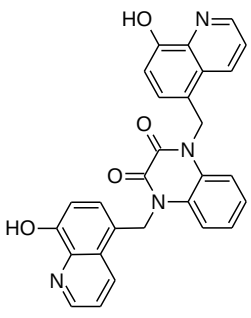

(34)

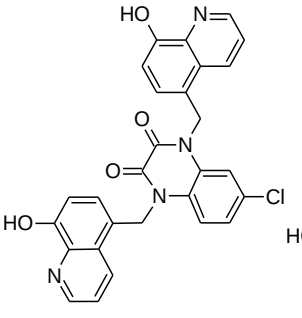

(35)

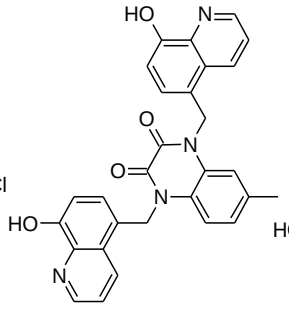

(36)

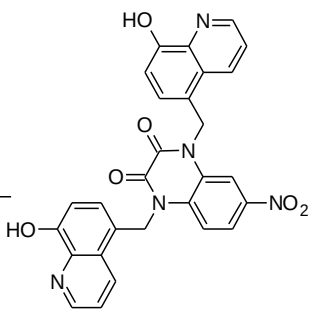

(37)

In 2015, Egor V. Verbitskiy *et al.,* reported an optoelectronic and electrochemical properties of some nitrogen containing heterocyclic compounds. Obtained compounds (**38** and **39**) have better photophysical properties by exhibiting absorption band at 327 nm to 637 nm. Further, theoretical studies reveal that compounds have better kinetic stability and photostability [120].

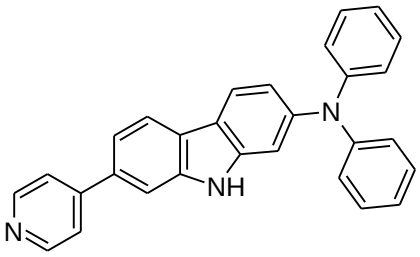

(38)

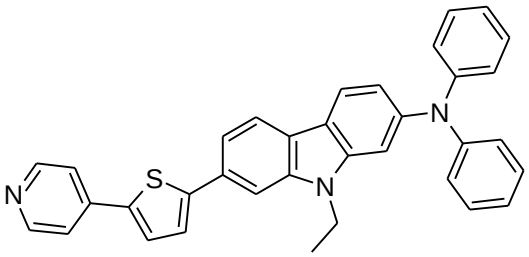

(39)

1.11.6 Dye derivatives:

In 2019, M.R. Maliyappa *et al.,* reported a benzothiazole based azo dyes (**40-43**) and studied their electrochemical and DFT applications. Synthesized azo dyes have shown good electrochemical behavior by exhibiting fine redox peak current [121].

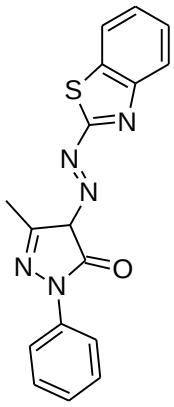

(40)

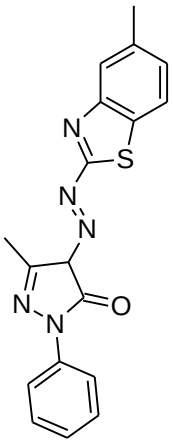

(41)

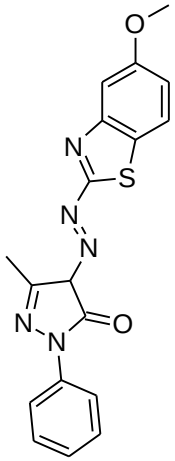

(42)

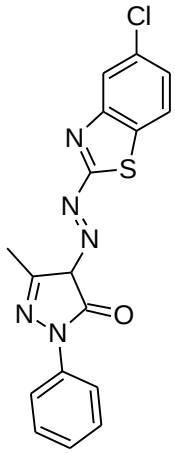

(43)

Nagaraj O *et al.,* reported a hydroxy coumarin substituted with nitrogen azo dyes (**44-47**) and evaluation of their anti-Tb activity. These dyes are said to be hard molecules by theoretically hence they have better photostability and kinetic stability, and act as anti-tubercular agents [122].

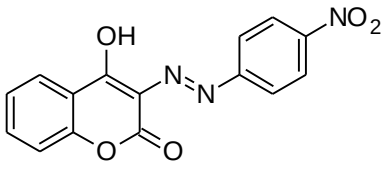

(44)

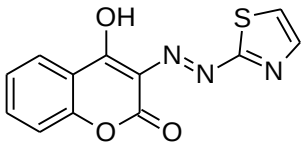

(45)

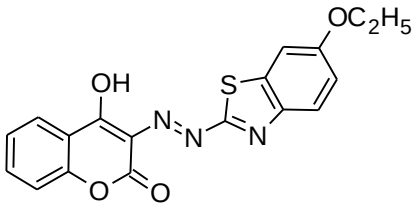

(46)

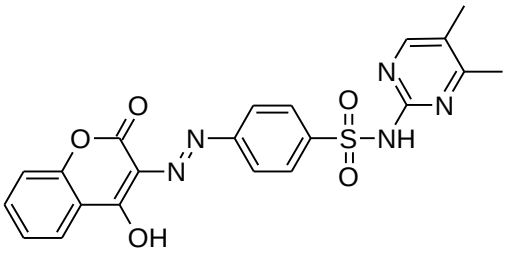

(47)

1.11.7 Latent Fingerprint application:

In 2018, M.K. Ravindra *et al.*, reported a 2-(1-(3,5-bis(trifluoromethyl) phenyl)-4,5-diphenyl-1*H*-imidazol-2-yl)phenol compound (**48**). Obtained compound has been used for development and visualization of LFPs and compounds shows ridges of fingerprint on different substrate [123].

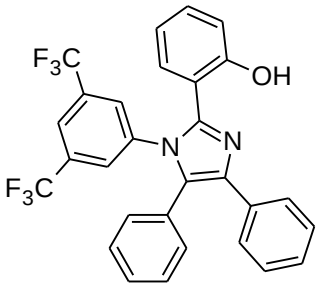

(48)

A new coumarin substituted heterocyclic compound (**49**) has been reported in the year 2020 by Naveen Kumar *et al.*, and studied for latent fingerprint. Development and visualization of LFPs approached by powder dusting method using synthesized compound and fine fingerprint ridges was observed under UV-light on surface of substrate [124].

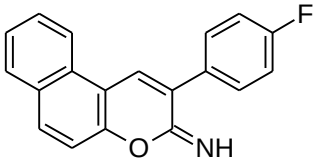

(49)

In 2021, M. Nirmala *et al.*, reported water-soluble pyrene-adorned imidazolium salts (**50**, **51**, **52**) and used for visualization of latent fingerprint on different surface materials, compounds were clearly visible the minutiae feature of developed fingerprint under UV-light. Further, solid-state emission behavior has been studied and emitted at red region [125].

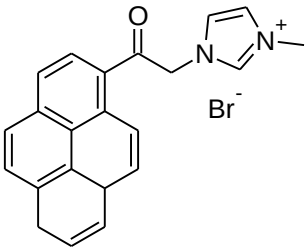

(50)

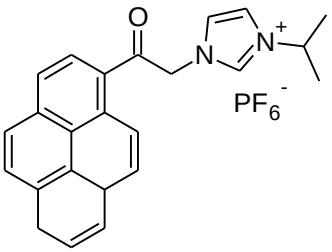

(51)

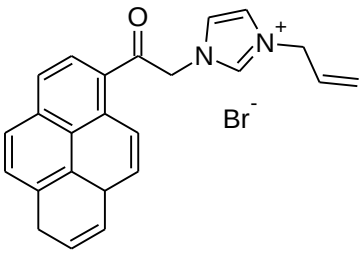

(52)

In 2020, Ghouse Khan and co-workers a reported new series of 1, 2, 4-triazole derivatives (**53**, **54**). The reported compounds have been used for development of fingerprints and screened for antibacterial activity and cytotoxicity against MDA-MB 231 and A375 cancer cell lines. Clear visualization of fingerprints has been found on surface, and show better antibacterial activity by exhibiting higher zone of inhibition at 15.02 ± 0.10. Also, compounds were potential anti-cancer agents by showing higher the CTC_{50} (22.18±1.3) value [126].

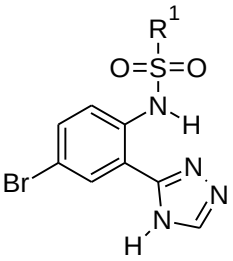

(53)

56a: R^1= C_6H_5 CH_3
56b: R^1= C_6H_5 Cl
56c: R^1= C_6H_5 NO_2
56d: R^1= C_6H_5 Br

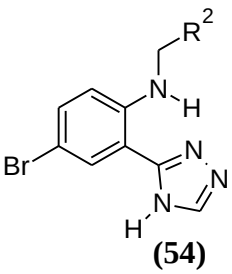

(54)

57a: R^1= C_6H_5 OCH_3
57b: R^1= C_6H_5 3,4 Cl,
57c: R^1= C_6H_5 F
57d: R^1= C_6H_5 4-CH_3

1.11.8 Corrosion inhibitors:

K.R. Ansari and coworkers reported a new cyano substituted amino pyridine derivatives [2-amino-6-(2,4-dihydroxyphenyl)-4-(4-methoxyphenyl)nicotinonitrile (**55**) and 2-amino-4-(4-methoxyphenyl)-6-phenylnicotinonitrile) (**56**)] as a corrosion inhibitor over N80 mild steel. The compounds found good corrosion inhibitors by increased inhibition efficiency with increase in inhibitors concentrations and theoretical calculation has been calculated to understands the intrinsic and extrinsic properties [127].

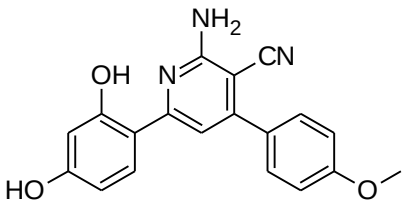

(55)

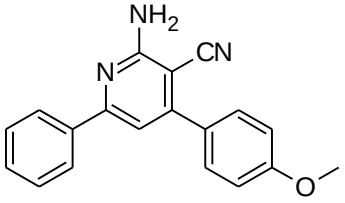

(56)

S.K. Ahmed *et al.,* reported a novel substituted triazole derivatives (**57-60**) as corrosion inhibitors for low-carbon steel in 0.5 M HCl using weight loss method. Synthesized compounds follow the Langmuir absorption isotherm with high negative value of heat of adsorption. The compounds show better corrosion inhibitors by increasing in concentration with inhibitor efficiency exceeding 96.02 % [128].

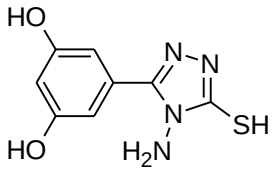

(57)

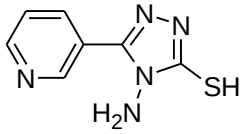

(58)

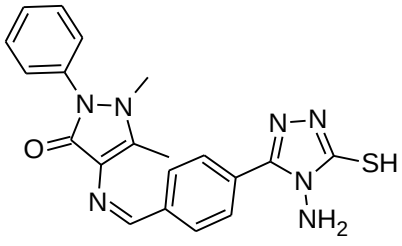

(59)

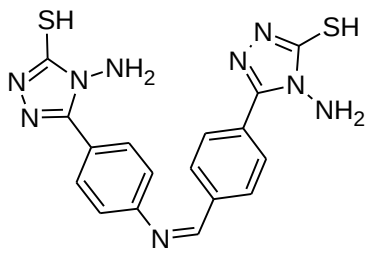

(60)

In 2019, R. Pakkath *et al.*, reported a new substituted pyrimidine derivative as corrosion inhibitors (**61-63**). The compounds have been found better corrosion inhibitor and with higher HOMO values due to presence of electron donor and acceptors groups [129].

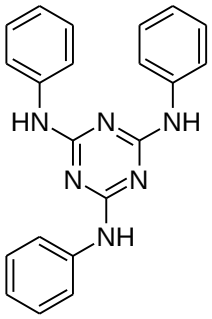

(61)

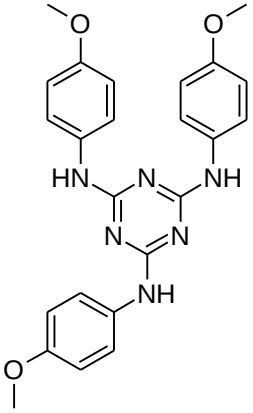

(62)

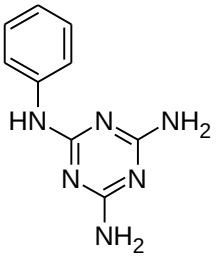

(63)

Based on the above reports, we have synthesized nitrogen-containing heterocyclic compounds and studied their optoelectronic, theoretical and current-voltage characteristics with latent fingerprint applications.

1.12. Organization of the work.

The research work entitled **"SYNTHESIS, CHARACTERIZATION AND APPLICATIONS OF SOME NOVEL NITROGEN HETEROCYCLIC COMPOUNDS"** is systematically presented in the five chapters and is as follows.

1. **Chapter-1:** Introduction
2. **Chapter-2:** This chapter has been divided into two sections:

   Section 2A: One-pot synthesis of some new 7-hydroxy-5-(4-substituted phenyl)-9-methyl-1,5-dihydro-2*H*-dipyrimido[1,2-a:4',5'-d]pyrimidine-2,4(3*H*)-dione derivatives and it's optoelectronic, DFT, photocatalytic studies and latent fingerprint applications.

   Section 2B: Facile synthesis and in-vitro cytotoxicity study of some 5-(4-substitutedphenyl)-7-hydroxy-9-methyl-2-thioxo-2,3-dihydro-1*H*-dipyrimido[1,2-a:4',5'-]pyrimidin-4(5*H*)-one derivatives and their optoelectronic, DFT and LFPs applications.
3. **Chapter-3:** Development and visualization of level II, III features of latent fingerprints using some new 4-(4-substitutedphenyl)-6-(4-substitutedphenyl)-2-oxo-1, 2-dihydropyridine-3-carbonitrile derivatives: Synthesis, characterization, optoelectronic and DFT studies.
4. **Chapter-4:** This chapter has been divided into two sections:

   Section 4A: Synthesis, characterizations of new Schiff base heterocyclic derivatives and their optoelectronic & computational studies with level II & III features of LFPs.

   Section 4B: Optoelectronic, DFT and current-voltage performance of new Schiff base 6-nitro-benzimidazole derivatives.
5. **Chapter-5:** Facile synthesis of 7-(4-substitutedphenyl)-5-(4-substitutedphenyl)-1,3-dimethyl-1 *H*-pyrimido [4,5-d]thiazolo [3,2-a]pyrimidine-2,4(3*H*,5*H*)-dione derivatives and their optoelectronic, DFT and level II & III of LFPs applications.

1.13. Reference.

1. I. L. Finar, Organic Chemistry, Vol.1,6th Ed., *Person Eduction Ltd.,* (**2002**).
2. M. Hossain, A.K. Nanda, *J. Chem. Sci.,* 6 (**2018**) 83-95
3. V. Polshettiwar, R. S. Varma. *Curr. Opin. Drug Discovery Dev.,* 10 (**2007**) 723-737.
4. C.J. Li, *Cheni. Chem. Soc. Rev.,* 35 (**2006**) 68-82.
5. R.S. Varma, *Org. Chem*., 52 (**2007**) 11-21.
6. N. Dege, M.A. Raza, O.E. Dogan, T. Agar, M.W. Mumtaz, *J. Iran. Chem. Soc.*, 18 (**2021**) 2345-2368.
7. D. Robert, *Organic synthesis.,* (**2018**) 1-5.
8. A.R. Katritzky and J.A. Boulton, *Adv. Hete. Chem.,* (Ed.), Academic Press, New York, 27 (**1963**)1-40.
9. S. Pathania, R.K. Narang, R.K. Rawal, *Eur. J. Med. Chem.*, 180 (**2019**) 486-508.
10. P.H. Narnaware, N.S. Prashant, *Int. J. Cur. Eng. Sci. Res.,* 5 (**2018**) 159-169.
11. P. Arrora, V. Arrora, H.S Lamba, D. Wadhwa, *IJPSR.,* 3 (**2012**) 2947-2962.
12. A. Pandith, R.G. Siddappa, Y.J. Seo, *J. Photochem. Photobiol. C: Photochem. Rev.,* 40 (**2019**) 81-116.
13. T.L. Gilchrist, *Hete. Chem., 3rd Ed. Addison Wesley*: Essex, England, (**1997**) 414.
14. R.K Bansal, Heterocyclic Chemistry, (**2008**).
15. D. Rajiv, S. Suman, S.K. Sonwane, S.K Srivastva, *Adv. Bio. Res.,* 5 (**2011**) 120-140.
16. Dickson D. B, Saritha R. G, Sambandam. A.V.A. Airody, *Dyes and Pigm.,* 112 (**2015**) 183-191.
17. R.S. Ansar, M. Farooqui, R.H. Satpue, S. Abed, *J. Drug Delivery & Therap.,* 7 (**2017**) 67-78.
18. F. Hemmerling, F. Hahn, Beilstein, *J. Org. Chem.,* 12 (**2016**) 1512-1532.
19. H. Venkatachalam, V.N.A Kumar, *Heterocycles -Synthesis and Bilogical Activities*, 1 (**2020**)

20. P.G. Alan, W. Schwartz, Geochim, *Cosmochim. Acta.,* 45 (**1981**) 563-569.

21. K. Nagaraju, G. Lalitha. S. Maddila, K.K Gangu, S.B. Jonnalagadda, *Molecules*, 1 (**2020**) 25-40

22. X.L.C. Zhencai, H. Hongli, L. Xuxu, T. Yingzi, C. Huajie, P. Yong T. Songting, *J. Power Sources*, 248 (**2014**) 400-406.

23. C. Xia, X. Fan J. Locklin, R.C. Advincula, *J. Org. Lett.*, 4 (**2002**) 2067-2080.

24. K.R. Idzik, P. Ledwon, R. Beckert, S. Golba. J. Frydel, M. Lapkowski, *J. Electrochim. Acta.*, 55 (**2010**) 7419-7432.

25. A. Mermer, T. Keles, Y. Sirin, *Bioorg. Chem.*, 114 (**2021**) 105076-105090.

26. N. Depa, H. Erothu, Rasayan *J. Chem.,*15 (**2022**) 1-9.

27. J. Zhu, J. Mo, H.Z. Lin, Y. Chen, H.P. Sun, *Bioorg. Med. Chem.,* 26 (**2018**) 3065-3075.

28. A.E.S. Hassan, A.M. Hesham, *J. Iran. Chem. Soc.*, 16 (**2019**) 723-732.

29. R. Ziessel, G. Ulrich, A. Harriman, M.A.H. Alamiry, B. Stewart, P. Retailleau, *J. Chem. A Eur.,* 15 (**2009**) 1359-1369.

30. C. Simon, T. Constantieux, J. Rodriguez, *Eur. J. Org. Chem.,* 24 (**2004**) 4957-4980.

31. K.P. Sahu, K.P. Sahu, S.M. Kaurav, M. Messali, S.M. Almutairi, P.L. Sahu, D.D. Agarwal, *ACS Omega.,* 3 (**2018**) 15035-15042.

32. A. Mermer, T. Keles, Y. Sirin, *Bioorg. Chem.*, 114 (**2021**) 105076-105090.

33. A. Agresti, *N J: John Wiley & sons, Inc,* (**2002**) 876-883.

34. P. Kumar, S. Singh, B. K. Gupta, *Nanoscale.,* 8 (**2016**) 14297-14305.

35. K. Braeckmans, S.C. De Smedt, C. Roelant, M. Leblans, R. Pauwels, J. Demeester, *Nat, Mater.,* 1 (**2003**) 169-175.

36. H. Nam, K. Song, D. Ha, T. Kim, *Sci. Rep.,* 1 (**2016**) 385-387.

37. B.M. Weckhuysen, P., Van Der Voort, G. Catana, (Eds), *Leuvan University Press,* (**2000**) 221-225.

38. Forster, H., Seebode, J. Fejes, P. Kiricsi, *J. Chem. Soc. Faraday Trans.,* (**1987**) 1109-1113.

39. Y. Sendoda, Y. Ono, T. Keii, *J. Catal.,* 28 (**1975**) 357-361.

40. F. Murphy, M. Middleton, *Annual.,* 85 (**2012**) 334-338.

41. G.L. Patrick, II., 25 (**2005**) 456-459.

42. A. Das, B.K. Banik, *Sustainable Drug Design.,* (**2020**) 123-128.

43. A. Demeter, *Anthropic Awareness.,* 139 (**2015**) 234-239.

44. A.A. Altaf, A. Shahzad, Z. Gul, N. Rasool, A. Badshah, B. Lal, E. Khan, *J. Dur. Des. Med. Chem.,* 1 (2015) 1-11.

45. T. Anderson, *Ann. Phys.,* 60 (**1846**) 86-98.

46. D. Bora, B. Deb, A.L Fuller, A.M.Z Slawin, J. D. Woollins, D.K. Dutta, *Inorg. Chim. Acta.,* 363 (**2010**) 1539-1549.

47. S. Saito, H. Yamamoto, K. Oshima, T. Tzitzikas, A.L. Chandgude, A. Dömling. *Chem. Rec*., 15 (**2015**) 1-13

48. C. Allais, J.M. Grassot, J. Rodriguez, T. Constantieux, *Chem. Rev.,* 114 (**2014**) 10829-10868

49. G.D. Henry, *Tetrahedron.,* 60 (**2004**) 6043-6061.

50. S. Shimizu, N. Watanabe, T. Kataoka, T. Shoji, N. Abe, S. Morishita, H. Ichimura *Weinheim: Wiley-VCH.* (**2016**).

51. N.B. Patel, S.N. Agravat, F.M. Shaikh, *Chem. Res*., 20 (**2011**) 1033-1041.

52. N.B. Patel, S.N. Agravat, *Chem. Heterocycle. Compd*., 45 (**2009**) 1343-1353.

53. A. Sivastava, S.N. Pandeya, *Int. J. Curr. Pharm. Rev. Res*., 4 (**2011**) 5-8.

54. T.J Tucker, J.T. Sisko, R.M. Tynebor, T.M. Williams, P.J. Felock, J.A. Flynn, M. Lai, Y. Liang, G. McGaughey, M. Liu, *J. Med. Chem.,* 51 (**2008**) 6503-6511.

55. G.K. Sims, E.J. O'Loughlin, *Crit Rev Environ Sci Technol.,* 9 (**2009**) 309-340.

56. M. Josipa, J. Marijana, I. Hamit, S. Dijana, B. Željka, T. Tana, V. Robert, Opačak- T. Bernardi, L. Glavaš-Obrovac, B. Žinić, *Nucleo. Nucleot. Nucleic Acids.,* 40 (**2021**) 470-503.

57. N. Shahabadi, A. Akbari, M. Jamshidbeigi, R. Khodarahmi, *Nucleo. Nucleot. Nucleic Acids.,* 35 (**2016**) 315-333.

58. F.S. Rojas, C. Bosch Ojeda, *Analytica Chimica Acta.*, 635 (**2009**) 22-44.

59. W.L.F. Armarego, C.L.L Chai, *5th Ed.; Butterworth-Heinemann: Amsterdam; Boston* (**2003**) 445-447.

60. P.C. Ray, J.M.C. Tummanapalli, S.R. Gorantla, *Google Patents:* (**2011**) 276-287.

61. B.M. Weckhuysen, V.D. Voort, P. Catana, G., (Eds), *Leuvan University Press*., (**2000**) 221-224.

62. F. Basolo, R.C. Johnson, W.A. Benjamin, *Coord. Chem. Rev.,* 8 (**1964**)

63. A.M.S. El-Sharief, M.S. Ammar, Y.A. Ammar, M.E. Zak, *Ind. J. Chem*., 22 (**1983**) 700-712.

64. H.J. Kimble, M. Dagenais, L. Mandel, *Phys. Rev. Lett.*, 39 (**1977**) 691-698

65. M. Tebyetekerwa, J. Zhang, Z. Xu, T.N. Truong, Z. Yin, Y. Lu, S. Ramakrishna, D. Macdonald, H.T. Nguyen, *ACS Nano.,* 14 (**2020**) 14579-14604.

66. M. Kira, F. Jahnke, S.W. Koch, *Phys. Rev. Lett.*, 82 (**1999**) 3544-3557.

67. J. Lv, T. Liu, S. Cai, X. Wang, L. Liu, Y. Wang, *J. Inorg. Biochem. Acta*., 1760 (**2006**) 814-834.

68. A.S. Gaballa, M.S. Asker, A.S. Barakat, S.M. Teleb, *Spectrochim Acta. Part A. Mol Biomol Spectors*., 1 (**2006**) 1-12.

69. L. Leonat, S. Gabriela, I.V. Branzoi, *U.P.B. Sci. Bull. Series B.,* 75 (**2013**) 111-119.

70. I. Yilmaz, M.B. Kocak. *J. Polyhedron.,* 23 (**2004**) 1279-1285.

71. E.M. Espinoza, J.A. Clark, J. Soliman, J.B. Derr, M. Morales, V.I. Vullev, *J. Electrochem. Soc.,* 166 (**2019**) 3175-3187.

72. S. Prasada, R.K. Agarwala, B.A. Kumar, *J. Iran. Chem. Soc.,* 8 (**2011**) 825-839.

73. M. Sonawane, K. Tayade, S.K. Sahoo, C.P Sawant, A. Kuwar, *J. Coord. Chem.*, 69 (**2016**) 2785-2792.

74. P. Hohenberg, W. Kohn, *Phys. Rev. B.*, 136 (**1964**) 864-874.

75. W. Kohn, L.J. Sham, *Phys. Rev. A.*, 140 (**1965**) 1133-1144.

76. E. Erdem, E.Y. Sari, R. Kilincarslan, R. Kabay, *Trans. Met. Chem.*, 34 (**2009**) 167-174.

77. C. Anitha, C.D. Sheela, P. Tharmaraj, S. Sumathi, *Spec. Chim. Acta, Part A.*, 96 (**2012**) 493-500.

78. N. Venugopal, G. Krishnamurthy, H.S. Bhojya naik, P. Murali Krishna, *J. Mol. Struct.*, 1183 (**2019**) 37-51.

79. M. El-Behery, H. El-Twigry, *Spec. Chim. Acta A: Mol. Biomol. Spectrosc.*, 66 (**2007**) 28-36.

80. R. Parr, G. Donnelly, R.A. Lev, M.W.E. Palke, *J. Chem. Phys*., (**1977**) 3801-3807.

81. J. Jia, J. Wen, *Tetrahedron Lett.,* 61 (**2020**) 4028-4039.

82. J.P. Perdew, Y. Wang, *Phys. Rev. B.,* 45 (**1992**) 13244-13256.

83. R.G. Parr and W. Yang, *Springer, Berlin.,* (**1990**) 1123-1134.

84. W. Kohn and P. Vashishta, *Plenum, New York.,* (**1983**) 79-147

85. S.K. Weng, W.L. Jing, C.C. Woon, L.P. Yean, C.S Lan, *Environ. Sci. Pollut. Res.*, 27 (**2020**) 2522-2565.

86. M.R. Khan, A.S.W. Kurny, G. Fahmida, *App. Wat. Scienc.*, 170 (**2009**) 520-529.

87. C. Hachem, F. Bocquillon, O. Zahraa, M. Bouchy, *Dyes and Pigm.,* 49 (**2001**) 117-125

88. K.N. Harish, H.S. Bhojya Naik, P.N. Prashanth Kumar, R. Vishwanath, G.S. Yashwanth Kumar, *Arch. App. Sci. Res.,* 5 (**2013**) 42-51.

89. N. Ganji, V.K. Chityala, P.K. Marri, R. Aveli, Vamsi, K. Narendrula, S. Daravath, J. Shivaraj, *Photochem. Photobiol. B.,* 175 (**2017**) 132-140.

90. C. Christophe, L. Chris, M. Pierre, S. Milutin, *Boca Raton, London, New York, Washington, DC: CRC Press*; (**2004**) chapter 4.

91. M. Srinivas, G.R. Vijayakumar, K.M. Mahadevan, H. Nagabhushana, H.S. Bhojya naik, *J. Sci. Adv. Mater. Devices.,* 2 (**2017**) 156-164.

92. K.A. Vishnumurthy, M.S. Sunitha, K. Safakath, R. Philip, A.V. Adhikari, *Polymer (Guildf,).,* 19 (**2011**) 4174-4183.

93. R.B. Basavaraj, G.P. Darshan, B.D. Prasad, S.C. Sharma, H. Nagabhushana, *J. Rare Earths.,* 37 (**2019**) 32-44.

94. G.P. Darshan, H.B. Premkumar, H. Nagabhushana, S.C. Sharma, B.D. Prasad, S.C. Prashantha, R.B. Basavaraj, *J. Alloys Compd.,* 686 (**2016**) 577-587.

95. R.B. Basavaraj, H. Nagabhushana, G.P. Darshan, B.D. Prasad, S.C. Sharma, K.N. Venkatachalaiah, *J. Ind. Eng. Chem.,* 51 (**2017**) 90-105.

96. J. Janczak, *J. Polyhedron,* 38 (**2012**) 75-87.

97. M. Dhanalakshmi, H. Nagabhushana, G.P. Darshan, R.B. Basavaraj, B.D. Prasad, *J. Sci. Adv. Mater. Devices.,* 2 (**2017**) 22-33.

98. N. Sengottuvelan, D. Saravanakumar, M. Kandaswamy, *J. Polyhedron.,* 26 (**2007**) 3825-3835.

99. R. Akhil Chakravarty, A.N. Pattubala Reddy, K. Bidyut Santra, M. Anitha Thomas, Proc. *Indian Acad. Sci. (Chem. Sci.).,* 114 (**2002**) 391-402.

100. Y. Saegusa, S. Harada, S. Nakamura, *J. Het. Chem.*, 27 (**1990**) 739-748.

101. B.G. Tweedy, *Phyto Pathology.,* 55 (**1964**) 910-922.

102. S Mishra, R. Dahima, *J. drug delivther.*, 9 (**2019**) 366-369.

103. S. Achelle, C. Baudequin, *Targets Heterocycl Syst.,* 17 (**2013**) 1-34.

104. R. Komatsu. S. Hisahiro. K. Junji, *J. Photon. Energy.*, 8 (**2018**) 032108-032128.

105. A. Sylvain, J. Rodríguez-López, M. Larbani, R. Plaza-Pedroche, F Robin-le Guen, *Molecules.*, 24 (**2019**) 1742-1751.

106. V.D. Suryawanshi, A.H. Gore, L. Walekar, S. Anbhule. P.V, Patil, S.R, Kolekar, *J. Mol. Liq.,* 184 (**2013)** 1125-1140.

107. E.V. Verbitskiy, E. Cheprakova. J.O Subbotina, A.V. Schepochkin, P.A. Slepukhi, G.L. Rusinov, V.N. Charushin, O.N. Chupakhin, N. Makarova, A.V Metelitsa, V.I Minkin, *Dyes and Pigm.,* 100 (**2014**) 201-220.

108. J. Weng, Q. Mei, Q. Fan, Q. Ling, B. Tongc, W. Huang, *RSC Adv.,* 3 (**2013**) 21877-21892.

109. T. Heba, Abdel-Mohsen, F.A.F. Ragab, M.M. Ramla, H.I. El Diwani, *Eur. J. Med. Chem.*, 45 (**2010**) 2336-2344.

110. A.A. Abd Elhameeda, N.S. El-Goharya, E.R. El-Bendarya, M.I. Shaaban, S.M. Bayomi, *Bio Org. Chem.*, 81 (**2018**) 299-310.

111. K. Mohammed. Abd elhameida, N. Ryadb, Al-Shorbagy MY, M.R. Mohammed, M. M. Ismaila, S.El. Meligiea, *Chem. Pharm. Bull*., 18 (**2018**) 00269-00278.

112. C.T. Devaiah, B. Hemavati, M.B. Ros, J.B. Rosa, M. Tejedor, K.K. Sadasivuni, T.N. Ahipa, *J. Mol. Liq.,* 255 (**2018**) 233-243.

113. M. Yu. Ievleva, N.S. Mayorova, M.A. Shishlikovaa, M.Yu. Belikova, I.N. Bardasova, O.V. Ershova, *Russ. J. Org. Chem.,* 57 (**2021**) 1961-1967.

114. A.S.V. Anand, K. Mahesh, V. Priyanka, S. Karpagam, *J. Mat. Sci. Mat. Electr*., 29 (**2018**) 10949-10961.

115. K.V. Basavarajappa, Y.A. Nayaka, R.O. Yathisha, K.B. Manjunatha, *J. Fluoresc.*, 29 (**2019**) 1201-1211.

116. K.V. Basavarajappa, Y.A. Nayaka, H.T. Purushotham, R.O. Yathisha, M.M. Vinay, B.J. Rudresh, K. Manjunatha, *J. Mol. Struct.,* 1199 (**2020**) 126946-126958.

117. K.V. Basavarajappa, Y.A. Nayaka, H.T. Purushothama, M.M. Vinay, A. Antony, P. Poornesh, *Int. J. Environ. Anal. Chem.*, (**2019**) 1-14.

118. B. Hemavathi, J.V. Pradhan, S.C. Gokul, G.J. Kusuma, G.K. Chandrashekara, P.C Ramamurthy, R.K Pai, K.N. Narayanan Unni, T.N. Ahipa, S. Suraj, R.G Balakrishna, *Sol. Energy.,* 174 (**2018**) 1085-1096.

119. A. El Assyry1, I. Rafiq, M. Rbaa, A. Derouiche, B. Lakhrissi, *Trends Sci.*, 19 (**2022**) 6173-6187.

120. E.V. Verbitskiy, E.M. Cheprakova, J.O. Subbotina, A.V. Schepochkin, P.A. Slepukhin, G.L. Rusinov, V.N. Charushin, O.N. Chupakhin, N.I. Makarova, A.V. Metelitsa, V.I. Minkin, *Dyes and Pigm.,* 98 (**2015**) 302-314.

121. M.R. Maliyappa, J. Keshavayya, M. Mahanthappa, Y. Shivaraj, K.V. Basavarajappa, *J. Mol. Struct.,* 1199 (**2020**) 126959-126970.

122. O. Nagaraja, Y.D. Bodke, I. Pushpavathi, S. Ravi Kumar, *Heliyon.*, 6 (**2020**) 04245-04256.

123. M.K. Ravindra, K.M. Mahadevan, R.B. Basavaraj, G.P. Darshan, S.C. Sharma, M.S. Raju, G.R. Vijayakumar, Kiran B. Manjappa, D.Y. Yang, H. Nagabhushan, *Mater. Sci. Eng. C.*, 101 (**2018**) 564-574.

124. N. Kumar, Udayabhanu, K.M. Mahadevan, G. Nagaraju, *J. Sci. Adv. Mat. Dev.*, 5 (**2020**) 520-526.

125. M. Nirmala, R. Vadivel, S. Chellappan, J.G. Malecki, P. Ramamurthy, *ACS Omega.*, 6 (**2021**) 10318-10332.

126. G. Khan, S. Sreenivasa, G. Shivaraja, V. Chandramohan, P.R. Shetty, *J. Hete. Chem.*, (**2020**) 1-14.

127. K.R. Ansari, M.A. Quraishi, A. Singh, *Measurement.*, 76 (**2015**) 136-147.

128. S. K. Ahmed, W.B. Ali, A.A. Khadom, *J. Bio and Tribo Corrosion.*, 5 (**2019**) 15-22.

129. P. Rajeesh, E. K. Reddy, S. Kuriakose, C. Saritha, A.M. Sajith, R.P. Karuvalam, K.R. Haridas, *J. Korean Chem. Soc.*, 63 (**2019**). 352-359.

Chapter-2A

One-pot synthesis of some new 7–hydroxy-5-(4-substitutedphenyl)-9-methyl-1,5-dihydro-2*H*-dipyrimido [1,2- *a* :4 _ ,5 _ - *d*]pyrimidine-2,4(3*H*)–dione derivatives and it's optoelectronic, DFT, photocatalytic studies and latent fingerprint applications

2A.1 Introduction

Multicomponent reaction (MCR) is an approach of green chemistry which plays a vital role in organic synthesis, which helps to synthesize large diversity of products in a simple reaction with more than two reactants [1, 2]. The main use of MCRs is the synthesis of polyfunctional organic compounds such as 1,4 additions, nitration, 1,3 dipolar cycloadditions, and hanzsch reaction using various organic catalysts [3, 4]. In past years these polyfunctional organic compounds were synthesized to be used in pharmaceutical chemistry as biological agents and also gained interest use in material science applications such as organic fluorescent materials, light emitting diodes, electroluminescent indicators, as dyes in energy conversion devices, and forensic science [5, 6]. It has many advantages in comparison with classical reactions, such as fewer isolation and purification steps, high atom economy, low cost and energy consumption, short reaction time etc. MCRs have been carried out predominantly to synthesize nitrogen-bearing heterocyclic compounds and were used in many applications [7, 8].

Metal-free organic dye compounds containing heterocyclic moieties like coumarin indole, pyridine, pyrimidine, etc., are shows better light absorption and light-emitting properties due to their aromatic conjugations and electronic transitions [9-10]. In general, pyrimidines are well-known drugs in the field of medicinal chemistry as anti-analgesic, anti-microbial, anti-inflammatory and anti-cancer agents [11-13]. As known drug molecules, researchers have gained interest to develop and design pyrimidine moieties as photonic materials, optical chemosensors and photo-sensitizers due to their better photophysical properties, high electron affinity and act as a π-acceptor character. Particularly, pyrimidine exhibited higher fluorescent

properties when having different electron-withdrawing and donating groups [14, 15]. Moreover, it acts as an electron-withdrawing character due to its π-deficient nature hence increasing color sensitivity and higher molar extinction co-efficient with solvatochromic behavior.

Photocatalysts play a important role in purifying the water pollution caused by the textile, leather, pulp and paper industries. Till now, Nanocomposite metal oxides have been used as photocatalysts under UV-irradiation by dye degradation method. Due to the insolubility of metal oxide nanoparticles and the formation of byproducts in the water molecule, researchers are interested to design and develop simple metal-free organic light-absorbing and emission materials as photocatalysts [16]. Additionally, these metal-free organic compounds can be used to develop latent fingerprints on porous/nonporous materials and visualized under UV light. [17, 18]. Latent fingerprints are commonly and predominantly used by every forensic analyzer due to the invisible to the naked eye [19, 20] hence chemical or physical treatment is required to develop for visualization. The visualization of LFPs requires a good optical contrast and adherence between fingerprints ridges and materials to develop. In earlier days, there are several methods were carried out for the visualization of LFPs such as powder dusting, iodine fuming, electrochemistry, vacuum metal deposition, mass spectrometry and fluorescence spectroscopy [21-23]. Among these approaches, the powder dusting method was commonly encouraged to use at crime spots because of the easiest method and because data can be stored for a longer time. However, in general, there are three types of powders were well-known to use such as regular, metallic and organic fluorescent materials. Regular powders contain polymers and colorant powders which are hard to develop on a difficult surface and metallic powders are injurious to humans due to metals [24-26]. Among these

powders, organic fluorescent powders have been used recently due to their high emission properties and found a good optical contrast between fingerprint ridges and surface materials, therefore organic fluorescent materials are needed to design and develop a visualization of LFPs. Some of the reported biological and material science applications of important heterocyclic compounds have been discussed below.

Bharti Mohana *et al.*, reported in the year 2020, a new series of bis uracil derivatives obtained by the reaction of 6-amino-1,3-dimethyl pyrimidine-2,4(1*H*,3*H*)-dione with aromatic benzaldehyde in solvent media (ethanol) using acid catalyst, Targeted compound (**1**) shown better photophysical properties at 400 nm to 600 nm, hence, these compounds have luminescence character [27].

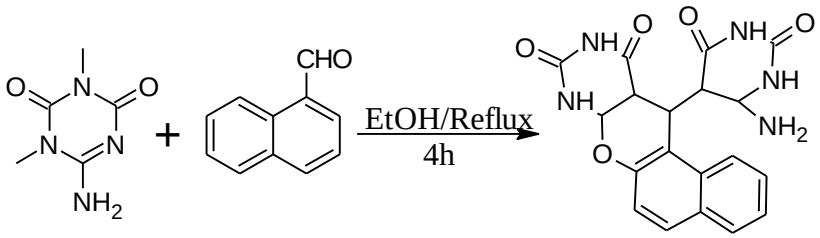

(1)

S. Sunil *et al.*, reported a novel pyrimidine-5-carbonitrile derivatives (**2**) in the year 2021 by the reaction of aromatic aldehyde, malononitrile, and guanidine hydrochloride in solvent media using $Fe(acac)_3$ as a catalyst. Obtained targeted compound analysis for both biological and optical properties. The compound shows excellent optical properties by absorbing bands at longer wavelengths (352 nm to 402 nm) and emitted at bathochromic shift (425 nm to 570 nm) [28].

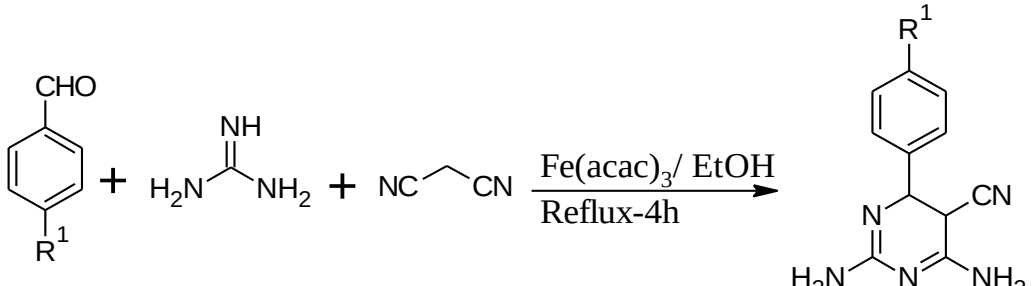

R^1= NO_2, Cl, OCH_3, OH, CH_3

(2)

Hassan *et al.,* reported a 4-oxo-pyrido[2,3-d]pyrimidine derivatives (**3**) in the year 2019 with a good yield. The obtained compounds display better photophysical properties, where absorb at 370 nm to 455 nm and are emitted at 427 nm to 482 nm [29].

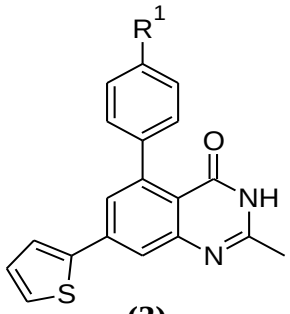

R^1 = OH, NO_2, Cl, Br, OCH_3

(3)

Shinde *et al*., synthesized a new pyrimido [4,5-d] pyrimidine-2-(1*H*)-one derivatives (**4**) under solvent-free conditions using L-proline as catalyst. These compounds have better optical properties, whereas both absorption and emission bands were located at a longer wavelength (320 nm to 526 nm), and exibhits excellent electrochemical behavior. Further, targeted compounds also show a better anti-cancer agent with the least IC_{50} value of 23±18 [30].

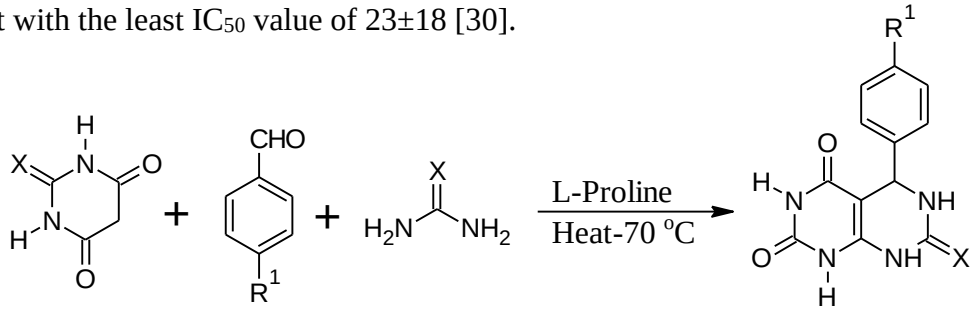

X= O, S. R^1 = CH_3, NO_2, OH, F **(4)**

Jagwani and Joshi reported a green approach for the synthesis of [4-(4-hydroxyphenyl)-6-methyl-2-oxo-1,2,3,4-tetrahydropyrimidin-5-yl](oxo)acetic acid (**5**) and this method was found to be easier and got better yield in shorter reaction time. Obtained compounds have shown better optical properties and absorption bands that move to the redshift at 380 nm to 460 nm, emitted at a longer wavelength (425 nm to 560 nm) and also show good anti-cancer agents [31].

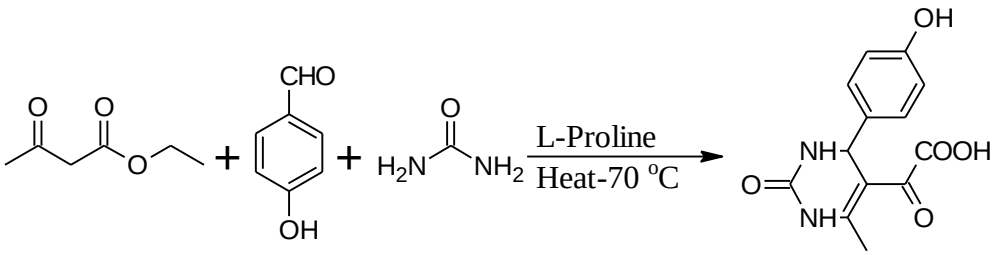

(5)

Ethyl-3-amino-2-cyano-6-hydroxy-7,12-dioxo-2,7,12,12a-tetrahydro-1*H* benzo[g]pyrimido[1,2-a]quinoline-5-carboxylate (**6**) has been reported by Nadia A.A. *et al.,* in 2020 and studied for optoelectronic properties in solvent media. The optical bands appeared at visible regions (400 nm to 560 nm) with better redox behavior [32].

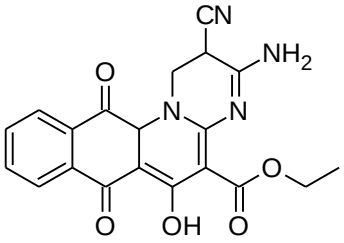

(6)

Based on the above-obtained results, in this chapter, we report; a one-pot synthesis of some novel 7-hydroxy-5-(4-substituted phenyl)-9-methyl-1,5-dihydro-2*H*-dipyrimido[*1,2-a:4,5*-]pyrimidine-2,4(3*H*)–dione derivatives **4**(**a-d**) using a catalytic amount of L-Proline and studied their optical, electrochemical, theoretical, photocatalytic studies and latent fingerprint application.

2A.2 Present Work.

In this chapter, we have developed a simple and coinvent method for the synthesis of some new 7-Hydroxy-5-(4-substitutedphenyl)-9-methyl-1,5-dihydro-2*H*-dipyrimido[*1,2-a:4-,5-d*]pyrimidine-2,4(3*H*) dione derivatives **4**(**a-d**) through the multicomponent reaction of 2-amino-4-hydroxy-6-methyl pyrimidine (**1**), barbituric acid (**2**) with aromatic aldehydes (**3**) in 20 mL ethanol using L-Proline as a catalyst.

The synthetic pathway of synthesized substituted pyrimidine derivatives **4(a-d)** have been demonstrated in **Scheme 1.**

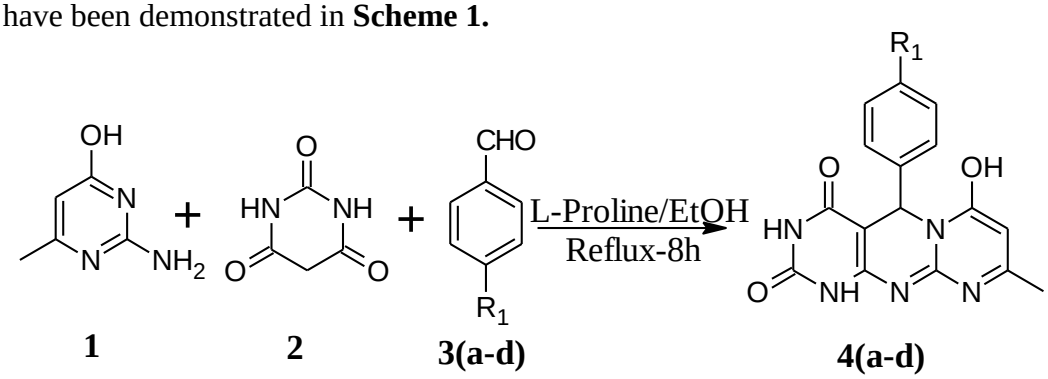

1 **2** **3(a-d)** **4(a-d)**

Entry	R_1
4a	OH
4b	Cl
4c	OH, OCH_3
4d	Br

Scheme-1: Synthesis of new 7-Hydroxy-5-(4-substitutedphenyl)-9-methyl-1,5-dihydro-2*H*-dipyrimido[*1,2-a:4',5'-d*]pyrimidine-2,4(3*H*)-dione derivatives **4**(**a-d**).

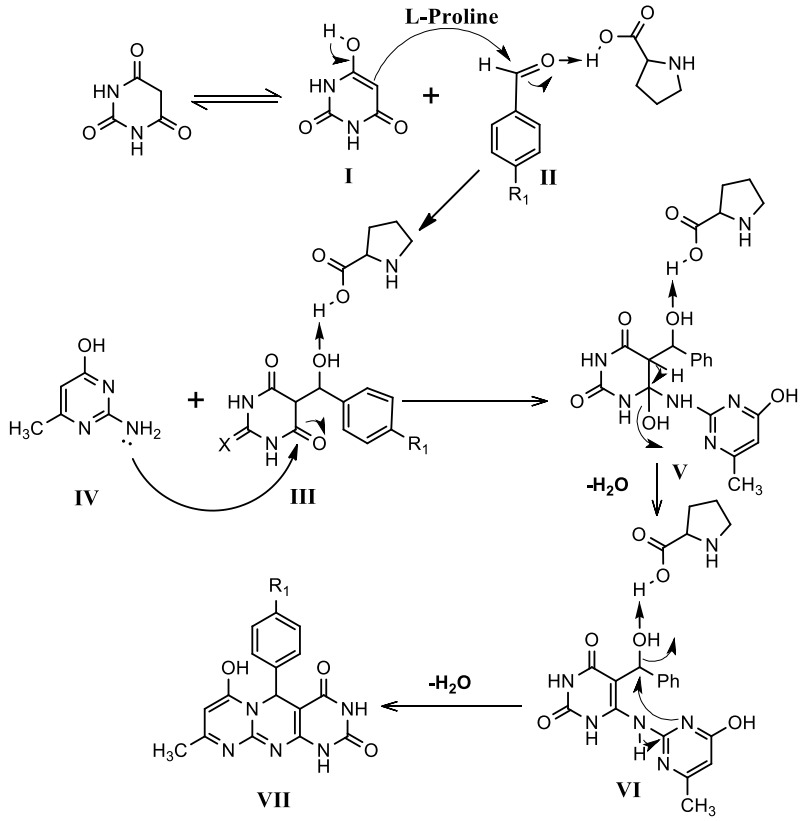

Scheme 2: Possible mechanism of synthesized substituted pyrimidine derivatives **4**(**a-d**).

Possible mechanism for formation of new 7-hydroxy-5-(4-substitutedphenyl)-9-methyl-1,5-dihydro-2*H*-dipyrimido[*1,2-a:4',5'-d*]pyrimidine-2,4(3*H*)-dione derivatives proposed in **Scheme 2**. The enol (**I**) from barbituric acid attack substituted benzaldehyde (**II**) through L-Proline and was coordinated through a hydrogen bond to oxygen atom (**III**). Nucleophilic attack from primary amine (**IV**) to the carbonyl group of the activated benzaldehyde (**III**) and formation of Knoevenagel intermediate (**V**). Michael addition reaction has taken place from pyrimidine ring leads to formation of intermediate (**VI**). Further, cyclo-condensation to afford the targets (**VII**) **4**(**a-d**) [33].

2A.3 Spectral characterization.

The structures of newly synthesized compounds 7-Hydroxy-5-(4-substitutedphenyl)-9-methyl-1,5-dihydro-2*H*-dipyrimido[*1,2-a:4',5'-d*]pyrimidine-2,4(3*H*)-dione derivatives **4(a-d)** were confirmed by different spectroscopic techniques such as FTIR, ^{1}H & ^{13}C- NMR and HRMS.

In the IR spectrum of synthesized compound **4a** showed a stretching vibration band at 3427 cm^{-1} due to the hydroxyl group and another band at 3267 cm^{-1} which correspond to starching vibration of amide functionality. Aromatic stretching frequency appeared at 3184 cm^{-1} and absorption band at 1663 cm^{-1} correspond to C=O stretching carbonyl functionality. In ^{1}H-NMR spectrum of compound **4a** exhibited two singlet peaks at δ 11.22 and 11.09 ppm due to two NH protons of the pyrimidine nucleus and another two singlet peaks appeared at δ 10.77 and 10.79 ppm corresponds to two OH protons. Furthermore, the doublet peaks at δ 8.30-8.28 ppm of two aromatic protons and a singlet peak at δ 8.16 ppm correspond to aromatic proton, another doublet peak observed at 6.84-6.82 ppm due to another two aromatic protons. A singlet peak has been observed at δ 5.73 ppm of junction proton between

the phenyl and pyrimidine ring and another singlet peak appeared at 1.95 ppm corresponds to methyl protons. Also, ^{13}C-NMR spectra of compound **4a** shows a signal at δ 165.30 and 162.84 ppm due to the C=O carbon and δ 156.00 correspond to C=N carbons. Aromatic carbon peaks observed at 150.78 to 114.71 and a methyl carbon has been observed at δ 23.66 ppm. The high-resolution mass spectrum showed molecular ion peak $[M]^+$ at m/z is 341.3083 corresponding to molecular weight of the compound **4a.**

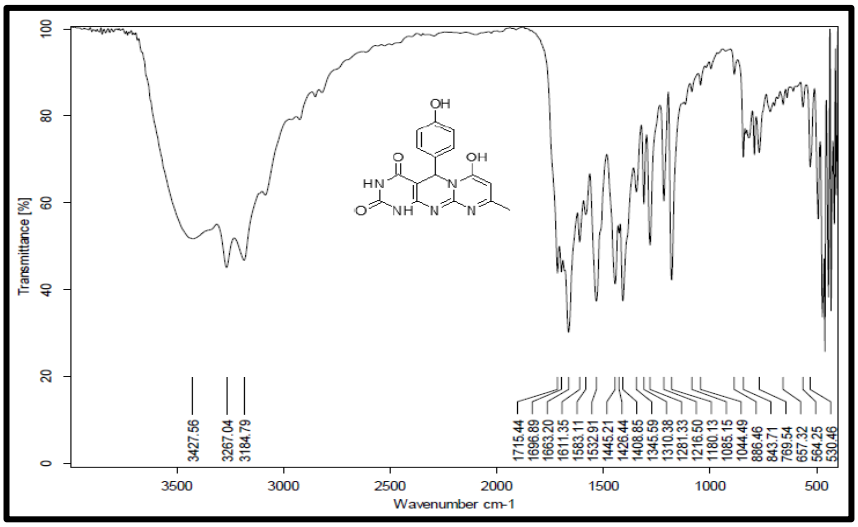

FTIR spectrum of compound 4a

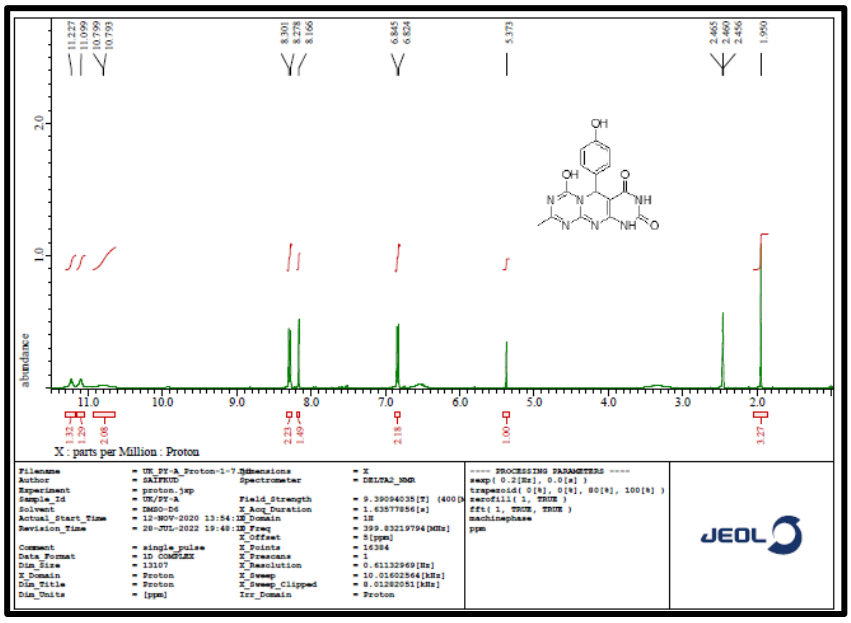

^{1}H-NMR spectrum of compound 4a

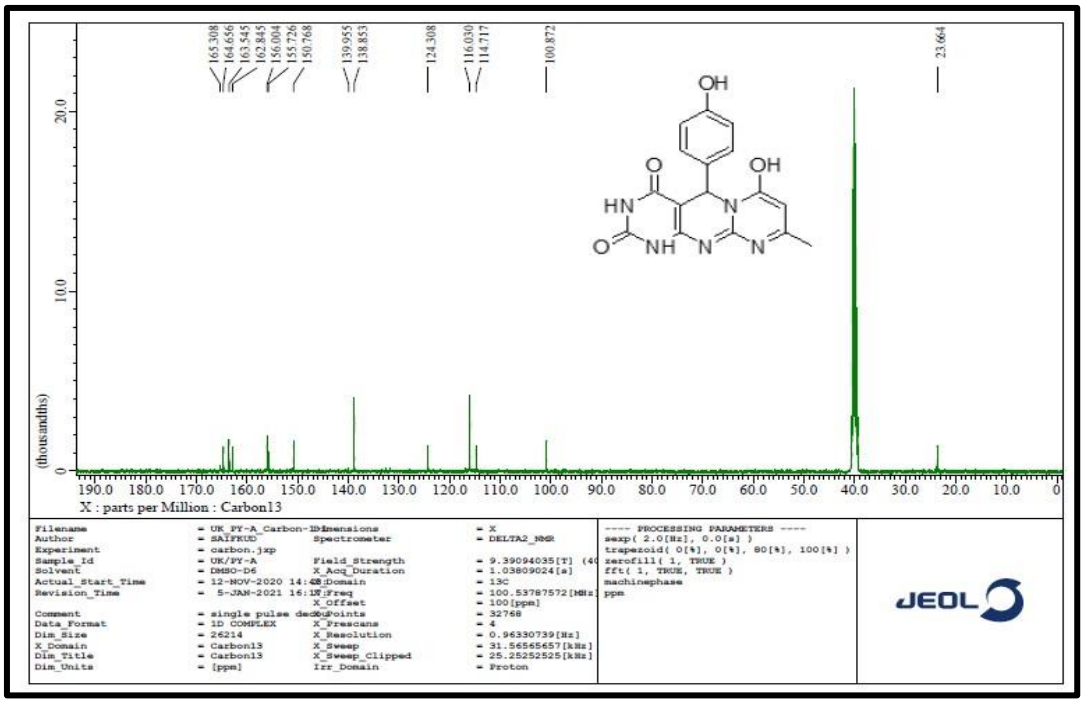

^{13}C-NMR spectrum of compound 4a

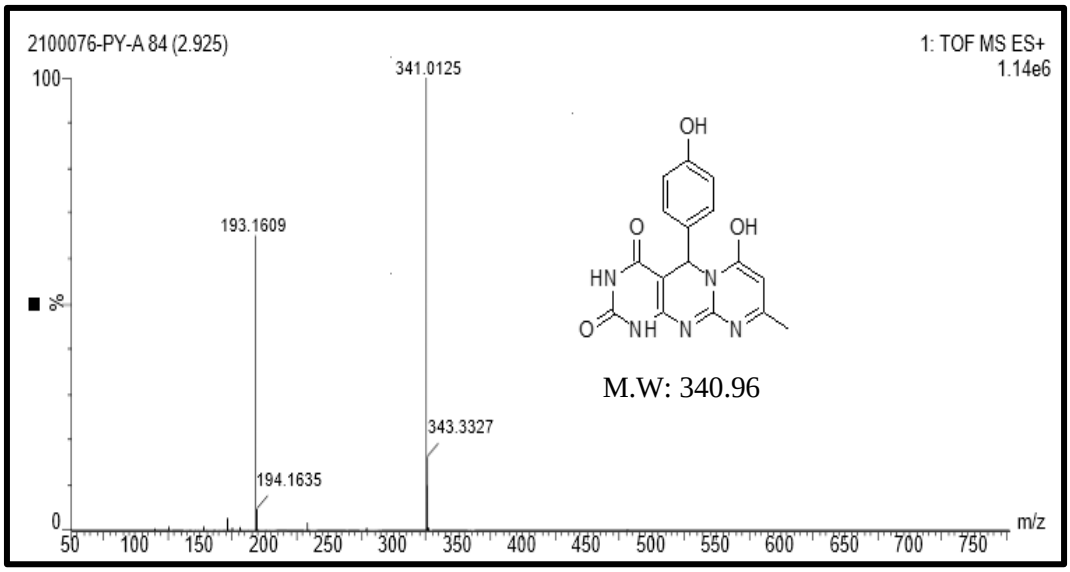

MASS spectrum of compound 4a

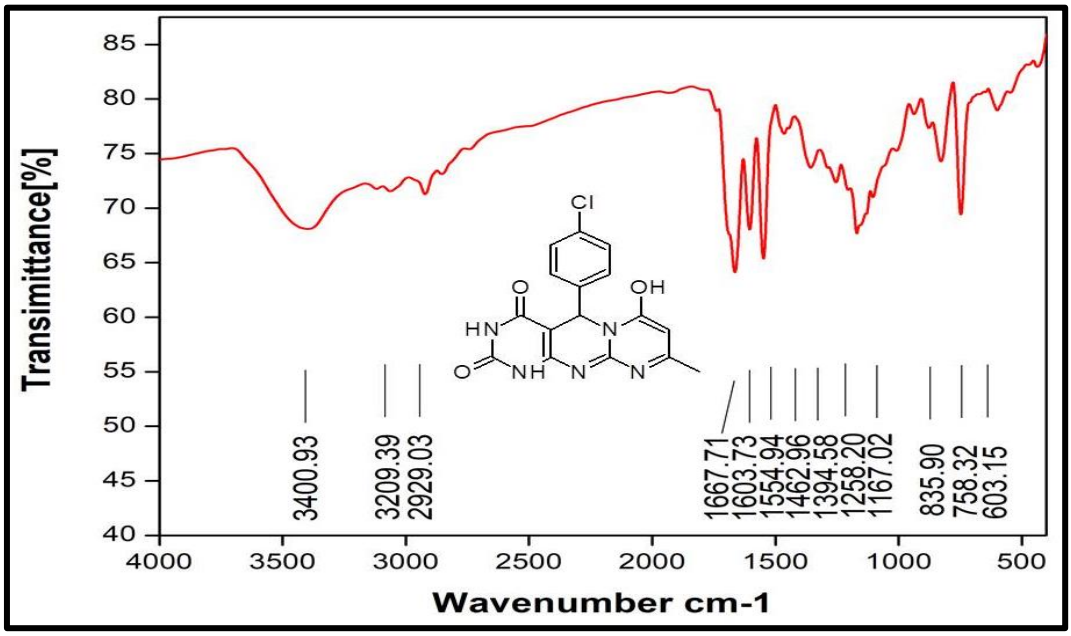

FTIR spectrum of compound 4b

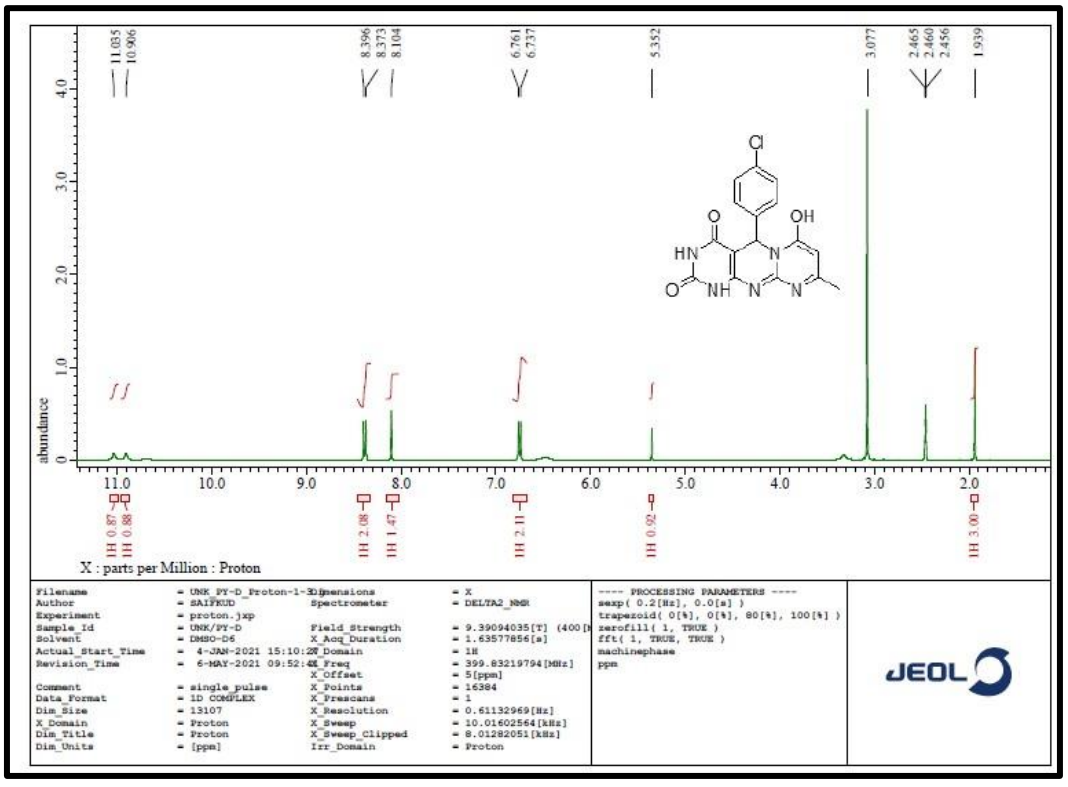

^{1}H-NMR spectrum of compound 4b

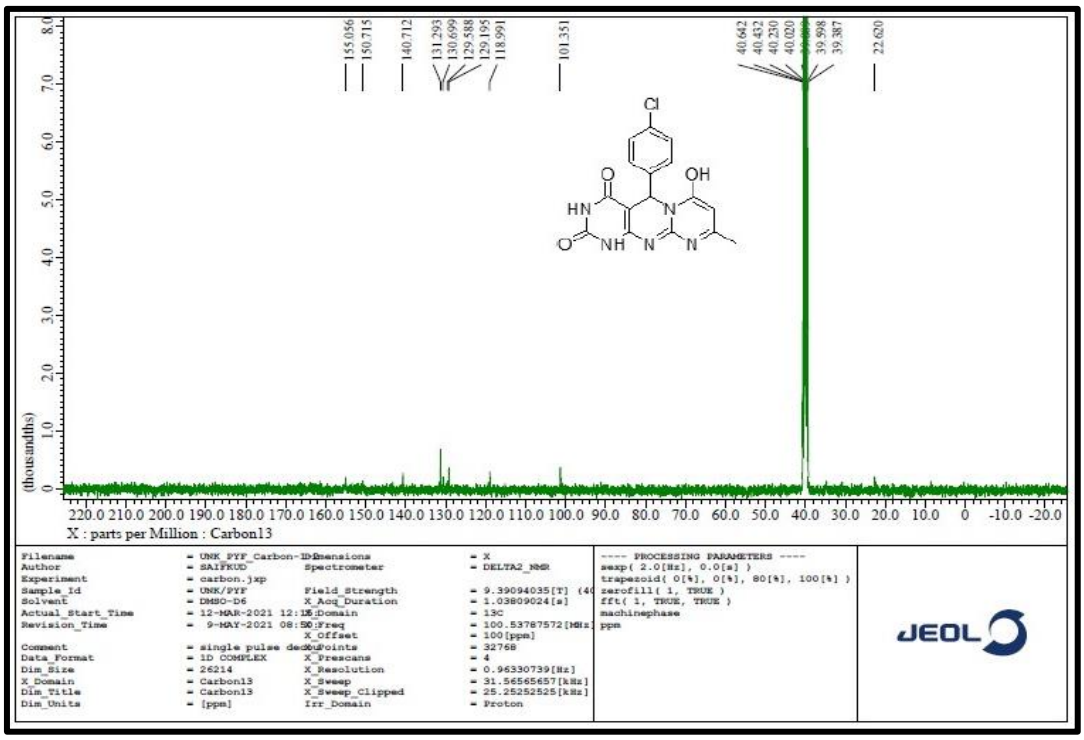

^{13}C-NMR spectrum of compound 4b

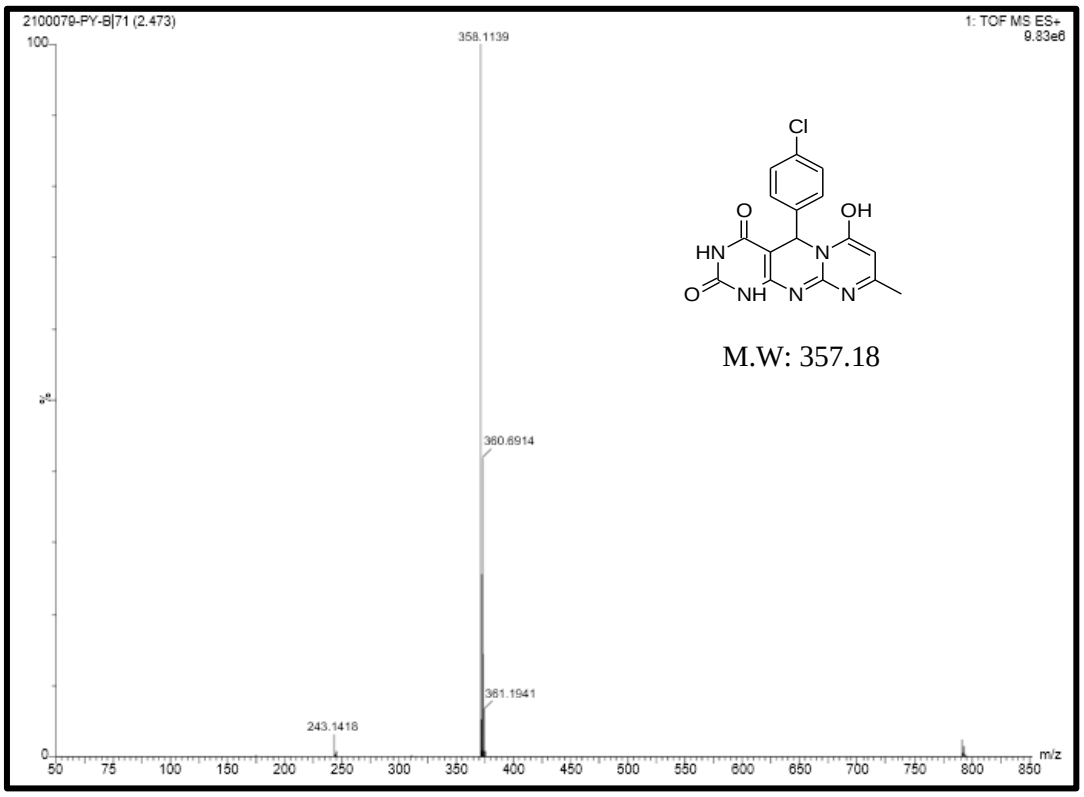

MASS spectrum of compound 4b

2A.4 Experimental.

2A.4.1 General Information.

The chemicals and reagents were brought form Sigma Aldrich company and used without any further purifications. Analytical thin-layer chromatography was used with E. Merck silica gel GF254 glass plates, to check the progress of reaction mixture. 254 UV-light chambers were used for visualization of developed chromatogram. Melting points were determined using Shimadzu DS-50 thermal analyzer and are uncorrected. FTIR spectra were recorded using KBr pellets on Bruker analytical. The ^{1}H-NMR and (400 MHz) and ^{13}C-NMR (100 MHz) spectrum were recorded on Jeol delta 5.3.1 instrument using DMSO-d_6 solvent and data were measured in chemical shift δ ppm with TMS as internal standard. The molecular weight of compounds was recorded from Shimsdzu, 2010A High-Resolution mass spectrometry. Absorption spectra was recorded by UV-Visible spectrophotometer (USB-4000, Ocean optics, USA) and the emission spectra was recorded by Shimadzu RF-5301 PC spectrophotometer. The electrochemical studies were done in Cyclic Voltammograms (CHI66OD) potentiostat CH instrument using Pt wire as a counter electrode, non-aqueous Ag/AgCl as reference electrode and Glassy Carbon paste as a working electrode in 1 M KOH solution as electrolyte. Geometrical optimized structure, FMOs, quantum parameters, UV-Visible, FTIR and COSMO-RS values were estimated theoretically in Gaussian 09 program at the gaseous phase. A photocatalytic experiment was carried out for the degradation of the malachite green (MG) dye compound using a UV-Vis spectrophotometer. Latent Fingerprint application was carried out by powder dusting method using synthesized compounds **4(a-d)** on the different substrates (Knife, steel coin and mobile phone) and pictures were photographed under UV light.

2A.4.2 General Procedure for the synthesis of 7-hydroxy-5-(4-substitutedphenyl)-9-methyl-1,5-dihydro-2*H*-dipyrimido[*1,2-a:4',5'-d*]pyrimidine-2,4(3*H*)-dione derivatives 4(a-d):

Equimolar quantity of 2-amino-4-hydroxy-6-methyl pyrimidine (**1**, 1 mmol) barbituric acid (**2**, 1 mmol) and different aromatic aldehydes (**3**, 1 mmol) in the presence 20 mL distilled ethanol using 10 mol % L-Proline as a catalyst. The reaction mixture was refluxed with constant stirring for about 8 h and reaction progress was monitored by TLC (Ethyl acetate and Petroleum ether). After the completion of the reaction mixture was cooled to room temperature and poured into the 100 mL flake ice with vigorous stirring to get solid coloured precipitated. The crude mixture was filtered, washed and recrystallized with hot ethanol to afford pure solid products **4(a-d)** (**Scheme 1**).

7-Hydroxy-5-(4-hydroxyphenyl)-9-methyl-1,5-dihydro-2H-dipyrimido[1,2-a:4',5'-d] pyrimidine-2,4(3H)-dione derivatives (4a):

Reddish orange solid; Yield: 84 %; MP: 235-238 ^{o}C; Mol. Formula: $C_{15}H_{12}N_5O_5$; FTIR (υ, cm^{-1}): 3427 (OH), 3267 (NH), 3185 (CH), 1663 (C=O), 1611 (C=N); ^{1}H-NMR (δ ppm): 11.22 (s, 1H, NH), 11.09 (s, 1H, NH), 10.77 (s, 2H, OH), 8.30-8.28 (d, *J* = 8 Hz, 2H, Ar-H), 8.16 (s, 1H, Ar-H), 6.84-6.82 (d, *J* = 8 Hz, 2H, Ar-H), 5.73 (s, 1H, CH) and 1.95 (s, 3H, CH_3); ^{13}C-NMR (δ ppm): 165.30, 164.65, 163.54, 162.84, 156.00, 155.72, 150.76, 139.99, 138.85, 124.30, 116.03, 114.71, 100.87, 23.66; HRMS: (m/z): 341.0125 [M^{+}1]; Anal. Calcd for C 56.64, H 3.86 and N 20.64 %; Found: C 55.25, H 3.75 and N 18.97 %.

7-Hydroxy-5-(4-chlorophenyl)-9-methyl-1,5-dihydro-2H-dipyrimido[1,2-a:4',5'-d] pyrimidine-2,4(3H)-dione derivatives (4b):

Pale yellow solid; Yield: 85 %; MP: 230-235 ^{o}C; Mol. Formula: $C_{16}H_{12}ClN_5O_3$, FTIR (υ, cm^{-1}): 3400 (OH), 3209 (NH), 2929 (CH), 1668 (C=O), 1554 (C=N), 758 (C-Cl); ^{1}H-NMR (δ ppm): 11.03 (s, 1H, NH), 10.90 (s, 1H, NH), 8.39-8.37 (d, *J* = 8, Hz, 2H, Ar-H), 8.10 (s, 1H, Ar-H), 6.76-6.73 (d, *J* = 9.6 Hz, 2H, Ar-H), 5.35 (s, 1H, CH), 1.93 (s, 3H, CH_3); ^{13}C-NMR (δ ppm): 165.19, 164.23, 155.05, 150.71, 140.71, 131.29, 130.69, 129.58, 129.19,118.99, 101.35, 22.62; HRMS (m/z): 358.1139 [M^{+}1], [M^{+}3] 361.1941; Anal. calcd for C 53.73, H 3.38, N 19.58 %; Found: C 53.55, H 3.20, N 19.48 %.

7-Hydroxy-5-(4-hydroxy-3-methoxyphenyl)-9-methyl-1,5-dihydro-2H-dipyrimido[1,2-a:4',5 '-d]pyrimidine-2,4(3H)-dione derivatives (4c):

Pale yellow solid; Yield: 87%; MP: 237-239 ^{o}C; Mol. Formula: $C_{17}H_{15}N_5O_5$; FTIR (υ, cm^{-1}): 3355 (OH), 3176 (NH), 2952 (Ar-OCH_3), 2849 (CH), 1661 (C=O), 1555 (C=N); ^{1}H-NMR (δ ppm): 11.24 (s, 1H, NH), 11.11 (s, 1H, NH), 9.97 (s, 1H, OH), 8.44-8.43 (d, *J* = 8, Hz, 2H, Ar-H), 8.18 (s, 1H, Ar-H), 7.77-7.75 (d, *J* = 8 Hz, 1H, Ar-H), 5.391 (s, 1H, CH), 3.78 (s, 3H, OCH_3), 1.96 (s, 3H, CH_3); ^{13}C-NMR (δ ppm): 164.72, 164.53, 156.40, 155.67, 153.59, 147.454, 133.09, 124.70, 118.46, 115.83, 114.49, 100.97, 55.99, 23.34; HRMS (m/z): 369.9939 [M^{+}1]; Anal. calcd for C 55.28, H 4.09 and N 18.96 %, Found: C 55.12, H 4.00 and N 18.72 %.

7-Hydroxy-5-(4-bromophenyl)-9-methyl-1,5-dihydro-2H-dipyrimido[1,2-a:4',5'-d]pyrimidine-2,4(3H)-dione derivatives (4d):

Red solid; Yield: 85 %; MP: 230-232 ^{o}C; Mol. Formula: $C_{16}H_{12}BrN_5O_3$; FTIR (υ, cm^{-1}): 3550 (OH), 3282 (NH), 3157 (-CH), 1675 (C=O), 678 (C-Br); ^{1}H-NMR (δ ppm): 11.03 (s, 1H, NH), 10.90 (s, 1H, NH), 8.39-8.37 (d, *J* = 8, Hz, 2H, Ar-H), 8.10 (s, 1H, Ar-H), 6.76-6.73 (d, *J* = 9.6 Hz, 2H, Ar-H), 5.35 (s, 1H, CH) 1.93 (s, 3H, CH_3); ^{13}C-NMR (δ ppm): 165.25, 163.27, 155.98, 155.87, 154.65, 150.85, 139.61, 120.48, 111.71, 110.02, 100.35, 23.92; HRMS (m/z): 401.9598 [M^{+}1], 402.9841 [M^{+}2]; Anal. calcd for C 47.78, H 3.01, N 17.41 %, Found: C 47.69, H 2.99, N 17.39 %.

2A.4.3 Preparation of Carbon paste electrode.

The Carbon electrode paste was chosen as the working electrode and is prepared by mixing 75 % of the graphite powder and 10 % of silicone oil added (20 °C, 0.98-1.0 g/mL and 370-500 mP as viscosity) with a mass ratio of 15:70:15. Then it was manually mixed in a mortar for about 25 minutes to enhance the mechanical strength of the electrode. The well-grinded mixture was pasted into a homemade Teflon cavity (0.3 mm of surface area) tube and then the surface was smoothed, pressing gently on weighing paper to ensure better electrical contact [34].

2A.4.4 Electrochemical studies.

Electrochemical studies were analyzed in CH Potentiostat CHI604D electrochemical workstation using three-electrode systems by increasing the scan rate (10 mVs^{-1} to 50 mVs^{-1}). The electrochemical cell was constructed with an electrode of Ag/AgCl (reference), Glassy carbon paste (Working) and Pt wire (Counter) in 1M KOH aqueous electrolyte solution [35]. Further, redox onset potential was determined to calculate the energy molecules (HOMO-LUMO).

2A.4.5 Computational study.

Optimized structure and FMOs have been estimated using the Gaussian 09 program and Gauss View 6.0.16 graphical interference. Quantum chemical parameters were calculated using a gaseous phase in density functional theory (DFT) with the help of the (DFT)/B3LYP method using a 6-311++ G (d, p) basis set [36].

2A.4.6 Photocatalytic activity.

UV-Vis spectrophotometer (Shimadzu's model 2600) was used to carry out the photocatalytic activity. Malachite green dye was chosen as the dye model and the 20 ppm of 250 mL aqueous dye solution was prepared followed by the addition of 60 mg of synthesized compounds as a catalyst. The mixture was stirred in a glass reactor at a dark condition before irradiation of light, for every 15 min, the UV-light was irradiated in open-air conditions and was recorded in UV-Vis range of 200-800 range [37].

2A.4.7 Latent fingerprints.

The powder dusting method was used for the development and visualization of the LFPs using synthesized compounds **4(a-d)**. A bear single hand was washed with sopy water and cleaned with deioniszed water, further, it was pressed with sweat pores on the selected porous/non-porous surface materials. Pressed fingerprint was developed by an ostrich feather fingerprint brush, further developed LFPs were photographed with the help mobile camera under normal light and 264 nm UV-light [38].

2A.5 Results and discussion.

2A.5.1 Absorption properties.

Absorption study have been carried out in different solvents at the concentration of 6×10^{-6} M using a UV-Visible spectrophotometer. **Fig. 2A.1a**, displays all the compounds have shown strong absorption bands at ~350-500 nm due to the π-π* and n-π* electronic transitions and aromatic conjugation, and also influenced by the electron-donating and withdrawing groups [39, 40]. Compound **4a** shows the dual absorbance peaks in DMSO solvent at visible region 383 nm and 469 nm due to the influence of two hydroxyl groups as an electron-donating group and high polarity of the solvent. Similarly, compound **4b** observed a dual absorption band appeared at redshift at 297 nm and 404 nm in DMSO, 295 nm and 376 nm in acetonitrile, 299 nm and 405 nm in methanol and 389 nm in acetone. While compounds **4a** and **4c** were shown redshifts due to being influenced by the hydroxyl on the pyrimidine ring and methoxy group on the phenyl ring [41]. These compounds **4(a-d)** have a higher molar extinction coefficient due to the extent of conjugation of phenyl rings.

Further, the theoretical absorption properties of synthesized compounds were analyzed and correlated with the time-dependent density functional theory (TD-DFT) method at the gaseous phase [42]. From the **Fig. 2A.1b**, compounds **4a** and **4c** showed three absorption bands at 316 nm, 328 nm, 383 nm and 317 nm, 341 nm and 384 nm respectively. Compound **4b** exhibited a peak at 328 nm, and 383 nm and **4d** showed only a single absorption band at 383 nm. From theoretical studies, all bands are observed at a bathochromic shift, while in the solvent system compounds observed dual absorption bands with higher intensity. The experimental and

theoretical absorption spectral data has been summarized in **Table 2A.1** and the optical band gap was calculated using equation (1) [43].

$$Eg = 1240/\lambda_{onset}\ \text{eV} \qquad \text{— (1)}$$

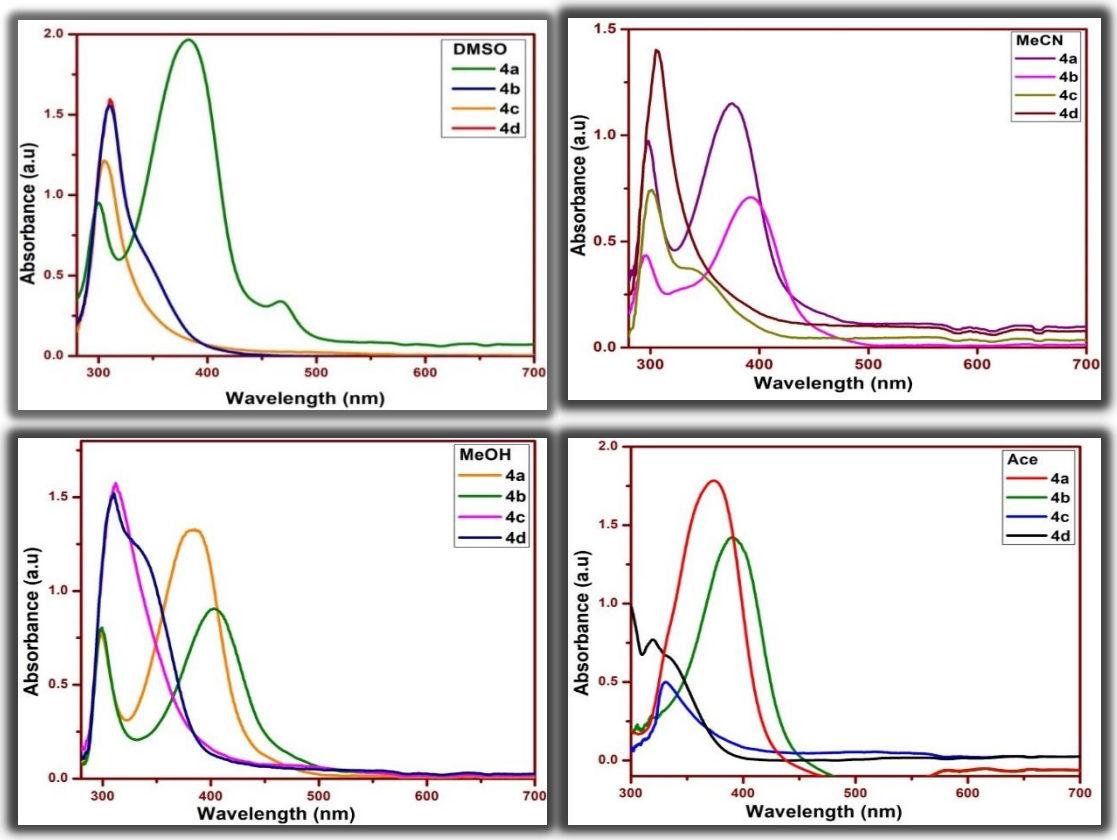

Fig.2A.1 a) Electronic absorption graphs of synthesized compounds **4(a-d)** in different solvents.

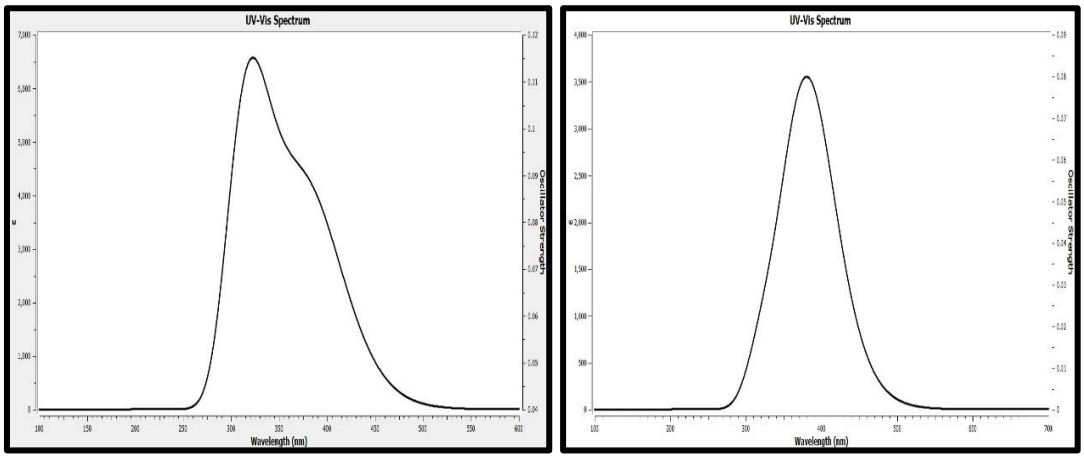

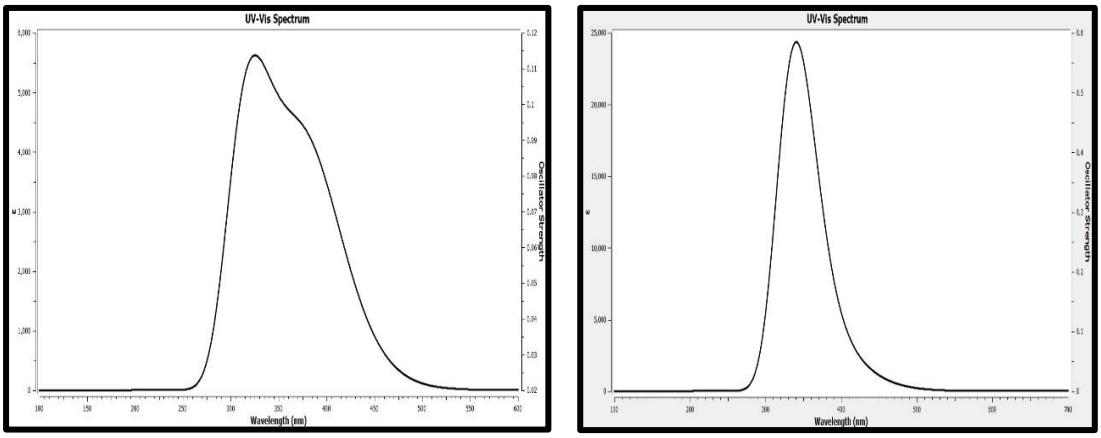

Fig.2A.1 b) Electronic absorption graphs of synthesized compounds **4**(**a-d**) estimated from theoretically, TD-DFT B3LYP method using 6- 311G (++, d, p) basis set at gaseous phase.

Table 2A.1. Experimental and theoretical absorption spectral data of synthesized compounds **4**(**a-d**).

Solvents	**Entry**	**Experimental** λ_{abs} **(nm)**	E_g^{OTP}**(eV)**	**Theoretical** λ_{abs} **(nm)**	E_g^{OTP}**(eV)**
Acetone	**4a**	374	3.31	317, 328, 383	3.90, 3.80, 3.24
DMSO		384, 469	3.22, 2.64		
Acetonitrile		374	3.31		
MeOH		385	3.22		
Acetone	**4b**	389	3.18	328, 383	3.78, 3.24
DMSO		297, 404	4.17, 3.06		
Acetonitrile		295, 376	4.20, 3.29		
MeOH		299,405	4.14, 3.06		
Acetone	**4c**	332	3.73	317, 341, 384	3.90, 3.64, 3.23
DMSO		307	4.03		
Acetonitrile		301, 331	4.11, 3.74		
MeOH		312	3.97		
Acetone	**4d**	335	3.70	383	3.24
DMSO		311	3.98		
Acetonitrile		306	4.05		
MeOH		334	3.71		

2A.5.2 Emission study.

The emission study of the synthesized compounds **4**(**a-d**) was recorded in DMSO solvent at the concentration of 6×10^{-6} M. The peaks were emitted with the corresponding excitation wavelength and moved towards the longer wavelength at 530 nm and 560 nm for **4a** and **4b** respectively. While compound **4c** has shown dual adsorption bands at 401 nm and 614 nm because of the hydroxyl group present on pyrimidine and phenyl rings as an electron donor and the methoxy group present on the phenyl ring as a withdrawing group. Similarly, compound **4d** has shown a longer emission peak at 622 nm due to the presence of a bromine group on the phenyl ring [44 45]. Emission spectrum have been displayed in **Fig. 2A.2** and values were listed in **Table 2A.2**.

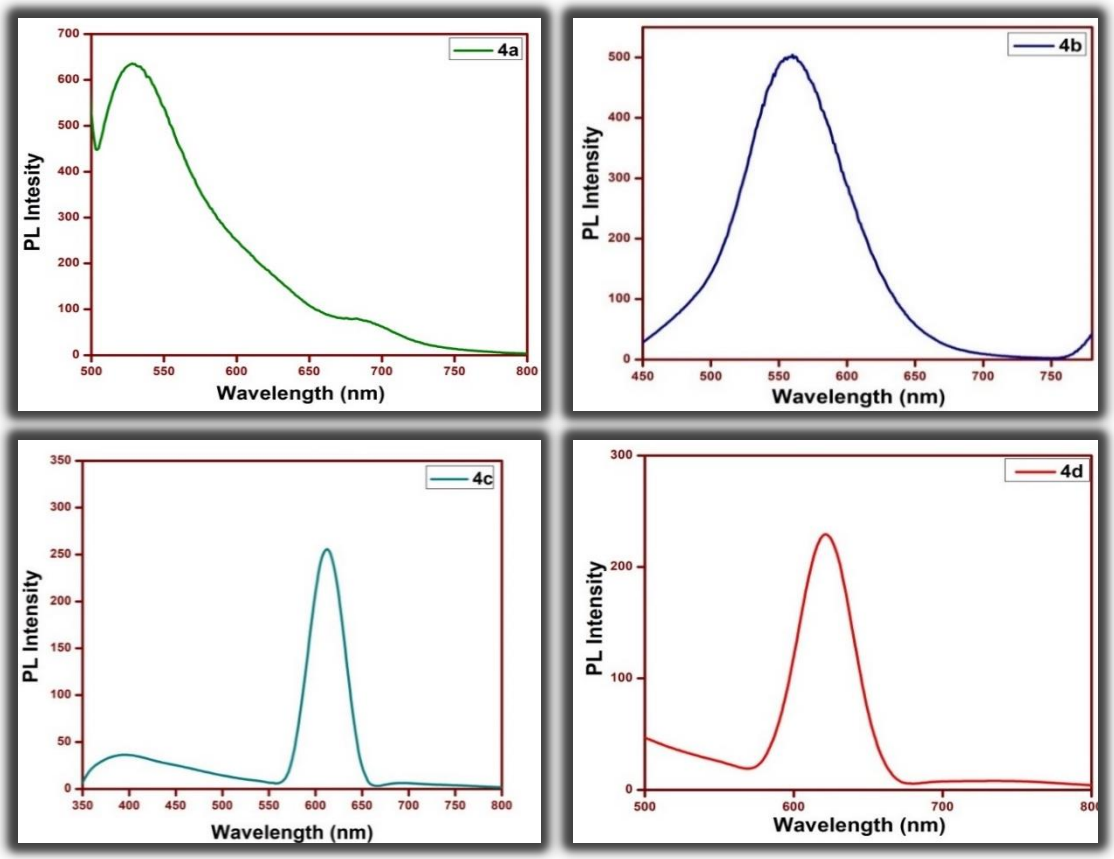

Fig. 2A.2 Emission graphs of synthesized compounds **4**(**a-d**) in DMSO solvent.

Table 2A.2. Emission spectral data of synthesized compounds **4**(**a-d**) in DMSO solvent.

Entry	λ_{exe} (nm)	λ_{emi} (nm)
4a	469	530
4b	404	560
4c	331	461, 614
4d	334	622

2A.5.3 CV study.

The electrochemical study of the synthesized compounds **4**(**a-d**) has been done with three-electrode systems in 1M KOH aqueous electrolyte. **Fig. 2A.3** shows find redox behavior at different scan rates (10 mVs^{-1} to 50 mVs^{-1}) and redox onset potentials have been measured. Compound **4a** has shown one-electron transfer of reversible reduction -0.64 V and quasi-reversible oxidation of -0.29 V, similarly **4b** and **4d** compounds have similar redox behavior that reversibility of reduction and quasi-reversible oxidation and due to the presence of halogen groups (Cl and Br) as electron-withdrawing groups -1.22 V, -0.62 V and -0.34 V, -0.21 V respectively. Further, the **4c** compound has shown reversibility electron transfer of redox potentials at 0.34 V and 0.39 V due to the presence of hydroxyl and methoxy groups on the phenyl ring [46, 47].

From the electrochemical studies, the redox onset potentials were used to calculate the HOMO and LUMO experimentally using equations (2 and 3) [48]. The HOMO of oxidation onset potential ($E_{(oxonset)}$) relates to the ionization potential (IP) and LUMO of reduction onset potential ($E_{(redonset)}$) relates to the electron affinity (EA). The estimated oxidation onset potential is -0.27 V, -0.62 V, 0.39 V, and 0.21V and gives -4.11 eV, -3.78 eV, -4.79 eV, and -4.61 eV of higher HOMO values respectively. Similarly, the quasi-reversible of cathodic reduction onset potential is -0.63 V, -1.2 V, 0.34 V and -0.34 V gives -3.77 eV, -3.20 eV, -4.74 eV and -4.06 eV lower values of LUMO for the compounds **4**(**a-d**). Further, theoretically calculated

energy molecules gives 4.11 eV, 3.78 eV, 4.79 eV, and 4.61 eV of HOMO for oxidation and reduction of LUMO gives the 3.77 eV, 3.20 eV, 4.74 eV and 4.06 eV respectively, for the compounds **4(a-d)** and we found good experimental results on compared to theoretical values [49, 50]. The calculated values have been appended in **Table 2A.3a** and **2A.3b**.

$$E_{(HOMO)} = -[E_{(ox\text{-}onset)} + 4.4]\ eV \qquad \text{— (2)}$$

$$E_{(LUMO)} = -[E_{(red\text{-}onset)} + 4.4]\ eV \qquad \text{— (3)}$$

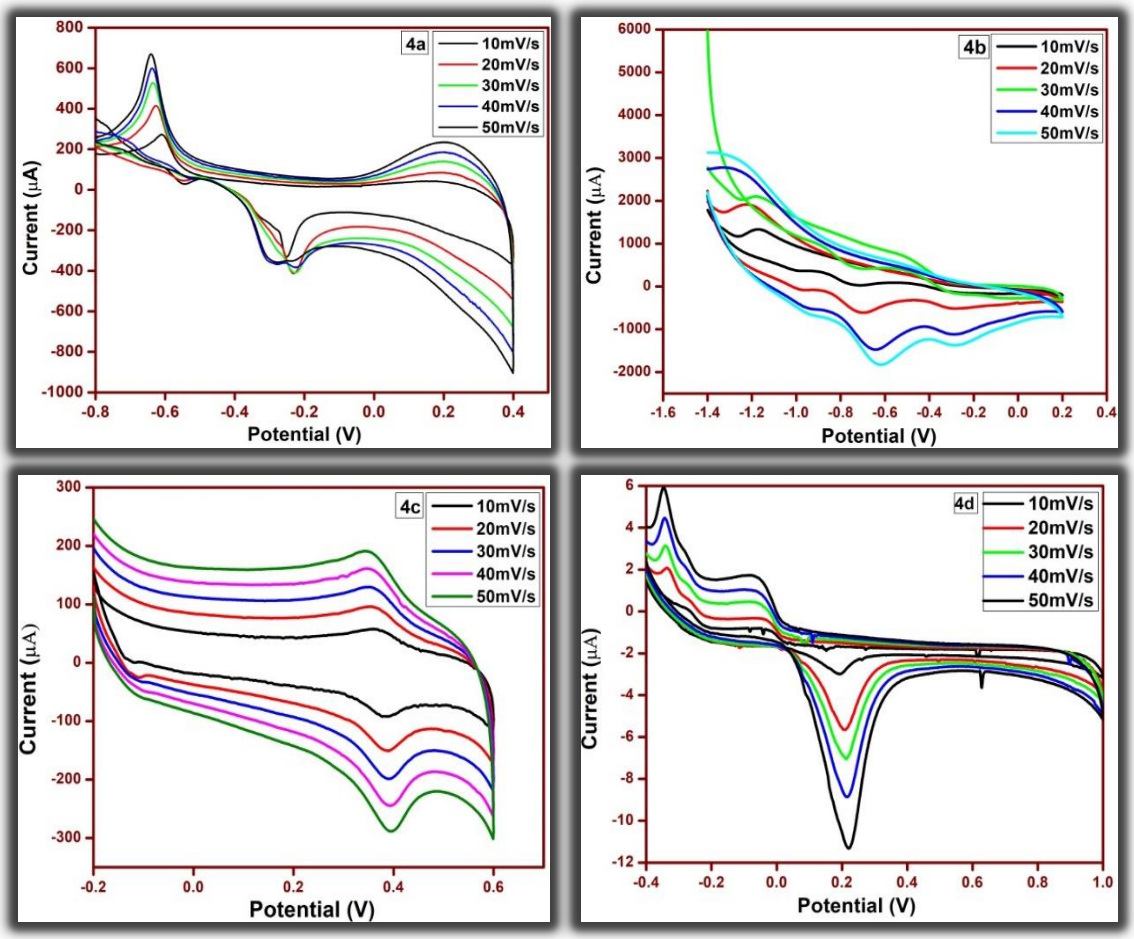

Fig. 2A.3 CV studies of synthesized compounds **4**(**a-d**) at different scan rate in 1M KOH

Table 2A.3a. CV Studies of synthesized compounds **4**(**a-d**).

Entry	E_{Pa} (*V*)	E_{PC} (*V*)	HOMO (*eV*)	LUMO (*eV*)
4a	-0.29	-0.63	-4.11	-3.77
4b	-0.62	-1.2	-3.78	-3.20
4c	0.39	0.34	-4.79	-4.74
4d	0.21	-0.34	-4.61	-4.06

Table 2A.3b. Experimental chemical parameters of synthesized compounds **4**(**a-d**).

Entry	*I* (eV)	*A* (eV)	η (eV)	σ (eV)	χ (eV)	μ (eV)	ω (eV)
4a	4.11	3.77	0.17	5.88	3.94	-3.94	45.65
4b	3.78	3.20	0.29	3.44	3.49	-3.49	20.64
4c	4.79	4.74	0.11	9.09	4.76	-4.76	102.7
4d	4.61	4.06	0.27	3.70	4.73	-4.73	41.43

2A.5.4 DFT.

2A.5.4.1. Frontier Molecular Orbitals (FMOs).

FMOs are the energy of the highest occupied molecular orbital (E_{HOMO}) and the energy of the lowest unoccupied molecular orbital (E_{LUMO}). Optimized structures are shown in **Fig. 2A.4** and **Fig. 2A.5** and both energy molecular orbital are the important parameters which describe the intrinsic and extrinsic properties of the synthesized compounds [51, 52].

To the synthesized compounds **4**(**a-d**), E_{HOMO} is associated with electron-donating ability to the empty orbital and values -0.222 eV, -0.233 eV, -0.219 eV and -0.237 eV respectively, Similarly, E_{LUMO} is commonly known for accepting the excited electron and the values are -0.103 eV, -0.139 eV, -0.078 eV and -0.141 eV, respectively. The reactivity and chemical stability of the compound was determined by the energy gap between E_{LUMO} and E_{HOMO} i.e $\Delta E = E_L - E_H$ [53]. An increase in the energy gap leads to the greater kinetic stability of molecules and chemical reactivity. Similarly, lower energy gap values reveal higher inhibition efficiency, chemical reactivity and biological active molecules [54]. The theoretically calculated energies of HOMO and LUMO values are given in **Table 2A.4**.

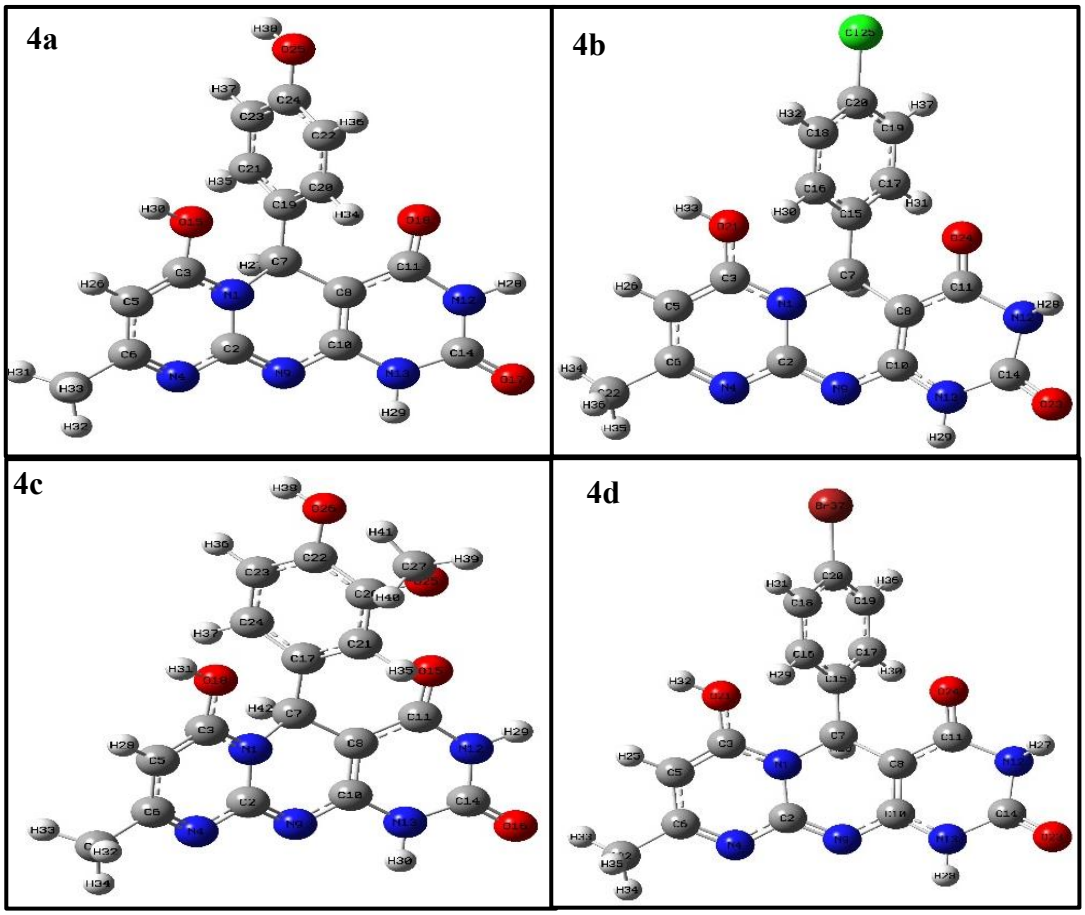

Fig. 2A.4. Optimized structure of synthesized compounds **4(a-d)**.

2A.5.4.2 Quantum chemical parameter.

Koopmans theorem describes ionization potential as directly proportional (IP) to E_{HOMO} and electron affinity (EA) is related to E_{LUMO}. The intrinsic and extrinsic properties were measured from the chemical hardness (higher energy gap) and softness (lower energy gap). The synthesized compounds are the hard molecules that show better intra-molecular charge transfer (ICT) and an increase in chemical reactivity and photostability.

Electronegativity tells the intrinsic properties, Chemical potential is the negative value of the electronegativity and the global electrophilicity index relates acceptance of electron on the metal surface as a corrosion inhibitor and increase in photostability where the synthesized compounds **4(a-d)** show higher electrophilicity

index gives 0.21 eV, 0.32 eV, 0.14 eV and 0.40 eV which increase in photostability. Dipole moment is another important parameter that informs the absorption between the metal surface and the chemical compound. While synthesized compound **4(a-d)** shows greater values 6.86 D, 9.05 D, 8.74 D and 7.62 D respectively, which increase the absorption on the metal surface [55, 56]. The quantum chemical parameters were calculated using the equations (4-8) and values have been appended in **Table-2A.5**.

$$[\eta = 1/2\ (I - A)] \quad \text{— (4)}$$

$$[\sigma = 1/\eta] \quad \text{— (5)}$$

$$[\chi = 1/2\ (I + A)] \quad \text{— (6)}$$

$$[\mu = -\chi] \quad \text{— (7)}$$

$$[\omega = \mu^2/2\eta] \quad \text{— (8)}$$

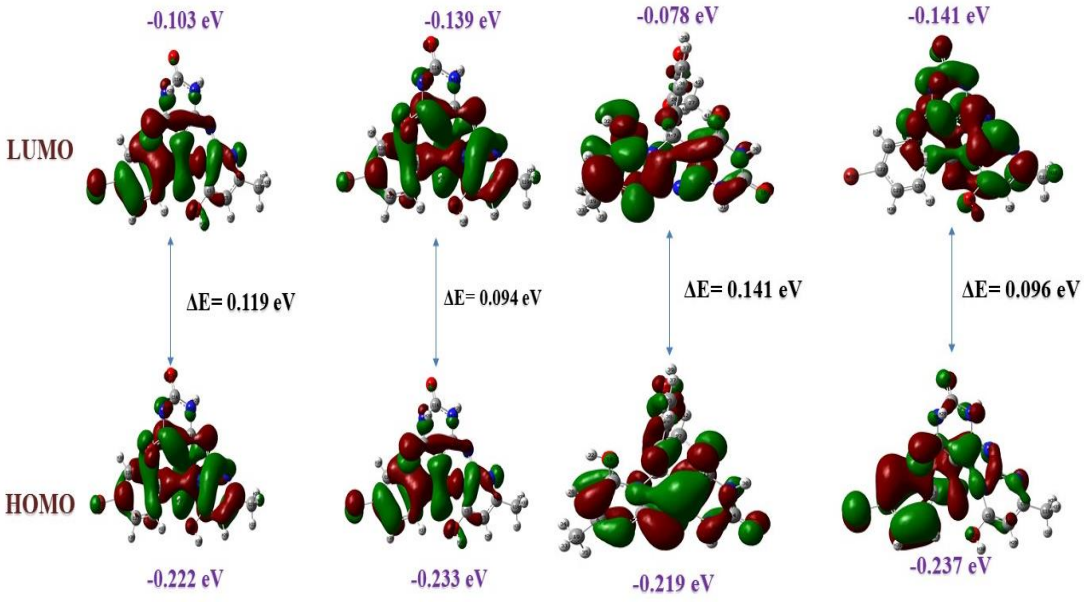

Fig. 2A.5, E_{HOMO}-E_{LUMO} structures of synthesized compounds **4(a-d)**.

Table 2A.4. Frontier molecular orbital's (FMOs) of synthesized compounds **4**(**a-d**).

Entry	E_{HOMO}	E_{LUMO}	ΔE
4a	-0.222	-0.103	0.119
4b	-0.233	-0.139	0.094
4c	-0.219	-0.078	0.141
4d	-0.237	-0.141	0.096

Table 2A.5. Theoretical chemical parameters of synthesized compounds **4**(**a-d**).

Entry	*I* (eV)	*A* (eV)	η (eV)	σ (eV)	χ (eV)	μ (eV)	ω (eV)	*D*
4a	0.22	0.10	0.06	16.6	0.16	-0.16	0.21	6.86
4b	0.23	0.13	0.05	20.0	0.18	-0.18	0.32	9.05
4c	0.29	0.07	0.11	9.09	0.18	-0.18	0.14	8.74
4d	0.23	0.14	0.04	22.2	0.18	-0.18	0.40	7.62

2A.5.4.3. Vibrations Analysis.

FT-IR spectral analysis of 7-hydroxy-5-(4-substituted phenyl)-9-methyl-1,5-dihydro-2*H*-dipyrimido[*1,2-a:4',5'-d*]pyrimidine-2,4(3*H*)-dione derivatives **4**(**a-d**) have been estimated theoretically at gaseous phase using (DFT)/B3LYP method using 6-311++ G(d, p) basis set [57]. Obtained compounds contain 38 atoms that lead to 108 to 120 fundamental vibrations which show the C_1 point group. The estimated theoretical FT-IR spectra were shown in **Fig. 2A.6** and obtained frequencies are appended in **Table 2A.6** with potential energy density (PED).

2A.5.4.3.1 O-H vibration.

The presence of hydroxyl group on the pyrimidine ring in the obtained compounds **4**(**a-d**) shows symmetric stretching frequency at 3823 cm^{-1}, 3824 cm^{-1}, 3826 cm^{-1} and 3820 cm^{-1} theoretically and found experimentally found at 3428 cm^{-1}, 3400 cm^{-1}, 3355 cm^{-1} and 3550 cm^{-1} respectively.

2A.5.4.3.2 N-H vibration.

Amide functionality is observed symmetric vibrations at 3200-3600 cm^{-1} in the IR region. The amide (N-H) group present in pyrimidine ring shows symmetric stretching frequency occurs at 3630 cm^{-1}, 3621 cm^{-1}, 3626 cm^{-1} and 3620 cm^{-1} by theoretically and experimentally found at 3267 cm^{-1}, 3274 cm^{-1}, 3176 cm^{-1} and 3282 cm^{-1} respectivly.

2A.5.4.3.3 C-H vibrations.

Generally, C-H vibration of aromatic compounds shows 3100-2800 cm^{-1}. In the titled compounds, symmetric stretching frequency are observed at 3185 cm^{-1} for compounds **4a**, 3054 cm^{-1}, 2894 cm^{-1} and 3157 cm^{-1} shows symmetric starching frequency of compounds **4b**, **4c** and **4d**. Further, found theoretically at 3213 cm^{-1}, 3204 cm^{-1}, 3213 cm^{-1}, 3212 cm^{-1}, 3203 cm^{-1}, and 3215 cm^{-1}, 3211 cm^{-1}, 3206 cm^{-1} to the synthesized compounds.

2A.5.4.3.4 C=O vibrations.

The carbonyl functional groups present in aromatic compounds have been shown in the region of 1780-1650 cm^{-1}. The predicted theoretical vibrations are 1683 cm^{-1}, 1728 cm^{-1}, 1728 cm^{-1}, 1720 cm^{-1}, and 1687 cm^{-1} for the titled compounds **4**(**a-d**). While we found at 1663 cm^{-1} and 1668 cm^{-1}, for the compounds **4a** and **4b** respectively. Similarly, compounds **4c** and **4d** have found at 1661 cm^{-1}, and 1675 cm^{-1} respectively.

2A.5.4.3.5 C=N vibrations.

After the carbonyl functional groups, the C=N starching frequency was observed at 1630-1590 cm^{-1} of aromatic compounds. Theoretically, compounds **4a** and **4b** have been observed C=N stretching frequency at 1683 cm^{-1} and 1589 cm^{-1} respectively, while **4c** and **4d** were observed at 1590 cm^{-1} and 1588 cm^{-1}. In the

experimental IR spectrum of compounds **4(a-d)** found at 1611 cm^{-1}, 1635 cm^{-1}, 1661 cm^{-1}, respectively and these results are in good agreement with PED calculations.

2A.5.4.3.6 C-Cl and C-Br.

Halogen functional groups showed stretching vibrations at fingerprint regions of the IR spectrum. In the aromatic compound, C-Cl and C-Br show starching vibrations at 850-650 cm^{-1}. The predicted bending vibrations value for C-Cl is 663 $cm^{-1}$and bending vibration for C-Br gives 693 cm^{-1}. In compounds, **4b** and **4d** have shown symmetric bending vibrations at 786 cm^{-1} and 678 cm^{-1} respectively [58-60].

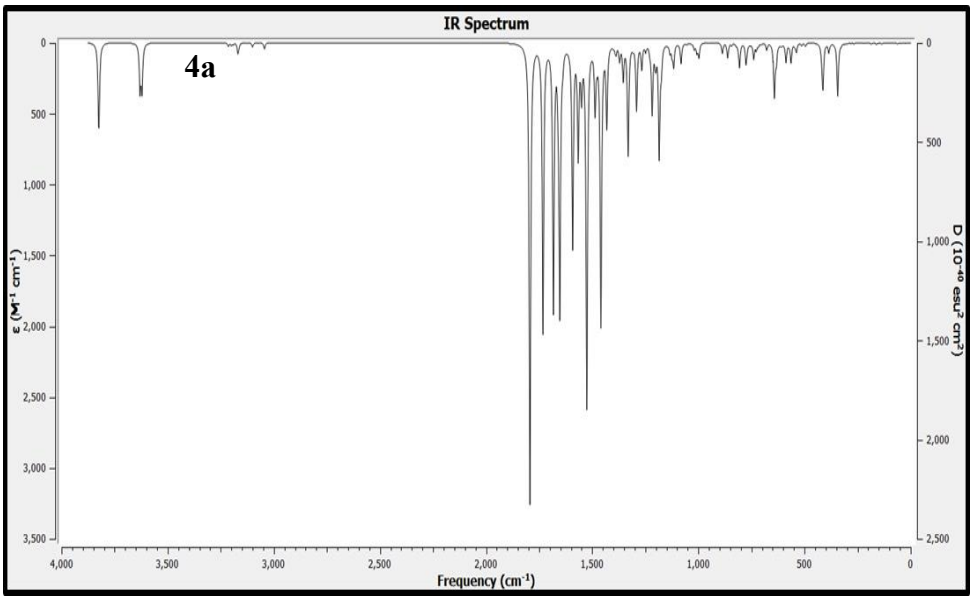

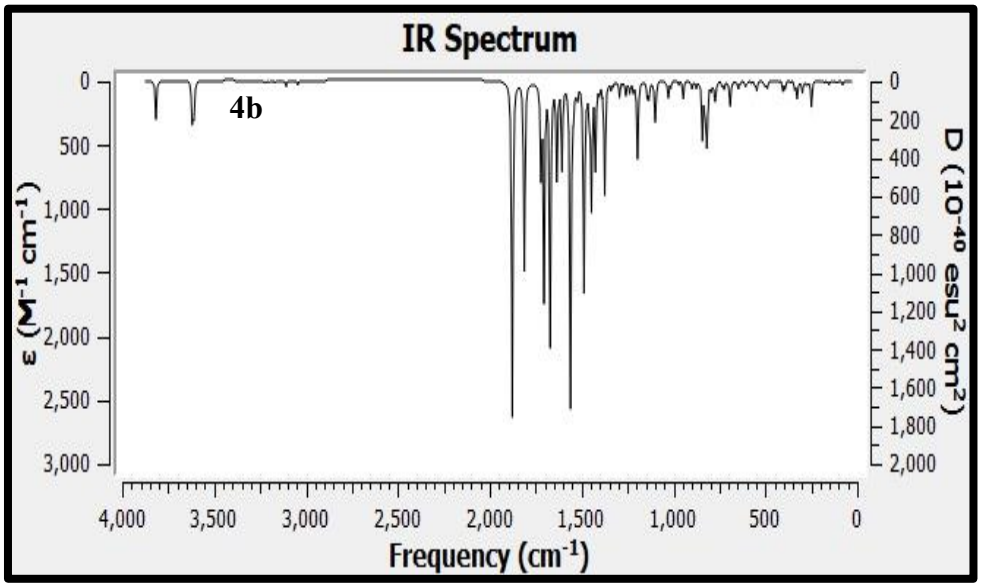

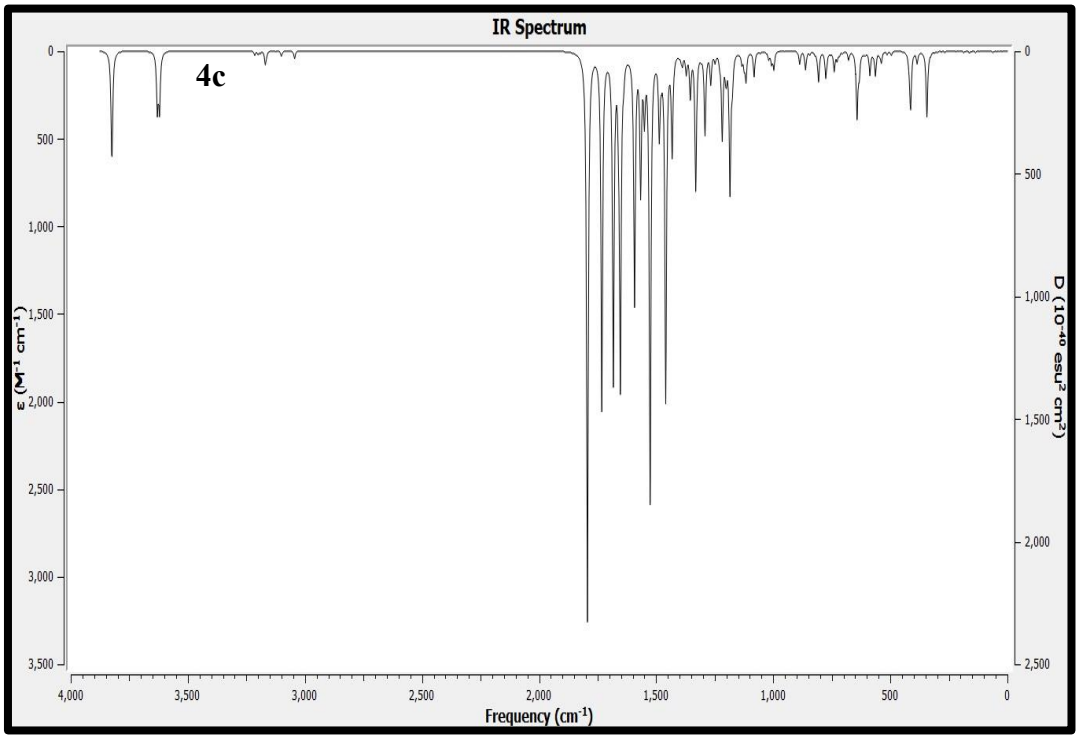

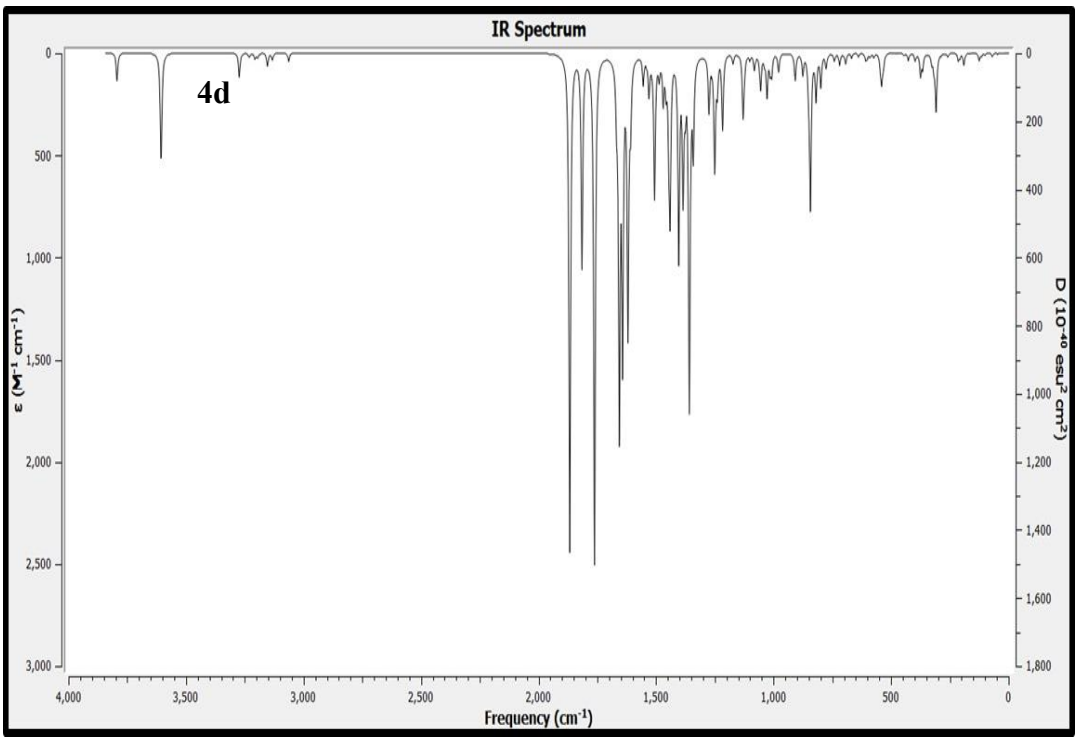

Fig. 2A.6, Theoretical FTIR spectras of synthesized compounds **4(a-d)**.

Table 2A.6. Theoretical vibrational Analysis of the compound **4(a-d)**.

SL. NO	4a	PED Assignment	4b	PED Assignment
1	3825.64	ν OH(99)	3816.77	ν OH(99)
2	3823.55	ν OH(99)	3619.58	ν NH(99)
3	3630.27	ν NH(99)	3609.79	ν NH(99)
4	3621.09	ν NH(99)	3228.23	ν CH(99)
5	3214.91	ν CH(99)	3220.70	ν CH(90)
6	3214.05	ν CH(97)	3213.36	ν CH(97)
7	3199.95	ν CH(97)	3197.49	ν CH(89)
8	3190.04	ν CH(87)	3170.06	ν CH(89)
9	3169.15	ν CH(93)	3121.61	ν CH(87)
10	3164.38	ν CH(89)	3107.66	ν CH(93)
11	3124.63	ν CH(99)	3044.84	ν CH(89)
12	3100.65	ν CH(87)	1877.28	ν OC(72)
13	3044.09	ν CH(93)	1811.83	ν OC(78)
14	1793.60	ν CO(74)	1721.31	ν ON(74)
15	1732.12	ν CO(72)	1704.67	ν NC(86)
16	1683.03	ν CN(78)	1671.17	ν NC(78)
17	1660.68	ν CN(76)	1663.31	ν ON(83)
18	1653.09	ν CC(76)	1635.10	ν NC(89)
19	1639.13	ν CC(78)	1627.01	ν CC(76)
20	1592.42	ν CC(52)	1606.86	ν CC(78)
21	1566.46	ν CC(55)	1560.25	ν CC(84)
22	1550.23	ν CC(59)	1543.99	ν CC(75)
23	1525.85	ν CC(67)	1528.99	ν CC(79)
24	1486.80	ν CC(58)	1521.32	ν CC(93)
25	1486.57	ν CC(60)	1487.02	ν NC(75)
26	1477.28	ν NC(29)	1470.80	ν CC(87)
27	1459.28	ν CC(60)	1457.18	ν NC(83)
28	1431.94	ν NC(57)	1452.79	ν CC(82)
29	1430.82	ν NC(10)	1449.72	ν NC(50)
30	1401.62	ν NC(12)	1446.45	ν OC(58)
31	1393.79	ν NC(12)	1424.66	ν NC(68)
32	1388.02	ν OC(29)	1404.52	ν NC(50)
33	1371.66	ν NC(22)	1386.66	ν NC(78)
34	1354.39	ν CC(62)	1374.09	ν CC(56)
35	1331.12	ν CC(13)	1340.35	ν CC(72)
36	1308.42	ν CC(48)	1327.24	ν NC(74)
37	1291.45	ν NC(22)	1293.95	ν CC(77)
38	1267.09	β CCC(59)	1277.97	ν NC(78)
39	1248.70	β CNC(52)	1259.34	β CCN(56)
40	1228.45	β CCC(47)	1238.63	β CCC(55)
41	1217.89	β NCC(45)	1218.75	β CNC(63)
42	1203.47	β HOC(43)	1206.17	β NCC(58)
43	1200.25	β HOC(45)	1196.00	β HOC(52)
44	1184.74	β HNC(63)	1191.26	β HNC(68)
45	1174.39	β HNC(59)	1143.14	β HNC(59)
46	1134.15	β HCC(75)	1133.73	β HCC(67)
47	1124.55	β HCC(79)	1103.32	β HCC(62)
48	1116.45	β HCC(66)	1099.41	β HCC (58)

49	1081.76	β HCH(64)	1094.84	β HCC (74)
50	1055.15	β HCH(62)	1043.39	β HCC (45)
51	1028.51	β HCC(47)	1027.99	β HCH(48)
52	1019.54	β HCH(56)	1025.59	β HCH(58)
53	1007.36	β HCC(68)	1013.95	β HCH(65)
54	997.52	β HCC(74)	971.24	β OCN(62)
55	974.59	β OCN(64)	946.29	β CCN(87)
56	951.37	β OCN(68)	899.69	β CCC(45)
57	887.37	β NCN(47)	876.39	β NCC(64)
58	862.17	β NCC(47)	842.57	β NCN(58)
59	843.09	β CCC(72)	828.78	β NCN(68)
60	822.31	β CCN(78)	818.89	β CCN(54)
61	812.73	β CCC(48)	814.83	β CCC(78)
62	806.58	β CCN(72)	794.75	β CNO(52)
63	775.90	β CCC(76)	776.33	β CCC(63)
64	770.69	β CNC(70)	773.21	β CNC(78)
65	755.43	β CNC(72)	770.43	β CNC(70)
66	739.80	β CCC(48)	736.64	β CNC(45)
67	728.82	β CNC(71)	733.78	β CCC (64)
68	726.89	β CCO(69)	723.98	β NCN(71)
69	717.09	β NCN(58)	706.12	β OCC (60)
70	704.01	βCNC(60)	694.48	β NCN(72)
71	678.43	β NCN(72)	691.19	β CNC(82)
72	648.23	β OCC(64)	675.22	β CCN(58)
73	642.30	β CCN(56)	661.10	β CCC (54)
74	632.85	τ HOCN(67)	646.42	β CCC (65)
75	613.58	τ HOCC(93)	633.77	β CCCl(79)
76	605.99	τ HNCN(55)	608.56	τ CCNC(82)
77	587.41	τ HNCN(79)	600.78	γ ONNC(55)
78	574.60	τ HCCC(55)	575.93	τ HNCN(68)
79	563.73	τ HCCC(57)	558.96	τ HCCC(67)
80	546.86	τ HCCC(74)	546.48	τ HCCC(72)
81	538.48	τ HCCC(68)	508.81	τ HCCC(82)
82	514.09	τ HCCC(66)	500.52	τ HCCN(65)
83	495.84	τ HCCC(67)	488.89	τ HCCC(68)
84	421.73	τ HCCC(71)	423.23	τ HCCC(58)
85	416.64	τ HCCC(67)	404.22	τ HCCC(54)
86	415.50	τ HCCC(59)	392.59	τ HCCC(59)
87	413.11	τ NCCC(60)	362.82	τ ONCC(57)
88	385.83	τ CCCC(43)	340.04	τ NCCC(85)
89	348.81	τ CNCC(54)	328.71	τ CCCC(54)
90	343.91	τ CCCC(74)	326.76	τ CNCN(65)
91	328.45	τ CCCC(69)	303.85	τ CCCC(68)
92	311.52	τ CNCC(39)	298.36	τ CCCC(58)
93	297.61	τ CNCC(55)	277.39	τ HOCN(54)
94	281.56	τ CNCC(39)	271.32	τ CNCC(45)
95	268.12	τ CCCN(54)	249.58	τ CNCC(58)
96	220.17	τ CNCN(39)	192.44	τ CNCC(47)
97	186.90	τ CNCN(41)	177.37	τ CCCN(49)
98	180.64	τ CCCN(33)	163.45	τ CNCN(42)

99	162.60	τ CNCN(57)	153.42	τ CNCC (44)
100	152.31	τ CNCC(67)	128.70	τ CNCC(97)
101	136.39	γ ONNC(91)	116.08	τ CNCN (68)
102	120.60	γ ONNC(91)	110.41	τ OCON(74)
103	62.13	γ OCCC(75)	103.66	τ HNCN(75)
104	54.44	γ CCNC(57)	81.52	τ HNCN(68)
105	46.25	γ CCNC(52)	78.28	τ CCCC (87)
106	44.32	γ NCNC(51)	62.66	γ ONCC(78)
107	34.81	τ CCCN(48)	56.44	γ NCCC(69)
108	23.29	γ CCCC(75)	35.79	γ CCNC(72)
109			24.30	γ CCCC(85)

SL. NO	4c	PED Assignment	4d	PED Assignment
1	3830.14	ν OH(98)	3793.85	ν OH (99)
2	3826.24	ν OH(98)	3795.85	ν OH (99)
3	3628.79	ν NH(98)	3607.35	ν NH (99)
4	3620.58	ν NH(98)	3605.32	ν NH (99)
5	3216.01	ν CH(98)	3273.59	ν CH(99)
6	3213.02	ν CH(99)	3233.53	ν CH(97)
7	3203.92	ν CH(97)	3229.71	ν CH(98)
8	3166.77	ν CH(99)	3207.20	ν CH(98)
9	3166.54	ν CH(89)	3195.42	ν CH(99)
10	3152.72	ν CH(87)	3183.60	ν CH(97)
11	3118.06	ν CH(93)	3153.68	ν CH(99)
12	3112.69	ν CH(87)	3132.56	ν CH(97)
13	3103.00	ν CH(98)	3063.09	ν CH(95)
14	3046.82	ν CH(98)	1867.29	ν OC (74)
15	3031.21	ν CH(98)	1815.44	ν OC(70)
16	1790.82	ν OC(75)	1761.83	ν NC(60)
17	1725.06	ν OC(76)	1668.09	ν CC (72)
18	1682.12	ν CC(69)	1656.56	ν NC (64)
19	1655.60	ν CC(70)	1642.77	ν NC(63)
20	1653.99	ν CC(71)	1620.03	ν CC(59)
21	1640.30	ν CC(72)	1608.57	ν CC(57)
22	1590.39	ν CC(73)	1554.71	ν NC(40)
23	1564.25	ν CC(74)	1540.68	ν OC(44)
24	1543.77	ν CC(75)	1530.41	ν OC(57)
25	1524.89	ν OC(72)	1518.14	ν CC (62)
26	1504.60	ν CC(78)	1506.53	ν CC(62)
27	1484.96	ν CC(67)	1486.8	ν CC (55)
28	1484.40	ν NC(83)	1469.7	ν OH (99)
29	1479.63	ν NC(98)	1459.51	ν NH (99)
30	1479.36	ν CC(78)	1457.29	ν NH (99)
31	1458.72	ν NC(59)	1445.71	ν CH(99)
32	1452.46	ν NC(62)	1440.39	ν CH(97)
33	1430.45	ν NC(50)	1403.55	ν CH(98)
34	1428.63	ν NC(51)	1385.35	ν CH(98)
35	1396.26	ν NC(52)	1375.58	ν CH(99)
36	1391.61	ν CC(55)	1358.52	ν CH(97)
37	1380.60	ν CC(64)	1341.86	ν CH(99)

38	1360.77	ν CC(61)	1275.02	ν CH(97)
39	1350.33	ν CC(62)	1262.86	ν CH(95)
40	1328.54	ν OC(55)	1250.72	ν OC (74)
41	1310.42	ν NC(27)	1239.62	ν OC(70)
42	1287.88	β CCC(65)	1217.15	ν NC(60)
43	1267.48	β CNC(55)	1172.52	ν CC (72)
44	1258.73	β CNC(49)	1129.86	ν BrC (62)
45	1243.24	β CCC(34)	1124.19	β CCC(65)
46	1227.77	β HOC(46)	1101.7	β CNC(55)
47	1217.97	β HOC(57)	1082.27	β CNC(49)
48	1205.71	β HNC(61)	1075.58	β CCC(34)
49	1192.43	β HNC (63)	1060.09	β HOC(46)
50	1176.08	β HCC(64)	1055.2	β HOC(57)
51	1166.91	β HCC(68)	1038.88	β HNC(61)
52	1166.71	β HCC(55)	1028.16	β HNC (63)
53	1131.01	β HCC(88)	1014.92	β HCC(64)
54	1127.42	β HCH(72)	1008.15	β HCC(68)
55	1115.70	β HCH(47)	978.77	β HCC(55)
56	1087.71	β HCH(69)	910.23	β HCC(88)
57	1049.31	β HCC(68)	907.89	β HCH(72)
58	1043.59	β HCH(67)	875.51	β HCH(47)
59	1019.17	β HCH(71)	851.18	β HCH(69)
60	1006.02	β HCH(67)	843.51	β HCC(68)
61	996.07	βCNC(68)	819.56	β HCH(67)
62	944.39	β NCO(62)	813.8	β HCH(71)
63	942.97	β NCC(56)	799.26	β HCH(67)
64	910.86	β NCN(70)	777.11	βCNC(68)
65	870.77	β CCN(63)	771.15	β NCO(62)
66	827.72	β HNC(45)	741.97	β NCC(56)
67	820.42	β CCC(49)	719.29	β NCN(70)
68	809.12	β CCC(64)	703.93	β CCN(63)
69	780.99	β CCC(78)	693.58	β HBr(45)
70	772.33	β CNC(71)	669.08	β CCC(49)
71	768.14	β CNC(75)	667.61	β CCC(64)
72	751.75	β CCC(68)	639.23	β CCC(78)
73	749.39	β CCO(57)	608.51	β CNC(71)
74	740.73	β NCN(98)	601.68	β CNC(75)
75	723.82	β CCC(87)	590.48	β CCC(68)
76	716.52	β CNC(68)	574.01	β CCO(57)
77	706.81	β OCC(57)	545.1	β NCN(98)
78	680.57	β OCC(54)	540.18	β CCC(87)
79	658.43	β CCN(68)	532.57	β CNC(68)
80	641.45	β COC(64)	477.17	β OCC(57)
81	633.50	β NCC(68)	445.25	β OCC(54)
82	615.68	τ HOCN(66)	427.09	β CCN(68)
83	606.70	τ HOCC(62)	397.83	β COC(64)
84	591.86	τ HNCN(68)	374.7	β NCC(68)
85	588.70	τ HNCN(75)	365.72	τ HOCN(66)
86	567.63	τ HCCC(74)	326.86	τ HOCC(62)
87	549.66	τ HCCC(78)	317.7	τ HNCN(68)

88	547.91	τ HCCC(61)	308.64	τ HNCN(75)
89	528.67	τ HCCC(43)	287.89	τ HCCC(74)
90	501.79	τ HCCC(54)	258.88	τ HCCC(78)
91	487.15	τ HCCC(57)	214.08	τ HCCC(61)
92	453.69	τ HCCC(59)	207.45	τ HCCC(43)
93	417.52	τ HCCC(45)	190.31	τ HCCC(54)
94	413.41	τ HCOC(40)	168.32	τ HCCC(57)
95	392.74	τ HCOC(57)	163.08	τ HCCC(59)
96	360.19	τ HCOC(36)	125.47	τ HCCC(45)
97	345.19	γ CCCC(49)	115.46	τ HCOC(40)
98	341.04	γ CCCC(45)	100.03	τ HCOC(57)
99	325.46	τ CCNC(57)	70.25	τ HCOC(36)
100	313.91	τ CCCC(45)	47.31	γ CCCC(49)
101	302.78	τ CCCC(56)	34.54	γ NCNC(45)
102	284.88	τ CCCC(47)	25.39	τ NNNC(57)
103	276.16	τ CNCC(78)		
104	267.57	τ CNCC(45)		
105	215.25	τ CCNC(45)		
106	192.25	τ CCNC(75)		
107	181.02	τ NCNC(61)		
108	168.65	τ CCNC(49)		
109	162.52	τ CNCN(56)		
110	151.90	τ COCC(58)		
111	144.93	τ NCCC(53)		
112	134.56	γ ONCC(45)		
113	110.70	γ ONNC(48)		
114	73.32	τ CCCN(47)		
115	63.26	γ OCCC (34)		
116	50.78	γ CCNC(85)		
117	41.46	γ OCCC (75)		
118	38.08	γ NCNC(78)		
119	32.31	τ CCNC(72)		
120	16.89	τ CCCN(89)		

ν= Stretching vibration, β= bending vibration, τ= Torson, γ=out of the plane.

2A.5.4.4 COSMO-RS.

Conductor like screening model for real solvent (COSMO-RS) is one of the theoretical approaches to predictions of thermodynamic properties of fluids and liquid mixtures. The values were calculated theoretically using materials studio software, $DMol_3$ calculation in solvation method at triple zeta valance polarized basis set (TVZP) [61-64]. This method describes the electrostatic interactions of synthesized compounds **4**(**a-d**) with the selected solvents and provides screening charge distribution (σ, sigma) of specific polarity on the molecular surface. Sigma (σ) profile

for each selected solvent was given in **Fig. 2A.7** along with the estimated COSMO-RS file of synthesized compounds which helps to predict the hydrogen bond interactions. The centre peak of σ profile is related to the molecule is nonpolar while the peak is far from the centre then the molecule is polar, similarly further peaks have appeared in -0.0084 e/Å^{-2} and +0.0084 e/Å^{-2} are regions of hydrogen bond donor and acceptor molecules. Further, the negative σ value indicates positive screening charges and positive σ values are the negative screening charges [65].

Here, we found noteworthy results, for all the synthesized compounds in selected solvents were observed more polar. Compound **4a** was observed peak at negative charge and presence of functional group will be more polarized than the solvent at 0.010 e/Å^{-2}, 0.012 e.Å^{-2} of hydrogen bond acceptor regions and -0.011 e.Å^{-2} of hydrogen donor regions associated with hydroxyl as amphoteric groups. Similarly, compound **4c** observed dual peaks corresponding to the negative charge density 0.0081 e.Å^{-2}, 0.012 e.Å^{-2} of hydrogen acceptor bonds and more polarized than the solvent used; also, gives screening charge density at -0.011 e.Å^{-2} of hydrogen donor regions and more polarity in acetonitrile solvent than the other solvent. Cation was present in compound **4b** associated with hydroxyl group will be more polar in selected solvent and attractive for strong hydrogen interaction and screening charge density gives the 0.011 e.Å^{-2}, at acceptor hydrogen molecules and -0.012 e.Å^{-2} at donor hydrogen bonds. While compound **4d** has observed dual peaks at 0.081 e.Å^{-2}, 0.012 e.Å^{-2} of hydrogen bond acceptor in selected solvent and the compound will be more polar and increase in a strong interaction of hydrogen bond donor atom [66]. Theoretically, estimated values are added in **Table-2A.7**.

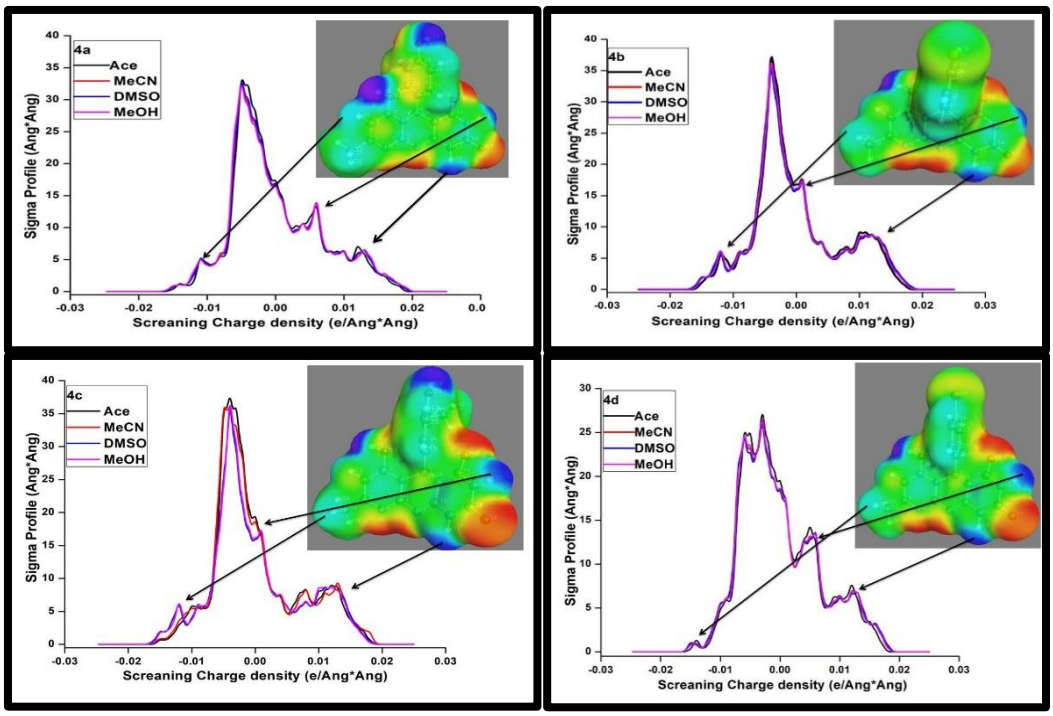

Fig. 2A.7. Sigma profiles for selected solvent using synthesized compounds **4**(**a-d**) estimated in Turbomole software

Table 2A.7. COSMO-RS values of synthesized compounds **4**(**a-d**) in selected solvents.

Solvents	**4a** **pK_a (kcal/mol)**	**4b** **pK_a (kcal/mol)**	**4c** **pK_a (kcal/mol)**	**4d** **pK_a (kcal/mol)**
DMSO	-25.78	-28.07	-29.11	-25.79
MeCN	-26.00	-27.76	-28.79	-25.49
Ace	-24.79	-27.71	-27.54	-24.39
MeOH	-26.31	-27.52	-28.56	-25.27

2A.5.5 Photocatalytic studies.

Catalytic activity was carried out using synthesized compounds **4**(**a-d**) over MG dye compound under the UV light; at triplicate studies (time interval, catalyst load, and variation of pH) [67, 68]. **Fig. 2A.8a** shows the intensity of absorption peaks were decrease continuously when an increase in time interval without changing any position of peaks and absorption was observed at 575 nm. Moreover, the absorbance of dye degradation is proportional to the concentration and at the initial

time being, the dye degradation was found to be very low, hence, the percentage of dye degradation increased with the time interval [69]. The percentage of dye degradation was calculated using equation (9) where C_o and C_t are dye concentrations of initial and final at time interval t [70-72]. An interesting result was found that lower catalytic efficiency was found to **4a** by reaching 65 % and higher catalytic efficiency was found to **4b** and **4c** by reliving 83 % and 87 % under the UV radiation.

$$\% \text{ Degradation} = C_0\text{-}C_t\ /C_0 \times 100 \qquad \text{— (9)}$$

2A.5.5.1 Photodegradation kinetics.

The photodegradation of MG dye compound using synthesized compounds **4**(**a-d**) under UV light irradiation exhibits the first-order reaction pseudo-first-order kinetics model (photodegradation kinetics) as shown in **Fig. 2A.8b**, respectively using equation (10).

$$\ln C_0/C_t = kt \qquad \text{— (10)}$$

Where C_t is the final concentration, C_0 is the initial concentration, t is the time interval and k apparent rate constant [73], the dye degradation rate was decreased with the increases of time. Hence, compounds **4**(**a-d**) are good photocatalysts over the MG in the presence of light. The calculated % of dye degradation rates were summarized in **Table 2A.8**.

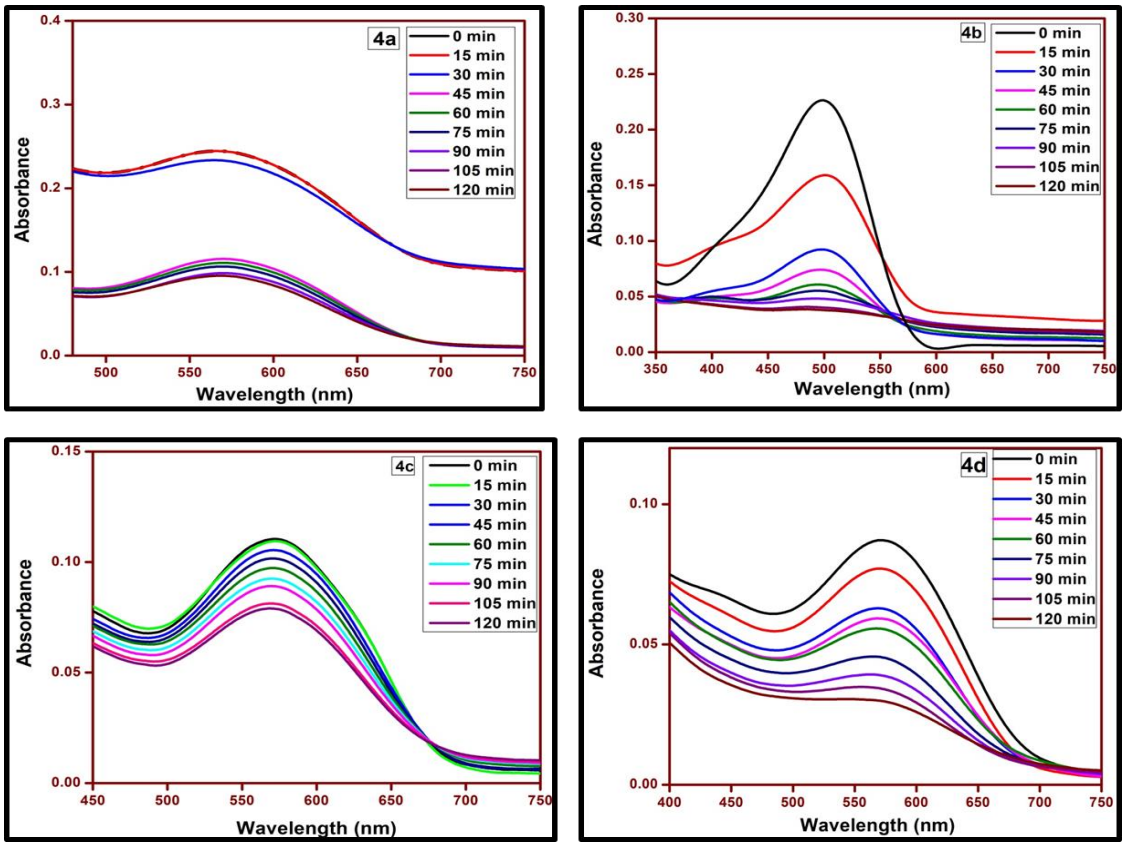

Fig. 2A.8a. UV absorbance spectra of MG dye during degradation using synthesized compounds **4**(**a-d**).

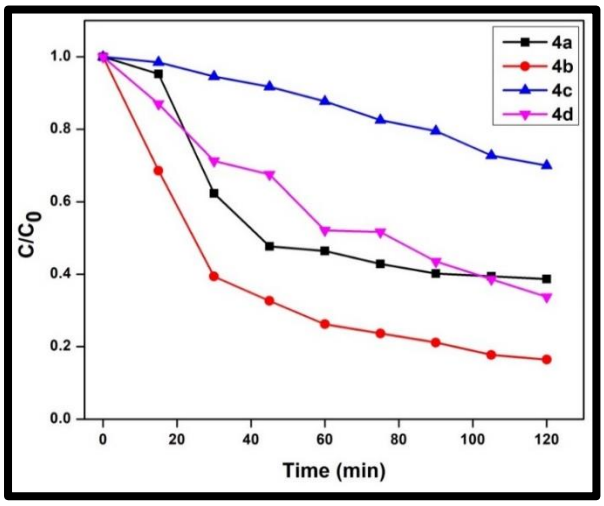

Fig. 2A.8b Kinetics study of dye degradation.

2A.5.5.2. Theoretical approaches of Photocatalytic.

In photocatalytic degradation, hydroxy (OH) groups play vital roles in the formation of hydroxyl and superoxide radicals after the incident of light and oxygen vaccines are also favourable for photocatalytic activity. Dye degradation of organic

dye compounds depends upon the chemical structure, aromatic rings, and presence of chromophores like nitro, hydroxyl and sulphur groups that act as active sites and bind to the malachite green dye compounds. Under UV light, the chromophores are enhancing the light towards the visible region and easily bind the pollutant compound and act as an efficient catalyst by the degradation method following the mechanism that has taken place [74].

$O_2 + e^- \rightarrow O_2^-$

$O_2^- + H^+ \rightarrow HO^\bullet_2$

$HO_2^\bullet + HO_2^\bullet \rightarrow H_2O_2 + O_2$

$H_2O_2 + e^- \rightarrow HO^\bullet + HO^-$

$H_2O_2 + O_2^- \rightarrow HO^\bullet + HO^- + O_2$

$H_2O_2 \rightarrow 2HO^\bullet$

$O_2 + HO^- \rightarrow O_2^- + HO$

Dye + HO → Degradation products

Dye $+h^+_{VB}$ → oxidation products

Dye $+ e^-_{CB}$ → reduction products

2A.5.5.3 Effect of time interval.

The photocatalytic activity was carried out over MG dye with a time interval of 0-120 min for each compound under UV light as shown in **Fig. 2A.9a** Among the synthesized compounds **4b** and **4c** have been found to have better photocatalytic activity by reaching dye degradation at 83 % and 87 % at 120 min. we didn't find any higher dye degradation after 120 min and hence compounds were better to have catalytic effects with respect to time.

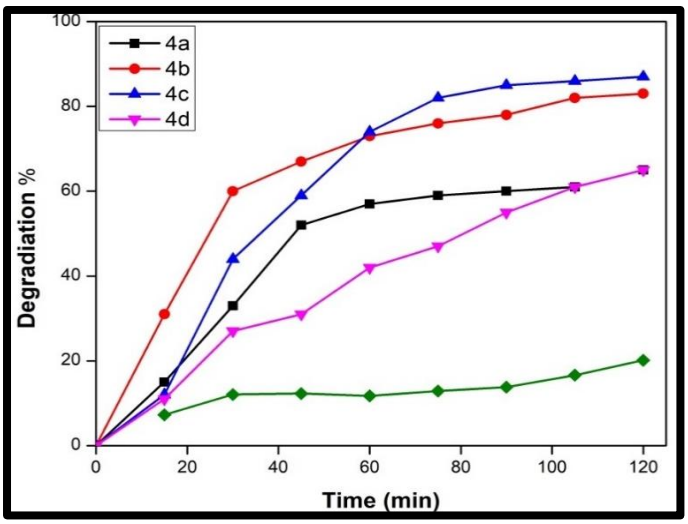

Fig. 2A.9a. Effect of a time interval of using synthesized compounds **4**(**a-d**) over MG dye degradation and error bars represent the standard deviation.

2A.5.5.4 Effect of catalyst.

Catalyst has been assessed over the MG dye compound keeping the dye concentration constant (20 ppm/250 mL aliquots). The catalyst load 40, 50, 60, 70 and 80 mg in 250 mL solution were analyzed as shown in **Fig. 2A.9b**. We observe variation in degradation rates and are increasing when a load of catalyst increases, compound **4b** and **4c** shows higher degradation rates at 85 % and 88 %. Similarly, compounds **4a** and **4d** have shown increased catalytic activity by reaching 68 % and 72 %. As the catalyst load increases, the particle suspension increases which affect by the UV radiations.

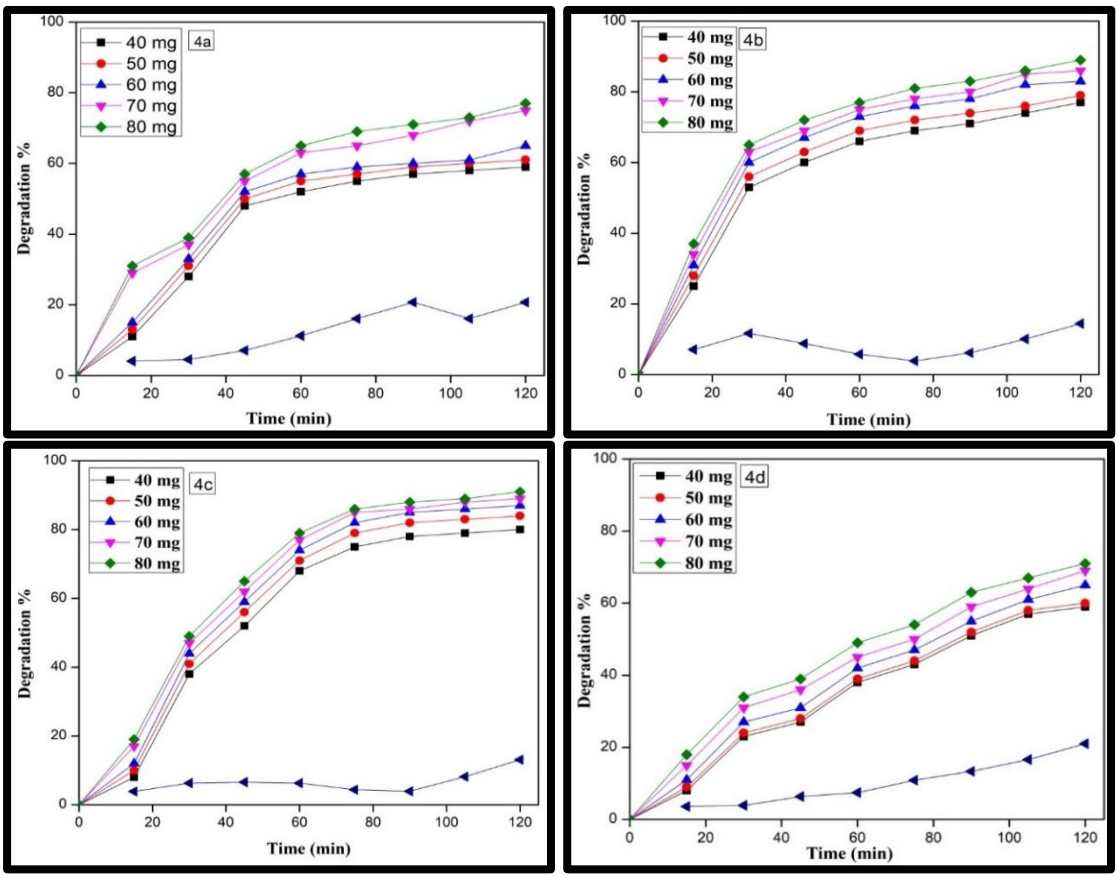

Fig. 2A.9b Graphs of % dye degradation with the effect of Catalyst in irradiation time of synthesized compounds **4**(**a-d**), error bars represent the standard deviation.

2A.5.5.5 Effect of pH.

Here we performed the photocatalytic activity using different pH variables at acidic (5 and 6), neutral (7) and basic (8 and 9) medium. In **Fig. 2A.9c**, we observed at neutral pH-7, the photocatalytic activity was found to be more effective in dye degradation of dye molecules by reaching 85 % and 88 % for **4b** and **4c** compounds. The dye degradation rates were decreasing when an increasing acidic medium, due to the absorption of protonated H^+ ions by the catalyst and as well as organic dye molecules, stays positive. Compounds **4a** and **4d** have shown moderate degradation by reaching 62 % and 64 % rates. The effect of parameters of compound **4c** was summarized in **Table 2A.9** [75-78]. Effects of parameters (pH, catalytic load and time interval) are carried out using compounds over MG dye and compound **4c** has been shown good catalytic activity under the UV light.

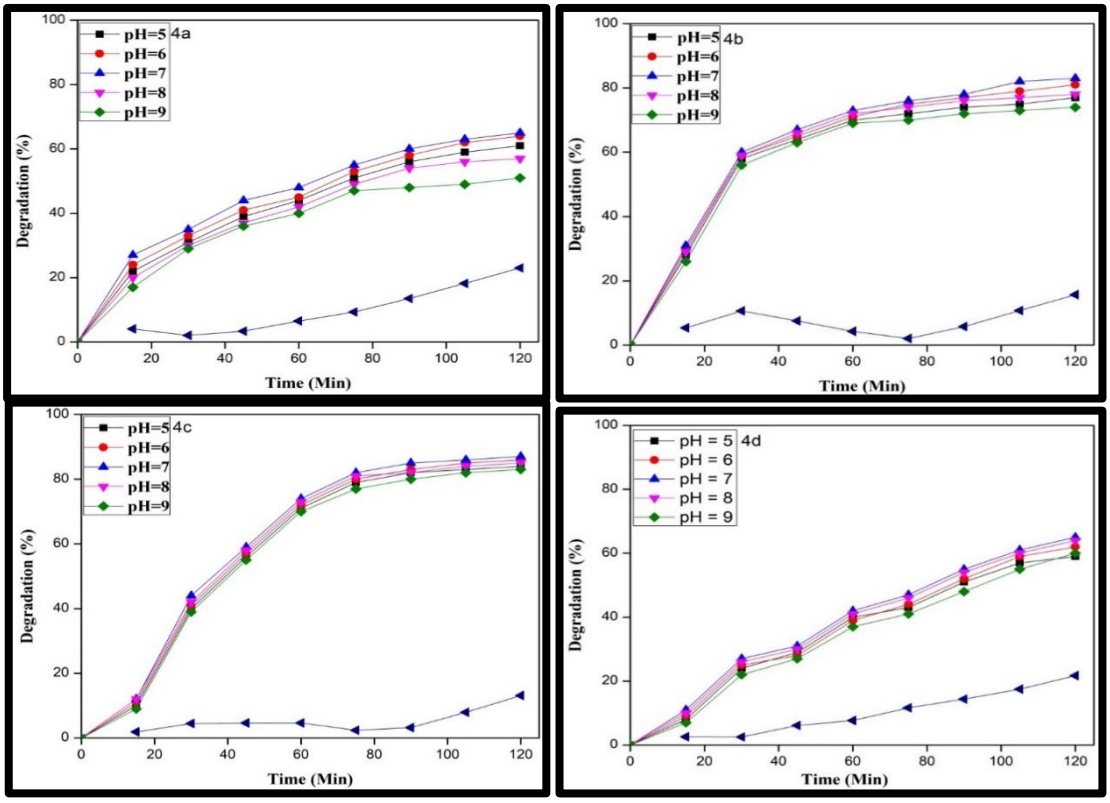

Fig. 2A.9c Graphs of % dye degradation with Effect of pH in irradiation time of synthesized compounds **4**(**a-d**), error bars represent the standard deviation.

Table 2A.8. Photocatalytic studies of synthesized compounds **4**(**a-d**).

A 20 ppm+60 mg synthesized compounds+UV light						
Time	**Entry**	**Concentration**	**C/C_0**	**log C/C_0**	**-log C/C_0**	**% D**
0		0.2452	1	0	0	0
15		0.2337	0.9530	-0.020	0.0200	15
30		0.1528	0.6231	-0.2054	0.2054	33
45		0.1158	0.4772	-0.3212	0.3212	52
60	**4a**	0.1138	0.4641	-0.3333	0.3333	57
75		0.1050	0.4282	-0.3683	0.3683	59
90		0.0986	0.4021	-0.3956	0.3956	60
105		0.0967	0.3943	-0.4017	0.4017	61
120		0.0949	0.3870	-0.4122	0.4122	65
0		0.2323	1	0	0	0
15	**4b**	0.1594	0.6861	-0.1636	0.1636	31
30		0.0915	0.3938	-0.4047	0.4047	60
45		0.0758	0.3263	-0.4863	0.4863	67

60		0.0609	0.2621	-0.5815	0.5815	73
75		0.0550	0.2367	-0.6258	0.6258	76
90		0.0491	0.2113	-0.6751	0.6751	78
105		0.0412	0.1773	-0.7512	0.7512	82
120		0.0382	0.1644	0.7840	0.7840	83
0		0.1113	1	0	0	0
15		0.1096	0.9847	-0.0066	0.0066	12
30		0.1053	0.9460	-0.0241	0.0241	44
45		0.1021	0.9173	-0.0374	0.0374	59
60	**4c**	0.0976	0.8769	-0.0570	0.0570	74
75		0.0919	0.8256	-0.0832	0.0832	82
90		0.0885	0.7951	-0.0995	0.0995	85
105		0.0810	0.7277	-0.1380	0.1380	86
120		0.0779	0.6999	0.1549	0.1549	87
0		0.0885	1	0	0	0
15		0.0770	0.8700	-0.0604	0.0604	11
30		0.0631	0.7129	-0.1469	0.1469	27
45		0.0598	0.6757	-0.1702	0.1702	31
60	**4d**	0.0461	0.5209	-0.2832	0.2832	42
75		0.0457	0.5163	-0.2870	0.2870	47
90		0.0385	0.4350	-0.3615	0.3615	55
105		0.0342	0.3864	-0.4129	0.4129	61
120		0.0299	0.3378	-0.4701	0.4719	65

Table 2A.9 Effect of parameters of synthesized compound **4c** for photocatalytic dye degradation of MG dye.

Effect of Time (in min)	**Degradation (in %)**	**Weight of photocatalyst (in mg)**	**Degradation (in %)**	**Effect of pH**	**Degradation (in %)**
0	0	40	68	5	75
30	44	50	70	6	76
60	74	60	75	7	89
90	85	70	80	8	79
120	87	80	88	9	78

2A.6. Latent Fingerprints (LFPs).

LFPs are one of the primary advance and promising methods used in criminal investigations. The powder dusting method was used to perform the experiment with the synthesized 7-hydroxy-5-(4-substitutedphenyl)-9-methyl-1,5-dihydro-2*H*-dipyrimido[*1,2-a:4',5'-d*]pyrimidine-2,4(3*H*)-dione derivatives **4**(**a-d**) on different substrates such as knife, mobile and steel coin which are collected form laboratory [79] and pictures were photographed under 365 nm UV light and normal light in canon digital camera as arranged in **Fig.2A.10**.

A noteworthy result was found that the compounds **4c** and **4d** developed on the knife and shows good contact on the substrate in UV light, similarly, **4a** and **4b** compounds also showed better contact on steel coin and mobile phone substrates. Here, we observe the powder dusting method was a useful method and compounds were physically and chemically stable in ambient as well as moisture atmospheres. Based on the results, the synthesized compounds have a greater potential to use as latent fingerprints in the forensic science department [80, 81].

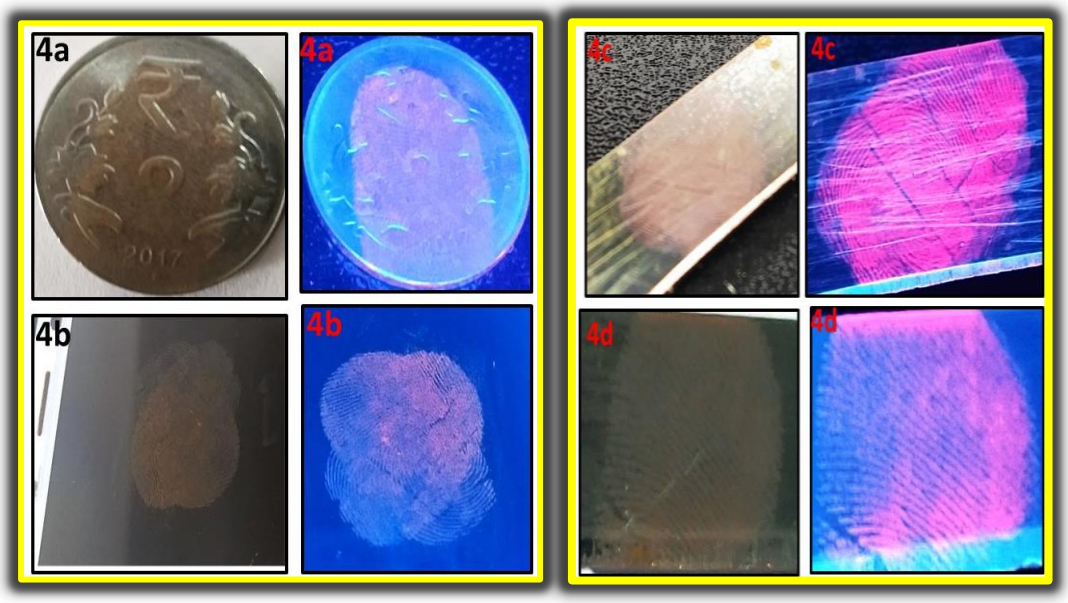

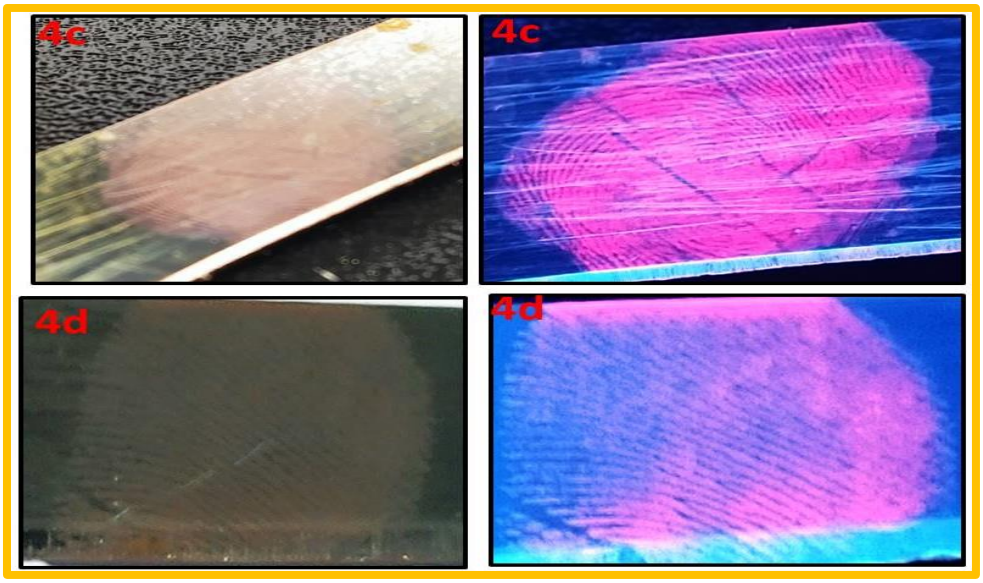

Fig. 2A.10 Latent fingerprints of synthesized compounds **4(a-d)** under normal light and UV-light.

2A.7. Conclusion.

In summary, this chapter describes, the one-pot synthesis of 7-hydroxy-5-(4-substitutedphenyl)-9-methyl-1,5-dihydro-2*H*-dipyrimido[*1,2-a:4',5'*-d]pyrimidine-2,4(3*H*)-dione derivatives **4(a-d)** using L-Proline as a catalyst and charcterrised by using spectroscopic techniques. Absorption and emission bands have appeared at a longer wavelength with higher intensity in solvent media. Similarly, redox peak current, have quasi-reversibility of an electron at different scan rate and experimental HOMO and LUMO informs the regeneration and recaptures of the injected electrons by the derivatives. Likewise, Theoretical studies are in good agreement with experimental results and revels that compounds are higher in chemical reactivity and photostability. The photocatalytic study over MG dye molecule at triplicate parameters was achieved at 65 %, 83 %, 88 % and 65 % dye degradation. Further, clear LFPs images were observed under UV light and compounds have better adherences over selected materials. Therefore, we conclude that synthesized compounds are potential materials to use in forensic science and phototonic materials.

2A.8 References.

1. D. Alexander, *Chem. Res.*, 106 (**2006**) 17-89.
2. H.Q. Xia, J. Wang, F.Q. Bai, H.X. Zhang, *Dyes and Pigment.*, 113 (**2015**) 87-95.
3. A. Mishra, M.K.R. Fischer, P. Bauerle, *Angew. Chem. Int. Ed.*, 48 (**2009**) 2474-2499.
4. T. Venkatesh, K. Upendranath, Y.A. Nayaka, *J. Solid State Electrochem*., 25 (**2021**) 1237-1244.
5. K.S. Pramod, K.S. Praveen, S.K. Manvendra, M. Mouslim, M.A. Saud, L.S. Puran, D.A. Dau, *ACS Omega.,* 3 (**2018**) 15035-15042.
6. X. Li, L. He, H. Chen, W. Wu, H. Jiang, *J. Org. Chem.,* 78 (**2013**) 3636-3646.
7. C.M.M. Santos, M. Freitas, E. Fernandes, *Eur. J. Med. Chem.*, 157 (**2018**) 1460-1479.
8. H.Q. Xia, J. Wang, F.Q, Bai, H.X. Zhang, *Dyes and Pigm.,* 113 (**2015**) 87-95.
9. A. Mishra M.K.R Fischer, P. Bauerle, *Angew. Chem. Int Ed.,* 48 (**2009**) 2474-2499
10. B.A.A. Rahaman El-Gazzar, H.N. Hafez, *Bioorg. Med. Chem. Lett.*, 19 (**2009**) 3392-3397.
11. A.A.A.R. Mahmoud, O.M. El-Hady, H. Salah, Z. Abo, E.M.M.A.E. Raheem, *J. Het. Chem.,* (**2015**) 1-6.
12. Z. Mario, L. Harald, T. Reinhard, *E. J. Med. Chem.,* 39 (**2004**) 1079-1088.
13. N. Vasu, C. Guochen, S. Qingning, J. Justin, F.S. Donald, *Bioorg. & Med. Chem. Lett.*, 19 (**2009**) 1425-1427.
14. G.B. Helio, P.C. Tainara, A.I. Bernardo, R.C.B. Iuri, N. Eufrânio, S. J.B.T. João, N.Z. Rocha, A.P.M. Marcos, *Tetrahedron Lett.,* 57 (**2016**) 5017-5021.
15. P.N. Kalaria, S.C. Karad, D.K. Raval, *Eur. J. Med. Chem.*, 158 (**2018**) 917-936.
16. S.K. Weng, W.L. Jing, C.C. Woon, L.P. Yean, C.S Lan, *Environ. Sci. Pollut. Res.*, 27 (**2020**) 2522-2565.
17. M.R. Khan, A.S.W. Kurny, G. Fahmida, *App. Wat. Scienc.*, 170 (**2009**) 520-529.

18. C. Hachem, F. Bocquillon, O. Zahraa, M. Bouchy, *Dyes Pigm.*, 49 (**2001**) 117-125.

19. C. Christophe, L. Chris, M. Pierre, S. Boca Raton, London, New York, *Washington, DC: CRC Press;* chapter 4 (**2004**).

20. S. Kulvir, S. Sahil, K.G. Rakesh, Egypt. *J. Forensic Sci.,* 3 (**2012**) 20-25.

21. W. Meng, L. Ming, Y. Aoyang, Z. Ye, Y. Mingying and M. Chuanbin, *Adv. Funct. Mater.*, 27 (**2017**) 1606243-1606259.

22. K.A. Vishnumurthy, M.S. Sunitha, K. Safakath, R. Philip, A.V. Adhikari, *Polymer (Guildf,)., 19* (**2011**) 4174-4183.

23. R.B. Basavaraj, G.P. Darshan, B. Daruka Prasad, S.C. Sharma, H. Nagabhushana, *J. Rare Earths.*, 37 (**2019**) 32-44.

24. M.K. Ravindra, K.M. Mahadevan, R.B. Basavaraj, G.P. Darshan, S.C. Sharma, M.S. Raju, G.R. Vijayakumar, Kiran B. Manjappa, D.Y. Yang, H. Nagabhushana, *Mater. Sci. Eng. C.*, 101 (**2018**) 564-574.

25. G.P. Darshan, H.B. Premkumar, H. Nagabhushana, S.C. Sharma, B. Daruka Prasad, S.C. Prashantha, R.B. Basavaraj, *J. Alloys Compd.,* 686 (**2016**) 577-587.

26. R.B. Basavaraj, H. Nagabhushana, G.P. Darshan, B.D. Prasad, S.C. Sharma, K.N. Venkatachalaiah, *J. Ind. Eng. Chem.,* 51 (**2017**) 90-105.

27. M. Bharti, M. Choudhary, G. Kumar, S. Muhammad, N. Das, K. Singh, A.G. Al-Sehemi, S. Kumar. *Synt. Commun.,* 50 (**2020**) 2199-2225.

28. S. Sunil, G.S. Khansole, A.R. Karad, N.B. Wadwale, Subhash, B. Junne, Vijay N. Bhosale *I. J. I. R. M. F.,* 11 (**2021**) 142-148.

29. S.V. Shinde, W.N. Jadhav, N.N. Karade, Orient. *J. Chem.,* 26 (**2010**) 307-315.

30. D. Jagawani, P. Joshi, *I.J.P.S.R.*, 5 (**2015**) 783-795.

31. H. Sachdeva, R. Saroj, S. Khaturia, S.S Chauhan, *Hetero. Lett.,* 1 (**2011**) 297-310.

32. A.A. Nadia Elkanzia, A.A.M. Faragc, N. Roushdye, A.M. Mansourf, *J. Optik*, 216 (**2020**) 164882-164896

33. S.H. Sukanya, T. Venkatesh, S.J. Aditya Rao, M.N. Joy, *J. Mole. Str.,* 1247 (**2021**) 131324-131330.

34. C. Pratapkumar, S.C. Prashantha, H. Nagabhushana, D.M. Jnaneshwara, *J. Sci. Adv. Mat. Dev*., 4 (**2018**) 464-470.

35. B. Avinash, C.R. Ravikumar, M.R. Anil Kumar, H.P. Nagaswarupa, M.S. Santosh, A.S Bhatt, D. Kuznetsov, *J. Phy. Chem. Sol*., 134 (**2019**) 193-200.

36. A.D. Becke, *Phys. Rev. A.,* 38 (**1998**) 3098-3100.

37. C. Pratapkumar, S.C. Prashantha, H. Nagabhushana, M.R. Anilkumar, C.R. Ravikumar, H.P. Nagaswarupa, D.M. Jnaneshwara. *J. Allo. Comp.,* 728 (**2017**) 1124-1138.

38. C. Hachem, F. Bocquillon, O. Zahraa, M. Bouchy, *Dyes and Pigm.,* 49 (**2001**) 117-125.

39. A.A. Nadia, Elkanzi, A.A.M Farag, N. Roushdy, A.M. Mansour, *Optik,* 216 (**2020**) 164882-16895.

40. M.M. Duvenhagel, O.M. Ntwaeborwal, H.G. Visser, H.C. Swart, *J. Cond. Matt.,* 439 (**2014**) 46-49.

41. T. Sutradhar, A. Misra, *J. Phy. Chem. A.,* 122 (**2018**) 4111-4120.

42. T. Venkatesh, Y.D. Bodke, M.J. Nibin, B.M. Vinoda, S. Yellappa, B.L. Dhananjaya, *Lett. In Org. Chem.,* 13 (**2016**) 1-12.

43. R.O. Yathisha and Y.A. Nayaka, *SN Appl. Sci.,* 2 (**2020**) 451-467.

44. K. Yasuhiro, O. Yousuke, F. Kazumasa and M. Masaki, *J. Org. Chem.,* 78 (**2013**) 7058-7067.

45. Y. Takakazu, L.L Bang, *Macromolecules.,* 35 (**2002**) 2993-2999.

46. A. Esvet, L. Abdulkadir, G. Selçuk, R.S. Mehmet, A. İnci, *Bull. Kor. Chem. Soc.,* 31 (**2010**) 3632-3638.

47. D. Stephane, S.H. Garry, W.G Skene, *J. Phys. Chem. B.,* 111 (**2007**) 11407-11418.

48. L. Leonat, S. Gabriela, I.V. Branzoi, *U.P.B. Sci. Bull. Series B.,* 75 (**2013**) 111-119.

49. A.R. Lopes Da Silva, A. Jhones Dos Santos, C.A. Martínez-Huitle, *RSC Adv.,* 8 (**2018**) 3483-3492.

50. A.J.S. Ahammad, S. Sarker, M. Aminur Rahman, J.J. Lee, *Electroanalysis.*, 22 (**2010**) 694-700.

51. I. Fleming, *Wiley.*, (**1977**).

52. A. Akbar, K. Muhammad, F.R. Muhammad, H. Sadia, A. Arif, N.T. Muhammad A. Muhammad, R. Faiz, A.C.B Ataualpa, *ACS Omega.*, 5 (**2020**) 15115-15128.

53. S. Murugavel, C. Ravikumar, G. Jaabil, P. Alagusundaram, *J. Mol. Str.*, 1176 (**2019**) 729-742.

54. R. Parr, G. Donnelly, R.A. Lev, M.W.E Palke, *J. Chem. Phy.*, 68 (**1977**) 3801-3807.

55. P. Udhayakala, T.V. Rajendiran, S. Gunasekaran, *J. Comp. Meth. Mol. Des.*, 2 (**2012**) 1-15.

56. K.V. Basavarajappa, Y.A. Nayaka, R.O. Yathisha, P. Manjunatha, *J. Fluor.*, 29 (**2019**) 1201-1211.

57. C.S. Abraham, S. Muthu, J.C. Prasana, S.J. Armaković, S. Armaković, F.B. Rizwana, A. S. B. Geoffrey, *Comput. Biol. Chem.*, 77 (**2018**) 131-145.

58. S. Renuga, S. Muthu, *Spectrochim. Acta. Part. A.*, 118 (**2014**) 702-715.

59. N.R. Rajagopalan, P. Krishnamoorthy, K. Jayamoorthy, M. Austeria, *J. Mod. Sci.*, 2 (**2016**) 219-225.

60. J.S.P.P. Leela, R. Hemamalini, S. Muthu, A.A. Al-Saadi, *Spectrochim. Acta A.*, 146 (**2015**) 177-186.

61. A. Klamt, *Fluid Phase Equilib.*, 407 (**2016**) 152-158.

62. A. Klamt, *Wiley Interdiscip. Rev. Comput. Mol. Sci.*, 8 (**2018**) 1-11.

63. F. Eckert, A. Klamt, *J. Comput. Chem.*, 27 (**2006**) 11-19.

64. M. Larriba J. D Riva, P. Navarro, D.Moreno, N.D. Noemí, J. García, V.R. Ferro, F. Rodríguez, J. Palomar, *Sep. Purif. Technol.*, 190 (**2018**) 211-227.

65. S. Gusarov, S.R. Stoyanov, *J. Phys. Chem. Lett.*, (**2020**), 9408-9414,

66. S. Balchandani, R. Singh, *ACS Omega.*, 6 (**2021**) 747-761.

67. M.A.S. Amulya, H.P. Nagaswarupa, M.R. Anil Kumar, C.R. Ravikumar, K.B. Kusuma, *J. Phys. Chem. Sol.,* 148 (**2021**) 109661-109672.

68. B. Avinash, C.R. Ravikumar, M.R. Anil Kumar, M.S. Santosh, C. Pratapkumar, H.P. Nagaswarupa, H.C. Ananda Murthy, V.V Deshmukh, A.S Bhatt, A.A Jahagirdar, M.W. Alam, *App. Surf. Sci. Adv.,* 3 (**2021**) 100049-100062.

69. B. Abebe, H.C.A. Murthy, E. Amare, *J.E.A.S.*, 8 (**2018**) 225-255.

70. M.A.S. Amulya, H.P Nagaswarupa, M.R. Anil Kumar, C.R. Ravikumar, K.B. Kusuma, S.C. Prashantha, *J. Phy. Chem. Sol.,* 148 (**2021**) 109756-109769.

71. G. Nagaraju, Udayabhanu, Shivaraj, S.A. Prashanth, M. Shastri, K.V. Yathish, C. Anupama, D. Rangappa, *Mater. Res. Bull.*, 94 (**2017**) 54-63.

72. B.R. Kirthan, M.C. Prabhakara, H.S.B. Naik, R. Viswanath, P.H.A. Nayak, *J. Mol. Struct.,* 1244 (**2021**) 130917-130928.

73. B. Modak, K. Srinivasu, S. K. Ghosh, *J. Chem. Phys.,* 16 (**2014**) 24527-24535.

74. S.P. Yew, H.Y. Tang, K. Sudesh, *Polym. Degrad. Stab.*, 91 (**2006**) 1800-1807.

75. M.M. Naik, M. Vinuth, K. Karthik, B. Suresha, G. Nagaraju, H.R. Sujatha, AIP *Conf. Proc.*, (**2020**) 2274-2287.

76. M.M. Naik, H. S.B Naik, G. Nagaraju, M. Vinuth, H.R Naik, K. Vinu, *J., Microchem.*, 146 (**2019**) 1227-1235.

77. M.M. Naik, H.S.B. Naik, G. Nagaraju, M. Vinuth, K. Vinu, S.K. Rashmi, *J. Mater. Sci. Mater. Electron.*, 29 (**2018**) 20395-20414.

78. Z. Baoya, R. Guojuan, T. Mingyu, C. Fang, Q. Fengyu, W. Chungang, S. Zhongmin, *Dyes and Pigm.*,149 (**2018**) 686-695.

79. Y.J. Park, S.J. Park, H.K. Yang, *J. Lumin.,* 201 (**2018**) 285-273.

80. M. Dhanalakshmi, H. Nagabhushana, G.P. Darshan, R.B. Basavaraj, B.D. Prasad, *J. Sci. Adv. Mater. Devices.,* 2 (**2017**) 22-33.

81. J. Lee, M.M. Joullié, *Tetra. Lett.*, 56 (**2015**) 3378-3381.

Chapter-2B

Facile synthesis and *i*n-vitro cytotoxicity study of some 5-(4-substituted phenyl)-7-hydroxy-9-methyl-2-thioxo-2,3-dihydro-1*H*-dipyrimido[*1,2-a:4',5'*-d]pyrimidin-4(5*H*)-one derivatives and their Optoelectronic, DFT and LFPs applications.

2B.1 Introduction

Cancer is one of the leading causes of death worldwide and the survival rate is also less without proper medication [1, 2]. In recent years, lung cancer is the most frequently diagnosed cancer and the second-most frequent cause of cancer-related deaths in men and women which are majorly found in developed countries. Generally, lung cancer is caused by smoking and many hormonal, viral and genetic abnormalities [3,4]. Chemotherapy and radiotherapy are present suitable medications, but only a modest increase in survival rate is found after the application of radiotherapy and chemotherapy. Recent reports reveal that many heterocyclic compounds show a broad range of pharmacological agents in which pyrimidine acts as an anti-cancer against various cell lines such as lung, breast, ovary and leukaemia [5].

Latent fingerprints (LFPs) having II and III levels have been used as physical evidence in criminal investigations by the forensic department since the 19th century [6, 7]. Generally, fingers contact with porous/non-porous surfaces leaves an imprint of ridges on the surface due to eccrine sweat and oily sebum by the fingers [8, 9]. The powder dusting method was one of the easiest method in development and the visualization of fingerprints using organic fluorescent powders because it avoids a background hindrance has better sensitivity and a good contract between the surface and fingermarks [10, 11] presently organic with luminescence characteristics have been attracted in the field of material science applications, in that nitrogen substituted have concentrated much more.

Pyrimidine or pyrimidione derivatives have been given great attention by medical scientists in the past few years and literature surveys inform about pyrimidines are well-known drugs in the pharmaceutical field. They have been known as anti-microbial [12, 13], anti-malarial [14], anti-convulsant [15], anti-cancer [16] anti-inflammatory [17], analgesic [18, 19] anti-tubercular [20] agents. Similarly, pyrimidines exhibit higher fluorescent properties and hence can be used in optoelectronic-oriented applications like OLEDs, sensor materials, and electroluminescent materials [21]. In presence of anchoring (electron-withdrawing and donating) groups, they show biological as well as optical properties and themselves act as an electron-withdrawing group due to their π-deficient nature which reason for increased color sensitivity, luminous properties and solvatochromic behavior with bio charactears [22-24]. Recently reported pyrimidine substituted derivatives with biological activities and material science applications have been discussed below.

Sravanakumar *et al.*, reported a new indeno-fused pyrido[2,3-b]pyrimidines (**1**) in the year 2017. Compounds have been synthesized using different catalysts such as I_2, $SnCl_2$, and CAN, and compounds show excellent fluorescence properties. Absorption bands are moves redshift at 250 nm to 380 nm and emitted from 381 nm to 430 nm at the blue region [25].

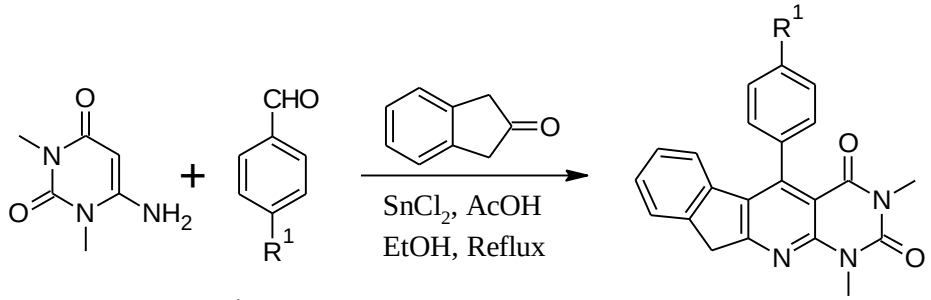

R^1= OCH_3, $N(CH_3)_2$, CN, OEt **(1)**

J.D. Tadi´c *et al.,* reported (2018) a new dihydropyrimidinone derivatives (**2**) as azo dyes through multicomponent reaction in microwave using acid catalyst. Synthesized compounds have been studied for optical properties in ethanol, where absorption bands have appeared at visible regions 350 nm to 480 nm. Further, synthesized compounds were analyzed theoretically, such as vibrational, FMOs and calculated chemical quantum parameters [26].

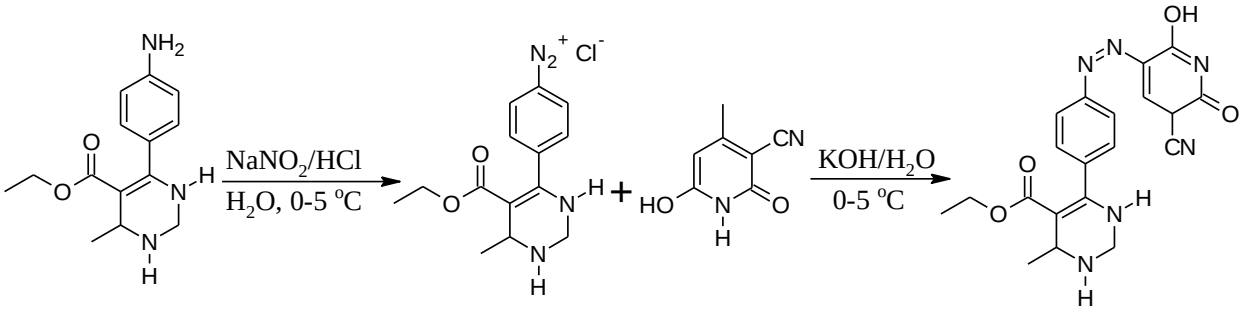

(2)

Pasha *et al.,* reported (2015) a novel 3,4-dihydropyrimidine-2(1*H*)-ones/thiones (**3**) using 10 mol % efficient Zinc chloride as catalyst under the microwave irradiation through multicomponent reaction. All the compounds have been tested for anti-cancer and anti-microbial activites, and compounds were exhibits the least IC_{50} values of 21.74±0.26 µg/mL and higher zone of inhibition 13.2±0.07 at higher the concentration [27].

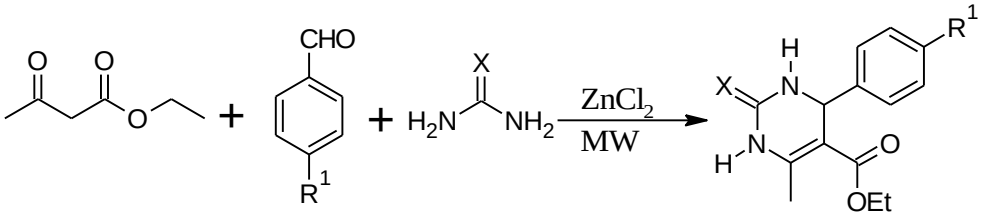

X- O. S, $R^1 = NO_2$, OH, OEt, C_6H_5, OCH_3, CN **(3)**

In 2016, Puripat and co-workers reported a new multicomponent reaction of pyrimido [*4,5*-d] pyrimidine-2-(1*H*)-one (**4**) in solvent-free condition using urea as a catalyst. The synthesized compounds have been screened for anti-cancer activity against human lung cancer A549 cell line and obtained least IC_{50} values of 23.69±0.53 [28].

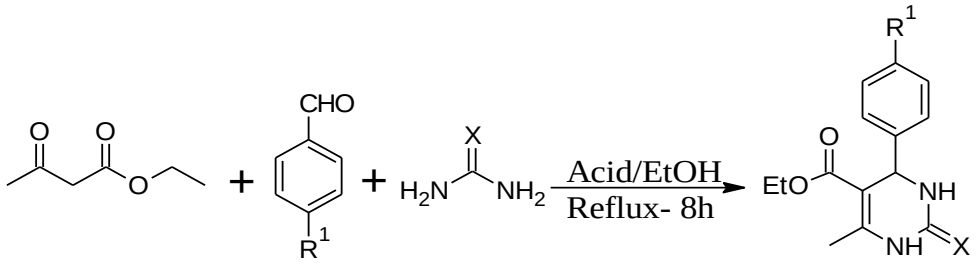

X = O. S, R^1 = Cl, Br, C_6H_5, Pyridine, Thiophene **(4)**

Sahand Safari *et al.,* reported a new 3,4-dihydropyrimidine derivatives as potential anti-cancer agents (**5**). The synthesized compounds have shown better activity agianist MCF-7, HepG-2, and A549 cancer cell lines. These compouds Compounds was found more potent against assessed cell lines by exibhiting the 65.54 ± 9.06, 73.71 ± 4.26 and 43.97 ± 0.45 IC_{50} values [29].

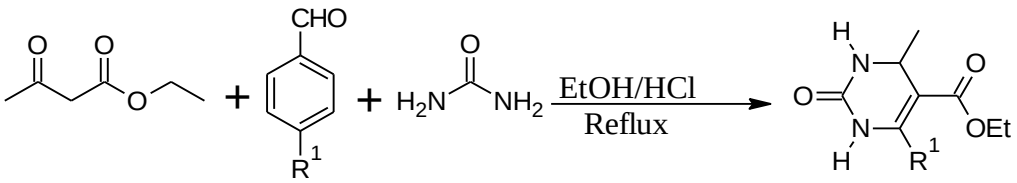

R^1= C_6H_5, F, Br, Cl, OCH_3, **(5)**

Hassan *et al.,* reported a new series of 2-substituted-4-oxo-pyrido[*2,3*-d] pyrimidines (**6**) from the acylation reaction of α-aminonicotinonitrile with aroyl chlorides, diethyl malonate and morpholine-4-carboxylate in presence of formic acid under solvent-free conditions. Obtained compounds are exhibits well fluorescence properties in solvent medium with least concentration of longer wavelength at 427-482 nm [30].

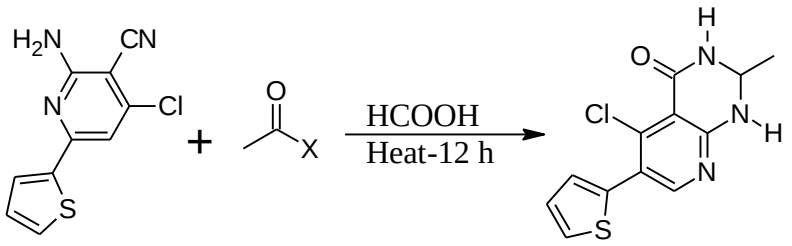

X= NH_2, Cl, OEt, OH **(6)**

Concerning the above literature survey, pyrimidine derivatives were gaining interest to use as efficient materials material science applications. Given reaction methods and the nature of pyrimidine compounds, we encouraged to synthesise some novel 5-(4-substitutredphenyl)-7-hydroxy-9-methyl-2-thioxo-2,3-dihydro-1*H*-dipyrimido[1,2-a:4',5'-d]pyrimidin-4(5*H*)-one derivatives **4**(**a-c**) using L-proline as a catalyst in ethanol and studied their optoelectronic, DFT, Latent fingerprint and *i*n-vitro cytotoxicity with molecular docking studies.

2B.2 Present work.

From the above reported results, considerable with biological and optoelectronic properties, we had gain interest to carry out multicomponent reaction of 2-amino-4-hydroxy-6-methyl pyrimidine (**1**) (1 mmol), 2-thio-barbutric acid (**2**) (1 mmol) and substituted aromatic aldehydes (**3**) (1 mmol) using, L-Proline as an organocatalytic under solvent media.

The reaction pathway of novel pyrimidine derivatives has been displayed in **Scheme 2** and the proposed mechanism has been discussed in previous **Chapter- 2A.**

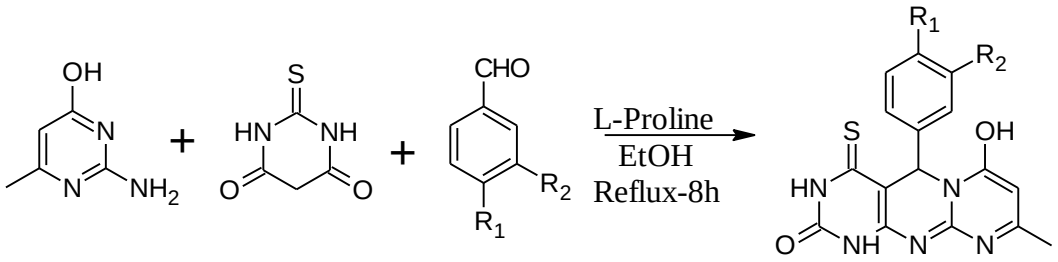

1 **2** **3(a-c)** **4(a-c)**

Entry	R_1	R_2
4a	Cl	NO_2
4b	Br	H
4c	OH	OCH_3

Scheme 2: Multicomponent reaction of some new 5-(4-substitutredphenyl)-7-hydroxy-9-methyl-2-thioxo-2,3-dihydro-1*H*-dipyrimido[*1,2-a:4',5'*-d]pyrimidin-4(5*H*)-one derivatives **4**(**a-c**).

2B.2.2 Spectral characterization.

The Structures of the targets were confirmed by using different spectroscopic techniques such as FTIR, NMR and Mass spectrometry.

In the FTIR spectrum, compound **4a** shows a starching vibrational band at 3452 cm^{-1} is correspond to the hydroxy functionality and another vibrational band at 3179 cm^{-1} due to the amide functionality. The vibration band at 2954 cm^{-1} correspond to the aromatic CH group and the carbonyl functionality of starching frequency has appeared at 1653 cm^{-1}. Further, the starching frequency obtained at 1289 cm^{-1} is correspond to C=S functionality. In ^{1}H-NMR spectrum, compound **4a** exhibited a singlet peak appeared at δ 11.95 ppm for OH proton and another two singlet peaks at δ 11.65 ppm and δ 11.57 ppm corresponds to the barbituric nucleus N-H protons. Doublet peaks appeared at 7.37-7.35 pmm is corresponds to the two aromatic protons and another doublet peaks obtained at δ

7.31-7.29 ppm correspond to one aromatic proton. Another doublet peaks obtained at δ 6.94-6.89 ppm is corresponds to two aromatic protons. A singlet peak at δ 5.88 ppm correspond to pyrimidine junction CH proton and another singlet peak obtained at δ 2.05 ppm correspond to the methyl protons. In ^{13}C-NMR spectrum, compounds **4a** exhibits signals at δ 174.09 ppm and δ 162.83 ppm corresponds to thiol (C=S) carbon and carbonyl (C=O) carbons respectively. A signals apperead at δ 154.00, 148.28, 147.78, 145.63, 132.83, 132.47, 131.44, 123.84, 121.88 110.74 and 95.30 ppm corresponds to aromatic carbons. A signal at δ 21.02 ppm due to methyl carbons. In addition, the mass spectrum exhibits a molecular ion peak at m/z 419.9934 and isotopic peak at 421.9872 is correspond to the molecular weight of the compound **4a.**

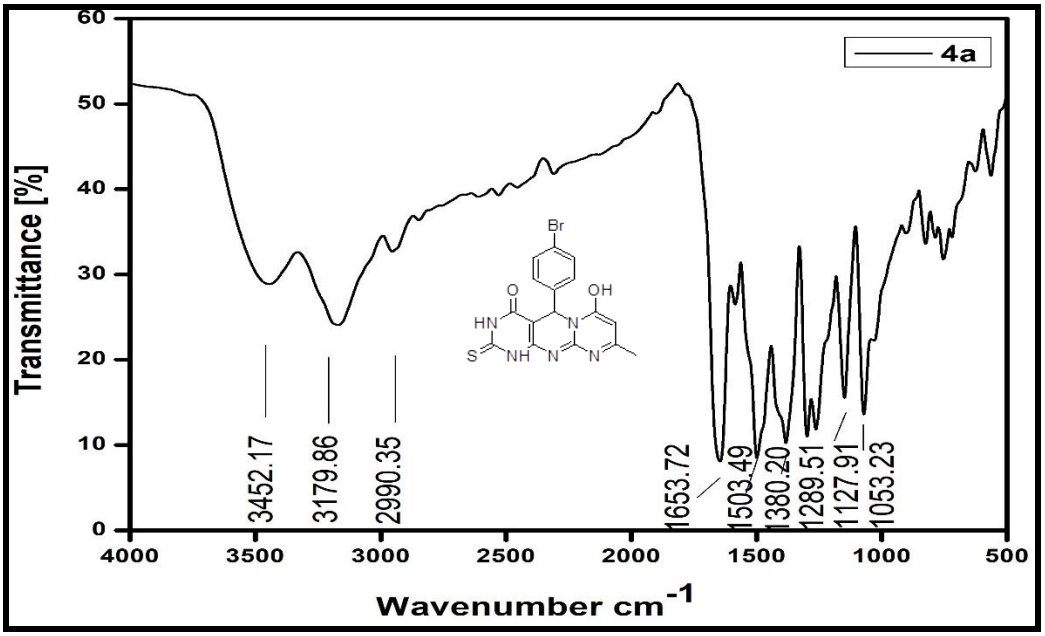

FTIR spectrum of compound 4a

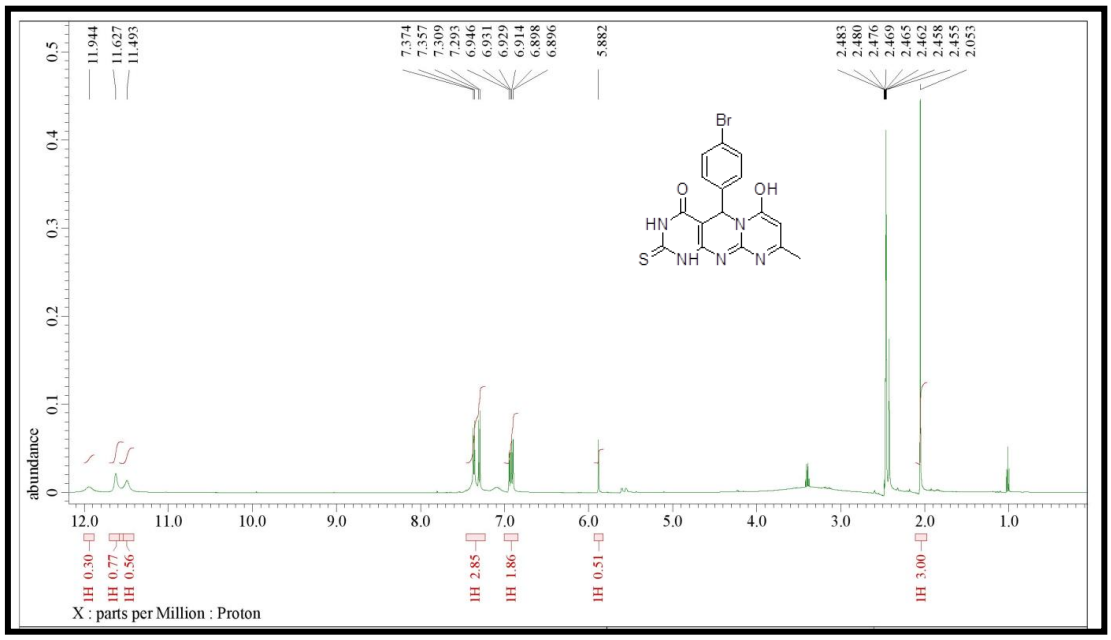

[1]H-NMR spectrum of compound 4a

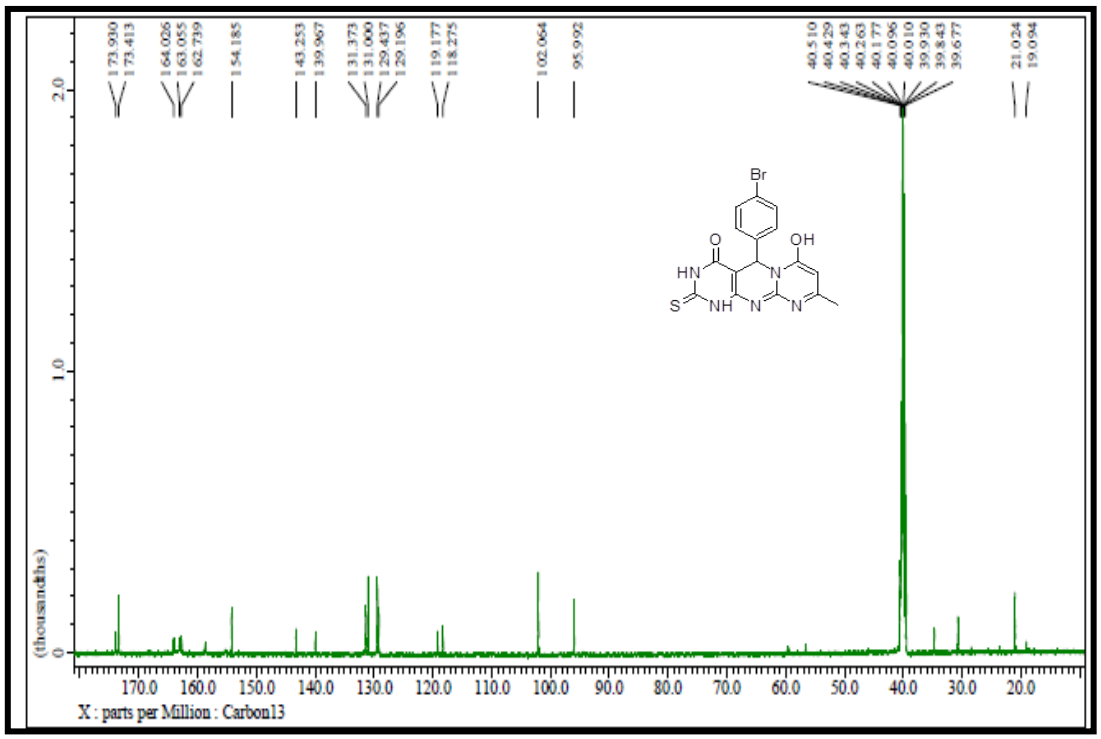

[13]C-NMR spectrum of compound 4a

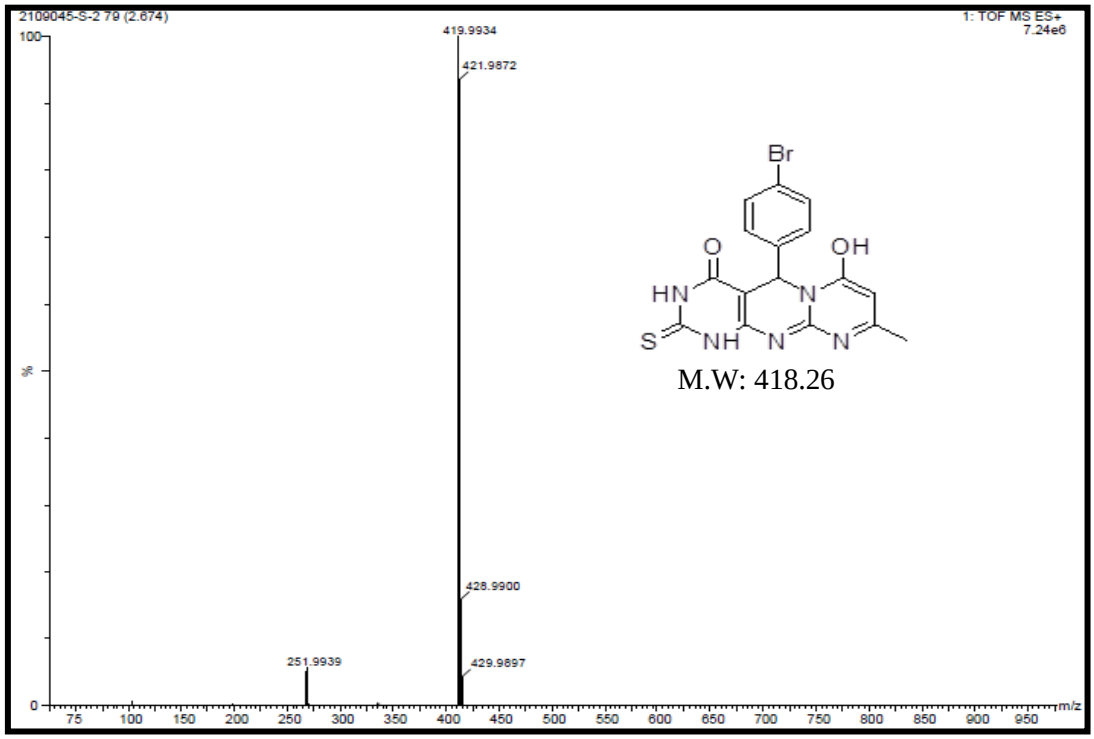

Mass Spectrum of compound 4a

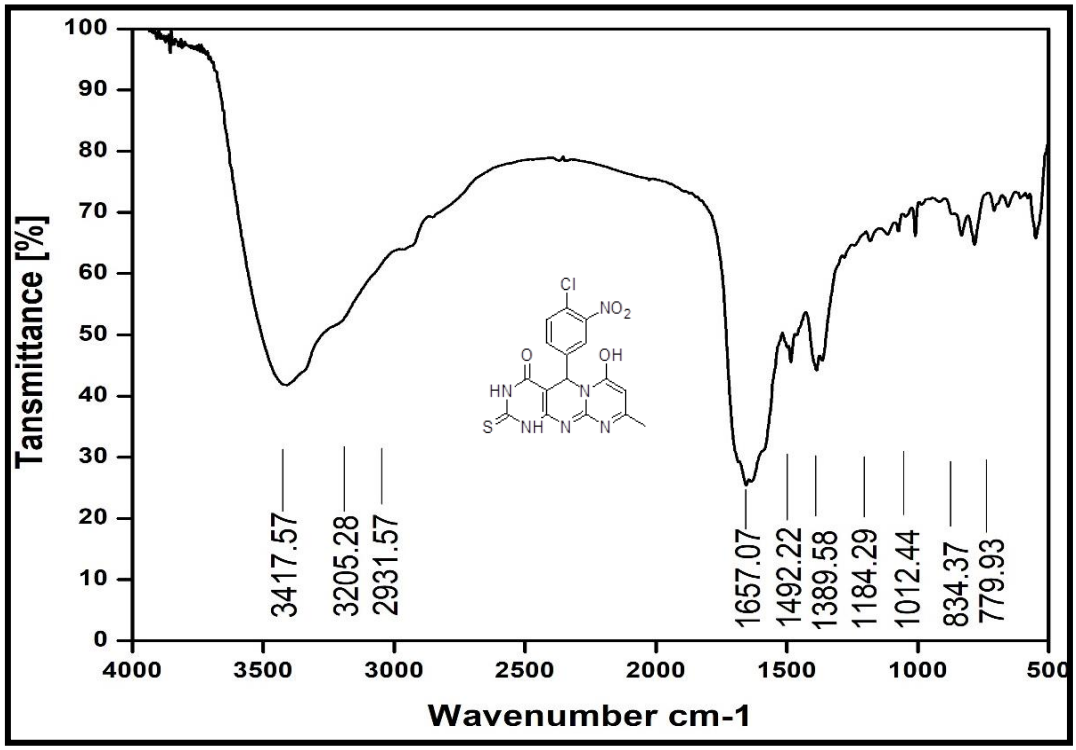

FTIR spectrum of compound 4b

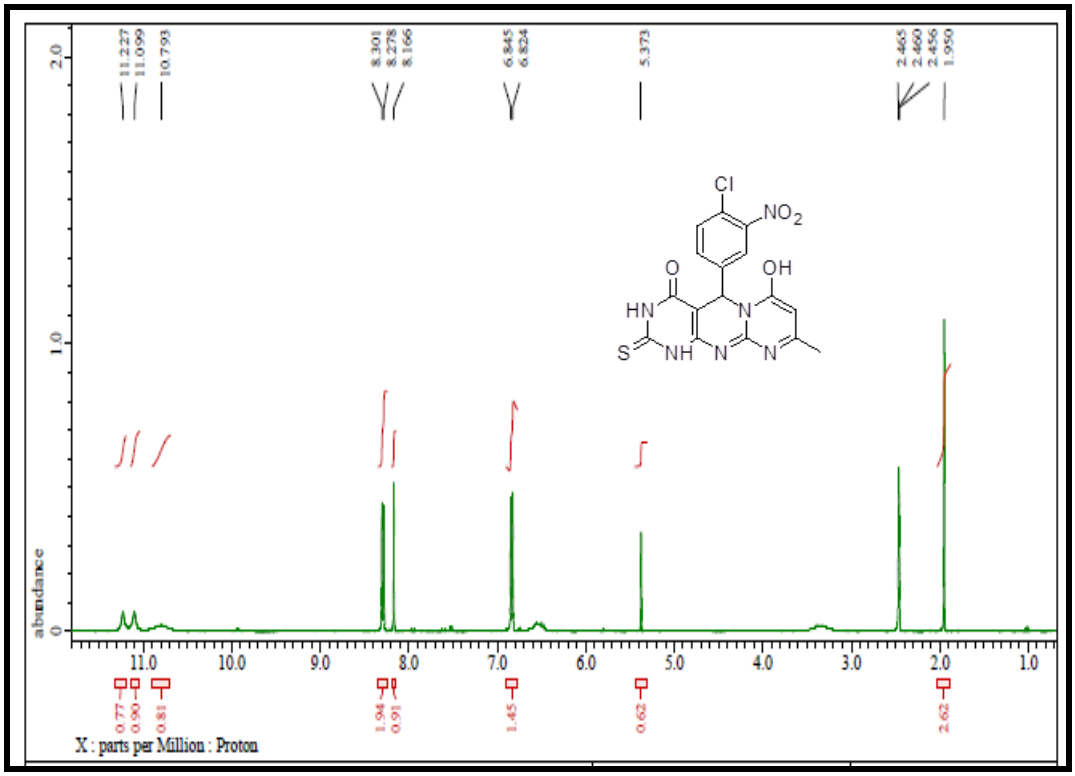

[1]H-NMR spectrum of compound 4b

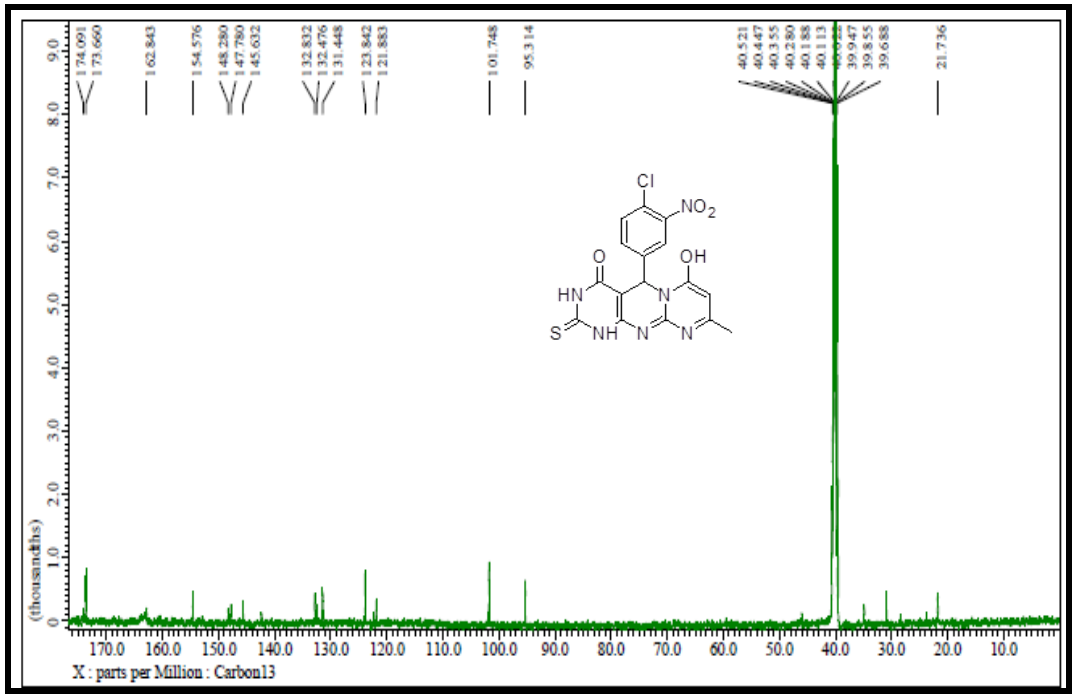

[13]C-NMR spectrum of compound 4b

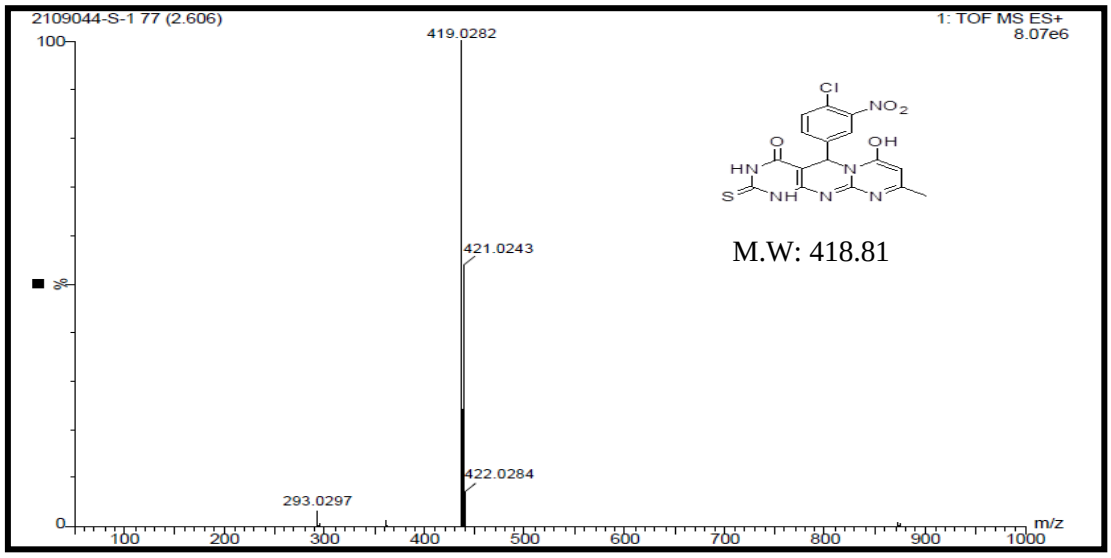

Mass spectrum of compound 4b

2B.3 Experimental

2B.3.1 General information.

The general information regarding the various solvent, reagents, and instruments, used for analysis has been discussed in the experimental section **2A.3** of the **Chapter - 2A.** Further the in-vivo cytotoxicity activities were performed in the Dept.of Martha madndal NGH Institute of Dental Science and Research Center, Belagum, Karnataka and molecular docking studies were carried out using Auto Dock Veena.

2B.3.2 General Procedure.

Synthesis of new 5-(4-substitutedphenyl)-7-hydroxy-9-methyl-2-thioxo-2,3-dihydro-1*H*-dipyrimido[*1,2-a:4',5'*- d]pyrimidin-4(5*H*)-one 4(a-c);

An equimolar mixture of 2-amino-4–hydroxy-6-methyl pyrimidine (**1**) (1 mmol) 2-thio-barbituric acid (**2**) (1 mmol) and different aromatic aldehydes (**3**) (1 mmol) in 20 mL ethanol, using 10 mol% of L-Proline as catalyst followed by according to reported procedure (**Chapter-2A**) (**Scheme 1**).

5-(4-Chloro-3-nitrophenyl)-7-hydroxy-9-methyl-2-thioxo-2,3-dihydro-1H-dipyrimido[1,2 a:4',5'- d]pyrimidin-4(5H)-one (4a):

Creamy solid; Yield: 85 %; MP: 202-204 ^{o}C; Mol. Formula: $C_{16}H_{11}ClN_6O4_5S$; FTIR (υ cm^{-1}): 3452 (OH), 3179 (NH), 2954 (C-H), 1653 (C=O), 1289.51 (C=S); ^{1}H-NMR (δ ppm): 11.95 (s, 1H, OH), 11.65 (s, 1H, NH), 11.57 (s, 1H, NH), 7.37-7.35 (d, 2H, CH), 7.31-7.29 (d, *J* = 8 Hz, 1H, Ar-H), 6.94-6.91 (d, *J* = 8 Hz, 1H, Ar-H) 6.91-6.89 (d, *J* = 8 Hz, 1H, Ar-H), 5.88 (s, 1H, CH) and 2.02 (s, 3H, CH_3); ^{13}C-NMR (δ ppm): 174.09, (C=S), 162.83 (C=O), 154.00, 148.28, 147.78, 145.63, 132.83, 132.47, 131.44, 123.84, 121.88 (C=C), 110.74, 95.30 (C=CH) 21.77 (C-CH_3); HRMS (m/z): 419.9934 [M^{+}1] and 421.9872 [M^{+}2]; Anal. Calcd for C 45.88, H 2.65 and N 20.07 %; Found: C 43.25, H 2.35 and N 19.97 %.

5-(4-Bromophenyl)-7-hydroxy-9-methyl-2-thioxo-2,3-dihydro-1H-dipyrimido[1,2-a:4',5'-d]pyrimidin-4(5H)-one (4b):

Creamy solid; Yield: 86 %; MP: 200-201 ^{o}C; Mol. Formula: $C_{16}H_{12}BrN_6O_4S$; FTIR (υ cm^{-1}): 3417 (OH), 3205 (NH), 2931 (C-H), 1657 (C=O), 1184 (C=S); ^{1}H-NMR (δ ppm): 11.22 (s, 1H, NH), 11.09 (s, 1H, NH), 10.79 (s, 1H, OH), 8.30-8.27 (d, *J* = 8 Hz, 2H, Ar-H), 8.16 (s, *J* = 8 Hz, 1H, Ar-H), 6.84-6.82 (d, *J* = 8 Hz, 2H, Ar-H), 5.37 (s, 1H, CH), 1.95 (s, 3H, CH_3); ^{13}C-NMR (δ ppm): 173.93, (C=S), 164.02 (C=O), 163.05 (C-Br), 162.79, 154.18, 143.25, 139.96, 131.37, 131.37, 131.00, 129.43, 129.14, (C=C), 119.17, 118.27, 102.06, 95.99 (C=CH), 21.02 (C-CH_3); HRMS (m/z): 419.0282 [M^{+}1] and 421.0243 [M^{+}2]; Anal. Calcd: for C 45.94, H 2.89 and N 16.74 %; Found: C 45.25, H 2.06 and N 15.97 %.

5-(4-Hydroxy-3-methoxyphenyl)-7-hydroxy-9-methyl-2-thioxo-2,3-dihydro-1H-dipyrimido[1,2-a:4',5'-d]pyrimidin-4(5H)-one (4c):

Yellow creamy solid; Yield: 87 %, MP: 210-212 ^{o}C; Mol. Formula: $C_{17}H_{15}N_5O_4S$; FTIR (υ cm^{-1}): 3385 (OH), 3284 (NH), 3118 (C-H), 2986 (OCH_3), 1714 (C=O), 1596 (C=N), 1284 (C=S); ^{1}H-NMR (δ ppm): 11.87 (s, 2H, OH), 11.53 (s, 1H, NH), 11.39 (s, 1H, NH), 7.03 (s, 1H, Ar-CH), 6.59-6.57 (d, *J* = 8 Hz, 1H, Ar-H), 6.48-6.46 (d, *J* = 8 Hz, 1H, Ar-H) 6.36-6.34 (d, *J* = 8 Hz, 1H, Ar-H), 5.83 (s, 1H, CH), 3.52 (s, 3H, OCH_3), 1.99 (s, 3H, CH_3); ^{13}C-NMR (δ ppm): 173.70 (C=S), 163.43 (C=O) 163.05 (C=C-NH), 155.30, 147.75, 145.19, 144.55, 130.91, 119.66, 119.20, 115.70, 115.33, 112.03, (C=C), 115.62, 101.22, 96.71 (C=CH), 56.22 (C-OCH_3), 22.85 (C-CH_3); HRMS (m/z): 387.00 [M^{+}1]; Anal. Calcd for C 52.98, H 3.92 and N 18.17 %; Found: C 51.75, H 3.10 and N 18.00 %.

2B.3.3 Cytotoxicity.

In vitro cytotoxicity was assessed by the MTT assay method [31] against A549 (Human Lung cancer) cell line. The cells were seeded in a 96-well flat-bottom microplate and maintained at 37 ºC in 95 % humidity and CO_2 overnight. Different concentrations (100, 50, 25, 12.5 6.25 and 3.125 µg/mL) have been carried out and the cells were incubated for another 48 h, further, the wells were washed twice with PBS. 20 µL of MTT staining solution was added to each well, and the plate was incubated at 37 ºC. After 4 h, 100 µL of DMSO was added to each well to dissolve the formazan crystals, and absorbance was recorded at 570 nm using a microplate reader. The percentage of cell survival was calculated by using the following equation (1) [32].

$$\% \text{ of cell survival} = \frac{\text{Mean OD of test compound}}{\text{Mean OD of Negative control}} \times 100 \qquad \text{— (1)}$$

2B.3.4 Molecular docking studies.

The molecular interactions of the synthesized compounds **4**(**a-c**) at the binding pocket of EGFR Kinase protein were studied using automated docking by employing the Autodock Vina program [33]. The co-crystallized structure of Epidermal Growth Factor Receptor Kinase (EGFR Kinase) (PDB ID: 1M17) was retrieved from the protein databank and their substrate binding sites were identified using pdbsum server [34]. A grid box of dimensions 25 x 25 x 25 Å with X, Y and Z coordinates at 21.96, 0.994 and 54.093 for EGFR Kinase was created. The grid box was set around the residues forming the active pocket. The binding interactions were visualized using Bio-via Discovery Studio Visualizer V.20.1 [35]. The receptor structure was prepared before use in the docking study using the protein preparation module of the HEX modelling package. During the protein preparation, all hetero and water molecules were removed from the crystal structure except water molecules within 2.6 Å from the ligand. All the molecules docked at the binding sites of the receptor structures. The *in silico* molecular docking scores give useful information concerning the capability of the newly synthesized compounds to bind the active sites of the receptor.

2B.3.6 ADME studies.

Various physicochemical features and pharmacokinetic descriptors were calculated through the online web tool Swiss ADME [36]. The oral bioavailability of the synthesized compounds (**4a-c**) was predicted using the Lipinski rule-of-five (RO5) filter to derive the candidate drug's pharmacokinetic (PK) [37, 38]. The structural properties used in the RO5 filter are derived using Osiris Data warrior V.4.4.3 software [39]. The bioavailability scores were predicted using the molinspiration server [40].

2B.4 Results and discussion

2B.4.1 Optical properties.

The absorption and emission properties have been studied for synthesized compounds in DMSO solvent at the concertation of 6×10^{-6} M. From **Fig. 2B.1** compound **4**(**a-c**) has displayed absorption bands appeared at longer wavelength ~290-300 nm of bathochromic shift and emitted at ~358-370 nm of the blue region with respect of excitation wavelength. These compounds involve aromatic conjugation and electronic transition like π-π* and n-π*, and also the presence of electron-donating and withdrawing groups that act as auxochromes and which help to increase bands towards redshift [30].

The average difference between emission spectra and absorption spectra is said to be stokes shift. The lesser spectral gap of 72 nm and 70 nm of stokes shift for compounds **4a** and **4b,** and compound **4c** gives 63 nm stokes shift [31]. Moreover, the stokes shift is caused due to solute and solvent interaction, here all the compounds have better solute-solvent interactions. Obtained spectral values are summarized in **Table 2B.1** with an optical band gap.

$$Eg = 1240/\lambda_{onset}\ \text{eV} \qquad \text{— (2)}$$

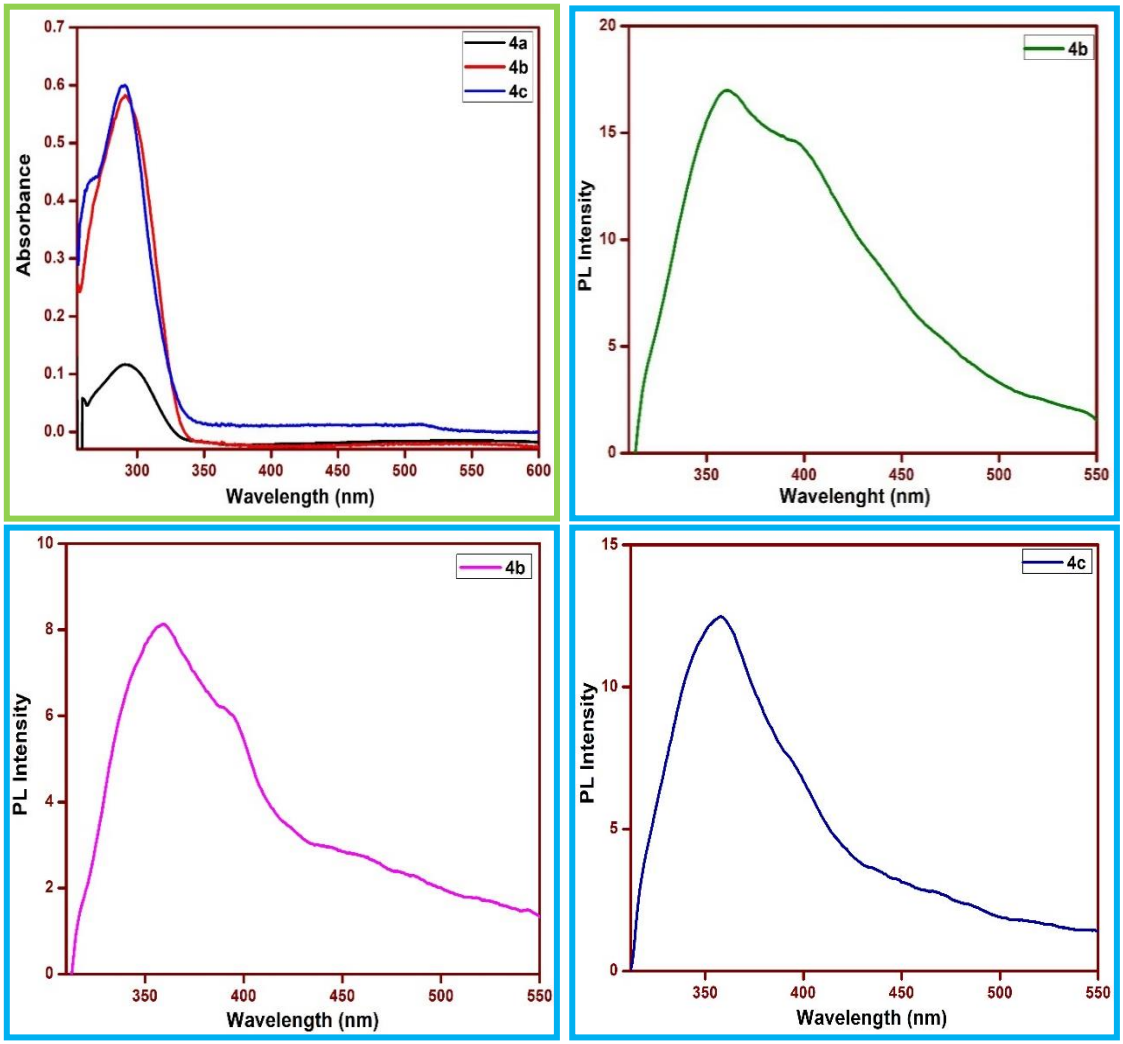

Fig. 2B.1. Graph of UV-Visible and Photoluminescence spectra of compounds **4**(**a-c**).

Table 2B.1. Optical spectral values of compounds **4(a-c)** in a solvent system.

Entry	Solvent	λ_{abs} (*nm*)	λ_{emi} (*nm*)	Stoke shift	E_g^{OTP} (*eV*)	Molar absorptivity ($\varepsilon \times 10^{-5}$ L mol^{-1} cm^{-1})
4a		298	370	72	4.16	4.9
4b	DMSO	290	360	70	4.28	5.0
4c		295	358	63	4.21	4.7

2B.4.2 Cyclic Voltammetry analysis.

The electrochemical properties of **4a**, **4b**, and **4c** compounds were analyzed using a cyclic voltammetry instrument in 1M KOH with help of a three-electrode system [32]. The cell was constructed with Ag/AgCl, carbon paste and Pt wire as a reference, working and counter electrodes at 100 mV/s to 500 mV/s scan rates [33].

A fine cathodic reduction and anodic oxidation peaks were observed in **Fig. 2B.2**, where all the compounds show quasi-reversibility electron transfer and redox onset potential has been listed in **Table 2B.2**. Compound **4a** has shown a quasi-reversible oxidation peak at -0.52 eV and reversibility of reduction at -0.03 eV respectively. Compounds **4b** and **4c** have shown reversibility of reduction on set potential is -0.14 eV and -0.82 eV, and quasi reversible oxidation peak is -0.55 eV and 0.17 eV. The compounds have shown fine redox behavior at a higher scan rate and also the presence of OH and C=O groups.

$$E_{(HOMO)} = -[E_{(ox\text{-}onset)} + 4.4]\ eV \qquad \text{— (3)}$$

$$E_{(LUMO)} = -[E_{(red\text{-}onset)} + 4.4]\ eV \qquad \text{— (4)}$$

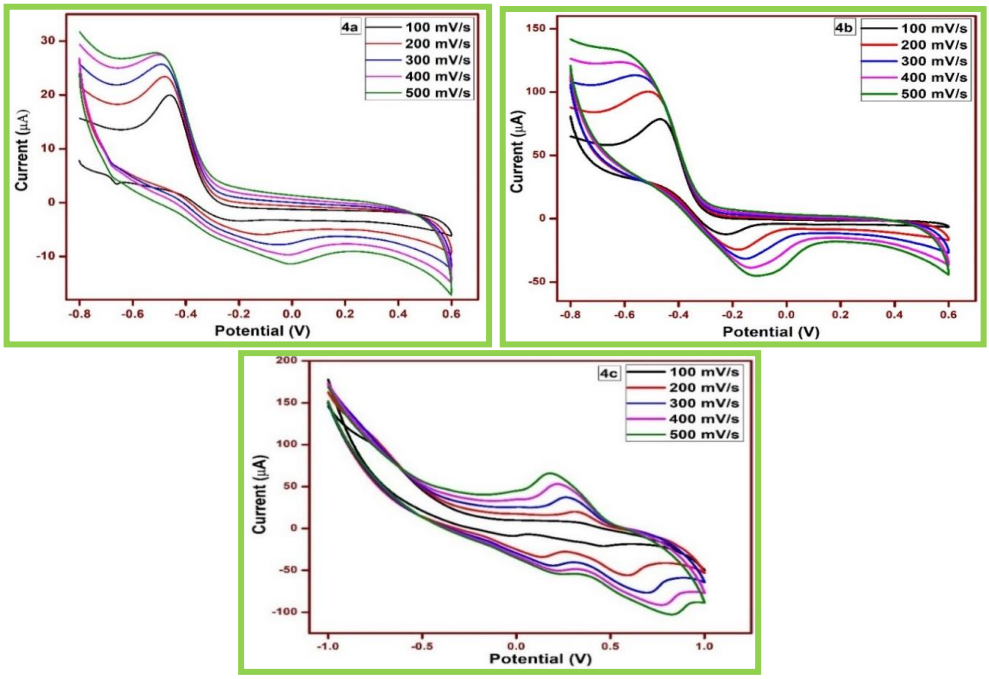

Fig. 2B.2 CV graphs of synthesized compounds **4**(**a-c**) at different scan rates.

Table 2B.2. CV spectral data and experimental HOMO-LUMO values **4**(**a-c**).

Entry	Reduction on set potential (V)	Oxidation on set potential (V)	E_{LUMO} (eV)	E_{HOMO} (eV)	$\Delta E = E_L - E_H$ (eV)
4a	-0.03	-0.52	-4.37	-3.88	-0.49
4b	-0.14	-0.55	-4.26	-3.85	-0.41
4c	-0.82	0.17	-3.58	-4.57	0.99

2B.4.3 DFT studies.

2B.4.3.1 Molecular geometry.

The newly synthesized compounds **4**(**a-c**) were subjected to complete geometry optimization in the ground state using the aforementioned level of theory [34]. The optimized molecular structure of these derivatives has been given in **Fig. 2B.3**. The optimized geometry results of these molecules show that the molecule belongs to C_1 point group symmetry.

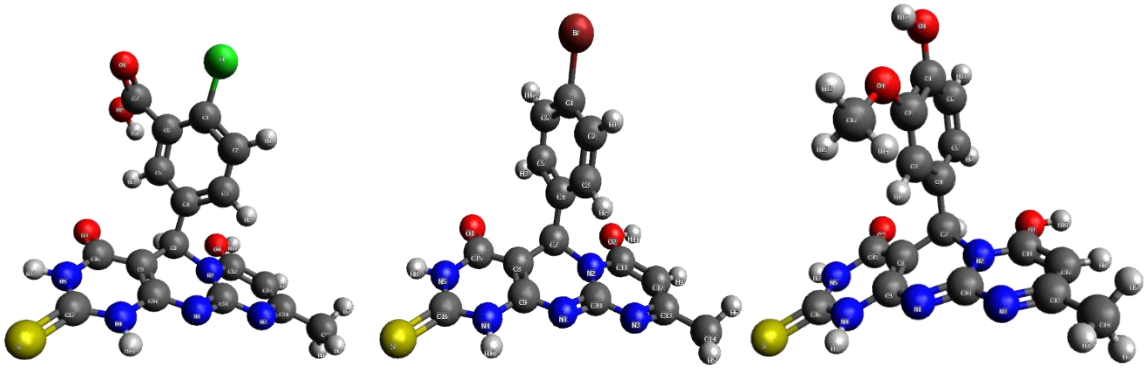

4a **4b** **4c**

Fig. 2B.3. Optimized structure of the pyrimidine derivatives **4**(**a-c**).

2B.4.3.2 Frontier Molecular Orbital (FMOs) analysis.

FMOs energy levels of synthesized compounds **4**(**a-c**) were calculated at above said theory and their energy to determine the molecular electrical transport properties, conductivity, biological properties, chemical reactivity, and kinetic stability [35]. The results are presented in **Fig. 2B.4** and the HOMO and LUMO are spread for **4a**, **4b** and **4c** compounds. Various reactive parameters have been proposed for understanding the chemical behavior of the molecules such as electron affinity (A), electronegativity (χ), chemical potential (μ), global hardness (η), global softness (S), and electrophilicity index (ω) were calculated using equations (5-9) and are summarized in **Table 2B.3a.** Generally, the large energy gap is concerned with good chemical reactivity and low kinetic stability, whereas a compound with a large energy gap value harder, and it was observed **4**(**a-c**) to be 3.662 eV, 3.668 eV, 3.673 eV and 3.384 eV respectively. From **Table 2B.3a**, it is observed that molecule **4c** has a higher electrophilicity index, hence compound **4c** acts as a good electrophile. Also, the value of global hardness for

compound **4c** has a lesser value compared to the other three molecules, hence it is found to be more reactive than the other synthesized compounds [36-38].

$$\chi = -\tfrac{1}{2}\,(E_{LUMO}+E_{HOMO}) \quad \text{— (5)}$$

$$\mu = -\chi = \tfrac{1}{2}\,(E_{LUMO}+E_{HOMO}) \quad \text{— (6)}$$

$$\eta = \tfrac{1}{2}\,(E_{LUMO} - E_{HOMO}) \quad \text{— (7)}$$

$$\sigma = 1/2\eta \quad \text{— (8)}$$

$$\omega = \mu^2/2\eta \quad \text{— (9)}$$

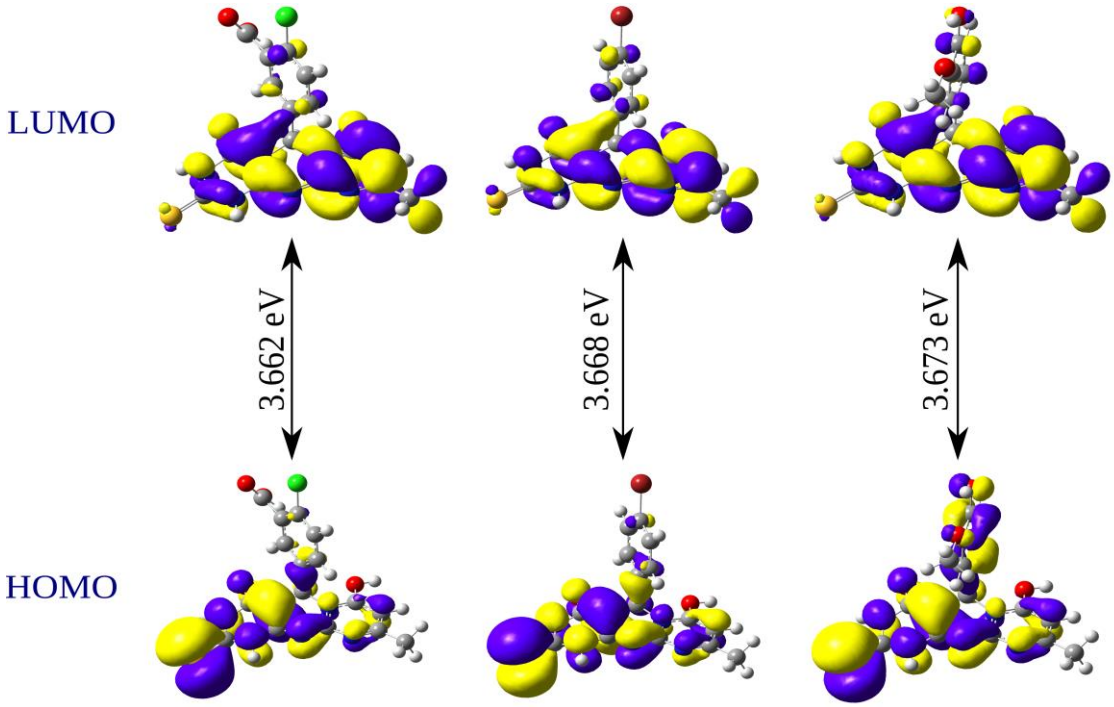

Fig. 2B.4. FMO structures of the synthesized compounds **4(a-c)**.

2B.4.3.3 Molecular electrostatic potential (MEP) surface analysis.

MEP is a color-coded plot of calculated electrostatic potential superimposed on an electron density surface. It is an important descriptor of the reactive sites present in the molecule and reactive ability providing a visual approach to the study of hydrogen bonding interactions, biological recognition and electrostatic potential regions. In the

MEP map, the maximum red colored region signifies the site for the electrophilic attack, and the maximum blue colored region indicates the site for the nucleophilic attack. The major significance of this MEP map gives information about molecular size, shape and positive, negative, and neutral electrostatic potential regions in terms of color code. Potential increases in the following order: red < green < blue [39, 40]. The 3D plots of MEP map synthesized compounds are illustrated in **Fig.2B.5** and show that the compounds have several possible sites for electrophilic attack over oxygen and nitrogen atom. For a plausible nucleophilic attack, the maximum positive region is found on the hydrogen atom attached to the oxygen in pyrimidine moiety. The overall volume of the surface, minimum and maximum electrostatic potential surface was listed in **Table 2B.3b.**

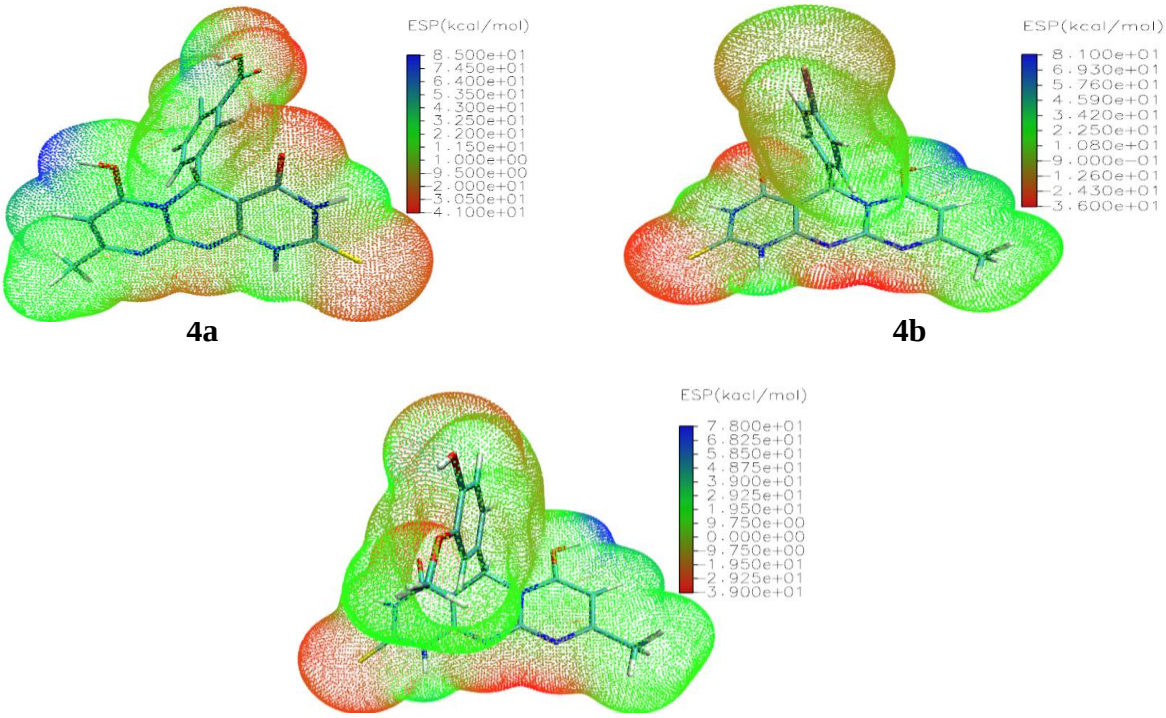

Fig 2B.5. MEP images of the pyridmidine derivatives (**4a-c**).

Table 2B.3a. Various reactive parameters for the molecules **4(a-c**).

Parameters	Values (eV)		
	4a	**4b**	**4c**
E_{HOMO}	-5.981	-5.770	-5.608
E_{LUMO}	-2.319	-2.102	-1.934
Energy gap (Δ)	3.662	3.668	3.674
Ionization energy (I)	5.981	5.770	5.608
Electron affinity (A)	2.319	2.102	1.934
Electronegativity (χ)	4.150	3.936	3.771
Chemical potential (μ)	-4.150	-3.936	-3.771
Global hardness (η)	1.831	1.834	1.837
Global softness (s)	0.546	0.545	0.544
Electrophilicity index (ω)	4.702	4.223	3.871

Table 2B.3b Volume of the surfaces and electrostatic potential of the compounds **4(a-c).**

Entry	Volume of the surfaces (Å^3)	Electrostatic potential (kcal/mol)	
		Minimum	**Maximum**
4a	426.259	-41.635	85.708
4b	401.533	-36.810	81.187
4c	415.192	-39.801	78.447

2B.4.4 Latent Fingerprints.

The chemical method (powder dusting) was the easiest method to use in the visualization of LFPs on porous/nonporous surfaces. In this present work, we employed the powder dusting method using synthesized compounds **4**(**a-c**) as shown in schematic representations **Fig.2B.6** [41].

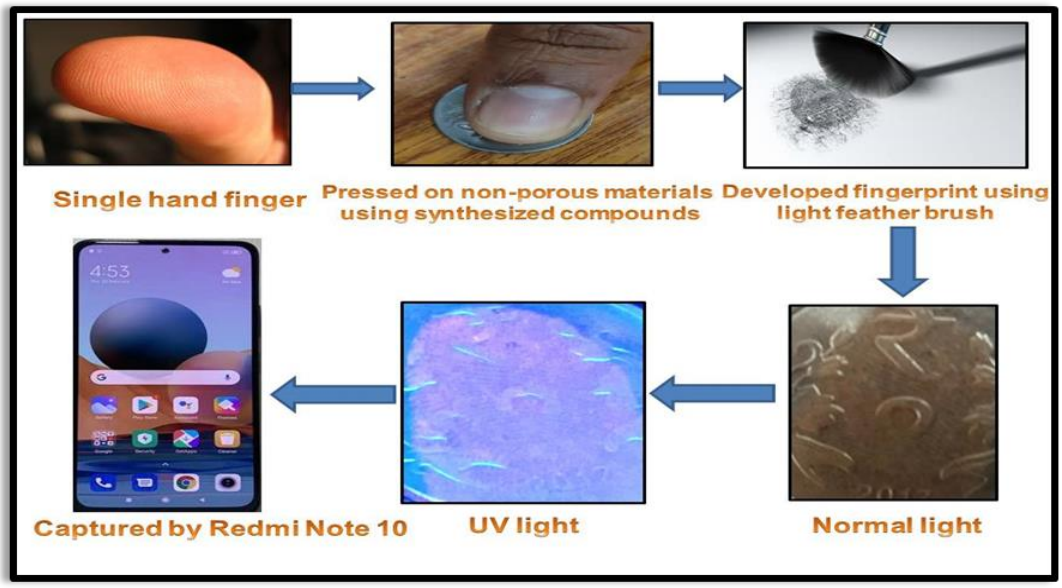

Fig 2B.6. Schematic reorientation of LFPs.

LFPs were developed and visualized under visible light as well as UV light on selected porous and non-porous materials. **Fig.2B.7** displays, all the compounds were potential materials to use in the forensic laboratory where compounds have a good contract between surface materials and sweat pores. Compound **4a** has been developed on a compact disk where we can observe the neat fingerprint ridges under normal and UV light (365 nm). Similarly, compounds **4b** and **4c** have been developed on the textbook, 250 mL beaker; there we can observe the clear visibility of fingerprint ridges on surface materials. Finger sweats consist of organic and inorganic residues such as amino acids, urea, peptides, fatty acids and chlorides along the water. Among these residues, amino acid contains core, polar and charged amino acid which covers the surface of a material and are in contact with solvent due to their ability for hydrogen bond can be formed. Here we observe the clear adherence between surface and compounds may be because of the electrostatic interaction between oxygen (O) atom present in the pyrimidine ring and the hydrogen (H) atom in amino acid [42-44].

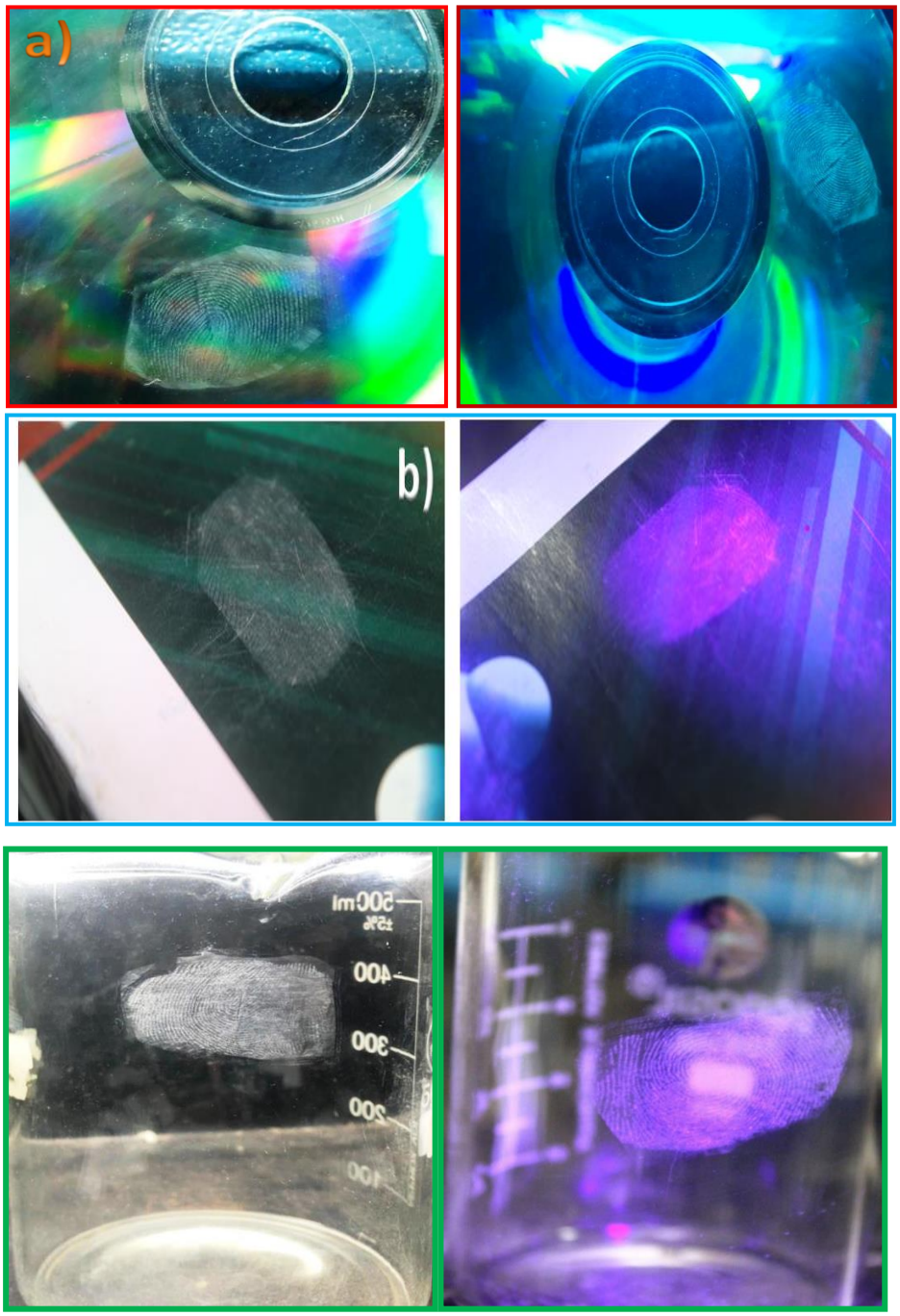

Fig.2B.7. Compound **4a** and **4b** on compact disk and text book, and **4c** on 250 mL beaker.

2B.4.5 Cytotoxicity study.

Evaluation of *in* vitro cytotoxicity of the synthesized compounds (**4a-c**) against the A549 (Human Lung cancer) cell line. A graph describing the concentration versus survival fraction and IC_{50} value of the compounds was plotted in **Fig. 2B.8** and the results were tabulated in **Table 2B.4a** with a comparison of the doxorubicin drug. Cytotoxicity results revealed that synthesized compounds exhibited considerable selectivity against the A549 cell line with noticeable IC_{50} values. The compound **4c** shows a significant cytotoxic effect with the least IC_{50} value of 16.74±0.23 µg/mL as compared to the standard drug doxorubicin (6.07±0.18 µg/mL). The remaining compounds also displayed a moderate cytotoxic effect with IC_{50} value in the range of 34.28±1.40 to 85.45±2.81 µg/mL.

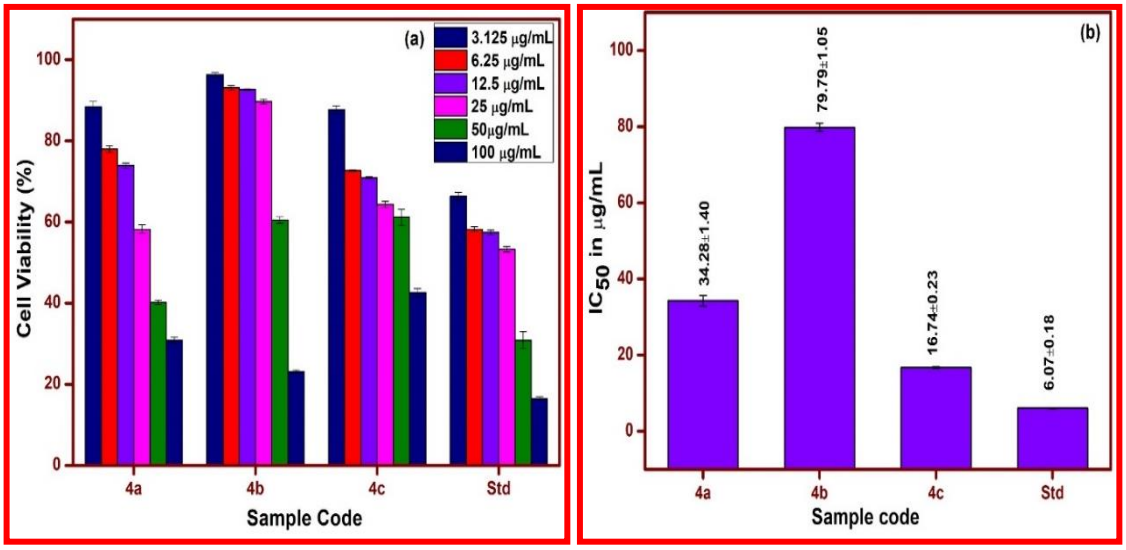

Fig 2B.8. A graph of % of surviving cells of synthesized compounds (**4a-c**) at different concentration against A549 cell line (**a**); A graph of IC_{50} value of compounds (**4a-c**) against A549 cell line (**b**).

Table 2B.4a Percentage of cell viability against A549 (Human Lung cancer) cell line of the synthesized compounds **4**(**a-c**).

Compd.	Mean cell Viability of A549 (Human Lung cancer) Concentration in µg/mL							IC_{50} in µg/mL
	NC	**3.125**	**6.25**	**12.5**	**25**	**50**	**100**	
4a	100	88.43±1.28	77.96±0.79	73.93±0.61	58.24±1.06	40.16±0.53	30.85±0.80	34.28±1.40
4b		96.30±0.55	93.08±0.53	92.64±0.15	89.71±0.55	60.50±0.80	23.13±0.40	79.79±1.05
4c		87.67±1.00	72.66±0.19	70.96±0.19	64.30±0.80	61.18±2.00	42.63±1.00	16.74±0.23
Std		66.29±1.01	58.24±0.61	57.45±0.56	53.29±0.69	30.84±2.11	16.50±0.46	6.07±0.18

Std-Doxorubicin, **NC-** Negative control

Values are Mean ±SE, N=3, *P<0.01 vs. Control

2B.4.6 *in silico* molecular docking study.

The docking receptor EGFR Kinase protein (**Fig. 2B.9**) with synthesized compounds **4**(**a-c**) showed well-established binding energies in their active pockets (**Table 2B.4b**). A molecular docking study helps to predict the binding modes and binding energies of the targeted compounds with active sites of the enzymes. The docking result shows that all the synthesized compounds **4**(**a-c**) exhibit a significant binding affinity in the range of -8.5 to -9.7 kcal/mol and the compounds were compared with standard drug doxorubicin (-9.3 kcal/mol). All the compounds showed encouraging binding energies and exhibited one or more hydrogen bonds with amino acids in their active pockets. Among them, compound **4c** exhibited the least binding energy of -9.7 kcal/mol and three hydrogen bonds with amino acid residues LYS721, ASP831 and THR766. The remaining compounds **4a** and **4b** were also established with good binding energies of -8.8, -8.5 and -8.5 kcal/mol respectively as compared to doxorubicin drug.

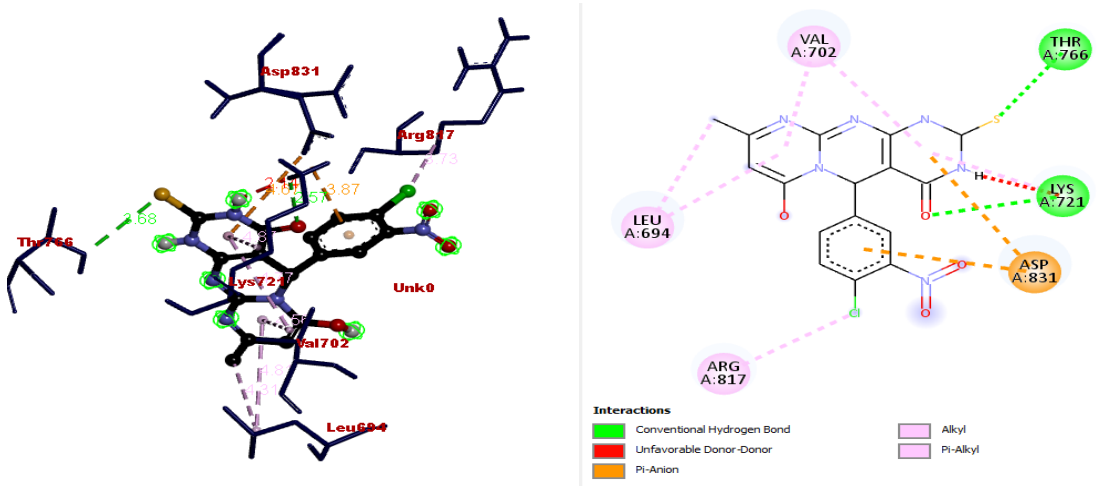

4a

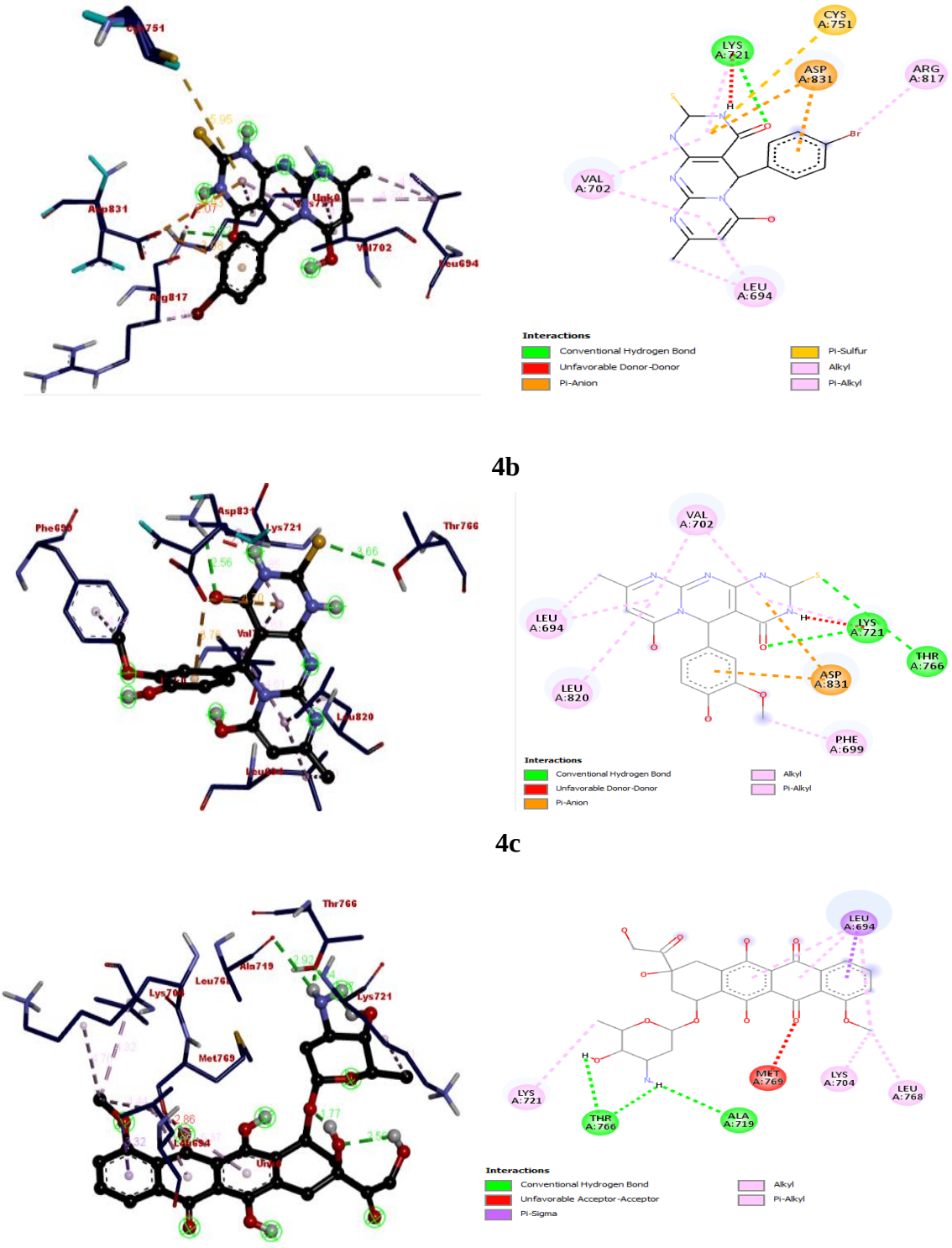

Doxorubicin

Fig.2B.9. 3D and 2D representation of molecular interactions between EGFR Kinase protein with synthesized compounds **4(a-c)** and doxorubicin.

Table 2B.4b Molecular interactions of synthesized compounds **4**(**a-c**) & Doxorubicin with EGFR Kinase protein.

Entry	Binding affinity (kcal/mol)	H bond	Hydrogen bond interaction	Hydrogen bond length in A°	Hydrophobic and other interactions
4a	-8.8	02	LYS721 THR766	2.57 3.68	ASP831, ASP831, LEU694, ARG817, LEU694, VAL702, VAL702, LYS721
4b	-8.5	01	LYS721	2.62	ASP831, ASP831, CYS751, LEU694, ARG817, LEU694, VAL702, VAL702, LYS721
4d	-9.7	03	LYS721 ASP831 THR766	2.23 2.31 2.50	ASP831, PHE699, LEU820, MET742, ALA719, LEU694, LEU768, VAL702, ALA719, VAL702, LYS721, VAL702, ALA719, LYS721
Doxorubicin	-9.3	03	THR766 ALA719 THR766	2.46 2.91 2.24	LEU694, LYS721, LEU694, LYS704, LEU768, LEU694, LEU694

2B.4.7 *ADME studies.*

2B.4.7.1 Physicochemical properties.

ADME study will help to novel drug design in the pharmaceutical field. A drug-likeness profile can be evaluated through some parameters such as molecular weight, the number of heavy atoms, HBA, HBD, rotatable bonds, molar refractivity and topological polar surface area (TPSA). These parameters were calculated for synthesized compounds **4**(**a-c**) and data was listed in **Table 2B.5a**.

The drug-likeness profiles were calculated based on Lipinski's (MW ≤ 500; HBA ≤ 10 and HBD ≤ 5), Ghose (160 ≤ MW ≤ 480; 40 ≤ MR ≤ 130 and 20 ≤ atoms ≤ 70), Veber (rotatable bonds ≤ 10 and TPSA ≤ 140), Egan (TPSA ≤ 131.6) and Muegge (200 ≤ MW ≤ 600; number of aromatic rings ≤ 7; number of rotatable bonds ≤ 15; HBA ≤ 10 and HBD ≤ 5). All the synthesized compounds obeyed Lipinski and Ghose rule, **4c** obeyed Veber, Egan and Muegge rule remaining compounds were not obeyed these rules. The rule-based score defines the compounds into four probability score classes *i.e.* 11 %, 17 %, 55 % and 85 %. The acceptable probability score is 55 % which indicates that it passed the rule of five [45, 46]. All the synthesized compounds showed a score of 55% indicating compounds having acceptable scores without any violations with good bioavailability. Further, the synthetic accessibility of the compounds was assessed to quantify the complexity of the molecular structure. The results showed that the score was in the range of 3.97-4.11 revealed that the compounds do not have complex synthetic routes (**Table 2B.5b**).

The mean predicted lipophilicity values were evaluated to decide whether the compounds were aqueous or non-aqueous solubility and they were calculated by considering the consensus log Po/w. According to this, if a molecule is more soluble then its consensus log Po/w values will be more negative. The results showed that the compounds were insoluble in a non-aqueous medium because Consensus Log Po/w values are positive. Consensus log S (if log S< −10: poorly soluble, <−6: moderately soluble, <−4: soluble, <−2: very soluble, and <0: highly soluble) values indicated that the compounds were having Log S value in the range of -3.62 to -2.64, hence all the compounds were soluble in an aqueous medium (**Table 2B.5c**).

The pharmacokinetic parameters like absorption, skin permeation, distribution, metabolism and excretion were predicted. Predicted distribution parameters of compounds **4**(**a-c**) suggested that all the synthesized compounds have low GI absorption (except **4b**). While all the compounds have no blood-brain permeant, hence there was no possibility of causing harmful toxicants in the brain and bloodstream. If the molecules have a more negative value of log Kp, it is said to be less skin permeant. Compounds **4**(**a-c**) have more negative log Kp values in the range of -8.59 to -8.03 cm/s, therefore these compounds are less skin permeant and results were tabulated in **Table 2B.6**.

Metabolism plays an important role in the bioavailability of drugs as well as drug-drug interactions [47, 48]. Metabolism parameters are important to understanding whether the compounds act as a substrate or non-substrate of the certain proteins. Hence, compounds **4**(**a-c**) were evaluated and the results found to be non-substrate of permeability glycoprotein (P-gp), CYP1A2, CYP2C19, CYP2C9, CYP2D6 and CYP3A4 inhibitors & the results were tabulated in **Table 2B.7**.

Table 2B.5a. Physicochemical properties of compounds (**4a-c**).

Entry	Formula	Molecular Weight (g/mol)	No. Heavy atoms	HBA	HBD	Rotatable bonds	Fraction Csp3	Molar Refractivity	TPSA (Å²)
4a	$C_{16}H_{11}ClN_6O_4S$	418.81	28	6	3	2	0.12	107.64	176.97
4b	$C_{16}H_{12}BrN_5O_2S$	418.27	18	4	3	1	0.12	101.51	131.15
4c	$C_{17}H_{15}N_5O_4S$	384.37	18	6	3	2	0.12	102.63	176.97

Table 2B.5b. Drug likeness, bioactivity and synthetic accessibility score of the synthesized compounds **4**(**a-c**).

Entry	Lipinski	Ghose	Veber	Egan	Muegge	Bioactivity Score	Synthetic accessibility
4a	Yes	Yes	No	No	No	0.55	4.01
4b	Yes	Yes	Yes	Yes	Yes	0.55	3.97
4c	Yes	Yes	No	No	No	0.55	4.01

Table 2B.5c. Predicted lipophilicity parameters of the synthesized compounds **4**(**a-c**).

Entry	Consensus Log Po/w	Consensus Log S	Solubility Class
4a	1.55	-3.36	Soluble
4b	2.46	-3.62	Soluble
4c	1.06	-2.77	Soluble

Table 2B.6. Predicted absorption & distribution parameters of the synthesized compounds **4**(**a-c**).

Entry	GI absorption	BBB permeant	Log Kp (cm/s)
4a	Low	No	-8.20
4b	High	No	-8.03
4c	Low	No	-8.59

Table 2B.7. Predicted metabolism parameters of the synthesized compounds **4**(**a-c**).

Entry	P-gp	CYP1A2 inhibitor	CYP2C19 inhibitor	CYP2C9 inhibitor	CYP2D6 inhibitor	CYP3A4 inhibitor
4a	No	No	No	No	No	No
4b	No	No	No	No	No	No
4c	No	No	No	No	No	No

2B.5 Conclusion

This chapter describes, synthesis of new 2-thioxo-2,3-dihydro-1*H*-dipyrimido[*1,2-a:4',5'*-d]pyrimidin-4(5*H*)-one derivatives through multicomponent reaction. Absorption bands appeared at redshift and emission bands at a longer wavelength. Cyclic voltammetry studies reveal that compounds are efficient materials for electrochemical applications by showing better redox behavior and higher values of HOMO-LUMO. Calculated quantum chemical parameters indicate that compounds are hard molecules which have higher chemical reactivity and kinetic stability. MEP images inform the compounds have good electrostatic potential, with nucleophilic attacking sites by showing color codes. All the compounds show clear ridges of fingerprints on selected materials. In addition, compound **4c** have been found potent *in-vitro* cytotoxicity effect with IC_{50} value 16.74±0.23 which was nearer to standard drug. Similarly, *in-silico* molecular docking results suggest that compounds have better binding energy affinity and energies. Further, from the ADME-toxicology studies compounds are nontoxic and have good oral bioavailability suitable as drug leads. Therefore, we conclude that these compounds are potential materials material science applications and pharmaceuticals.

2B.6. References.

1. M.Z. Bhatti, A. Alia, H.Q. Duongd, J. Chene, F. Ur. Rahman, *J. In. Org. Biochem*., 194 (**2019**) 52-64.
2. T. Venkatesh, Y.D. Bodke, S.J. Aditya Rao, *Chem. Data Collect.*, 25 (**2020**) 1-13.
3. F. Mottaghitala, M. Farokhib, Y. Fatahic, F. Atyabia, R. Dinarvand, *J. Contr. Rele*., **295** (2019) 250-267.
4. L.F. Magalhaes, F. Mello-Andrade, W.C. Pires, H.D. Silva, P.F.F. da Silva, L.M. Macedo, C. Henrique de Castro, C.C. Carneiro, C.G. Cardoso, P.R. de Melo Reis, L. Camargo de Oliveira, R.R. Caetano, A.A. Batista, E.P. Silveira-Lacerda, *Chem. Biol. Interact*., 278 (**2017**) 101-113.
5. R.L. Siegel, K.D. Miller, A. Jemal, *CA Cancer J. Clin*., 67 (**2017**) 7-30.
6. K. Upendranath, T. Venkatesh, M. Shashank, G. Nagaraju, K.M. Mussuvir Pasha, *J. Mol. Struct.*,1250 (**2021**) 131930-131949.
7. K.A. Vishnumurthy, M.S. Sunitha, K. Safakath, R. Philip, A.V. Adhikari, *Polymer (Guildf,).*, 19 (**2011**) 4174-4183.
8. R.B. Basavaraj, G.P. Darshan, B. Daruka Prasad, S.C. Sharma, H. Nagabhushana, *J. Rare Earths.*, 37 (**2019**) 32-44.
9. M.K. Ravindra, K.M. Mahadevan, R.B. Basavaraj, G.P. Darshan, S.C. Sharma, M. S. Raju, G.R. Vijayakumar, K.B. Manjappa, Ding-Yah Yang, H. Nagabhushan, *Mater. Sci. Eng. C.*, 101 (**2018**) 564-574.
10. G.P. Darshan, H.B. Premkumar, H. Nagabhushana, S.C. Sharma, B.D. Prasad, S.C. Prashantha, R.B. Basavaraj, *J. Alloys Compd*., 686 (**2016**) 577-587.
11. R.B. Basavaraj, H. Nagabhushana, G.P. Darshan, B.D. Prasad, S.C. Sharma, K. N. Venkatachalaiah, *J. Ind. Eng. Chem.*, 51 (**2017**) 90-105.
12. J. Cieplik, M. Stolarczyk, J. Pluta, O. Gubrynowicz, I. Bryndal, T. Lis, *Ac Polo Pharm Drug Res.*, 68 (**2011**) 57-65.
13. M.S. Mohamed, S.M. Awad, N.M. Ahmed, *J. App. Pharm. Sci.*, 1 (**2011**) 76-80.
14. M. Richa, B. Mishra, N. Moorthy, *Tre. Appl. Sci. Res.*, 3 (**2008**) 203-208.

15. J.R. Morgan, R. Haritakul, P.A. Keller, *Lett. Drug. Des. Discov.*, 5 (**2008**) 277-280.

16. T.A. Naik, K.H. Chikhalia, *Eur. J. Chem.*, 4 (**2007**) 60-6.

17. B. Ramesh, S.V. Kulakarni, *J. Glo. Pharma. Tech.*, 2 (**2010**) 110-122.

18. S.M. Sondhi, M. Dinodia, R. Rani, R. Shukla, R. Raghubir, *Ind. J. Chem.*, 49 (**2009**) 273-281.

19. Y. Pore, B. Kuchekar, *Dig. J. Nano. Biostr.*, 3 (**2008**) 293-298.

20. T.S. Chitre, M.K. Kathiravan, A.S. Chothe, V.K. Rakholiya, K.D. Asgaonkar, M. Shital, *J. Pharm. Res.*, 4 (**2011**) 1882-1893.

21. K.S. Pramod, K.S. Praveen, S.K. Manvendra, M. Mouslim, M.A. Saud, L.S Puran, D.A. Dau, *ACS Omega.*, 3 (**2018**) 15035-15042.

22. G.B. Helio, P.C. Tainara, A.I. Bernardo, R.C.B. Iuri, N. Eufrânio, S.J.B.T. João, N.Z. Rocha, A.P.M. Marcos, *Tetr. Lett.*, 57 (**2016**) 5017-5021.

23. A.E.S. Hassan, A.M. Hesham, *J. Iran. Chem. Soc.*, 16 (**2019**) 723-732.

24. R. Ziessel, G. Ulrich, A. Harriman, M.A.H. Alamiry, B. Stewart, P. Retailleau, *J. Chem. A Eur.*, 15 (**2009**) 1359-1369.

25. S. Manickam, S.K. Iyer, *Dyes and Pigm.*, 147 (**2017**) 300-312.

26. D. Russowsky, F.A. Lopes V.S.S. da Silva, K.F.S Canto, M.G.M D' Oca, M. N Godoi, *J. Braz. Chem. Soc*., 15 (**2004**) 165-175.

27. V.M. Joshi, S.K. Vyawhare, S.U. Tekale, S.B. Shinde, M. Fareesuddin, S.A. Dake, S.U. Shisodaia, R.P. Pawar, *Eur. Chem. Bull.*, 2 (**2013**) 481-490.

28. M.A. Pasha, N.R. Swamy, V.P. Jayashankara, *Ind. J. Chem.*, 44 (**2005**) 823-835

29. M. Puripat, R. Ramozzi, M. Hatanaka, W. Parsuka, V. Parasuka, K. Morokuma. *J. Org. Chem.*, 80 (**2015**) 6569-6580.

30. M. Brose, M. Patil, N. Patil, R. Shinde, *ISRN. Org. Chem.*, 6 (**2012**).

31. M.M. Duvenhagel, O.M. Ntwaeborwal, H.G. Visser, H.C. Swart, *Phys. Condens. Matter.*, 439 (2014) 46-49.

32. T. Sutradhar, A. Misra, *J. Phys. Chem. A.*, 122 (**2018**) 4111-4120.

33. K. Yasuhiro, O. Yousuke, F. Kazumasa, M. Masaki, *J. Org. Chem.,* 78 (**2013**) 7058-7067.

34. Y. Takakazu, L.L. Bang, *Macromolecules,* 35 (**2002**) 2993-2999.

35. A. Esvet, L. Abdulkadir, G. Selçuk, R.S. Mehmet, A. *Bull. Korean Chem. Soc.,* 31 (**2010**) 3632-3638.

36. D. Stephane, S.H. Garry, W.G. Skene, *J. Phys. Chem. B.*, 111 (**2007**) 11407-11418.

37. L. Leonat, S. Gabriela, I.V. Branzoi, *UPB Sci. Bull. Ser. B.,* 75 (**2013**) 111-119.

38. I. Fleming, Wiley., (**1977**).

39. R. Parr, G. Donnelly, R.A. Lev, M.W.E. Palke, *J. Chem. Phys.,* 68 (**1977**) 3801-3807.

40. P. Udhayakala, T.V. Rajendiran, S. Gunasekaran, *J. Comput. Methods Mol. Des.,* 21 (**2012**) 1-15.

41. U. Vanitha, R. Elancheran, V. Manikandan, S. Kabilan, K. Krishnasamy, *J. Mol. Struct*., 1246 (**2021**) 131212-131223.

42. J. Janczak, *J. Polyhed.,* 38 (**2012**) 75-87.

43. M. Dhanalakshmi, H. Nagabhushana, G.P. Darshan, R.B. Basavaraj, B.D. Prasad, *J. Sci. Adv. Mater. Devices.,* 2 (**2017**) 22-33.

44. J. Lee, M.M. Joulli´e, *Tetra. Lett*., 56 (**2015)** 3378-3381.

45. D. Navami, R.B. Basavaraj, G.P. Darshan, H.K. Inamdar, S.C. Sharma, H.B. Premkumar, H. Nagabhushana, *J. Optic. Mat.,* 88 (**2018**) 479-487.

46. K. Upendranath, T. Venkatesh, T.N. Lohith, M.A. Sridhar. *J. Mol. Stru*., 1264 (**2022**) 133231-133244.

47. M. Sham, Sondhi, N. Singh, A. Kumar, O. Lozach, *Bioorg. Med. Chem.*, 14 (**2006**) 3758-3765.

48. B. Andreas, Schreiner, E.P. Wolf-Winiski, A.G. Barlara Noverkis, 1991, 1999-27439, GB (**2001**) *2000-7511 Patent CA Section: 28 Section 1, 2, 32*.

CHAPTER-3

Development and visualization of level II, III features of latent fingerprints using some new 4-(4-substitutedphenyl)-6-(4-substitutedphenyl)-2-oxo-1,2-dihydropyridine-3-carbonitrile derivatives: Synthesis, characterization, optoelectronic and DFT studies

3.1. Introduction

Recent years, fingerprints are used in personal identifications such as mobile locks, banking sectors and biometric sensors, and they are considered primary evidence in the criminal investigations due to their unique identification [1-3]. There are two types of fingerprints were used to visualize crime spots, *i.e*. patent fingerprints and latent fingerprints (LFPs). LFPs are categorized into three different levels such as levels I, II and III. level I, consist of a whorl, arch and loop and level II consist of a core, delta and bifurcation [4]. Similarly, level III deals with pores, ridge path deviation, edge contour, breaks, creases, and scars [5]. Level III of finger marks give accurate quantitative data on each fingerprint and predominantly in fragmentary fingerprint comparison [6].

Many different techniques have been approached to visualize the LFPs through chemical reagents, such as silver nitrate spraying, powder dusting, ninhydrin and iodine fuming etc., [7]. From these techniques, the powder dusting method is one of the simplest methods by using organic fluorescent materials at crime spots without background hindrance [8].

Pyridine with electron-donating (D) and electron-accepting (A) groups are linked by a π-conjugated bridge that exhibits broad and intense absorption and emissions properties. Hence, it can be used as optoelectronic oriented materials [9, 10]. Pyridine is linked through a π-conjugated bridge and due to their chemical reactivity, π-deficient in nature, greater dipole moment and electron-deficient carbon atoms at α, β positions, and ring aromaticity. [11, 12]. The cyanopyridines and cyanopyridones are shows excellent photochemical and thermal stability with good optoelectronic properties. Moreover, cyano group have known as the better electron-

withdrawing group due to their smaller size and excellent behaviour under UV radiation [13].

Multicomponent reactions (MCRs) are one of the easiest methods for synthesizing poly-functional molecules in a single-step reaction with high competence over multistep synthesis [14]. Generally, MCRs are an efficient tool for the synthesis of new and several active drug molecules with advantages such as avoiding unnecessary expensive purification, high atom economy, toxic reagents and solvent consumptions. Over the past decades, polyfunctional molecules were gain interest to use as organic fluorescent materials in light-emitting fields and forensic science [15]. Some of the newly reported important cyanopyridine derivatives have been discussed below.

Hemanth *et al.,* reported a new 2-methoxy-4-(2-methoxynaphthalen-1-yl)-6-(thiophen-2-yl) nicotinonitrile (**1**) in the year 2020. The obtained compound has derived by the reaction of 2-methoxy-thiophene substituted naphthalene chalcone is reacted with malononitrile in presence of sodium ethoxide under solvent media. The compound has been tested for fluorescence properties in DMSO, and emission bands have appeared at longer wavelength 470 nm to 590 nm. Further, compounds were evaluated for CIE coordinates which emit in the orange region [16].

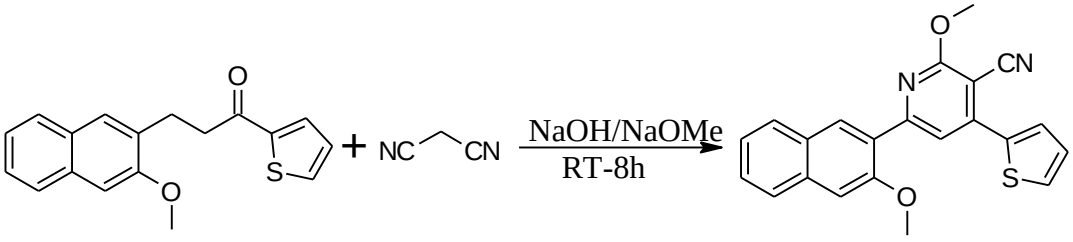

(1)

Feng Shi and co-workers reported an 2-amino-3-cyanopyridine derivatives (**2**) under microwave irradiation with ammonium acetate as catalyst in 2015. Synthesized compounds tested for luminescent properties and emission bands were obtained at blue regions of 500 nm-700 nm [17].

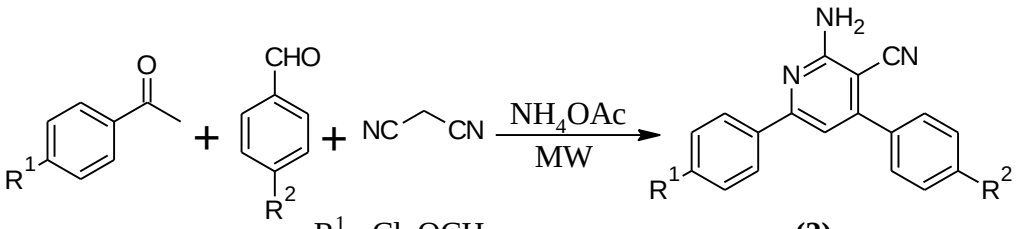

R^1= Cl, OCH_3,
R^2=Cl_2, F, CH_3, OCH_3

(2)

C. Trupthi Devaiah *et al.*, reported a series of new cyanopyridone derivatives (**3**) in 2016, by the reaction of aromatic acetophenones and substituted aldehydes with ethyl cyanoacetate in dioxane solvent using ammonium acetate. These synthesized derivatives were suited for optoelectronic properties, compounds were emitted at 550 nm to 625 nm and shows better redox behavior [18].

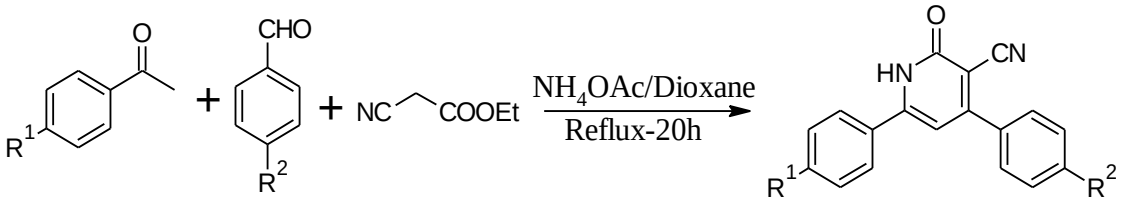

R^1= Br, Br
R^2= CH_3, CH_3

(3)

Manohara *et al.*, reported a 4-(3,4-dialkoxyphenyl)-2-methoxy-6-(ptolyl) nicotinonitrile (**4**) in 2017 by the reaction of chalcone and malononitrile in MeOH using sodium methoxide as a catalyst at room temperature for 24 h. The output of the research work is compounds have shown fine redox behavior in aqueous electrolyte. Optical properties of both absorption and emission bands are obtained at 384 nm to 578 nm of longer wavelength [19].

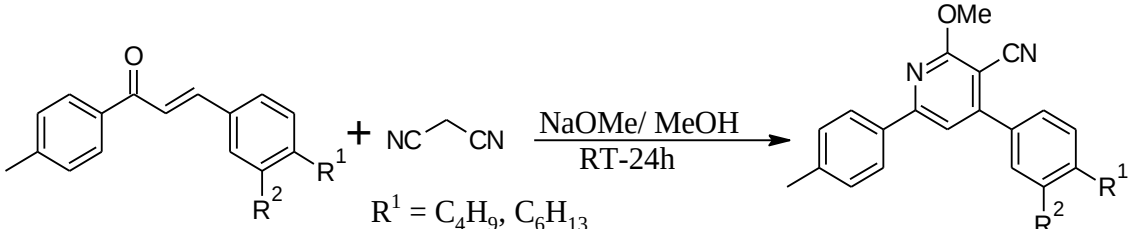

R^1 = C_4H_9, C_6H_{13}
R^2 = C_8H_{17}, $C_{16}H_{33}$

(4)

Dariush Khalili *et al.*, has carried out a one-pot synthesis of 2-amino-3-cyanopyridine derivatives (**5**) and reported in the year 2019, Graphene oxide was used as a reusable catalyst in an aqueous solvent. Synthesized derivatives were analyzed for their photophysical properties, where the optical properties of synthesized compounds show absorption bands at redshift (320 nm to 480 nm) and emit better solvatochromic behavior under UV radiation [20].

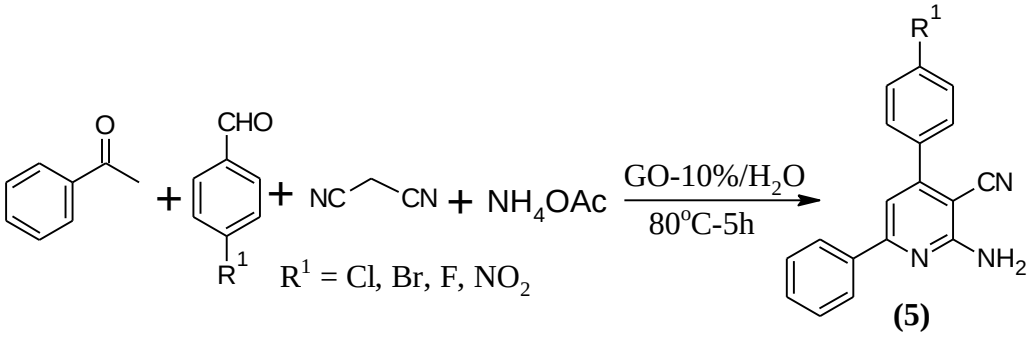

(5)

Swathi *et al.,* reported a new series of cyanopyridine derivatives (**6**) was obtained by the reaction of 2-acetyl thiophene with aldehyde in presence of ammonium acetate under solvent media. The targeted derivatives were analyzed for fluorescence properties, where all the emission bands are observed at the bathochromic shift of 450 nm to 600 nm [21].

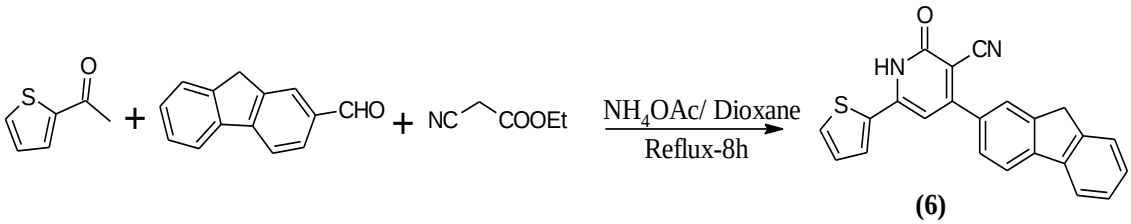

(6)

3.2. Present work.

In this chapter, we have synthesized novel cyanopyridine derivatives **4**(**a-d**) by one-pot synthesis of substituted acetophenones (**1**) substituted benzaldehydes (**2**) and ethyl cyanoacetate (**3**) in 20 mL ethanol using NH_4OAc as a catalyst and studied their optoelectronic, DFT and Latent fingerprint applications. The mode of reaction has been represented in **Scheme 3.**

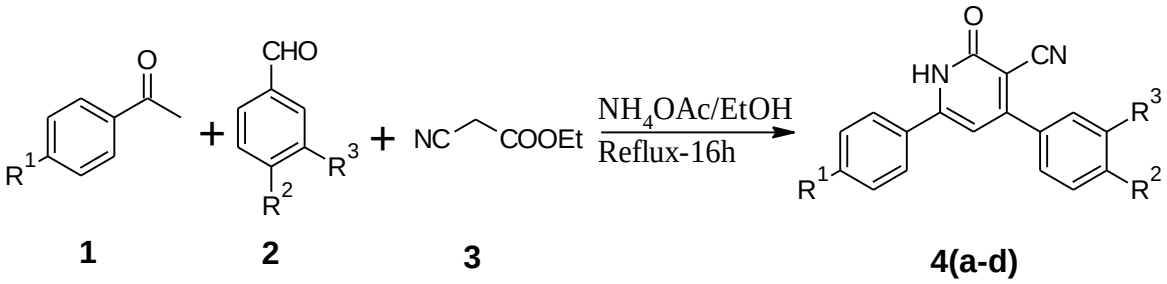

Entry	R^1	R^2	R^3
4a	OH	NO_2	H
4b	OH	Cl	NO_2
4c	NO_2	OH	OH
4d	NO_2	Br	H

Scheme 3: Synthesis of new 4-(4-substitutedphenyl)-6-(4-substitutephenyl)-2-oxo-1,2-di-hydropyridine-3-carbonitrile derivatives **4**(**a-d**).

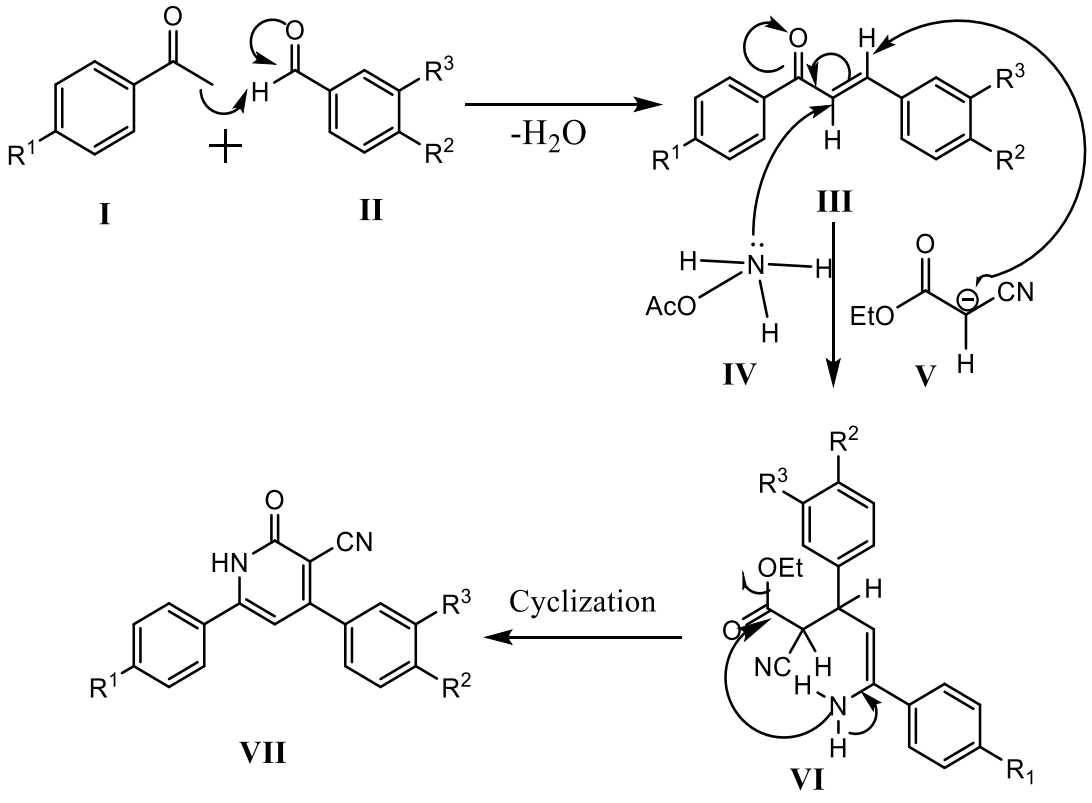

Fig. 3.1. Plausible mechanism of synthesized new 4-(4-substitutedphenyl)-6-(4-substitutedphenyl)-2-oxo-1,2-di-hydropyridine-3-carbonitrile derivatives **4**(**a-d**).

In the above mechanism (**Fig. 3.1**), the formation of α, β-unsaturated ketones from p-substituted acetophenones (**I**) and substituted aldehydes (**II**) as intermediate

by nucleophile attack and elimination of water (**III**). Nucleophilic attack from the lone pair of electrons of nitrogen atom from ammonium acetate (**IV**) and ethyl cyanoacetate (**V**) to α, β-unsaturated ketones through Michael addition reaction gives the intermediate (**VI**), further, cycloaddition and aromatization to afford the final product (**VII**).

In this work, we have concentrated on different reaction parameters (effect solvent, catalyst and temperature) to know the progress of the reaction. Initially, we tried the reaction by varying solvent media, other than ethanol we didn't find any greater yield and with the same solvent media, we continued the reaction by varying catalysts. Among the used catalyst ammonium acetate was found good catalyst and obtained a greater yield, similarly, the same reaction was carried out using different time period and was to find a greater yield in 16 h. Hence, we concluded that the reaction in ethanol as solvent and ammonium acetate as a catalyst with respect to time and temperature gives a high yield of synthesized targets (**Table 3.1**) [21, 22].

Table 3.1. Effect of reaction parameter of compound **4a.**

Entry	Catalyst	Solvent	Temperature (°C)	Time (h)	Yield (%)
1	**NH_4OAc**	**Ethanol**	**Reflux**	**16**	**89**
2	NH_4OAc	Water	Reflux	48	62 [31]
3	NH_4OAc	1,4-Dioxane	80	8	70 [33]
4	K_2CO_3	Ethanol	80	12	80 [32]
5	NH_4OAc	1,4-Dioxane	80	20	75 [25]
6	$ZnCl_2$	Ethanol	R.T.	12	38 [31]

3.2.1 Spectral Characterization.

Different spectroscopic techniques such as FT-IR, ^{1}H-NMR, ^{13}C-NMR, and HRMS were applied to confirm the structures of new compounds **4**(**a-d**).

The FTIR spectrum of **4a** showed a strong stretching vibration band at 3450 cm^{-1} correspond to the OH group and another band at 3331 cm^{-1} due to starching vibration of NH functionality of the pyridine ring. The sharp band was observed at 2205 cm^{-1} correspond to C≡N functionality and another absorption band at 1655 cm^{-1} correspond to C=O stretching frequency. In ^{1}H-NMR we observed two singlet peaks at δ 12.73 and 10.27 ppm due to two NH and OH protons of pyridine and phenyl rings respectively. A doublet peak obtained at δ 8.40-8.38 ppm for two aromatic protons and another doublet peaks were observed at 7.99-7.97 ppm corresponds to two aromatic protons. Similarly, another doublet peaks at 7.81-7.79 ppm for two aromatic protons, and 6.89-6.87 doublet peaks were observed at 6.89-6.87 for another two aromatic protons. A singlet peak has been observed at δ 6.79 ppm corresponds to the pyrimidine proton of the pyridine ring. In ^{13}C-NMR: a signal appears at 161.17 ppm corresponds to carbonyl carbon functionality, and signals at 148.82 ppm to 124.82 ppm correspond to the C=C groups. The HRMS showed a molecular ion peak [M^{+}1] at m/z is 334.0794 corresponding to a molecular weight of the compound **4a.**

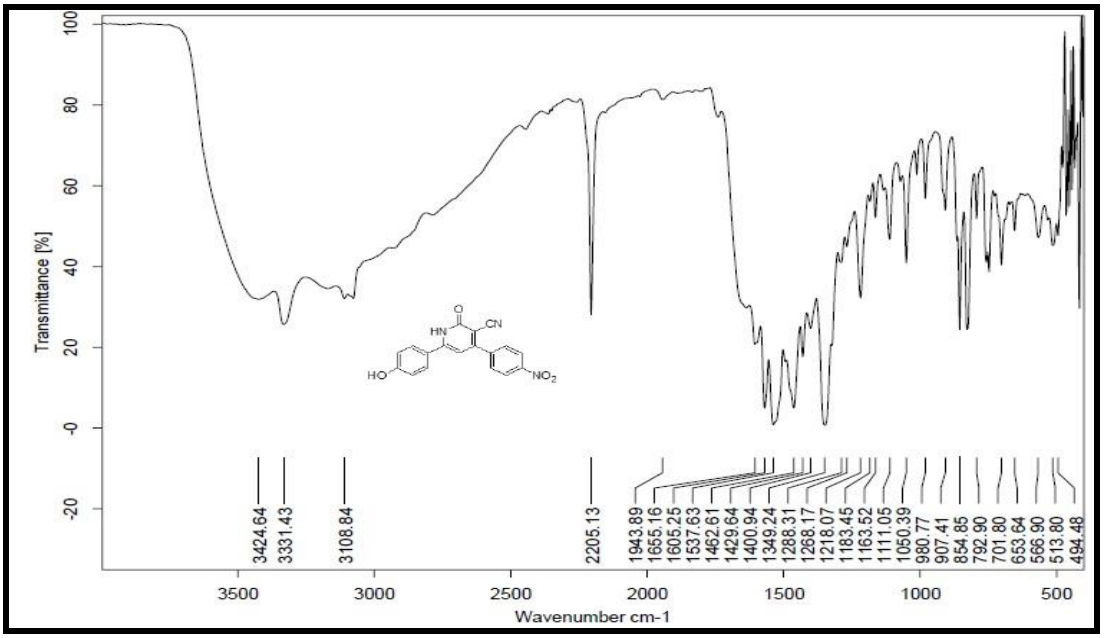

FTIR spectrum of compound 4a

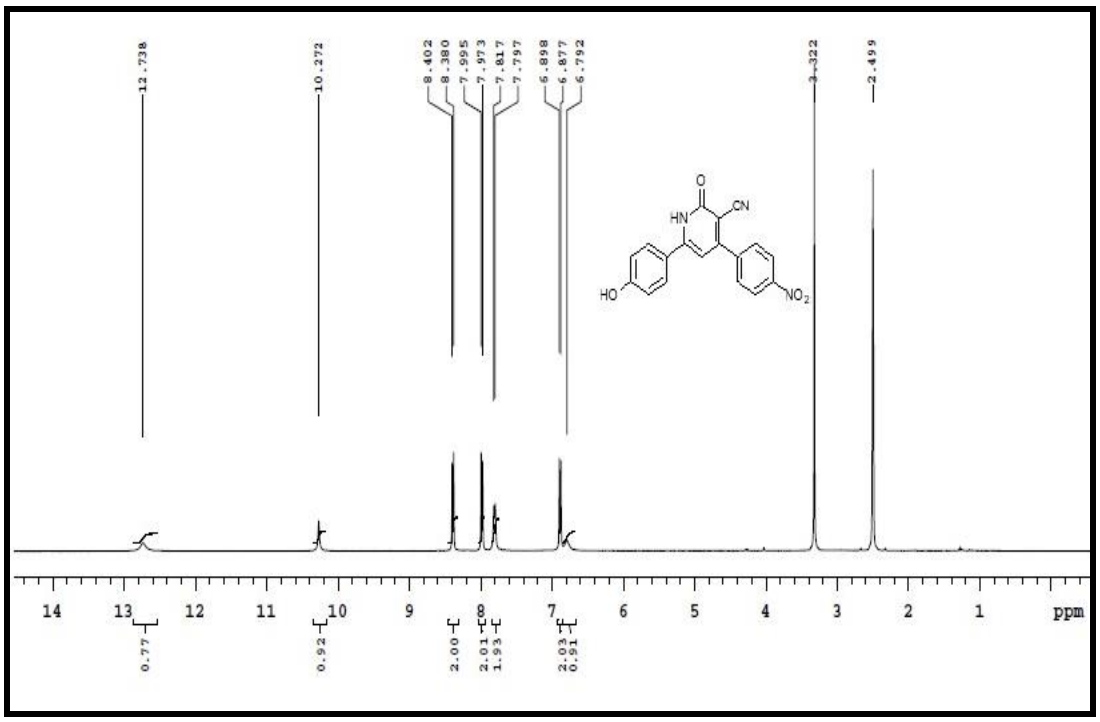

^{1}H-NMR spectrum of compound 4a

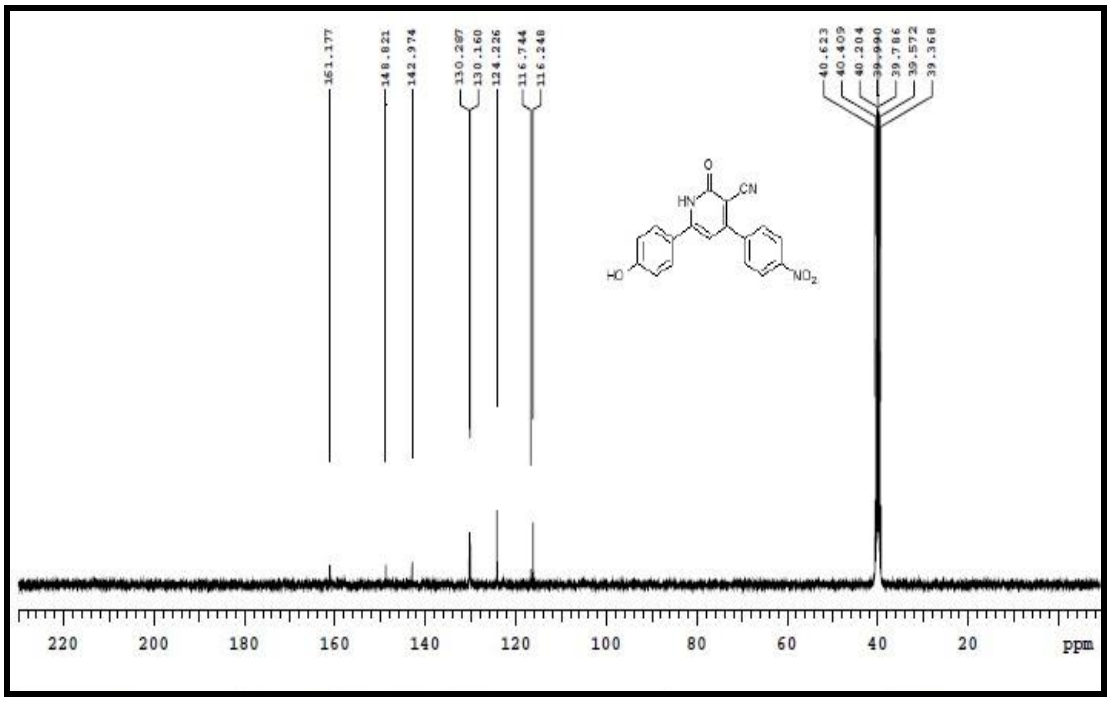

^{13}C-NMR spectrum of compound 4a

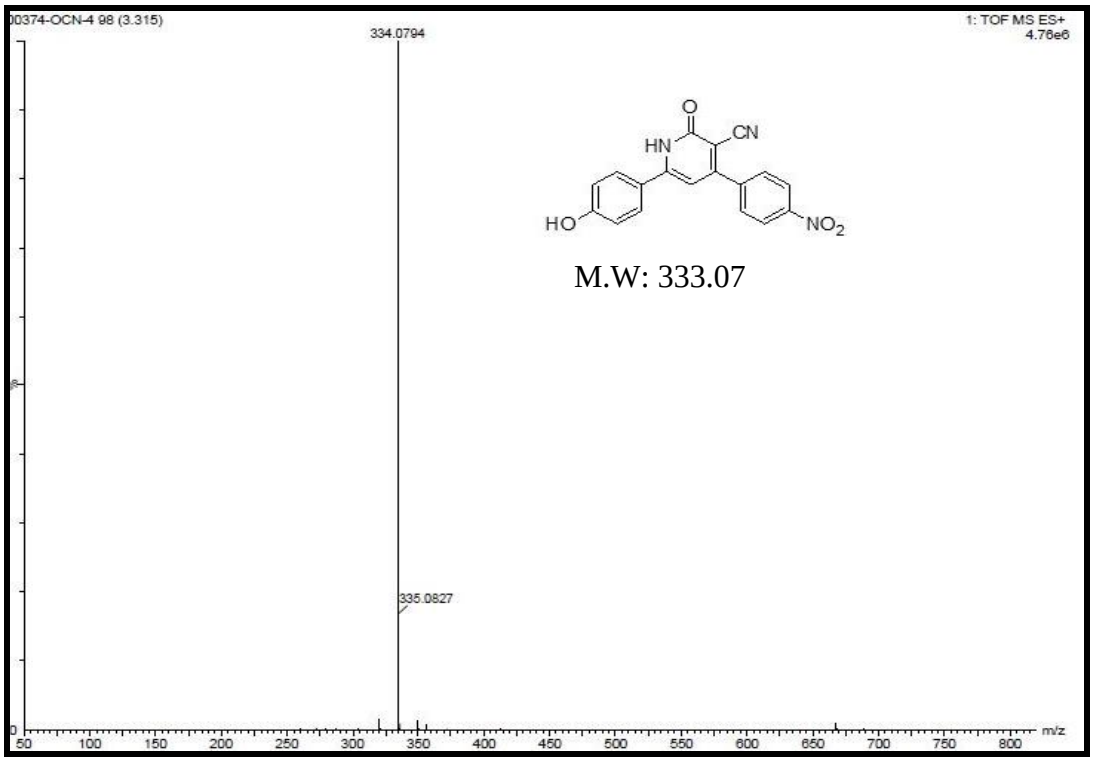

Mass spectrum of compound 4a

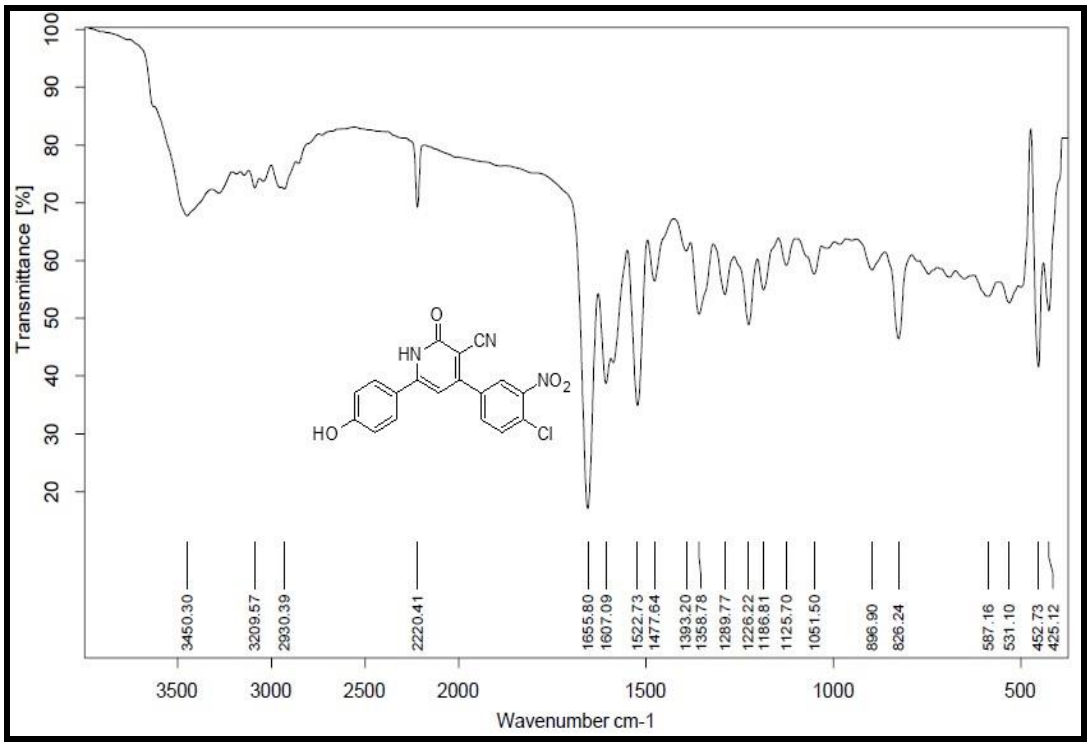

FTIR spectrum of compound 4b

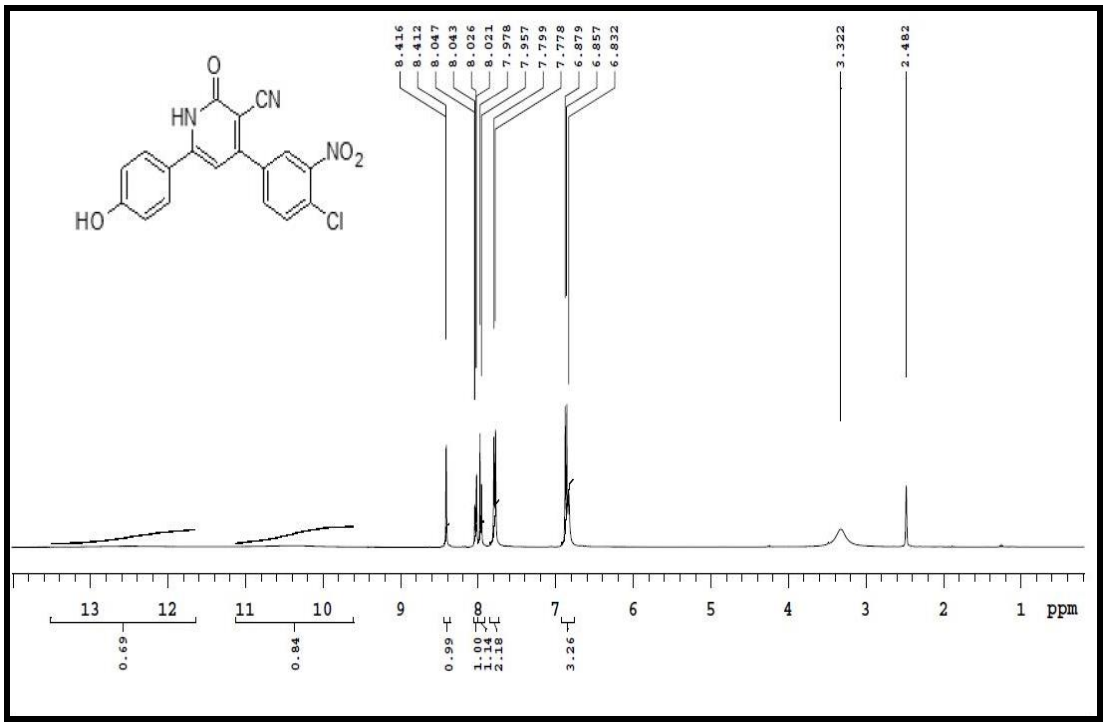

[1]H-NMR spectrum of compound 4b

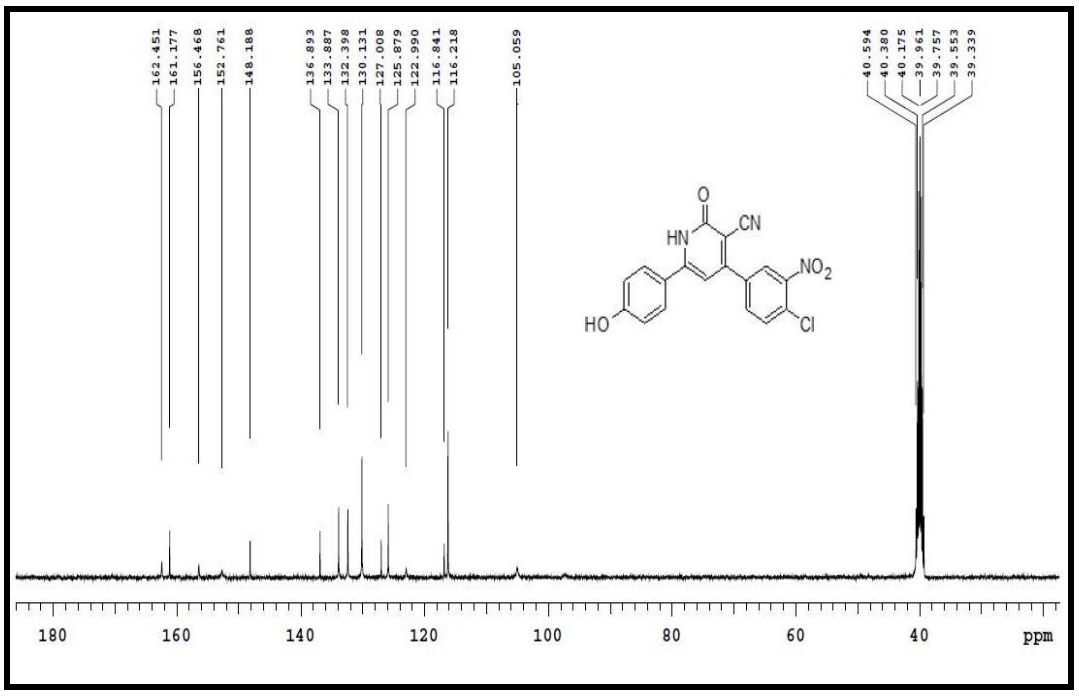

[13]C-NMR spectrum of compound 4b

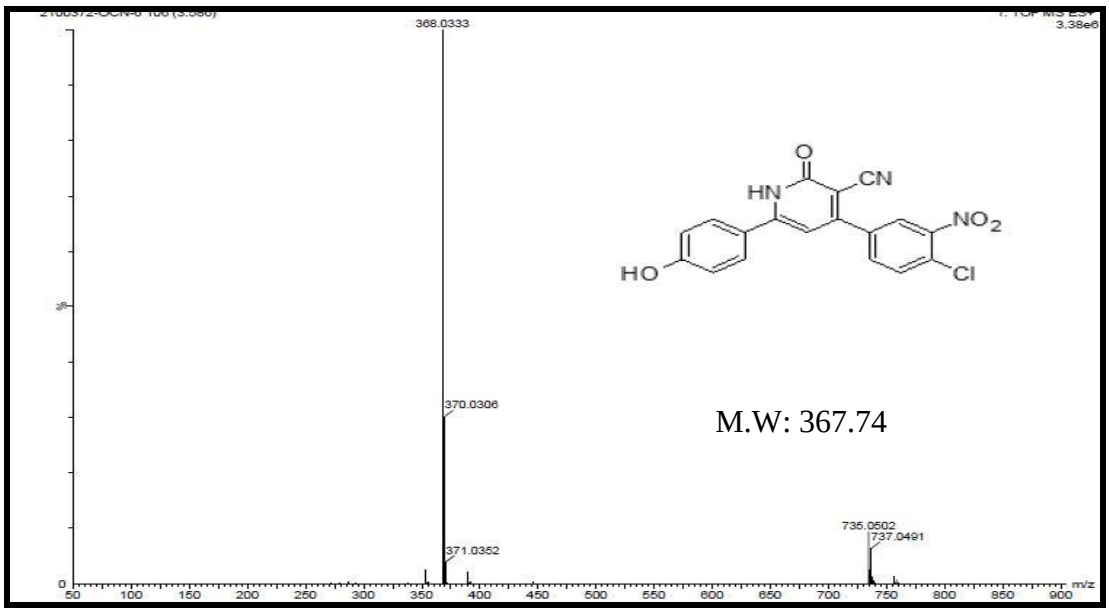

Mass spectrum of compound 4b

3.3 Experimental

3.3.1 General Information.

Details about purchased chemicals, reagents, and the used instrument for analysis, have been explained with an experimental procedure such as electrochemical, theoretical studies and development of LFPs in the previous **Chapter-2A** section **2A.3**.

3.3.2 General Procedure for one-pot synthesis of 4-(4-substitutedphenyl)-6-(4-substitutedphenyl)-2-oxo-1,2-di-hydropyridine-3-carbonitrile derivatives 4(a-d).

In a 100 mL round bottom flask, *p*-substituted acetophenones (**1**) (1 mM), substituted benzaldehydes (**2**) (1 mM), and ethyl cyanoacetate (**3**) (1.2 mM) were dissolved in (20 mL) ethanol. Quick addition of NH_4OAC (8 mM) as a catalyst to the reaction mixture was kept under the reflux temperature with constant stirring for about 16 h. progress of the reaction was monitored by TLC (ethyl acetate and pet. ether) and a colored crude precipitate was obtained after cooling at room temperature. Obtained crude filtered, dried, and recrystallized from absolute methanol and purified using column chromatography on silica gel with ethyl acetate and hexane (v/v, 1:10) to get pure targets **4**(**a-d**).

6-(4-Hydroxyphenyl)-4-(4-nitrophenyl)-2-oxo-1,2-dihydropyridine-3-carbonitrile (4a):

Yellow powder; Yield: 89 %; MP: <300 °C; Mol. Formula: $C_{18}H_{11}N_3O_4$; IR (υ, cm^{-1}): 3425 (OH), 3331 (NH), 3108 (C-H), 2205 (C≡N), 1655 (C=O), 1573 (C-NO_2), 1462 (C=C); ^{1}H-NMR (δ ppm): 12.73 (s, 1H, NH), 10.27 (s, 1H, OH), 8.40-8.38 (d, *J* = 8 Hz, 2H, Ar-H), 7.99-7.97 (d, *J* = 8 Hz, 2H, Ar-H), 7.81-7.79 (d, *J* = 8 Hz, 2H, Ar-H), 6.89-6.87 (d, *J* = 8 Hz, 2H, Ar-H), 6.79 (s, 1H, Pyridine CH); ^{13}C-NMR (δ ppm): 161.17 (C=O), 148.82, 142.97, 130.28, 130.16, 124.22 (C=C) 116.74 (C-C≡N), 116.24; HRMS (m/z): 334.0794 [M^+1]; Anal. Cal. for C 64.86, H 3.33 & N 12.61 %; Found: C 63.95, H 3.26 & N 11.97 %.

4-(4-Chloro-3-nitrophenyl)-6-(4-hydroxyphenyl)-2-oxo-1,2-dihydropyridine-3-carbonitrile (4b):

Yellow powder; Yield: 86 %; MP: <300 °C; Mol. Formula: $C_{18}H_{10}ClN_3O_4$; IR (υ, cm^{-1}): 3450 (OH), 3210 (NH), 2220 (C≡N), 1656 (C=O), 1522(C-NO_2), 1477 (C=C), 826 (C-Cl); ^{1}H-NMR (δ ppm): 12.50 (s, 1H, NH), 10.50 (s, 1H, OH), 8.42-8.41 (d, *J* = 4 Hz, 1H, Ar-H), 8.04-8.02 (dd, *J* = 8 Hz, 1H, Ar-H), 7.97-7.95 (d, *J* = 8 Hz, 1H, Ar-H), 7.79-7.77 (d, *J* = 8 Hz, 2H, Ar-H), 6.87-6.85 (d, *J* = 8 Hz, 2H, Ar-H), 6.83 (s, 1H, Pyridine CH); ^{13}C-NMR (δ ppm): 162.45 (C=O), 161.17 (C-NH), 156.46, 152.76, 148.18, 136.89, 133.88, 132.39, 130.13, 127.00, 125.99 (C=C), 116.84, 116.21 (C-C≡N), 105.05 (C=C-H); HRMS (m/z): 368.0333 [M^+1] and 370.0306 [M^+2]; Anal. Cal. for C 58.79, H 2.74 & N 11.43 %; Found: C 57.98, H 2.57 & N 11.27 %.

4-(3,4-Dihydroxyphenyl)-6-(4-nitrophenyl)-2-oxo-1,2-dihydropyridine-3-carbonitrile (4c):

Orange powder; Yield: 87 %; MP: <300 ºC; Mol. Formula: $C_{18}H_{11}N_3O_5$; IR (υ, cm^{-1}): 3426 (OH), 3296 (NH), 2218 (C≡N), 1656 (C=O) 1518, 1431 (C=C); ^{1}H-NMR (δ ppm): 12.50 (s, 1H, NH), 9.64 (s, 1H, OH), 9.35 (s, 1H, OH), 8.32-8.30 (d, *J* = 8 Hz, 2H, Ar-H), 8.16-8.13 (d, *J* = 9.2 Hz, 2H, Ar-H), 7.18-7.17 (d, *J* = 4 Hz, 1H, Ar-H), 7.09-7.07 (dd, *J* = 8 Hz, 1H, Ar-H), 6.89-6.87 (d, *J* = 8 Hz, 1H, Ar-H), 6.84 (s, 1H, Pyridine CH); ^{13}C-NMR (δ ppm): 149.00 (C=C), 148.65, 145.89, 129.63, 127.02, 124.21, 120.81, 117.08, 116.17 (C-C≡N), 116.13; HRMS (m/z): 350.0636 [M^+1]; Anal. Cal. for C 61.89, H 3.17, & N 12.03 %; Found: C 61.75, H 3.12 & N 12.00 %.

4-(4-Bromophenyl)-6-(4-nitrophenyl)-2-oxo-1,2-dihydropyridine-3-carbonitrile (4d):

Yellow powder; Yield: 83 %; MP: <300 ºC; Mol. Formula: $C_{18}H_{10}BrN_3O_3$. IR (υ, cm^{-1}): 3445 (OH), 3216 (NH), 2208 (C≡N), 1664 (C=O), 1531 (C-NO_2), 1491 (C=C), 699 (C-Br). ^{1}H-NMR (δ ppm): 8.29-8.27 (d, *J* = 8 Hz, 2H, Ar-H), 8.26-8.24 (d, *J* = 8 Hz, 2H, Ar-H), 7.75-7.73 (d, *J* = 8 Hz, 2H, Ar-H),7.64-7.62 (d, *J* = 8 Hz, 2H, Ar-H), 6.95 (s, 1H, Pyridine CH); ^{13}C-NMR (δ ppm): 168.07 (C=O), 156.13, 154.24, 148.44, 143.28, 136.83, 132.04, 130.81, 129.03, 124.02, 123.55 (C=C), 116.74 (C-C≡N), 106.60 (C=C-C), 95.92 (C-Br); HRMS (m/z): 395.9859 [M^+1] and 397.9841[M^+2]; Anal. Cal. for C 54.57, H 2.54, and N 10.61 %; Found: C 54.39, H 2.28, and N 10.40 %.

3.4 Results and Discussion

3.4.1 Absorption properties.

Both absorption and emission properties have been studied for synthesized compounds **4**(**a-d**) using a UV-Visible spectrophotometer at 3×10^{-6} M concentration using different solvents as shown in **Fig.3.2 (a-d)**. Here, all the compounds observed dual absorption bands at near-visible regions due to π-π* transitions and aromatic conjugation [24 25]. Compound **4a** has shown two absorption bands at ~304-400 nm of bathochromic shift due to the presence of electron-donating hydroxyl and electron-withdrawing nitro groups, which are strongly interacting through the solvent system and influence to move at the longer wavelength. Similarly, compound **4b** has also shown dual peaks in all polar solvents except ethyl acetate at 390 nm due to the lower dielectric constant of solvent and less interaction of solute-solvent because of the electron-withdrawing chloro group. Further, compound **4d** shows dual absorption bands in a high polar solvent and a single band in a less polar solvent due to the presence of an electron-withdrawing bromo group. Moreover, a more planar framework greater the extent of delocalization of π-electrons which increases the band gap and absorption peaks at the longer wavelength [26 27]. The optical band has been calculated using equation (1) [28]. The absorption spectral values are summarized in **Table 3.2**.

$$E_g = 1240/\lambda_{onset}\text{eV} \qquad \text{— (1)}$$

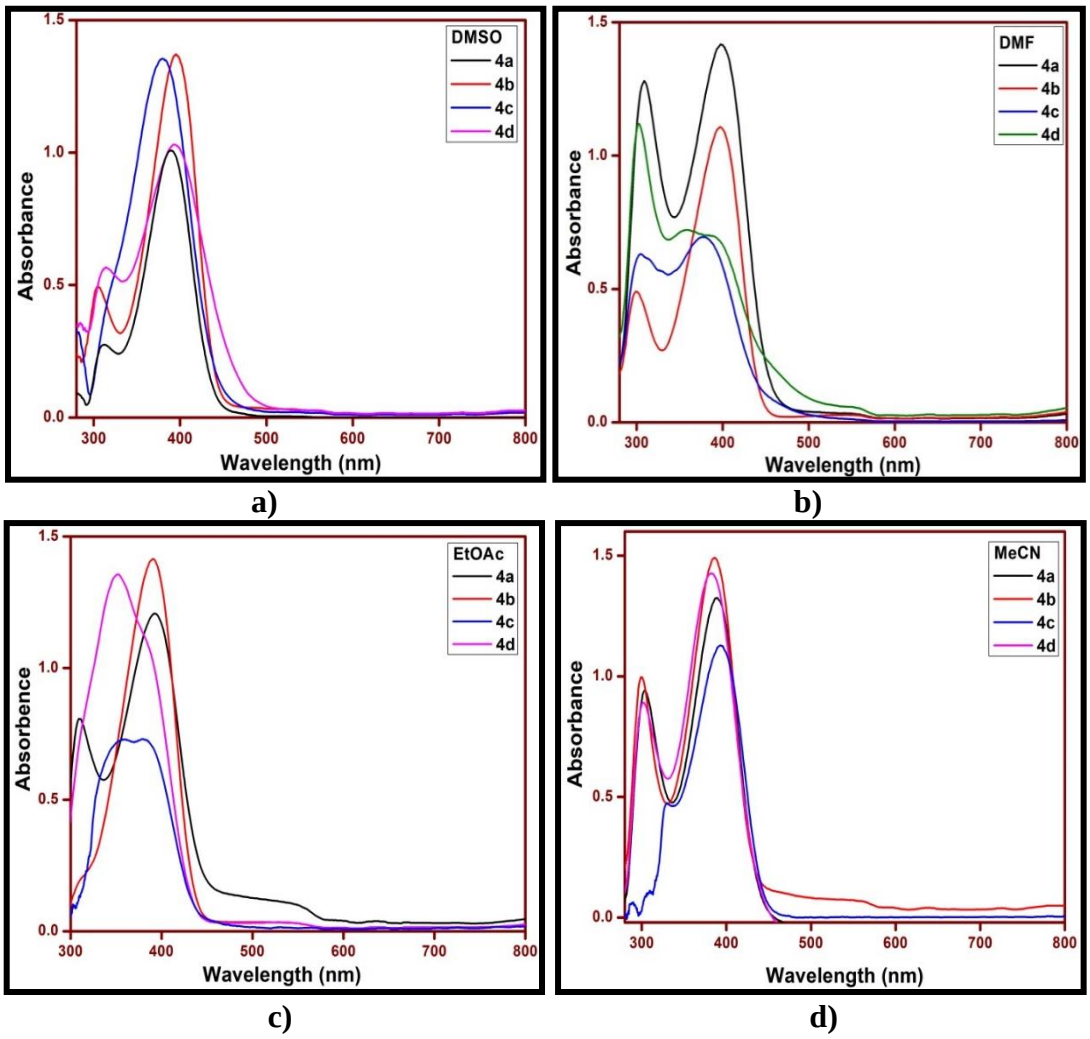

Fig. 3.2. Electronic absorption spectra of synthesized compounds **4**(**a-d**) in different solvents **a**), Di-methyl sulphoxide **b**), N, N- dimethyl formamide, **c**), Ethyl acetate **d**), Acetonitrile 3×10^{-6} M.

Table 3.2. Electronic absorption spectral data of synthesized compounds **4**(**a-d**).

Solvents	Entry	λ_{abs} (nm)	E_g^{OTP}(eV)	Molar absorptivity ($\varepsilon \times 10^{-5}$ L mol^{-1} cm^{-1})
DMSO	**4a**	312, 399	3.98 & 3.11	1.5 & 2.4
DMF		304, 400	4.08 & 3.10	2.1 & 2.3
Ethyl Acetate		309, 392	4.01 & 3.16	1.3 & 2.0
Acetonitrile		304, 390	4.08 & 3.18	1.5 & 2.2
DMSO	**4b**	306, 396	4.05 & 3.13	0.8 & 2.2
DMF		299, 397	4.15 & 3.12	0.7 & 1.6
Ethyl Acetate		390	3.18	2.3
Acetonitrile		300, 386	4.14 & 3.21	1.6 & 2.3
DMSO	**4c**	380	3.26	2.2
DMF		304, 381	4.08 & 3.25	1.0 & 1.1
Ethyl Acetate		376	3.73	0.81
Acetonitrile		300, 375	4.14	1.4 &1.8
DMSO	**4d**	314, 395	3.64 & 3.14	0.9 & 1.7
DMF		302, 391	4.11 & 3.17	1.8 & 1.1
Ethyl Acetate		353	3.51	2.2
Acetonitrile		302, 383	4.11 & 3.24	1.4 & 2.3

3.4.2 Photoluminescence properties.

All the compounds were emitted with respect to excitation values at longer wavelength ~467-547 nm (**Fig. 3.3**). Maximum spectral differences between absorption and emission are said to be stokes shift, hence **4a** and **4b** gives the 68 nm and 74 nm stokes shift at longer wavelength respectively. Similarly, compounds **4c** and **4d** have shown 153 nm and 152 nm stokes shifts. While compounds **4c** and **4d** has shown higher stokes shift values, this is due to the presence of electron-donating (Hydroxy) groups and electron-withdrawing (Bromo) group present on the benzene ring [29].

Moreover, the stokes shift was caused by the solute and solvent interaction and is also influenced by the aromatic π-conjugation system. Further, fluorescence quantum yield was calculated with standard reference procedure using quinine sulphate in 0.1 M sulfuric acid as a standard (Φf = 0.54) and compounds gives Φf = 0.28, 0.34, 0.45, and 0.49 respectively [30, 31]. The emission spectral data along with calculated stokes shift and quantum yield values were appended in **Table 3.3** and quantum yield has been calculated using equation (2) [32].

$$QE = \left(\frac{AR.Es.ns}{As.Er.nr}\right)^2 \qquad \text{— (2)}$$

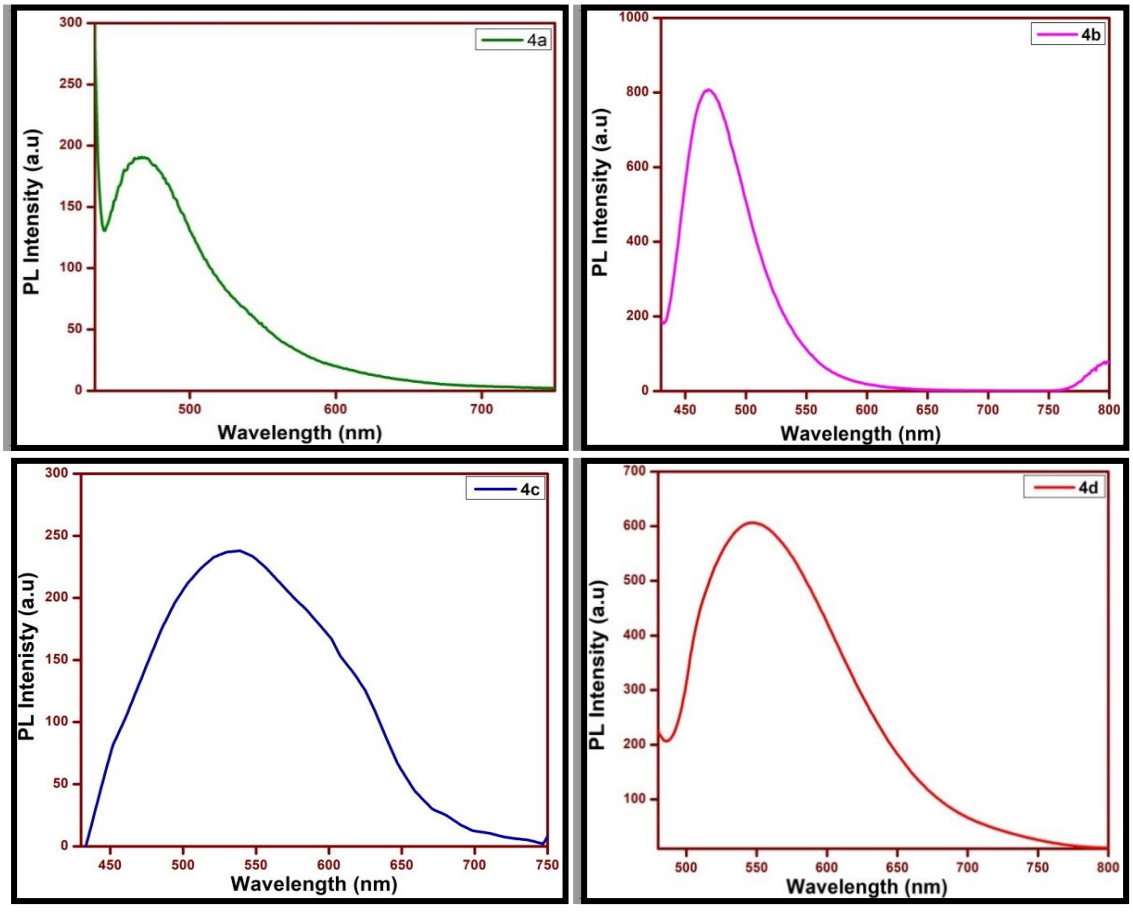

Fig. 3.3. Photoluminescence spectra of synthesized compounds in DMSO **4**(**a-d**).

Table 3.3. Photoluminescence spectral data of synthesized compounds **4**(**a-d**).

Entry	Solvent	λ_{exc} (nm)	λ_{emi} (nm)	Stokes shift (nm)	Φf
4a	DMSO	399	467	68	0.28
4b		396	470	74	0.34
4c		380	533	153	0.45
4d		395	547	152	0.49

3.4.3 CV study.

Electrochemical behavior of synthesized compounds **4**(**a-d**) has been studied using three-electrode system in CH instrument at increasing scan rates 10 mVs^{-1} to 50 mVs^{-1}. The cathodic reduction and anodic oxidation peak current were observed and the estimated redox onset potential was used to calculate experimental (E_{HOMO}-E_{LUMO}) energy molecules. Obtained results are appended in **Table 3.4**.

All the measurements were calibrated using the internal standard ferrocene. A noteworthy result was found that dual redox peaks have appeared for all the compounds as shown in **Fig. 3.4**. The compounds **4a**, **4b** and **4c** have shown quasi reversibility of electron transfer and show dual cathodic current peak (E_{pc}) and anodic peak current (E_{pa}) at -0.02 V & 0.39 V, -0.02 V & 0.38 V, -0.04 V & 0.39 V and 0.11 V & 0.46 V, 0.21 V & 0.47 V, 0.25 V & 0.49 V due to influence of electron-donating hydroxyl and withdrawing nitro groups present on phenyl ring respectively. Similarly, compound **4d** have shown quasi-reversibility of electron transfer -0.06 V & 0.32 V, -0.13 V & 0.53 V because of two electron-withdrawing nitro and bromide group, hence it appears the cathodic peak current at 0.07 V & 0.45 V, 0.17 V & 0.54 V and anodic peak current at 0.53 V respectively.

E_{HOMO} and E_{LUMO} have been calculated experimentally by substituting the redox onset potentials obtained from CV measurements using equations (3) and (4). The compounds have been found higher E_{HOMO} values where electron-donating and

withdrawing groups were attached to the conjugated system at para position which increases oxidation potential by decreasing the electron density of compounds which affects the energy molecules, increase in conjugation gets lower the E_{LUMO} and higher in E_{HOMO} values [33, 34]. Hence, compounds can be used as photosensitizer materials and estimated redox onset potentials with experimentally calculated energy molecules values were summarized in **Table 3.5**.

$$E_{(HOMO)} = -[E_{(ox\text{-}onset)} + 4.4]\ eV \quad \text{— (3)}$$

$$E_{(LUMO)} = -[E_{(red\text{-}onset)} + 4.4]\ eV \quad \text{— (4)}$$

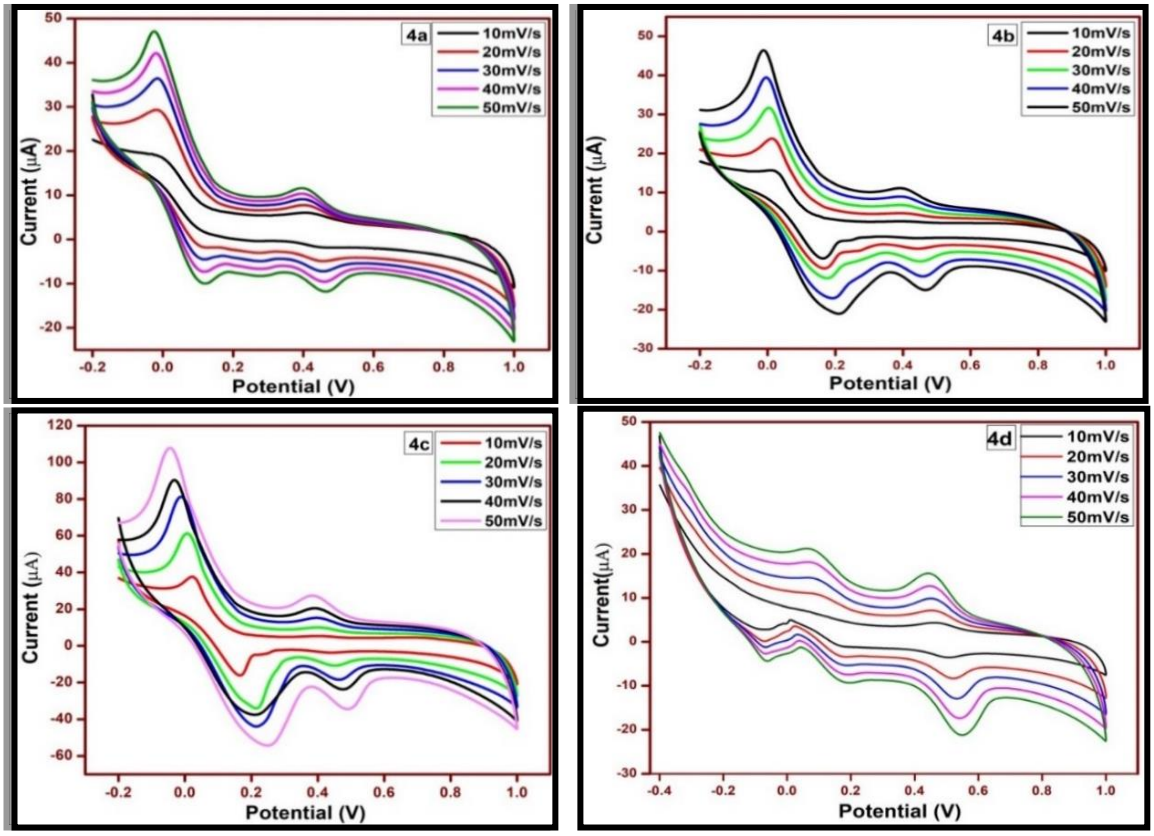

Fig. 3.4. CV studies of synthesized compounds **4**(**a-d**) at different scan rates in 1M KOH.

Table 3.4. Electrochemical parameters of synthesized compounds **4**(**a-d**).

Entry	E_{pc} (V)	E_{pa} (V)
4a	-0.02 & 0.39	0.11 & 0.46
4b	-0.02 & 0.38	0.21 & 0.47
4c	-0.04 & 0.39	0.25 & 0.49
4d	0.07 & 0.45	0.17 & 0.54

Table 3.5. Experimental redox on-sets potentials and E_{HOMO}-E_{LUMO} values of synthesized compounds **4**(**a-d**).

Entry	Reduction on set potential (V)	Oxidation on set potential (V)	E_{LUMO} (eV)	E_{HOMO} (eV)	$\Delta E = E_H - E_L$ (eV)
4a	-0.13 & 0.32	0.18 & 0.53	-4.70 & -5.12	-4.98 & -5.33	-0.28 & -0.21
4b	-0.02 & 0.30	0.37 & 0.55	-4.78 & -5.10	-5.17 & -5.35	-0.39 & -0.25
4c	-0.05 & 0.31	0.36 & 0.57	-4.75 & -4.49	-5.16 & -5.37	-0.41 & -0.88
4d	-0.06 & 0.32	0.13 & 0.53	-4.86 & 5.10	-5.33 & -5.37	-0.47 & -0.27

3.4.4 DFT study.

The entire quantum chemical calculations were carried out with the help of DFT/B3LYP method, 6-311++ G (d, p) basis set at the gaseous phase in Gaussian 09 software [35, 36].

3.4.4.1 Optimized structure.

The optimized structure of the synthesized compounds **4**(**a-d**) was subjected to geometry optimization in the ground state and the compounds were belongs to C_1 point group of symmetry as shown in **Fig. 3.5** with atom numbers.

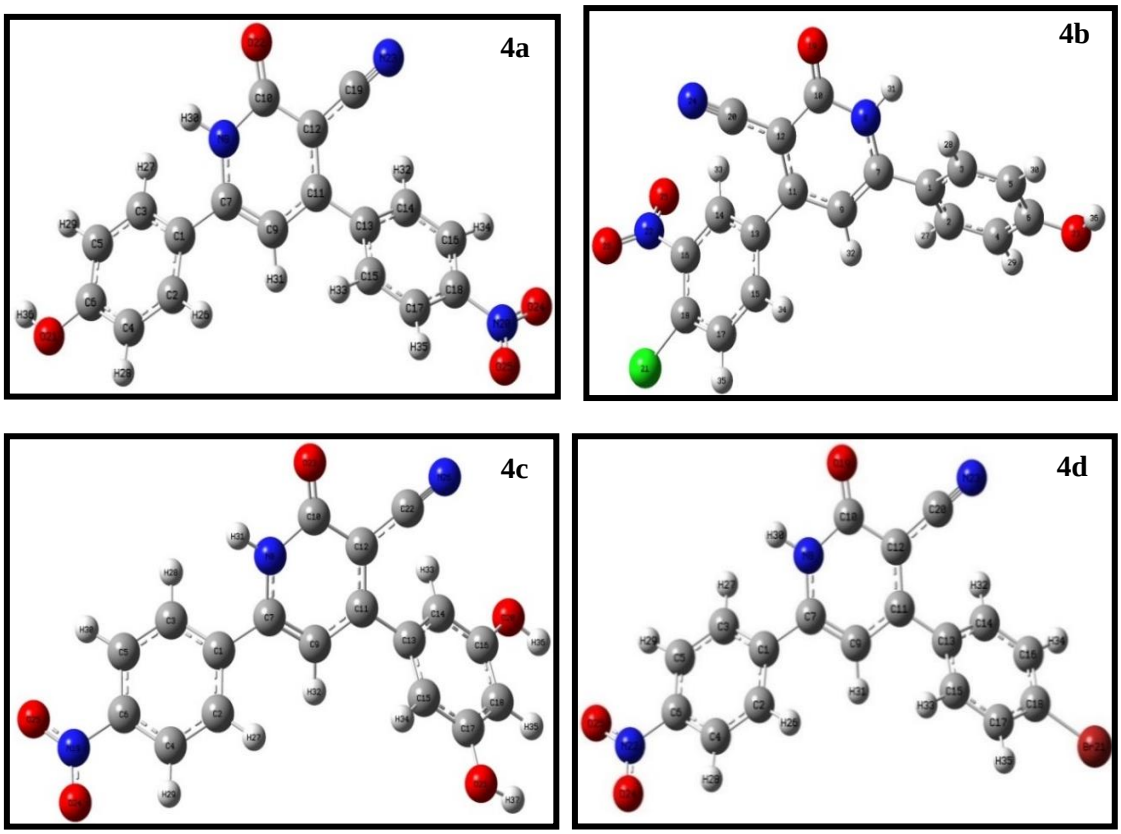

Fig. 3.5. Optimized structures of synthesized compounds **4**(**a-d**).

3.4.4.2 Frontier molecular orbitals (FMOs).

Frontier molecular orbitals (FMOs) are important parameters in theoretical studies, the E_{HOMO} is directly proportional to the ionization potential (IP) and the donation of electrons takes place. Similarly, the electron affinity is related to the E_{LUMO} and can easily accept the electrons. Compounds **4**(**a-d**) have shown higher values of E_{HOMO} -0.244 eV, -0.275 eV, -0.253 eV and -0.267 eV respectively as shown in **Fig. 3.6**. The energy gap is said to be the difference between frontier molecular orbitals. Compounds **4**(**a-d**) have been found higher the energy values *i.e* -0.125 eV, -0.164 eV, -0.122 eV, -0.131 eV respectively and results were tabulated in **Table 3.6**. A higher energy gap indicates higher kinetic stability and electron conductivity, while a lower energy gap informs higher chemical reactivity and biological stability.

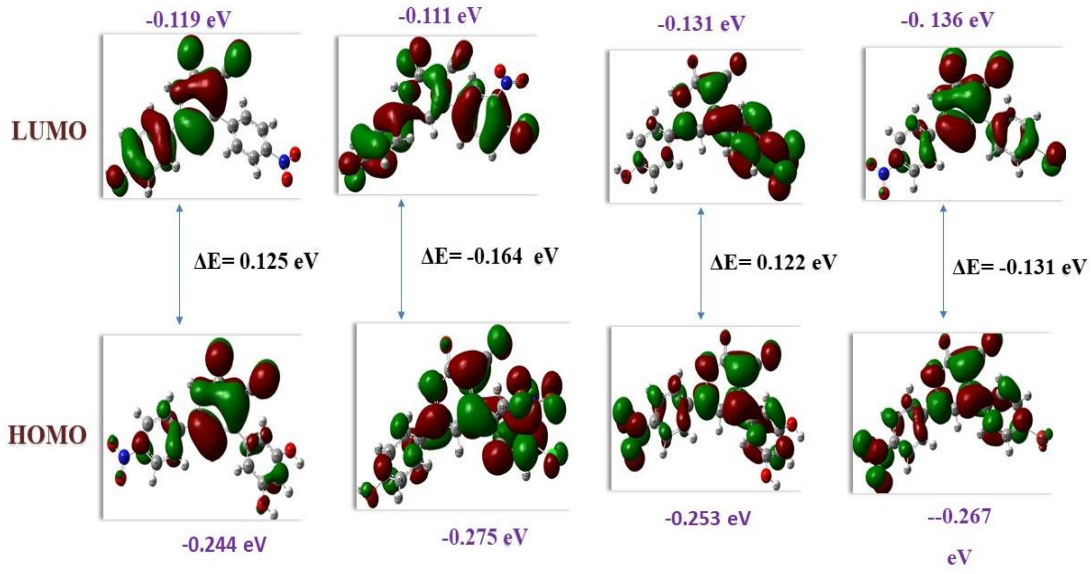

Fig.3.6 Frontier molecular orbital structures of synthesized compounds **4**(**a-d**).

3.4.4.3 Chemical parameters.

According to Koopmans theorems, chemical quantum parameters are calculated using the below equations (5 to 9) and results are summarized in **Table 3.7**. Chemical parameters help to understanding the chemical reactivity, photostability and intra-molecular charge transfer of the synthesized compounds **4**(**a-d**). Ionization potential known as E_{HOMO} (I) and electron affinity were known as E_{LUMO} (A). Chemical hardness and chemical softness were determined by the energy gap of E_{HOMO}-E_{LUMO}. The higher the energy gap is termed as chemical hardness and the lesser the energy gap is termed as chemical softness. Compounds **4**(**a-d**) have shown a higher energy gap, hence these are said to be hard molecules and hence, these molecules are shown greater photostability, higher chemical reactivity and higher intramolecular charge transfer.

The intrinsic properties of the compounds will be known by electronegativity. Chemical potential is the negative value of the electronegativity and the global electrophilicity index informs the photostability of compounds. Synthesized compounds show a higher electrophilicity index at 0.274 eV, 0.232 eV, 0.305 eV, and

0.312 eV respectively, which are greater in photostability. Another important parameter in theoretical studies is the dipole moment which informs the interaction of compounds. Higher the value increases in bonding interaction of compounds, **4a**, **4b** and **4c** have shown higher values of 12.00 eV, 13.63 eV and 6.871 eV respectively. While compound **4d** has shown a lower value of 4.655 eV due to the presence of highly electron-withdrawing nitro and bromo groups [37-39].

$$\eta = ½ (I - A) \quad \text{— (5)}$$

$$\sigma = 1/\eta \quad \text{— (6)}$$

$$\chi = ½ (I + A) \quad \text{— (7)}$$

$$\mu = -\chi \quad \text{— (8)}$$

$$\omega = \mu^2/2\eta \quad \text{— (9)}$$

Molecular electrostatic potentials (MEPs) are one of the important parameters in theoretical studies [40]. 3D images are shown in **Fig. 3.7** which helps to understand the electrostatic (electrophile, nucleophilic attack sites, biological detection, hydrogen bonding interaction) effects produced by the distribution of charges in compounds **4**(**a-d**). The MEPs surface computes with DFT B3LYP at 6-311++G (d, p) basis set and four regions of colors have appeared *i.e* red, blue, yellow and green [41]. The green color indicates higher negative electrostatic potentials and the blue color indicates highly positive electrostatic potentials. Similarly, yellow and red color indicate zero and electron-rich electrostatic potentials [42]. All the compounds have shown four colors in molecular electrostatic potentials where blue colors appear at phenyl ring with hydroxyl and amide groups. Similarly, the red color appears in the highly negative nitrile group with hydrogen and oxygen atoms [43].

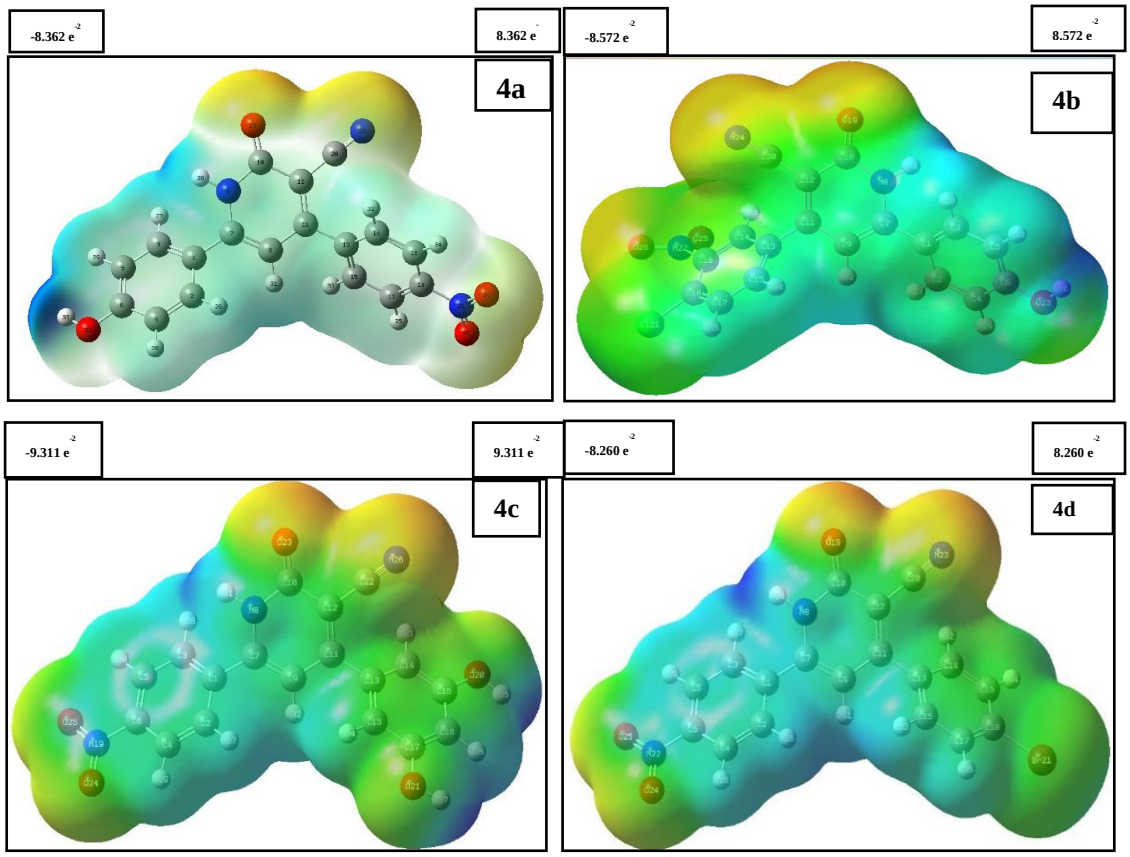

Fig. 3.7 Molecular electrostatic potential (MEP) images of synthesized compounds **4**(**a-d**).

Table 3.7. Quantum chemical parameters of synthesized compounds **4**(**a-d**).

Entry	*I* (eV)	*A* (eV)	*η* (eV)	*σ* (eV)	*χ* (eV)	*μ* (eV)	*ω* (eV)	*D*
4a	0.244	0.119	0.06	16.66	-0.181	-0.181	0.274	12.00
4b	0.275	0.111	0.08	12.50	-0.193	-0.193	0.232	13.63
4c	0.253	0.131	0.06	16.66	-0.192	-0.192	0.305	6.871
4d	0.267	0.136	0.06	15.38	-0.201	-0.201	0.312	4.655

3.4.5 Latent Fingerprints (LEPs).

LFPs have used identifications in banking sectors, access points and as evidenced by criminal investigations. LFPs developed easily using the powder dusting method using synthesized compounds **4**(**a-d**).

Under 365 nm UV light, the fingerprint was visualized clearly as shown in **Fig. 3.8** on selected porous/non-porous materials. Synthesized compounds are effective materials to use in forensic science by showing ridges of fingerprints. **Fig. 3.9** accurate level II and III features of latent fingerprint ridges on aluminium foil by using compound **4b** under 365 nm UV light. While the human sweat fingerprint consists of organic and inorganic residues such as amino acids, urea, peptides, fatty acids and chlorides along the water. The amino acids are in hydrophobic nature and contain charged, polar and cores amino acids, which covers all surface of porous and non-porous materials and well adhere to a molecule with the solvent through hydrogen bonds. When two electronegative atoms (nitrogen and oxygen) were reacts than hydrogen bond has been formed. The interaction between the donor hydrogen atom with an amide nitrogen atom and acceptor hydrogen with an oxygen atom, will cause of specific adherence between compounds and materials [44, 45].

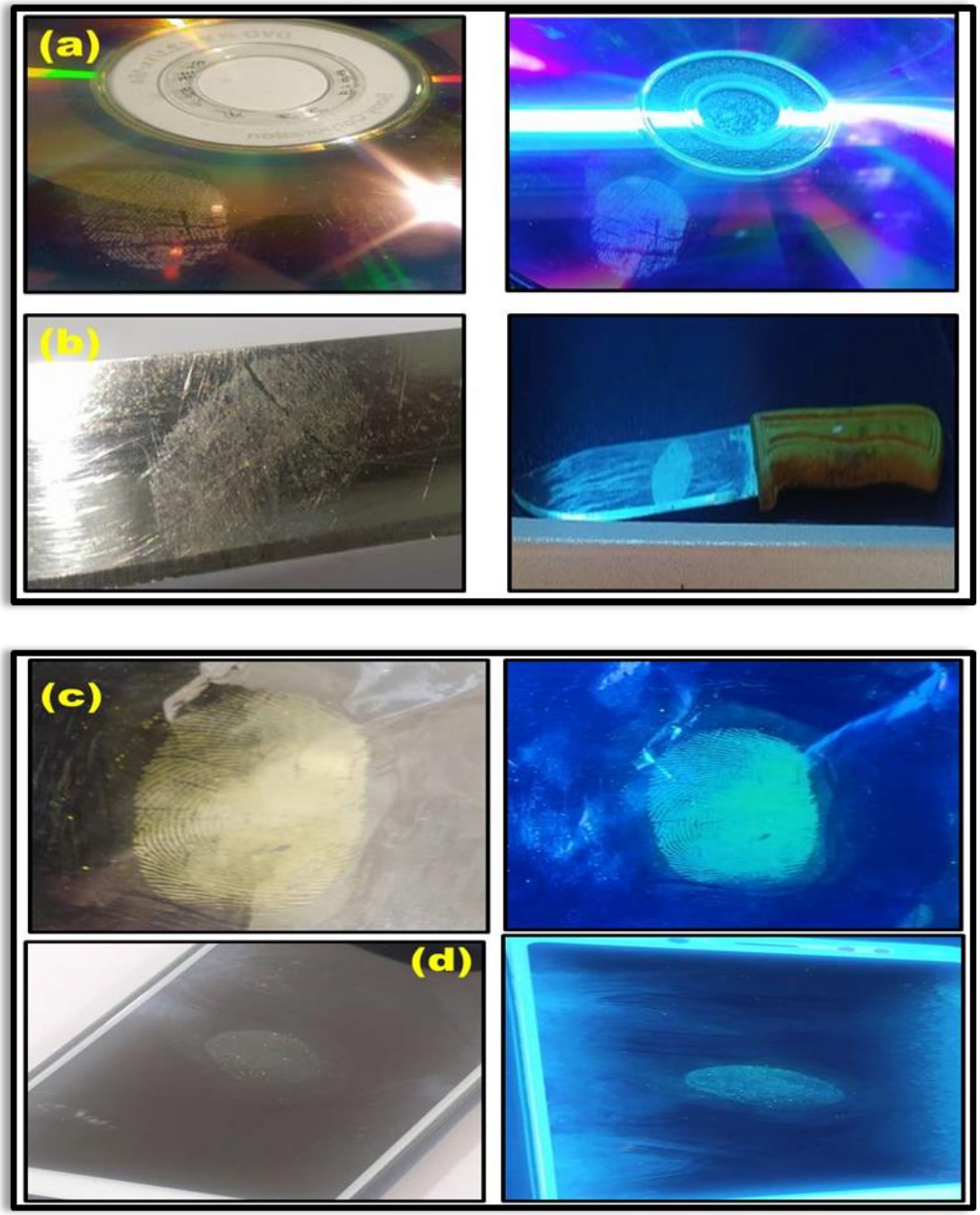

Fig. 3.8 Visualization of LFPs under normal and 365 UV-light. a) **4a**, b) **4c**, c) **4b** and d) **4d**.

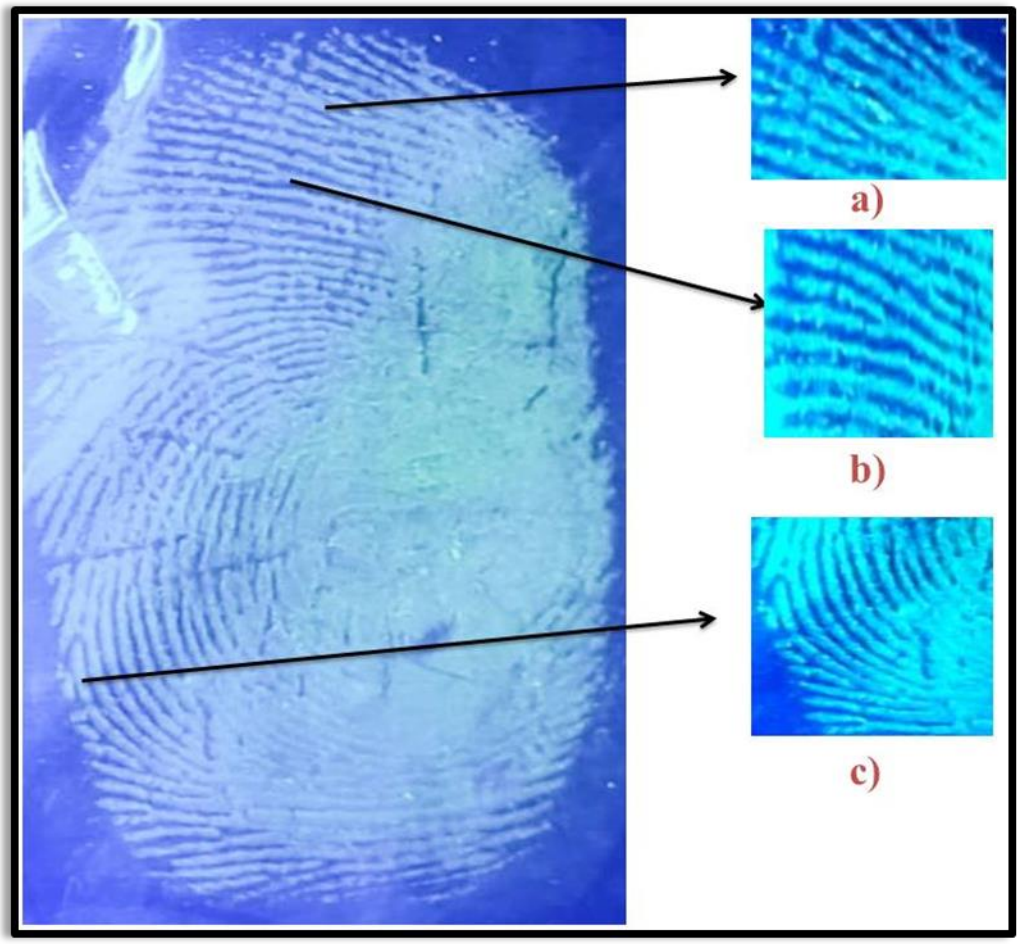

Fig. 3.9 Level II and III features of LFPs ridges on aluminum foil using synthesized compound **4b** in 365 nm UV-light, **a**) eye ridge, **b**) bifurcation and **c**) short ridge.

3.5 Conclusion

In this chapter, we have reported new 4-(4-substitutedphenyl)-6-(4-substitutedphenyl)-2-oxo-1,2-di-hydropyridine-3-carbonitrile **4**(**a-d**) derivatives and confirmed by different spectroscopic (FT-IR, ^{1}H-NMR, ^{13}C-NMR and Mass spectrometry) techniques. Compounds absorbed at a longer wavelength and emitted at the blue emission region in the solvent system due to π-π* and n-π* with aromatic conjugations and the presence of electron-withdrawing and donating groups. Further, compounds show reversible and quasi-reversible electrons in redox peak current energies experimentally. Theoretical results reveal that compounds are higher in chemical reactivity and photostability. MEPs images inform the compounds are having higher positive and negative electrostatic potentials by indicating red and blue colors. Similarly, compounds have electron-rich centers by showing green colors. A clear observation of bifurcation (level II), eye ridge and short ridges (level III) features of LFPs on different porous/nonporous materials without background hindrance and images were visualized under normal and 365 nm UV light.

3.6 Reference

1. C. Christophe, L. Chris, M. Pierre, S. Milutin, *Boca Raton, London, New York, Washington, DC: CRC Press*; chapter 4., (**2004**).
2. M. Srinivas, G.R. Vijayakumar, K.M. Mahadevan, H. Nagabhushana, H.S. Bhojya naik, *J. Sci. Adv. Mater. Devices.,* 2 (**2017**) 156-164.
3. K.A. Vishnumurthy, M.S. Sunitha, K. Safakath, R. Philip, A.V. Adhikari, *Polymer (Guildf,).,* 19 (**2011**) 4174-4183.
4. R.B. Basavaraj, G.P. Darshan, B.D. Prasad, S.C. Sharma, H. Nagabhushana, *J. Rare Earths.,* 37 (**2019**) 32-44.
5. M.K. Ravindra, K.M. Mahadevan, R.B. Basavaraj, G.P. Darshan, S.C. Sharma, M.S. Raju, G.R. Vijayakumar, K.B. Manjappa, D.Y. Yang, H. Nagabhushan, *Mater. Sci. Eng. C.,* 101 (**2018**) 564-574.
6. G.P. Darshan, H.B. Premkumar, H. Nagabhushan, S.C. Sharma, B.D. Prasad, S.C. Prashantha, R.B. Basavaraj, *J. Alloys Compd.,* 686 (**2016**) 577-587.
7. R.B. Basavaraj, H. Nagabhushana, G.P. Darshan, B.D Prasad, S.C. Sharma, K.N. Venkatachalaiah, *J. Ind. Eng. Chem.,* 51 (**2017**) 90-105.
8. B. Marappa, M.S. Rudresha, R.B. Basavaraj, G.P. Darshan, B.D. Prasad, S.C. Sharma, S. Sivakumari, P. Amudha, H. Nagabhushana, *Sensor. Actuator. B Chem.,* 264 (**2018**) 426-439.
9. Y. Ooyama, S. Inoue, T. Nagano, K. Kushimoto, J. Ohshita, I. Imae, K. Komaguchi, Y. Harima, *Angen. Chem. Intern. Ed.,* 32 (**2011**) 7429-7433.
10. A. Hovhannisyan, L. Aristakesyan, R. Hakobyan, G. Melikyan, *Chem. Biol.,* (**2015**) 9-13.
11. E.F.V. Scriven, R. Murugan, *Chem. Techn.,* 20 (**2005**) 1-53.
12. D. Seenaiah, P.R. Reddy, G.M. Reddy, A. Padmaja, V. Padmavathi, N.S. Krishna, *Eur. J. Med. Chem.,* 77 (**2014**) 1-7.
13. G.F. Zha, J. Leng, N. Darshini, T. Shubhavathi, H.K. Vivek, A.M. Asiri, H.M. Marwanic, K.P. Rakesha, N. Mallesha H.L. Qin, *J. Bioorg. Med. Chem. Lett.,* 27 (**2017**) 3148-3155.
14. D. Alexander, *Chem. Rev.,* 106 (**2006**) 17-89.

15. K.S. Pramod, K.S. Praveen, S.K. Manvendra, M. Mouslim, M.A. Saud, L.S. Puran, D.A. Dau, *ACS Omega.,* 3 (**2018**) 15035-15042.

16. W.J. Zhou, S.J. Ji, Z.L. Shen, *J. Orga. Chem.,* 691 (**2006**) 1356-1360.

17. F. Shi, S. Tu, F. Fang, L. Tuanjie, *A.R.K.I.V.O.C.*, (**2005**) 137-142.

18. C.T. Devaiah, B. Hemavathi, T.N. Ahipa, *Spectro. Act. Part A: Mol. and Biomol. Spectr*., 175 (**2017**) 222-228.

19. H.M. Manohara, C.T. Devaiah, B. Hemavathi, T.N. Ahipa, *J. Lum.,* 206 (**2019**) 284-291.

20. D. Khalili, *Tetra. Lett.,* 57 (**2016**) 1721-1723.

21. M.G. Swathi, T.N. Ahipa, *J. Mol. Liq.,* 265 (**2018**) 747-755.

22. J. Tang, L. Wang, Y. Yao, L. Zhang, W. Wanga, *Tetra.,* 52 (**2011**) 501-511.

23. H. Gezegen, M.B. Gürdere, A, Dinçer, O. Özbek, Ü.M. Koçyiğit, P. Taslimi, B. Tüzün, Y. Budak, M. Ceylan. *Arch. Pharm. DPhg.*, 354 (**2020**) 1-12.

24. M.A. Rauf, A.A. Soliman, M. Khattab, *J. Chem. Cent., 2* (**2008**) 1-9.

25. M.J. Sawicka, J.A. Soroka, M. Gąsiorowska, E.K. Wróblewska, *J. Solut. Chem.,* 41 (**2012**) 25-35.

26. J.B. Prieto, F.L. Arbeloa, V.M. Martinez, T.A. Lopez, F.A. Guerri, M. Liras, I.L. Arbeloa, *Chem. Phys. Lett.,* 385 (**2004**) 29-35.

27. M.G. Swathi, D. Devadiga, T.N. Ahipa, *J. Lumin.,* 217 (**2019**) 116818-116828.

28. R.O. Yathisha, Y.A. Nayaka, *SN Appl. Sci.,* 2 (**2020**) 451-467.

29. C.T. Devaiah, B. Hemavati, M.B. Ros, J.B. Rosa, M. Tejedor, K.K. Sadasivuni, T.N. Ahipa, *J. Mol. Liq.,* 255 (**2018**) 233-243.

30. H.J. Yvon, Stanmore, *Middlesex, UK*, (**2012**).

31. D.F. Eaton, *Pure Appl. Chem.,* 60 (**1988**) 1107-1114.

32. K.L. Wood, S. Upstone, K. Evans, Determination of Relative Fluorescence Quantum Yields Using the *FL6500 Fluorescence Spectrometer*.

33. J. Volke, V. Skála, *J. Electroanal. Chem*., 36 (**1972**) 383-388.

34. L. Leonat, S. Gabriela, I.V. Branzoi, *U.P.B. Sci. Bull. Series B.,* 75 (**2013**)111-119.

35. M.J. Frisch, G.W. Trucks, H.B. Schlegel, G.E Scuseria, M.A. Robb, J.R. Cheeseman, H. Nakatsuji, (**2009**). gaussian 09, Revision d. 01, Gaussian. *Inc., Wallingford CT*, 201.

36. I. Fleming, *Wiley.*, (**1977**).

37. R. Parr, G. Donnelly, R.A. Lev, M.W.E. Palke, *J. Chem. Phy.*, 68 (**1977**) 3801-3807.

38. J. Jia, J. Wen, *Tetra. Lett.,* 61 (**2020**) 0040-4039.

39. N. Pilicode, K.M. Nimith, M.N. Satyanarayan, A.V. Adhikari, *J. Photochem. Photobiol. A. chem.,* 364 (**2018**) 6-15.

40. J.S. Murray, T. Brinck, M.Ed. Grice, P. Politzer, *J. Mol. Str.,* 265 (**1992**) 29-45.

41. H.A. Arjun, R.K. Rajan, R. Elancheran, M. Ramanathan, A. Bhattacharjee, S. Kabilan, *Chem. data. Colle.,* 26 (**2020**) 100350-100365.

42. U. Vanitha, R. Elancheran, V. Manikandan, S. Kabilan, K. Krishnasamy, *J. Mol. Str.,* 1246 (**2021**) 131212-131223.

43. J. Janczak, *J. Polyhed.,* 38 (**2012**) 75-87.

44. M. Dhanalakshmi, H. Nagabhushana, G.P. Darshan, R.B. Basavaraj, B.D. Prasad, *J. Sci. Adv. Mater. Dev.,* 2 (**2017**) 22-33.

45. J. Lee, M.M. Joullié, *Tetra. Lett.*, 56 (**2015**) 3378-3381.

Chapter-4A

Synthesis, characterizations of new Schiff base heterocyclic derivatives and their optoelectronic, computational studies with level II & III features of LFPs

4A.1 Introduction

The Schiff base is a condensation reaction between primary amine and aldehyde which leads to a formation of imines or azomethine (-HC=N) [1]. These imines are considered as versatile organic compounds and received considerable attention in the field of pharmacological chemistry, and has proven their ability as antifungal, anti-microbial, antiviral, anti-cancer and anti-TB agents [2-6]. Apart from the biological agents, the researchers have concentrated on metal-free organic Schiff base compounds to prove their ability in the felid of electroluminescent, NLO, sensor and organic photovoltaic materials [7-9]. Moreover, the π-conjugated organic compounds exhibit mainly higher luminescence properties, by having an anchoring group such as electron-accepting and electron-donating groups and those were acting as D-π-A moieties. These anchoring groups may also help organic compounds to increase their optical as well as electrochemical behavior so that they can be used in the field of energy conversions and visualization of LFPs in the forensic science department [10]. Moreover, heterocyclic compounds are promising materials for photophysical-oriented applications, napthofurans are an important class of oxygen-containing heterocyclic compounds due to their natural abundance and they are found as well as biological agents mainly as antitumor agents because they have shown better cytotoxicity efficacy [11]. Especially, furan-containing heterocyclic compounds are expected to provide relatively high HOMO levels and hence can be used in electronic devices, such as organic light-emitting diodes (OLEDs), organic field-effect transistors (OFETs) and p-type semiconductors [12]. Similarly, indole is the nitrogen-containing heterocyclic compound, generally, it is a color compound used in many optical-oriented applications. Substituted indole derivatives are considered better pharmacologically active molecules. These derivatives will exhibit

fine luminescence properties when they are substituted with anchoring groups [13, 14]. Recently published Schiff base derivatives having luminescence characteristics was discussed below.

S. Singhal *et al.*, reported a newly synthesized benzimidazole substituted Schiff base organic derivatives (**1**) in 2019. Obtained derivatives have better fluorescence properties where the peaks have appeared at the longer wavelength of 354 nm to 380 nm. Further, synthesized compounds were screened for ct-DNA binding studies and the result shows compounds are well binded to ct-DNA [15].

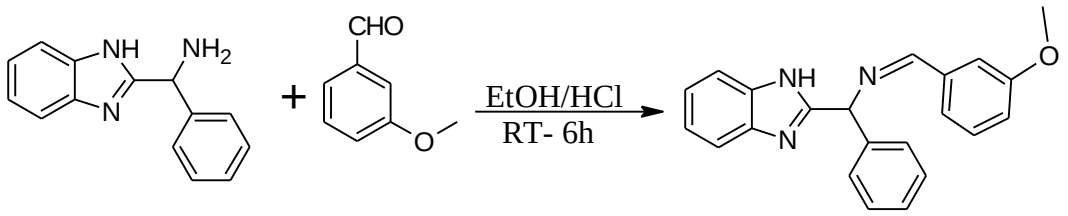

(1)

Abdullah M. Asiri *et al.*, reported a new Schiff base heterocyclic derivative 4-{(Z)-[(1,3-benzothiazol-2-yl)imino]methyl}-N,N-dimethylaniline (**2**) and obtained compounds have shown better photophysical properties in polar and non-polar solvents and absorption and emission bands appeared at a longer wavelength of 395 nm to 440 nm, and 418 nm to 558 nm [16].

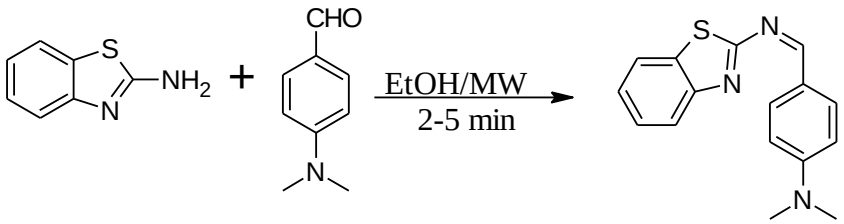

(2)

J. Liu *et al.*, synthesized a new triazole and benzotriazole Schiff base compounds (**3** and **4**) using an acetic acid catalyst. Both synthesized compounds were shows fine absorption and fluorescence properties in the solvent medium at the

concentration of 1×10^{-5} M. Absorption bands have appeared at 361 nm to 372 nm of longer wavelength, and emission peaks are obtained at 380 nm to 400 nm of blue regions [17].

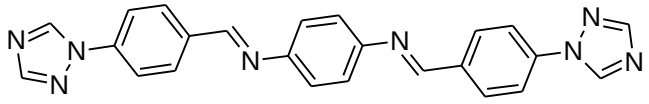

(3)

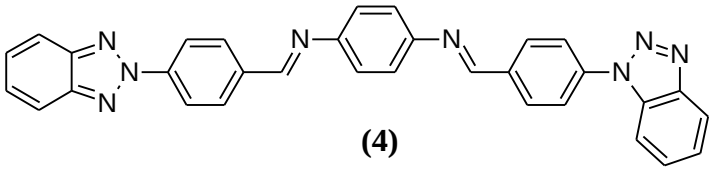

(4)

I. Kaya *et al.*, reported a pyridine Schiff base derivative (**5**) using ethanol at 3 h reflux condition. Reported compounds have been analyzed for their electrochemical and optical properties in organic solvent medium. The absorption bands appeared at 298 nm to 326 nm and emitted at 338 nm to 464 nm in DMSO. Further, compounds show fine redox peaks hence these compounds are potent materials for energy conversion devices [18].

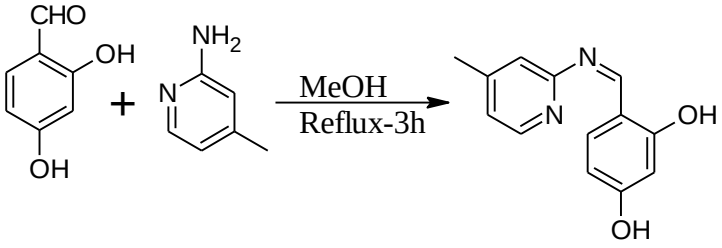

(5)

L. Shen and co-workers reported a N^2, N^6-bis(2-(2-hydroxynaphthalen-1-yl)phenyl)pyridine-2,6-dicarboxamide compound (**6**) in 2022. Reported compounds have exhibited fine photoluminescence character in the solvent medium at 369 nm to 475 nm and these compounds shown aggregation-induced emission properties under UV- light in THF/H_2O with different water fractions [19].

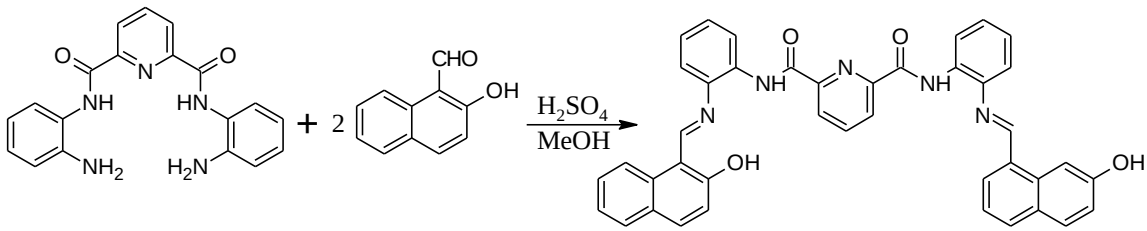

(6)

S. Ghosh *et al.*, reported a new pyrene-pyrimidine Schiff base compound (**7**) and used it for metal detection in an aqueous solution. Obtained compounds have better solvatochromic behavior in the solvent system with fine optical properties, where absorption bands appeared at 380 nm to 398 nm and emission bands appeared at 442 nm to 473 nm [20].

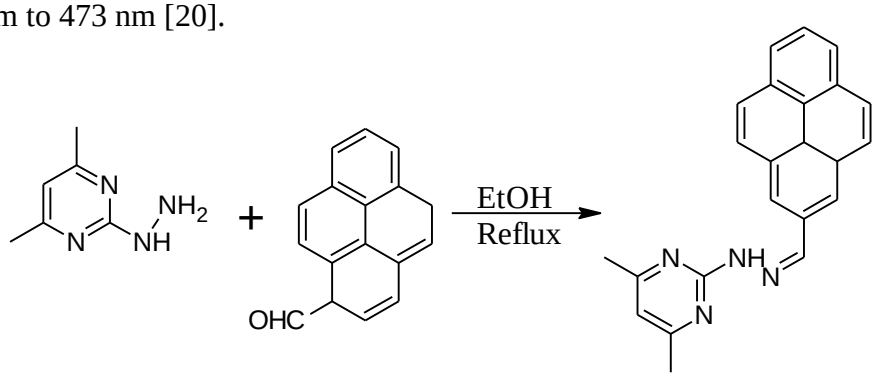

(7)

Concerning the above results, we have synthesized new Schiff base heterocyclic compounds using a catalytic amount of acetic acid and evaluated their optoelectronic, computational and LFPs studies.

4A.2 Present Work .

In this work, we have synthesized two new Schiff base [(4-hydroxy-3-methoxyphenyl)methylidene]naphtho[1,2-*b*]furan-2-carbohydrazide (**Sb1**) and 3-{[2-(2,4-dinitrophenyl)hydrazinylidene]methyl}-1*H*-indole (**Sb2**) and the mode of reaction pathway of new Schiff base derivatives has been demonstrated in the **Scheme 4a** and **4b.**

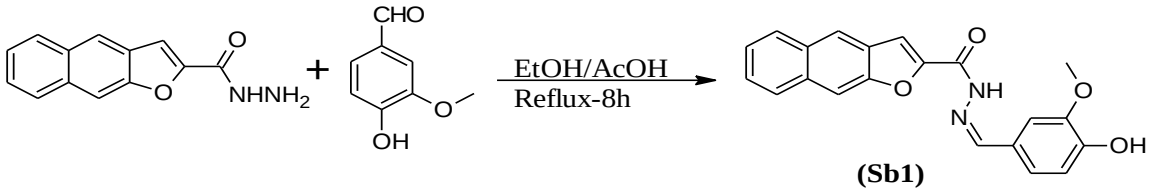

(Sb1)

Scheme 4a: Synthesis of [(4-hydroxy-3-methoxyphenyl)methylidene]naphtho[1,2-*b*]furan-2-carbohydrazide (**Sb1**)

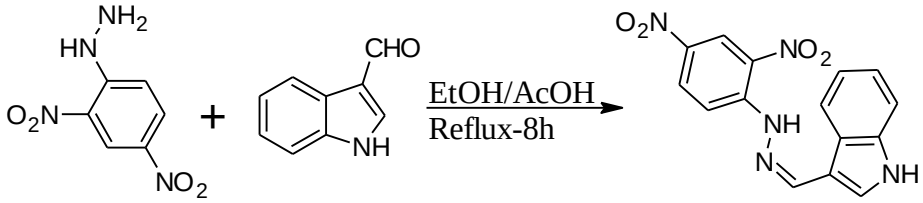

(Sb2)

Scheme 4b: Synthesis of 3-{[2-(2,4-dinitrophenyl)hydrazinylidene]methyl}-1*H*-indole (**Sb2**)

4A.2.1 Spectral characterization.

The structures of Schiff base heterocyclic compounds **Sb1** and **Sb2** were confirmed using spectral FT-IR, ^{1}H and ^{13}C-NMR, and Mass spectral characterization.

The IR spectra of the target compound **Sb1** showed a broad stretching vibration band at 3342 cm^{-1} due to OH functionality and another stretching band at region 3202 cm^{-1} correspond to the amide (NH) group. The stretching vibration band at 1663 cm^{-1} correspond to the carbonyl group (C=O) and another band at 1567 cm^{-1} correspond to azomethine (C=N) functionality. The ^{1}H-NMR spectrum of compound **Sb1** exhibited a singlet peak at δ11.67 ppm which correspond to the OH proton of the aromatic nucleus and another singlet peak at δ 9.66 ppm due to amide proton. Multiplet peaks were observed in the range of δ 8.88-7.48 ppm corresponds to aromatic protons and a singlet peak at δ 5.43 due to CH, proton, another a singlet peak at δ 3.26 due to methoxy protons. Similarly, the carbonyl carbon (C=O) has observed in a single peak

at 187.09 ppm and five-membered furan C-O carbon appeared at 148.95 ppm. Further, 137.75, 134.34, 130.46, 129.13, 125.68, 125.21, 121.26 ppm, (C=C), 110.44, 109.17 ppm corresponds to aromatic carbons. A peak obtained at 51.01 is corresponds to methoxy carbon (OCH_3). The mass spectrum showed molecular ion peak $[M]^+$at m/z 360.0911 which correspond to the molecular weight of the compound **Sb1.**

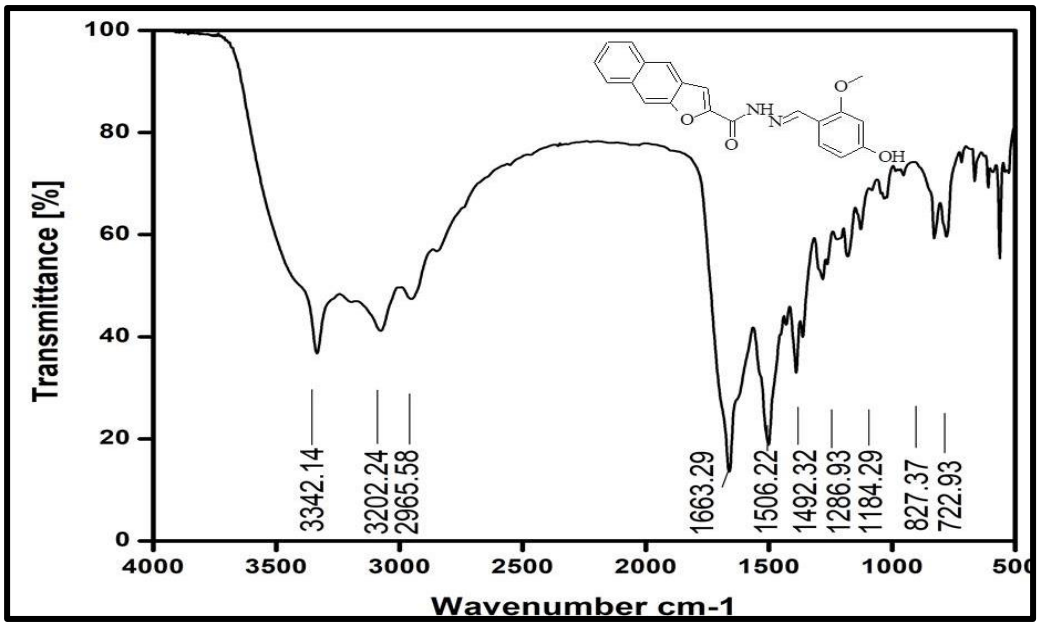

FTIR spectrum of compound Sb1

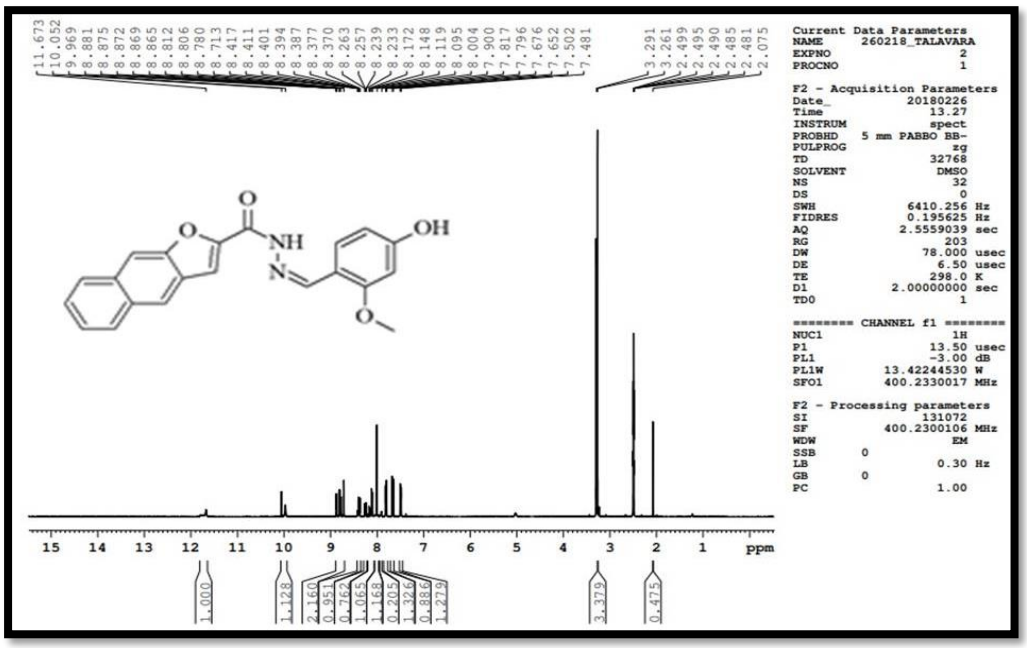

^{1}H-NMR spectrum of compound Sb1

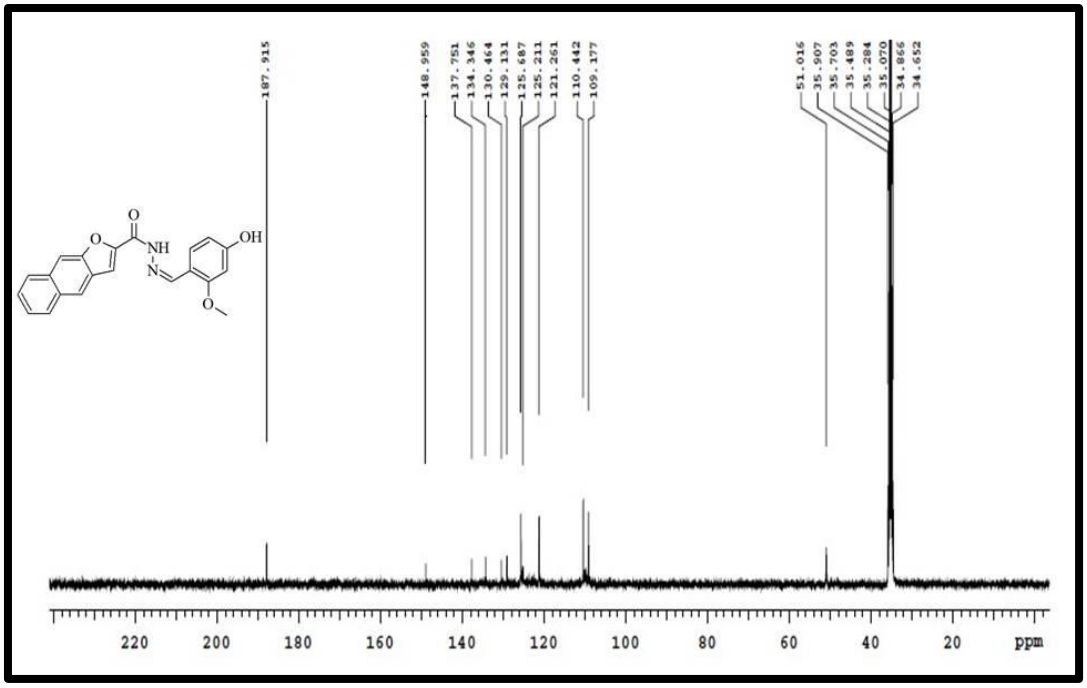

^{13}C -NMR spectrum of compound Sb1

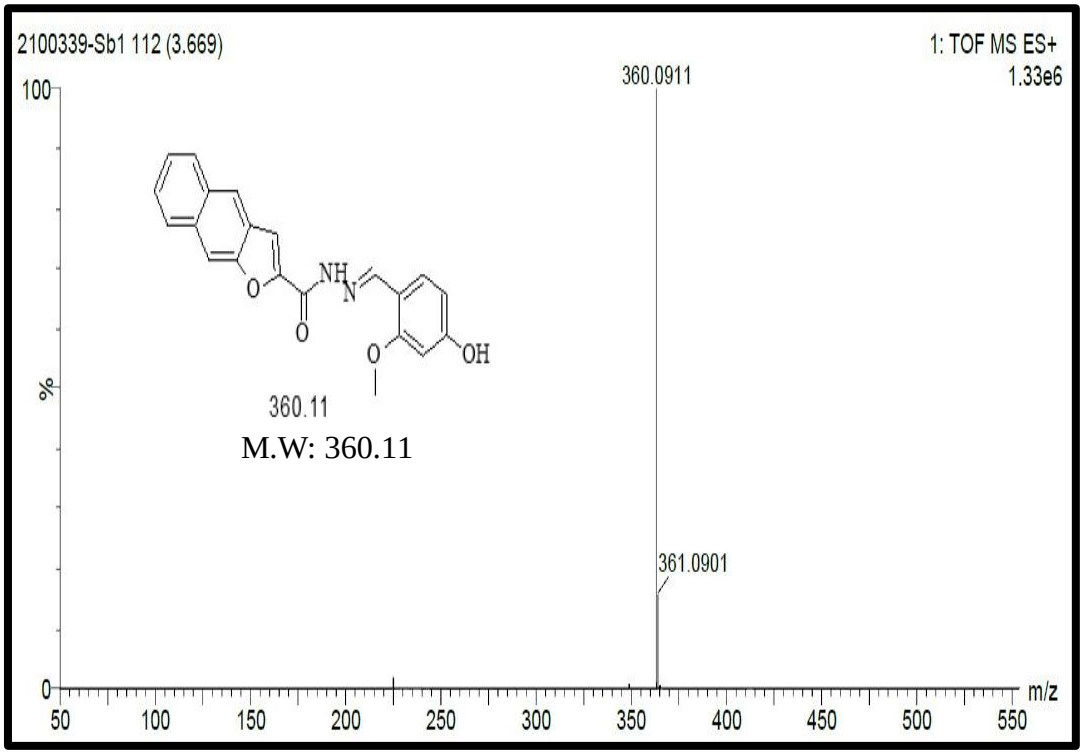

M.W: 360.11

Mass spectrum of compound Sb1

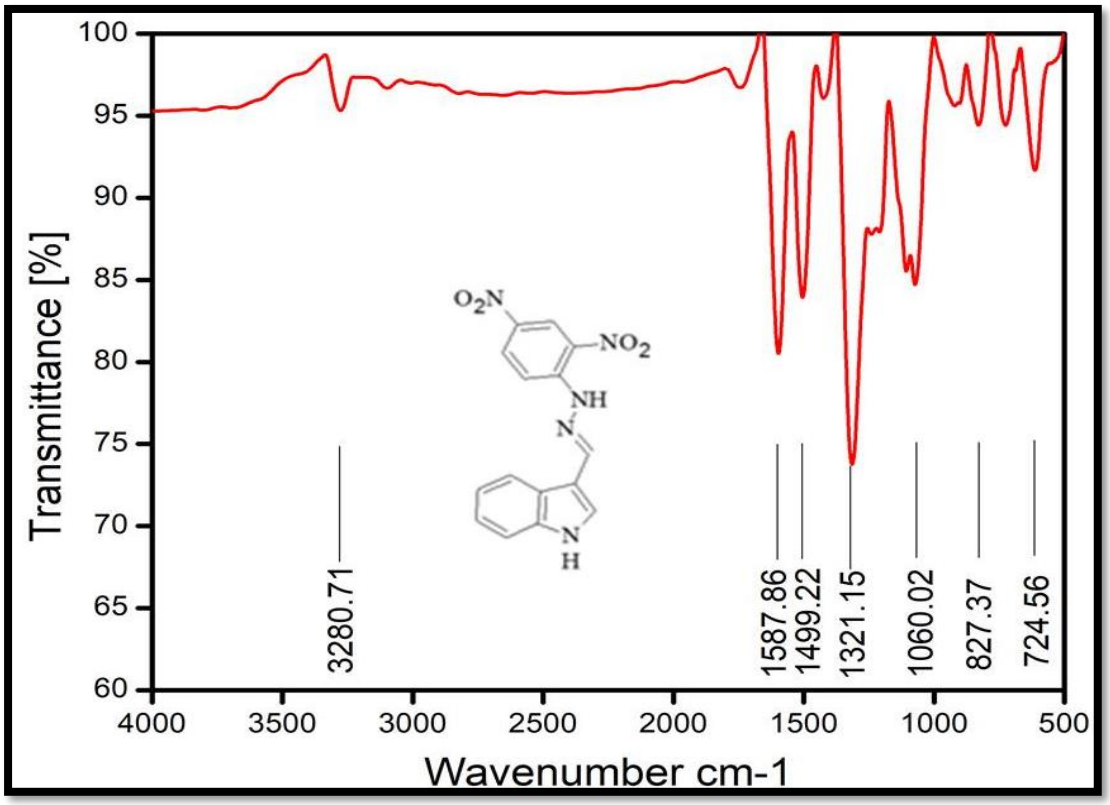

FTIR spectrum of compound Sb2

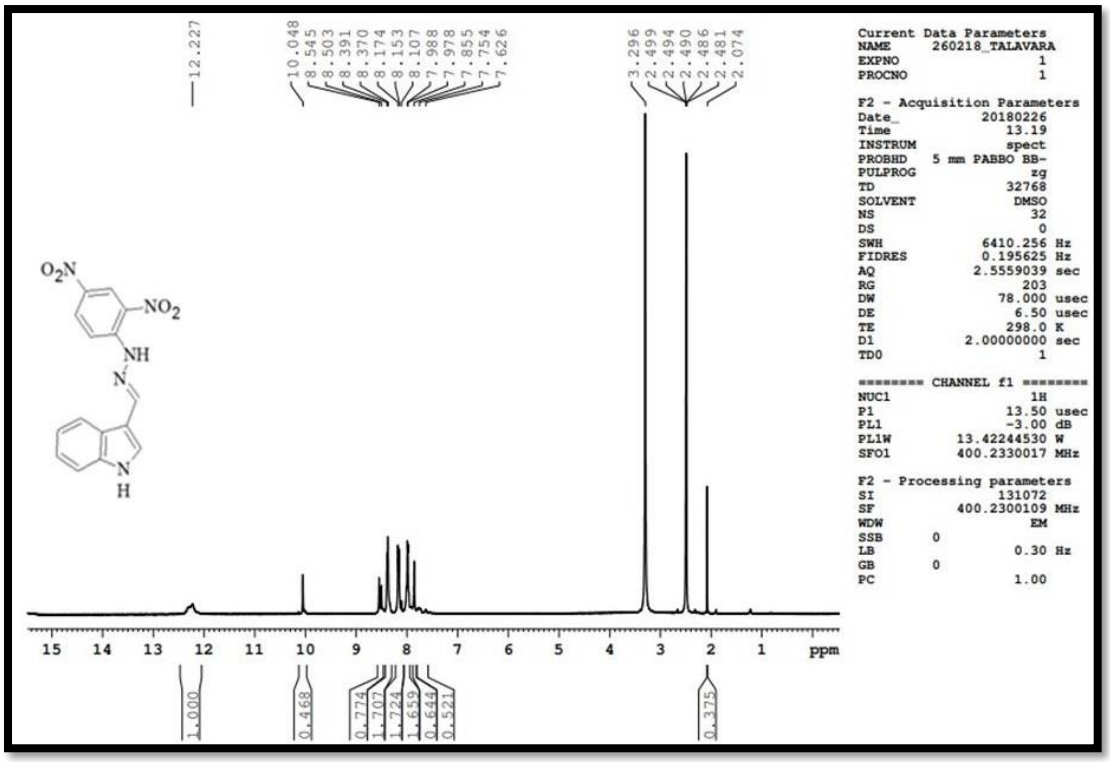

^{1}H-NMR spectrum of compound Sb2

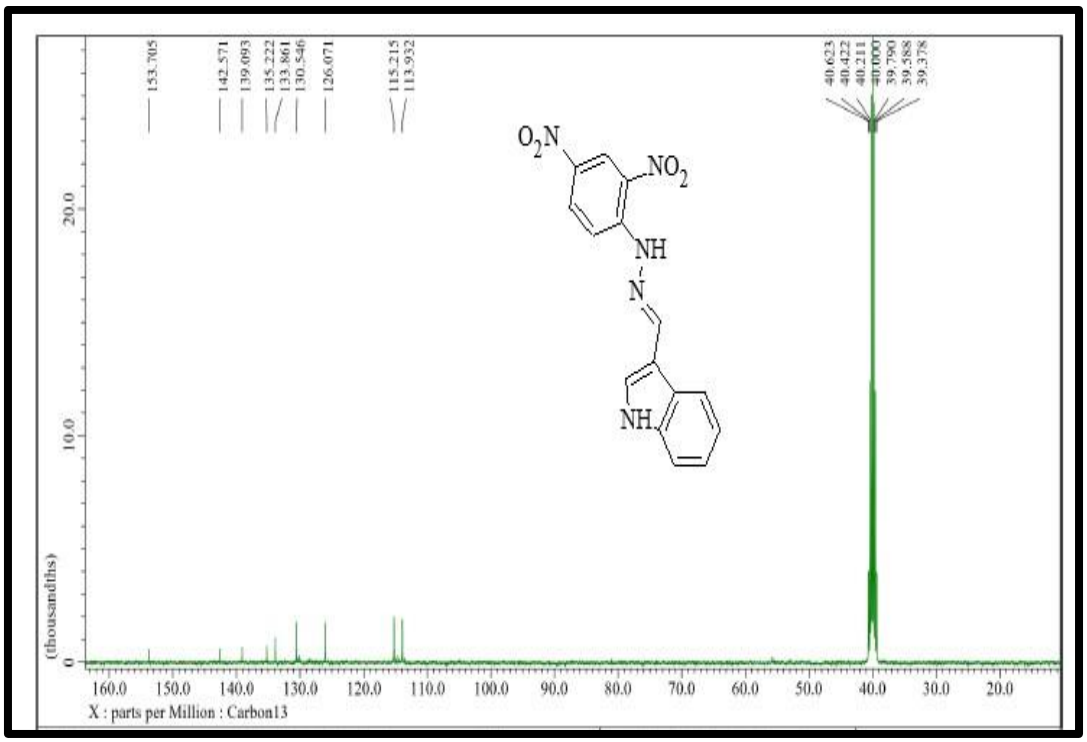

^{13}C -NMR spectrum of compound Sb2

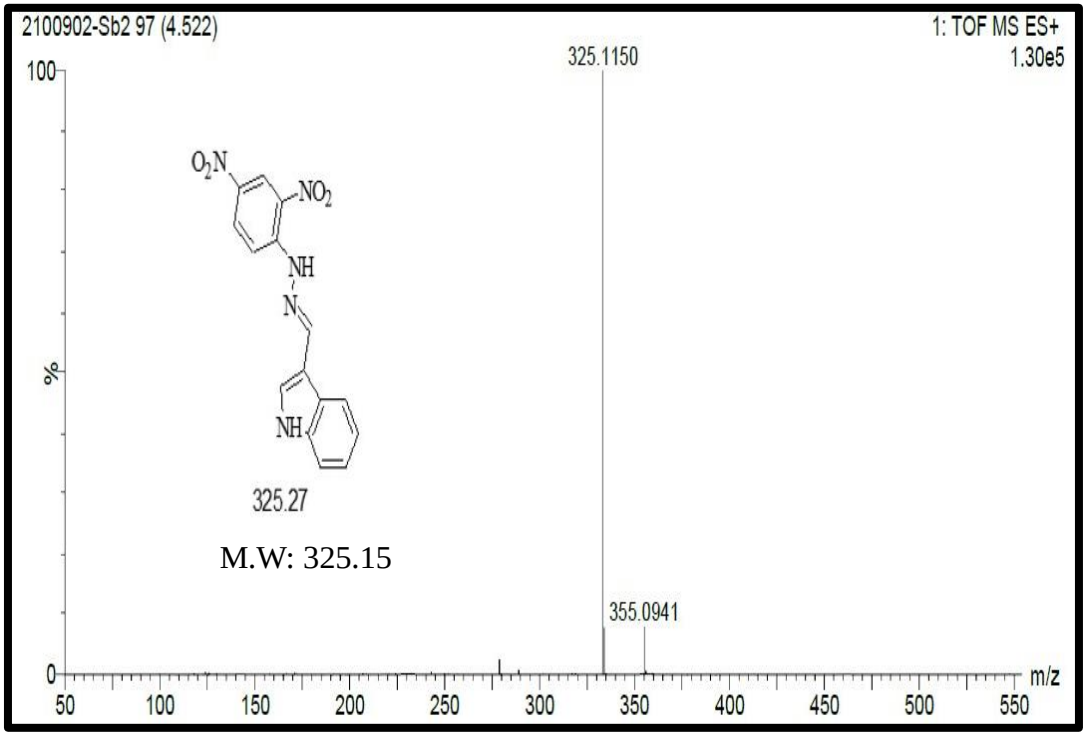

Mass spectrum of compound Sb2

4A.3 Experimental

4A.3.1 General information.

Regarding chemicals and reagents, glassware, instruments and methods carried for the analysis has discussed in previous **Chapter-2A**, and the experimental procedures (CV, DFT, LFPs) were detailed in the experimental section **2A.3**.

4A.3.2 Procedure for synthesis of new heterocyclic Schiff base compounds (Sb1 and Sb2).

N'-[(4-Hydroxy-3-methoxyphenyl)methylidene]naphtho[1,2-b]furan-2-carbohydrazide (Sb1):

An equimolar quantity of naphtho-[2,3-*b*]furan-2-carbohydrazide (1 mm) with vanillin (1 mm) using 3 drops of acetic acid in ethanol was taken in a round bottom flask and reflux with constant stirring for about 5 h. Simultaneously, the progress of the reaction was monitored by TLC (Ethyl acetate and Pet. ether). After the completion of the reaction, the mixture was poured into the 100 mL flake ice with vigorous stirring for 15 min till the solid residue separated, filtered then dried and recrystallized from absolute ethanol.

Dark brown solid; Yield: 85 %; MP: 320-322 °C; Mol. Formula $C_{21}H_{16}N_2O_4$; FTIR (υ cm^{-1}): 3342 (OH), 3202 (NH), 2965 (OCH_3), 1663 (C=O), 1567 (C=N); ^{1}H-NMR (δ ppm): 11.67 (s, 1H, OH), 9.96 (s, 1H, NH), 8.88-8.09 (m, 5H, Ar-H), 8.00 (s, 1H, Ar-H), 7.90 (s, 1H, Ar-H), 7.81-7.79 (d, *J* = 8, 1H, Ar-H), 7.67-7.65 (d, *J* = 8, 1H, Ar-H), 7.50-7.48 (d, *J* = 8, 1H, Ar-H), 5.43 (s, 1H, CH) and 3.26 (s, 3H, OCH_3); ^{13}C-NMR (δ ppm): 187.91 (C=O), 148.95 (Furan C-O), 137.75, 134.34, 130.46, 129.13, 125.68, 125.21, 121.26, 110.44, 109.17, 51.01 (OCH_3); HRMS: m/z 360.17 [M^+1]; Anal. Calcd for $C_{21}H_{16}N_2O_4$, C, 69.99; H, 4.48; N, 7.77 %; Found: C, 69.94; H, 4.43; N, 7.73 %.

3-{[2-(2,4-Dinitrophenyl)hydrazinylidene]methyl}-1H-indole (Sb2):

The compound (**Sb2**) was synthesized by the reaction of 2, 4-DNP (1 mm) and indole-3-carboxaldehyde (1 mm) and followed by synthesized compound (**Sb1**) procedure.

Red blood solid; Yield: 86 %; MP: 292-294 °C; Mol. Formula $C_{15}H_{11}N_5O_4$; FTIR (υ cm^{-1}): 3280 (NH), 1587 (C=N); ^{1}H-NMR (δ ppm): 12.22 (s, 1H, Indole-NH), 10.04 (s, 1H, NH), 8.54-8.50 (d, *J* =16, 1H, Ar-H), 8.39-8.37 (d, *J* = 8, 2H, Ar-H), 8.17-8.15 (d, *J* = 8, 2H, Ar-H), 7.98-7.97 (d, *J* = 4, 2H, Ar-H), 7.85 (s, 1H, Ar-H), 7.75 (s, 1H, CH); ^{13}C-NMR (δ ppm): 153.70 (C=NH), 142.57, 139.09, 135.22, 133.86, 130.54, 126.07, 115.21, 113.93; HRMS: m/z 325.1150 [M^+]; Anal. Calcd for $C_{15}H_{11}N_5O_4$, C, 55.39; H, 3.41; N, 21.53%; Found: C, 55.35; H, 3.38; N, 21.49 %.

4A.4 Results and discussion

4A.4.1 Electronic absorption studies.

The compounds **Sb1** and **Sb2** were dissolved in three different solvents ($CHCl_3$, DMSO, and EtOH) at a concentration of 6×10^{-6} M, to study their optical properties. **Fig. 4A.1** shows dual absorption peaks with higher intensity at ~250-420 nm due to the involvement of n-π* and π-π* electronic transition with aromatic ring conjugation. The compound **Sb1** has shown all the absorption bands at bathochromic shift and compound **Sb2** has shown a longer wavelength by the transition between p-orbital localized on the central bond of azomethine (HC=N) and the carbonyl (C=O) and presence of anchoring groups [21]. Compounds also have better solute and solvent interaction and have good light absorption properties hence these compounds used as photonic materials and will be in photovoltaic applications [22-25].

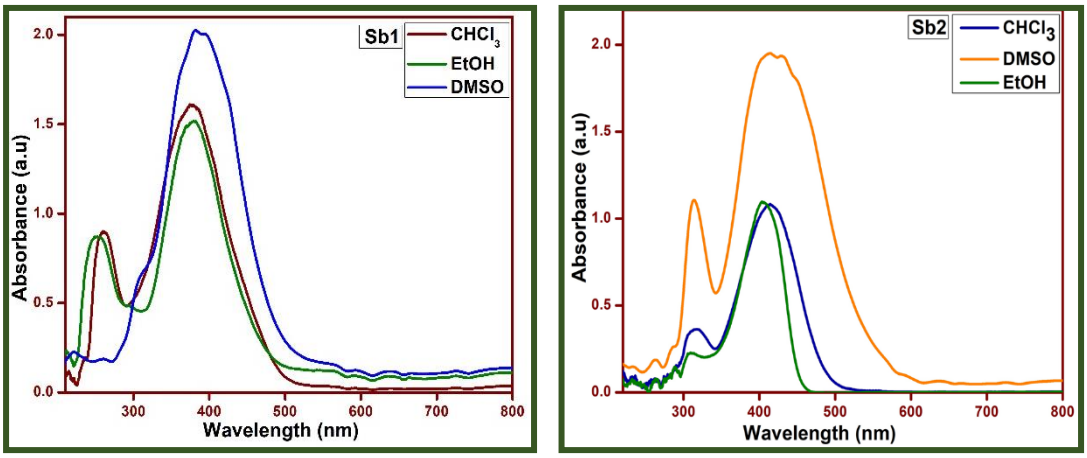

Fig. 4A.1 Electronic absorption spectra's of **Sb1** and **Sb2** in different solvents.

4A.4.2 Emission studies.

The emission properties help in determining the efficiency of charge carriers in semiconductors and the study has been carried out in DMSO solvent. From **Fig. 4A.2** (**a**) compounds emitted with respect to the excitation wavelength at longer shift 576 nm and 646 nm respectively. Here the compound **Sb1** and **Sb2** have shown larger stokes of 195 nm, and 232 nm respectively. In addition, fluorescence properties were also analyzed by the CIE systems of chromaticity coordinates. **Fig. 4A.2** (**b**) shows that calculated CIE data with coordinates X= 0.3093; Y=0.6404 results in the color enhancement and is represented by the star symbol located at the greenish-yellow region of **Sb1**, while reddish-orange at X=0.2996; Y=0.6786 for **Sb2**. Hence the synthesized compounds are potential materials for OLEDs applications and forensic science. Absorption, emission spectral and optical band gap values are appended in **Table 4A.1**.

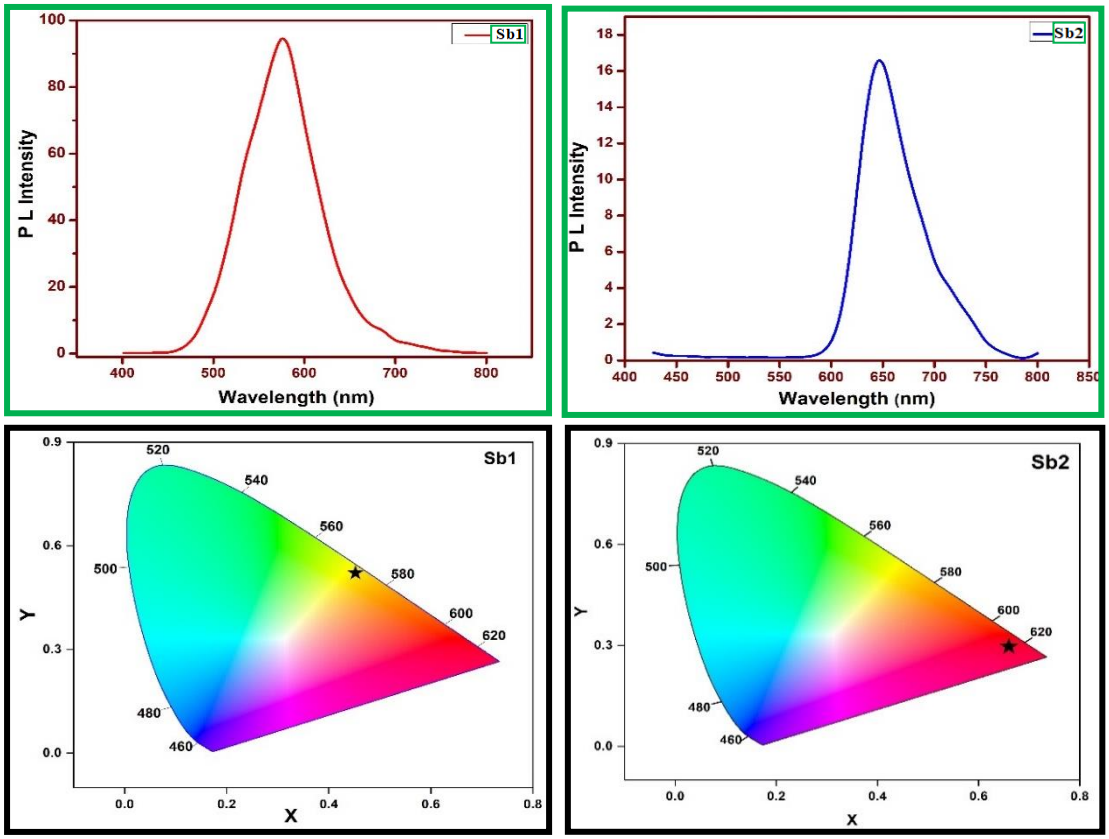

Fig. 4A.2 (a) Photoluminescence spectra spectrum **(b)** CIE spectrum of compounds **Sb1** and **Sb2**.

Table 4A.1. Absorption data of synthesized compounds **Sb1** and **Sb2** in different solvents.

Solvents	Entry	λ_{abs} (nm)	λ_{emi} (nm)	Stoke shift	E_g^{OTP} (eV)	Molar absorptivity ($\varepsilon \times 10^{-5}$ L mol^{-1} cm^{-1})
Chloroform		260, 376			4.76 & 3.29	2.3
DMSO	**Sb1**	221, 381	576	195	5.61 & 3.25	2.5
Ethanol		252, 379			4.92 & 3.27	1.6
Chloroform		272, 392			4.55 & 3.16	2.6
DMSO	**Sb2**	312, 414	646	232	3.97 & 2.99	0.3
Ethanol		257, 403			4.82 & 3.07	3.0

4A.4.3 Electrochemical studies.

The electrochemical studies for the compounds have been carried out using three-electrode cell system in DMSO as electrolyte and PBS as supporting electrolyte.

From the CV measurement (**Fig. 4A.2**) cathodic reduction peaks are observed for both the compounds **Sb1** and **Sb2** due to the presence of the carbonyl group (C=O). Moreover, nitro (NO_2) and keto groups undergo reduction. From the reduction onset potential, the LUMO was calculated using equation (2) and obtained -0.65 eV, -0.62 eV, -0.65 eV, and -0.68 eV respectively. Similarly, HOMO was calculated using equations (3 and 4). The lower HOMO ensures the effective regeneration and recaptures the injected electron by the synthesized compounds. Hence these compounds can be used in DSSCs application [26, 27]. Obtained HOMO-LUMO values are summarized in **Table 4A.3.**

$$E_{(LUMO)} = -[E_{(redonset)} + 4.4]\ eV \quad \text{— (2)}$$

$$E_{(HOMO)} = -[E_{(oxonset)} + 4.4]\ eV \quad \text{— (3)}$$

$$E_{(HOMO)} = E_{(LUMO)} - E_g^{OPT} \quad \text{— (4)}$$

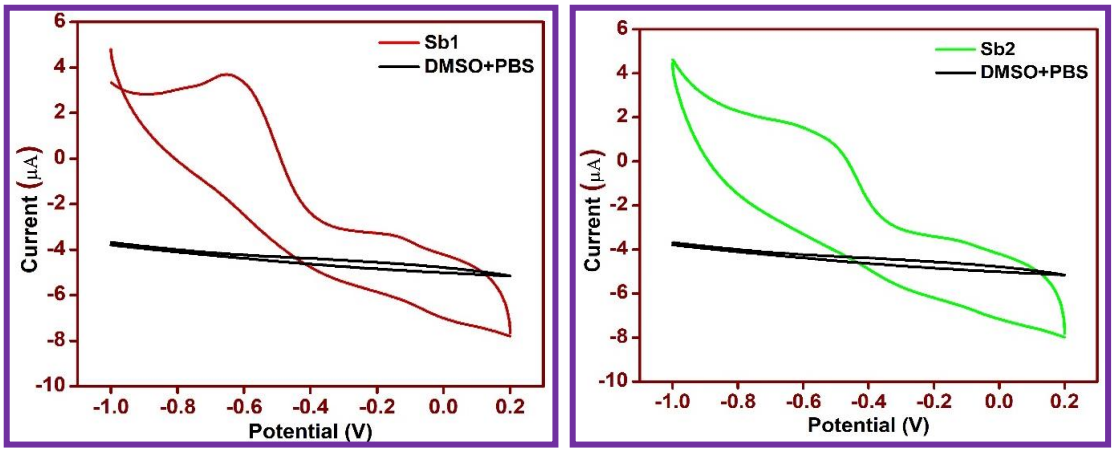

Fig. 4A.3 A graph of cyclic voltammetry of synthesized compounds **Sb1** and **Sb2.**

Table 4A.2. Electrochemical parameters of compounds **Sb1** and **Sb2.**

Entry	Oxidation onset potential (V)	Reduction onset potential (V)	E_{HOMO} (eV)	E_{LUMO} (eV)
Sb1	-	-0.65	-7.00	-3.75
Sb2	-	-0.62	-6.77	-3.78

Table 4A.3. Experimental quantum parameters of compounds **Sb1** and **Sb2.**

Entry	I (eV)	A (eV)	η (eV)	σ (eV)	χ (eV)	μ (eV)	ω (eV)	ΔE
Sb1	7.00	3.75	1.62	0.33	5.37	-5.37	8.90	3.25
Sb2	6.77	3.78	1.49	0.30	5.27	-5.27	9.28	2.99

4A.4.4 Computational study.

4A.4.4.1 FMOs.

HOMO and LUMO are known as FMOs and these play a vital role to assign the optical and electronic properties of the materials, donor of the electron is HOMO, and LUMO is the acceptor electron [28-31]. The energy gaps of the two heterocyclic Schiff base compounds are found to be 3.738 eV and 2.942 eV respectively and the pictorial representation of the HOMO-LUMO of these compounds as shown in **Fig 4A.4**. The higher value of separation energy between the HOMO and LUMO explains the charge transfer interaction within the molecule. Consequently, the lower value of the bandgap is essentially a consequence of the large stabilization of the LUMO due to the strong electron-acceptor ability of the electron-acceptor group. Therefore, the compound **Sb1** has a large energy gap due to less electronic conjugation compared to **Sb2** compound. The other chemical reactive parameters like electrophilicity index, chemical potential, global hardness, and softness were calculated using the standard equations as given below and values are listed in **Tables 4A. 4 and 4A.5**.

$\chi = -½ (E_{LUMO}+E_{HOMO})$ — (5)

$\mu = -\chi = ½ (E_{LUMO}+E_{HOMO})$ — (6)

$\eta = ½ (E_{LUMO} - E_{HOMO})$ — (7)

$\sigma = 1/2\eta$ — (8)

$\omega = \mu^2 /2\eta$ — (9)

From Table **4A.4** we observed that the compound **Sb2** has a higher electrophilicity index compared to **Sb1,** hence the compound **Sb1** acts as a good electrophile. Also, the value of global hardness for the compound **Sb2** is lesser as compared to **Sb1**. Hence the compound **Sb2** is more reactive than the **Sb1**.

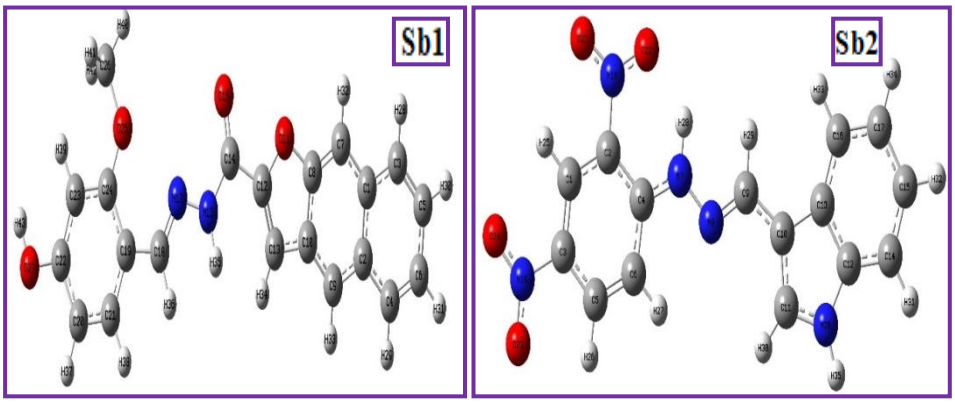

Fig.4A. 4 Optimized structures of compounds **Sb1** and **Sb2.**

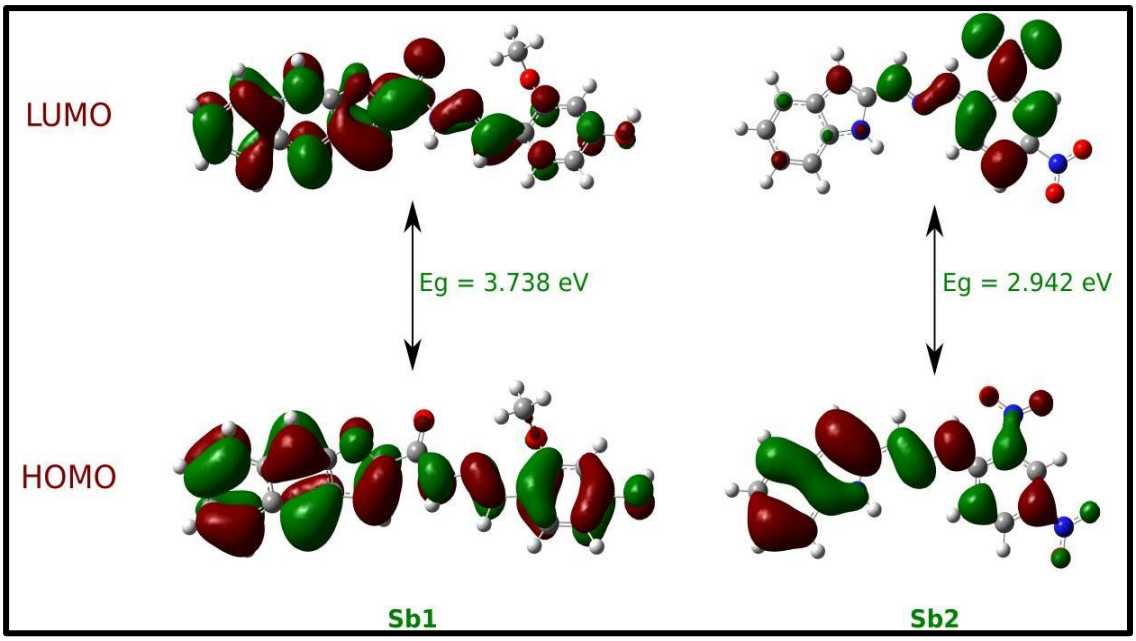

Fig. 4A. 5 Frontier molecular orbital (E_{HOMO}-E_{LUMO}) structures of synthesized compounds **Sb1** and **Sb2**

Table 4A.6 Frontier molecular orbitals of **Sb1** and **Sb2**.

Entry	E_{HOMO} (eV)	E_{LUMO} (eV)	ΔE
Sb1	-5.84	-2.10	3.73
Sb2	-6.04	-3.10	2.94

Table 4A.7. Theoretical Chemical Parameters of compounds **Sb1** and **Sb2.**

Parameters	Values (eV)	
	Sb1	**Sb2**
Ionization energy (I)	5.8432	6.0479
Electron affinity (A)	2.1048	3.1052
Electronegativity (χ)	3.9740	4.5765
Chemical potential (μ)	-3.9740	-4.5765
Global hardness (η)	1.8692	1.4714
Global softness (σ)	0.5350	0.6796
Electrophilicity index (ω)	4.2246	7.1174

4A.4.4.2 Molecular Electrostatic Potential (MEP) analysis.

The MEP map that is created in the space around a molecule by its nuclei and electrons is a useful tool to predict and study the reactive behavior and reactive sites present in the molecule. The MEP is related to the electronic density and is a very important descriptor for determining sites for electrophilic attack and nucleophilic reaction as well as hydrogen bonding interactions [32, 23]. The MEP maps of synthesized Schiff base compounds (**Sb1** and **Sb2**) as shown in **Fig. 4A 6.** With the MEP analysis, the reactive sites can be located by different color codes. The red color indicates an electron-rich site which is a negative region showing electrophilic attack while the blue color indicates an electron deficient site, which is a positive region showing the nucleophilic attack. From **Fig. 4A.6**, one can be observed that the negative regions in the molecules were found around the oxygen atom and the negative regions were found around the hydrogen atom attached to the nitrogen atom.

The overall surface for the compound **Sb1** is 427.77 $Å^3$, and for **Sb2** is 359.68 $Å^3$ respectively. The minimum and maximum electrostatic potential for the compound **Sb2** is -43.48 kcal/mol to 54.92 kcal/mol and for **Sb2** is 32.86 kcal/mol to 50.80 kcal/mol, respectively.

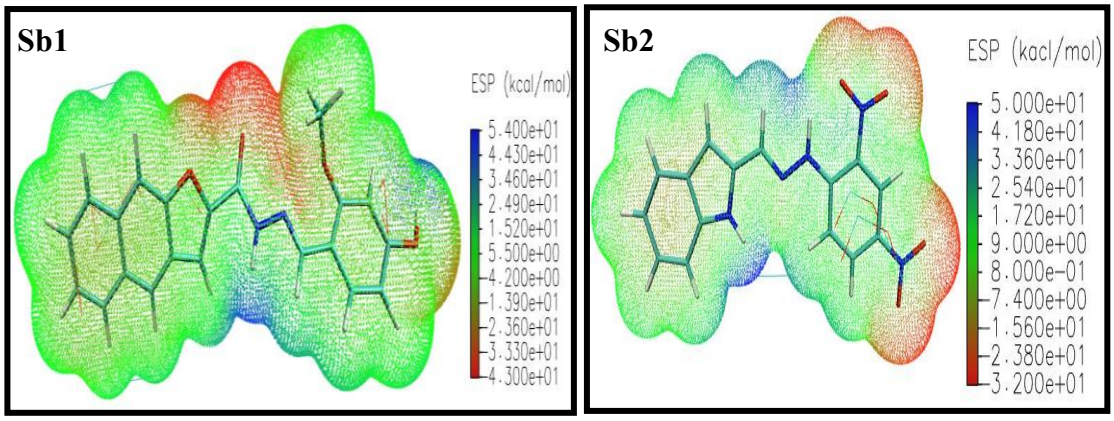

Fig. 4A. 6 Molecular electrostatic potential images of synthesized compounds **Sb1** and **Sb2**.

4A.4.5 Visualization of LFPs.

Every human has unique fingerprints, which are helpful to use in safety lockers in banks, mobile phones, and personal identification. Other than these helpful techniques fingerprints are used as a preliminary method of a criminal investigation. In general, LFPs are hard to visible to the naked eye, hence numerous methods have been followed to date for visualization among various techniques chemical method (powder dusting) was approached easily and a quick method was followed with fluorescence powder. **Fig.4A.8 (a)** and **(b)** shows developed LFPs on selected laboratory glasswares (500 mL beaker, spatula, aluminium foil) using synthesized compounds **Sb1** and **Sb2**, and visualization has proceed in normal light and UV light. Here we can observe the clear visualization of level II and level III fingerprint ridges without any background hindrance developed by the compounds **Sb1** and **Sb2.** The sweat pores have contained different organic and inorganic residues such as amino acids, urea, peptides, fatty acids, and chlorides along the water. Hydrophobic amino

acids contain the polar and core amino acids that play a vital role in adherence between material and synthesized compounds which shows clear and perfect images without any background hindrance. Hence the synthesized compounds are potential materials for latent fingerprint applications and can be used in forensic science [35-38].

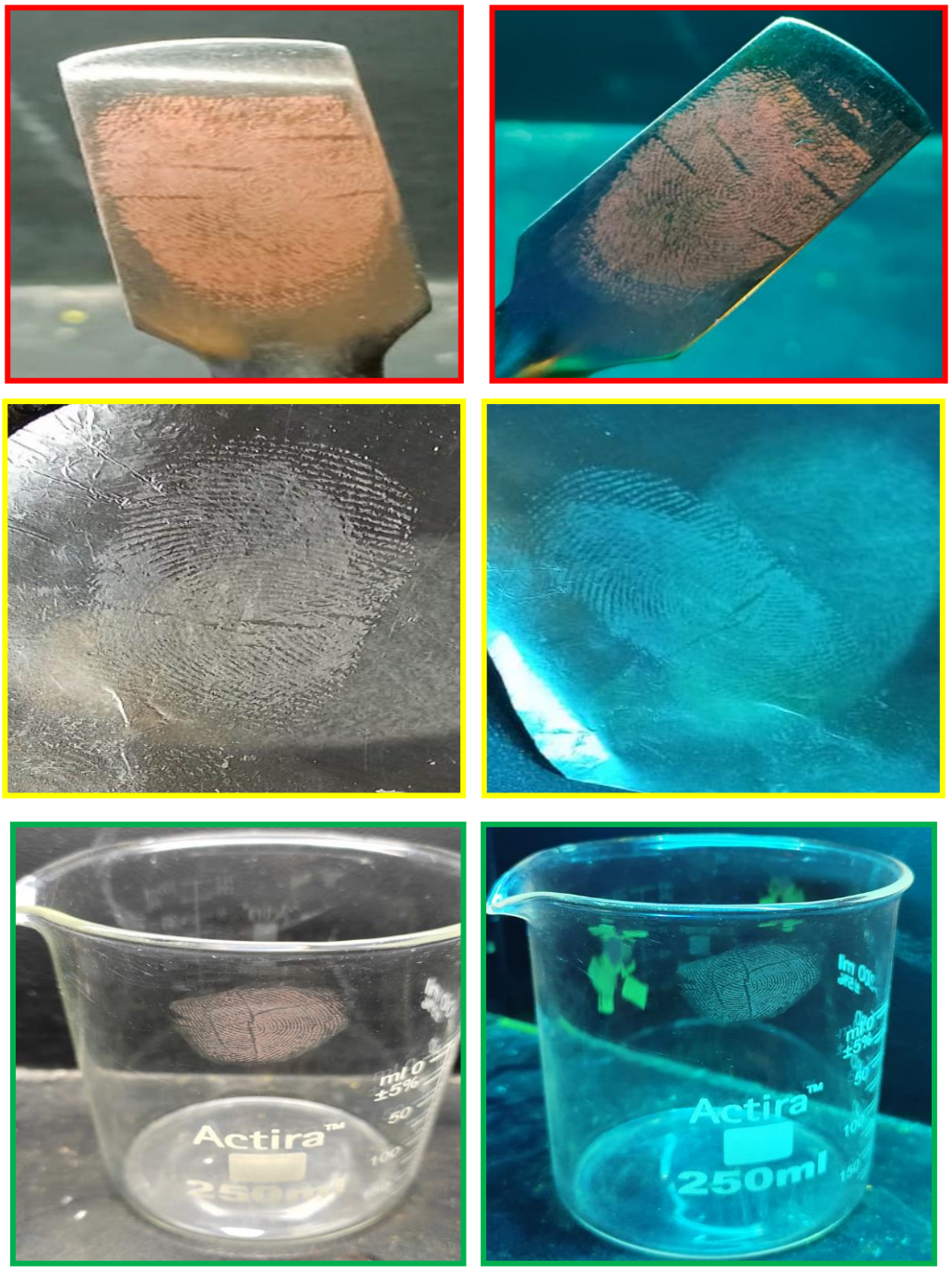

Fig. 4A.7 Developed LFPs on Spatula, Aluminum foil and Beaker using synthesized compounds **Sb1** and **Sb2**.

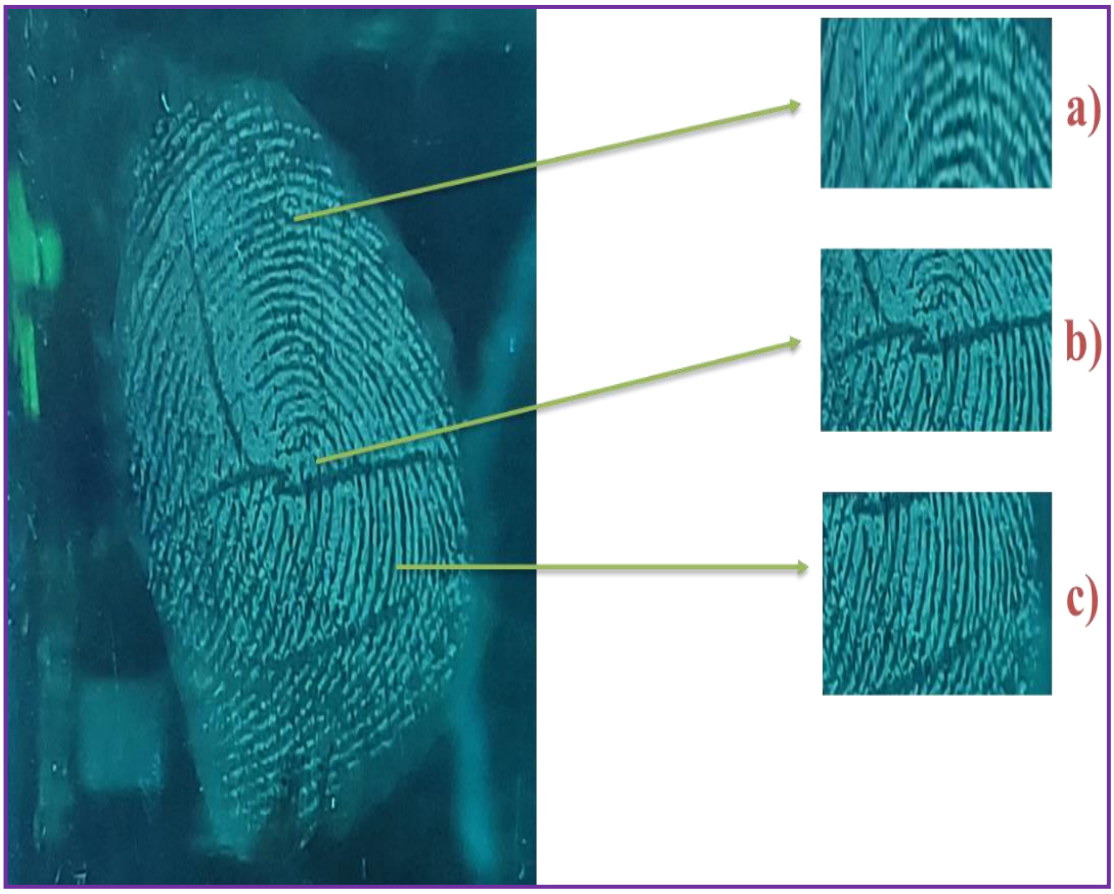

Fig.4A 8 Level II and III features of LFP ridges on 500 mL beaker using compound **Sb1**, a) bifurcation b) short ridge c) island.

4A.5 Conclusion

Chapter 4A describes that two new Schiff base heterocyclic compounds (**Sb1** and **Sb2**) were successfully synthesized using an acid catalyst in solvent media. These compounds have good electron absorption properties in a highly polar solvent by exhibiting a band at the visible region. Similarly, compounds also have better emission properties by emitting blue emissions, this emission was supported by the CIE coordinates. Redox onset potential (experimental HOMO-LUMO) reveals the electrochemical behavior and regeneration recaptures of the injected electron by the synthesized compounds. Further, computational studies and calculated quantum parameters reveal higher chemical reactivity and better emission properties. Compounds showed clear observation of level II and III features of fingerprints ridges on selected glasswares. Hence, these compounds are potential materials for OLEDs, DSSCs application-oriented materials and forensic science.

4A.6 Reference

1. N.H. Deepthi, G.P. Darshan, R.B. Basavaraj, B.D. Prasad, H. Nagabhushan, *Sensor. Actuator. B Chem.,* 255 (**2018**) 3127-3147.
2. W.S. Alwan, R. Karpoormath, M.B. Palkar, H.M. Patel, R.A. Rane, M.S. Shaikh, A. Kajee, K.P. Mlisana, *J. Eur. J. Med. Chem.,* 95 (**2015**) 514-525.
3. A.T. Farghalya, G.S. Masaret, Z.A. Muhammad, M.F. Harras, *J. Bioorg. Chem.*, 98 (**2020**) 103761-103774.
4. A. Kathiravan, K. Sundaravel, M. Jaccob, G. Dhinagaran, A. Rameshkumar, D.A. Ananth, T. Sivasudha, *J. Phys. Chem. B.,* 118 (**2014**) 13573-13581.
5. S.S. Jawoor, S.A. Patil, S.S. Toragalmath, *J. Coord. Chem.,* 71 (**2018**) 271-283.
6. V.R. Mishra, C.W. Ghanavatkar, S.N. Mali, H.K. Chaudhari, N. Sekar, *J. Biomol. Struct. Dyn.,* 38 (**2019**) 1772-1785.
7. V. Nishal, D. Singh, A. Kumar, V. Tanwar, I. Singh, R. Srivastava, P.S. Kadyan, *J. Org. Semicond.,* 2 (**2014**) 15-20.
8. M. Kose, G. Ceyhan, M. Tumer, I. Demirtas, I. Gonul, V. McKee, Monodentate, *Spectrochim. Acta A Mol. Biomol. Spectrosc.,* 137 (**2015**) 477-485.
9. K.M.P. Lokhande, K.K. Sonigara, M.M. Jadhav, D.S. Patil, S.S. Soni, N. Sekar, *Chem. Sel.,* 4 (**2019**) 4044-4056.
10. T. Venkatesh, K. Upendranath, Y.A. Nayaka, *J. Solid. State. Electrochem.*, 25 (**2021**) 1237-1244.
11. B.V. Lichitskii, V.G. Melekhina, A.N. Komogortsev, C.V. Milyutin, A.N. Fakhrutdinov, Y.O. Gorbunov, M.M. Krayushkin, *Org. Biomol. Chem.,* 12 (**2020**) 2501-2509.
12. H. Hagiwara, K. Sato, D. Nishino, T. Hoshi, T. Suzuki, M. Ando, *J. Chem. Soc., Perkin Trans.*, 1 (**2001**) 2946-2957.
13. M. Sayeda, O. Younisa, R. Hassanien, M. Ahmeda, A.A.K. Mohammed, A.M. Kamalc, O. Tsutsumi, *J. Photo. Chem. Photo. bio. A, Chem.*, 383 (**2019**) 111969-11971.
14. O. Younis, E.A. Orabi, A.M. Kamal, M. Sayed, R. Hassanien, R.L. Davis, O. Tsutsumi, M. Ahmed, *J. Opt. Mater*., 100 (**2020**) 109713-109813.

15. S. Singhal, P. Khanna, L. Khanna, *Heliyon.*, 5 (**2019**) 02596-02616.

16. A.M. Asiri, S.A. Khan, H.M. Marwani, K. Sharma, *J. Photo.chem. Photo.bio. B. Bio.*, 123 (**2013**) 82-89.

17. J. Liua, X. Menga, H. Duana, T. Xub, Z. Dinga, Yu Liuc, L. Lucia, *Sen. and Actu. B.*, 227 (**2016**) 296-303.

18. I. Kaya, M. Yıldırım, A. Avc, *Syn. Met.*, 160 (**2010**) 911-920.

19. S. Ghosh, D. Singharoy, S. Konar, J.P. Naskar, S.C. Bhattacharya, *J. Coor. Chem.*, 74 (**2021**) 1272-1283.

20. D. Sek, M. Siwy, K. Bijak, M. Filapek, G. Malecki, E.M. Nowak, J. Sanetra, A.J. Jedryka, K. Laba, M. Lapkowski, E.S. Balcerzak, *J. Electroanal. Chem.*, 751 (**2015**) 128-136.

21. T. Sutradhar, A. Misra, *J. Phys. Chem. A.*, 122 (**2018**) 4111-4120.

22. K.H. Ibnaouf, A.O. Elzupir, M.S.A. Salhi, A.S. Alaamer, *J. Opt. Mater*., 76 (**2018**) 216-221.

23. A.A. Gabr, *Spectrochim. Acta Part Mol. Spectrosc.*, 46 (**1990**) 1751-1757.

24. E. Ermis, K. Durmus¸ *J. Mol. Struct.*, 1217 (**2020**) 128354-128360.

25. M.M. Duvenhagel, O.M. Ntwaeborwal, H.G. Visser, H.C. Swart, *J. Condens. Matter Phys.*, 439 (**2014**) 46-49.

26. L. Leonat, S. Gabriela, I.V. Branzoi, *U.P.B. Sci. Bull. Series B.*, 75 (**2013**) 111-119.

27. K.V. Basavarajappa, Y.A. Nayaka, R.O. Yathisha, K.B. Manjunath, *J. Fluoresc*., 29 (**2019**) 1201-1211.

28. A. Becke, *Phys. Rev. A.*, 38 (**1988**) 3098-3100.

29. A. Bendjeddou, T. Abbaz, A.K. Gouasmia, D. Villemin, *J. Pure Appl. Chem.*, (**2016**) 1-9.

30. A. Mahmood, S.U. Khan, U.A. Rana, M.R.S.A. Janjua, M.H. Tahir, M.F. Nazar, Y. Song, *J. Phys. Org. Chem.*, 28 (**2015**) 418-422.

31. M.I. Abdullah, M.R.S.A. Janjua, M.F. Nazar, A. Mahmood, *Bull. Chem. Soc. Jpn.*, 86 (**2013**) 1272-1281.

32. A. Erdemir, S. Li, Y. Jin, *Int. J. Mol. Sci.*, 6 (**2005**) 203-218.

33. M.F. Nazar, A. Badshah, A. Mahmood, M.N. Zafar, M.R.S.A. Janjua, M.A. Razaa, R. Hussaind, *J. Phys. Org. Chem.*, 29 (**2016**) 152-160.

34. Lee, M.M. Joullié, *Tetra. Lett.*, 56 (**2015**) 3378-3381.

35. D. Navami, R.B. Basavaraj, S.C. Sharma, B.D. Prasad, H. Nagabhushan, *J. Alloys Compd.*, 762 (**2018**) 763-779.

36. D. Navami, R.B. Basavaraj, G.P. Darshan, H.K. Inamdar, S.C. Sharma, H.B. Premkumar, H. Nagabhushana, *J. Optic. Mati.*, 88 (**2018**) 479-487.

37. R.B. Basavaraj, H. Nagabhushana, G.P. Darshan, B.D. Prasad, S.C. Sharma, K.N. Venkatachalaiah, *J. Ind. Eng. Chem.*, 51 (**2017**) 90-105.

38. M. Dhanalakshmi, H. Nagabhushana, R.B. Basavaraj, G.P. Darshan, B.D. Prasad, *ACS Sustain. Chem. Eng.*, 6 (**2018**) 5214-5226.

Chapter -4B

Optoelectronic, DFT and Current-Voltage performance of new Schiff base 6-nitro-benzimidazole derivatives

4B.1 Introduction.

The growth of population and industrial sector leads to greater demands for the use of renewable energy sources such as wind, water and solar [1-4]. To reduce human efforts and to reach industrial demands, researchers have been interested in the development of metal-free organic dyes as an organic semiconductor to use in energy conversion devices by absorbing the sunlight. Photovoltaic cells (PV cells) or dye-sensitized solar cells (DSSCs) are considered energy conversion device that generates electricity using dye compounds under sunlight. DSSCs were known as third-generation photovoltaic cells and nowadays it is much more fascinating than silicon-based solar cells by using organic dyes as semiconductors [5]. The previous reports reveal that many metal complexes as dyes were used in OLEDs, organic-thin film transistors (OTFTs), and PV cells due to their better optical and intramolecular charge transportation with molar extinction co-efficient properties [6, 7]. Metal complexes found some drawbacks such as lower efficacy, high cost of metals and lengthy step reactions. To overcome these challenges, simple metal-free organic dyes as organic semiconductors are concentrated to increase the efficiency of the DSSCs.

Simple metal-free organic dyes consisting of chalcones [8], benzimidazole [9], coumarins [10] having D-π-A groups are known as electrooptical materials are the future due to their structural characteristics, ease of synthesis and fabrication as well as low-cost productions on an industrial scale [11]. Chalcones are open-chain π-conjugated organic compounds connected by α, β-unsaturated carbonyl compound, where the molecules belong to one of the most important families of flavonoids in the plant kingdom [12]. π-conjugated open-chain systems were nominated as electro-optical materials because of their unique structural properties and the presence of

carbonyl group act as an acceptor group, hence it's attracting towards energy storage materials such as optoelectronics, OLEDs, supercapacitors and NLO devices etc., [13, 14]. Chalcones and benzimidazole exhibit noble spectral and optical properties which may use as fluorescent sensors, electro-optical, and laser dyes when they consist of donor and acceptor materials linked by π-spacer [15, 16]. The presence of anchoring groups such as electron-donating groups (CH_3, OH, OCH_3 etc.) and electron-accepting groups (COOH, NO_2, CN) exhibits high electroluminescent properties in the visible region and the easy electron-hole transfer occurs when absorbed by light [17, 18]. Similarly, the benzimidazole molecule act as a π-spacer having an anchoring group and aromatic conjugation will increase color sensitivity and also may help to absorb the sunlight [19-21].

Mohd Shakir *et al.,* reported a new chalcone derivatives as donor-π-acceptor moieties as organic charge transfer and non-linear optical materials (**1**). Obtained compound gives a better absorption band at 290 nm to 320 nm of the visible region and theoretical studies of energy molecules reveal that synthesized compound are hard molecules hence they have better photostability [22]. In 2020, Shruthi *et al.,* reported a new chalcone compound (**2**) and have exhibits better non-linear optical properties and show good emission behaviour by exhibiting at 510 nm of longer wavelength [23].

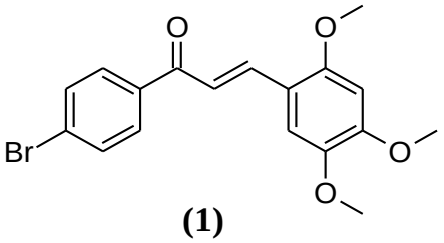

(1)

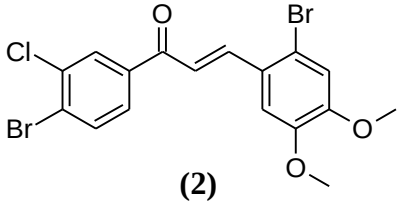

(2)

D. Halesheppa and co-workers reported a new compound (*E*)-1-(thiophen-2-yl)-3-(4-chlorophenyl)prop-2-en-1-one (**3**) in 2021. The reported compound has better optoelectronic properties where absorption and emission band show at bathochromic shifts. Also synthesized compound has better NLO properties which are proven by both theoretical and experimental studies. Further, the structure of the synthesized compound was confirmed by single-crystal XRD [24].

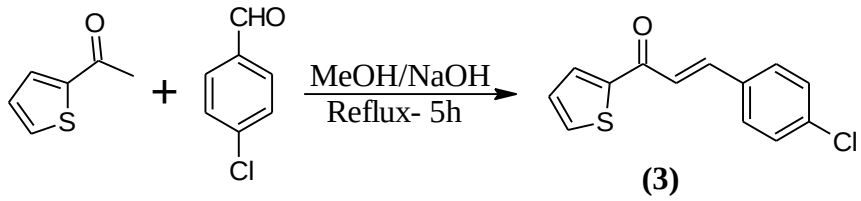

(3)

Marwa N *et al.,* reported (2021) a new thiophene-substituted chalcone compound (**4**) obtained by the reaction of 2-thio acetophenone and 9-phenanthrenecarbaldehyde in alcoholic conditions using sodium hydroxide as a catalyst. Obtained product has a solvatochromic effect under UV-light, and the compound shows better photophysical properties in solvent medium where absorption and emission band appeared at redshift (320 nm to 582 nm) [25].

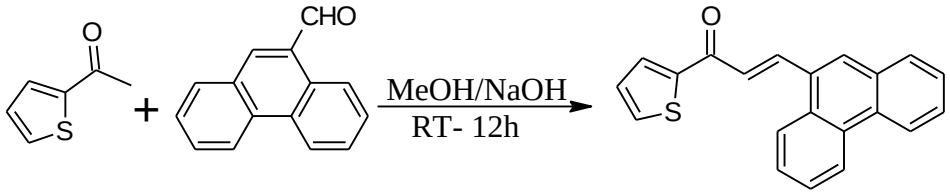

(4)

Chalcone derivatives are promising materials for optoelectronic applications, hence, in the year 2017, Kien Yung Teo *et al.*, reported a bis chalcone compounds (**5**). Obtained compound were used as dyes for the application of DSSCs and reached 0.30% efficiency on ITO conductive glass [26].

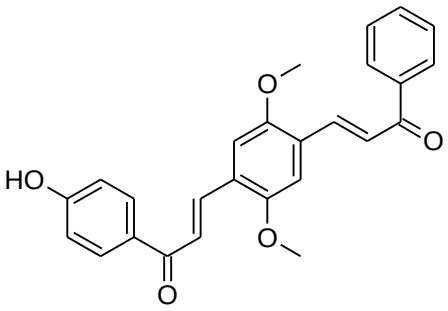

(5)

Sanjan *et al.,* reported a Schiff base of bis chalcone compound (**6**) in 2021. The targeted compound shows better photophysical properties where bands appear at a longer wavelength (328 nm to 498 nm) and have good electrochemical behaviour. Further, theoretical studies reveal that compound said to be hard molecule, therefore it has greater photostability [27].

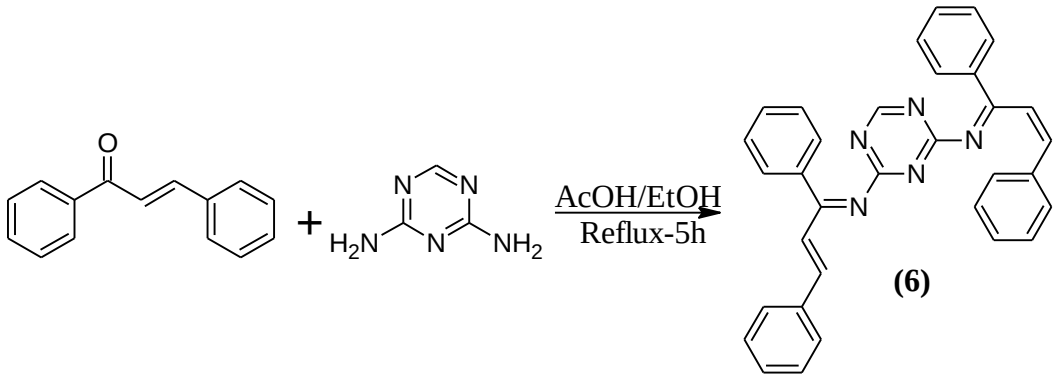

(6)

The above reported chalcone derivatives have shown better optical and electrochemical properties due to π-conjugation in the phenyl ring. Hence, they are promising materials for material science applications such as DSSCs, OLEDs, and sensor applications.

4B. 2 Present Work.

Keeping all observations and considering the above results, we have synthesized new Schiff base benzimidazole containing chalcone derivatives using an acetic acid catalyst in methanol and studied their optoelectronic, DFT and current-voltage studies.

The reaction pathway has been represented as **Scheme-4B**

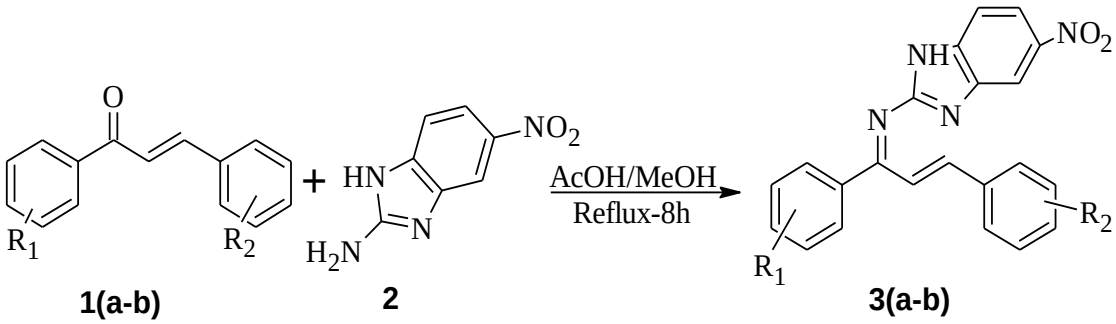

1(a-b) **2** **3(a-b)**

Entry	R_1	R_2
3a	OCH_3	OH
3b	OCH_3	NO_2

Scheme 4B: Synthesis of Schiff base substituted chalcone containing 6-nitro-benzimidazole derivatives (**3a** and **3b**).

4B.2.1 Characterization.

The structures of targets were confirmed by using different spectroscopic techniques such as FTIR, ^{1}H and ^{13}C-NMR and Maas spectrometry.

The FTIR spectrum of synthesized compound **3a** shows a stretching vibration band at 3284 cm^{-1} due to the N-H functionality of the benzimidazole ring and another vibration band at 2844 cm^{-1} correspond to the methoxy (OCH_3) group. The absorption band at 1638 cm^{-1} is correspond to the C=N stretching frequency. In ^{1}H-NMR spectrum of **3a**, a singlet peak obtained at δ 8.74 ppm corresponds to NH proton and

peaks at δ 8.65-7.05 ppm correspond to eleven aromatic protons (Ar-11H). Two doublet peaks at δ 6.98-6.96 and 6.91-6.89 ppm corresponds to two CH protons, and a singlet peak at δ 3.84 ppm corresponds to methoxy proton. In the ^{13}C-NMR, a peak at δ 159.14 ppm correspond to N=C-NH, and δ 148.95 to 122.54 aromatic carbons a peak at δ 56.16 ppm corresponds to methoxy carbon. The molecular ion peak m/z at 442.0471 corresponds to the molecular weight of targeted compound **3a**.

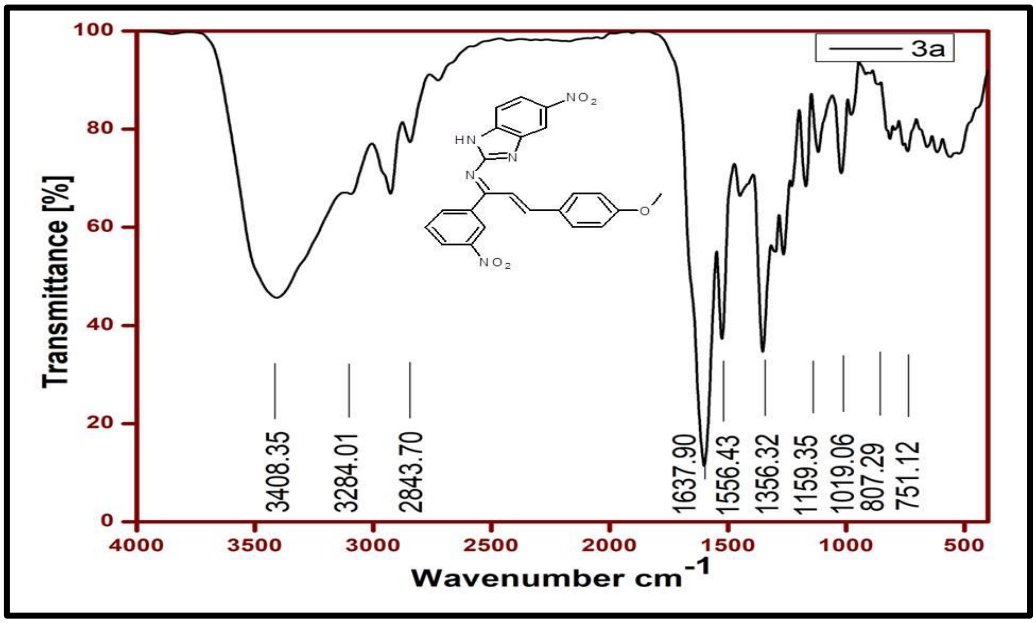

FTIR spectrum of compound 3a

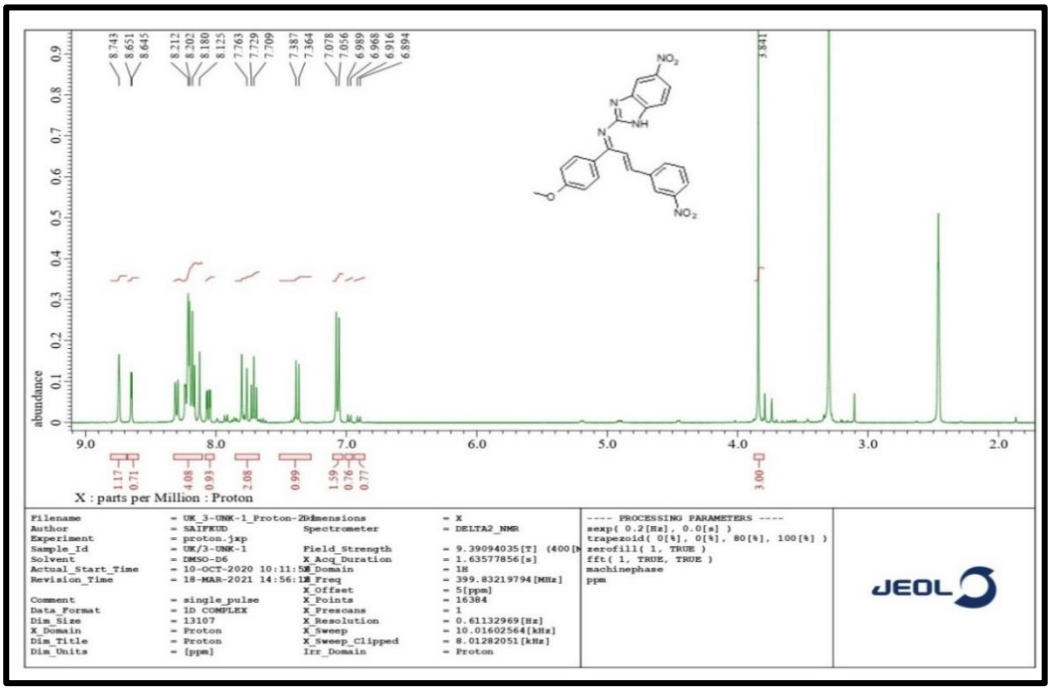

^{1}H-NMR spectrum of compound 3a

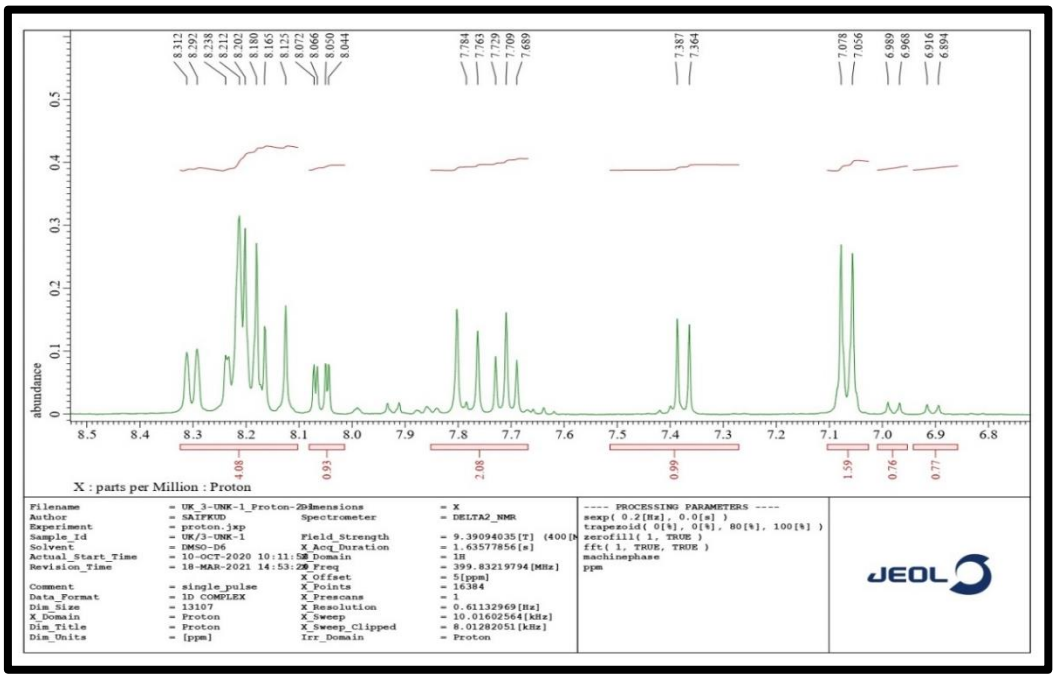

Expansion of ^{1}H-NMR spectrum of compound 3a

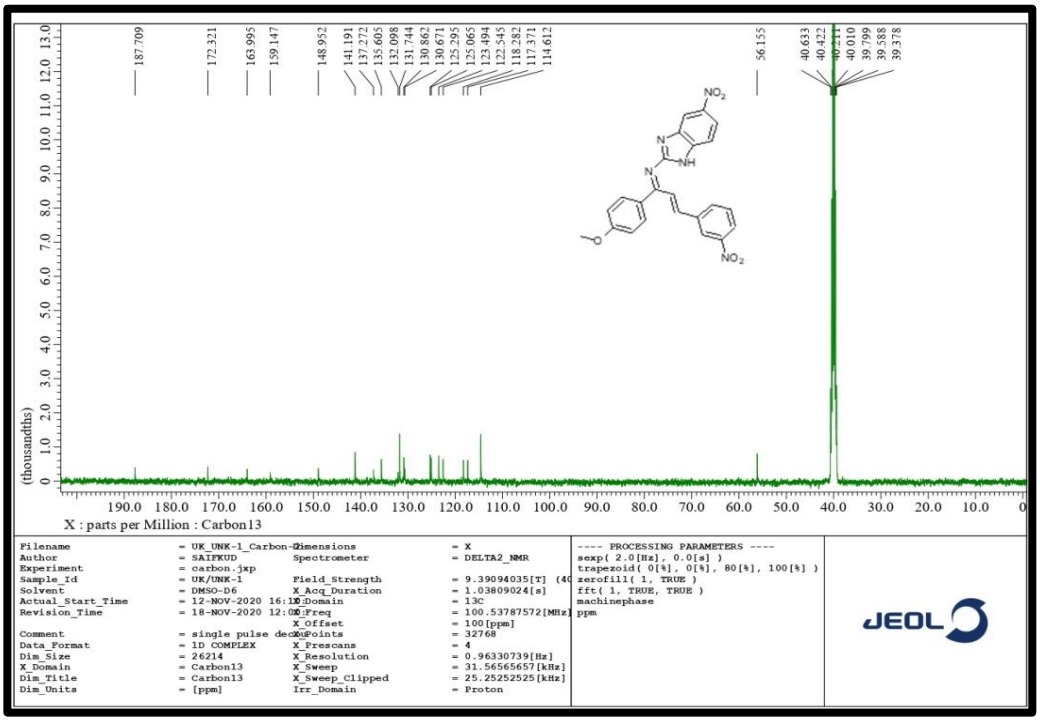

^{13}C-NMR spectrum of compound 3a

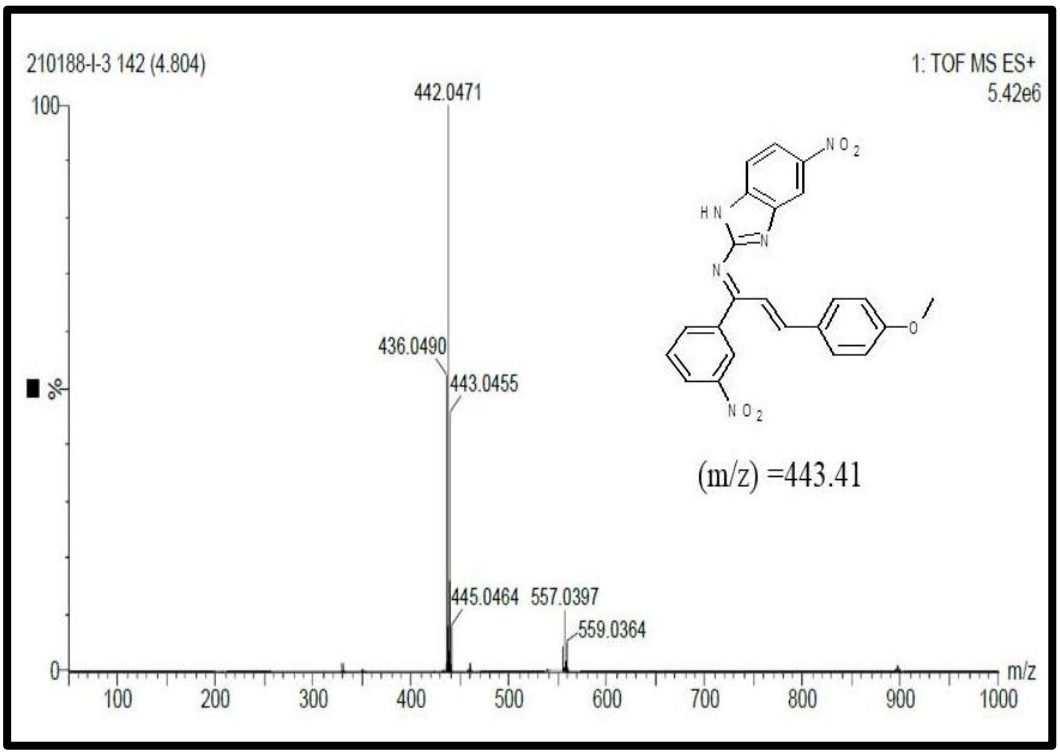

Mass spectrum of compound 3a

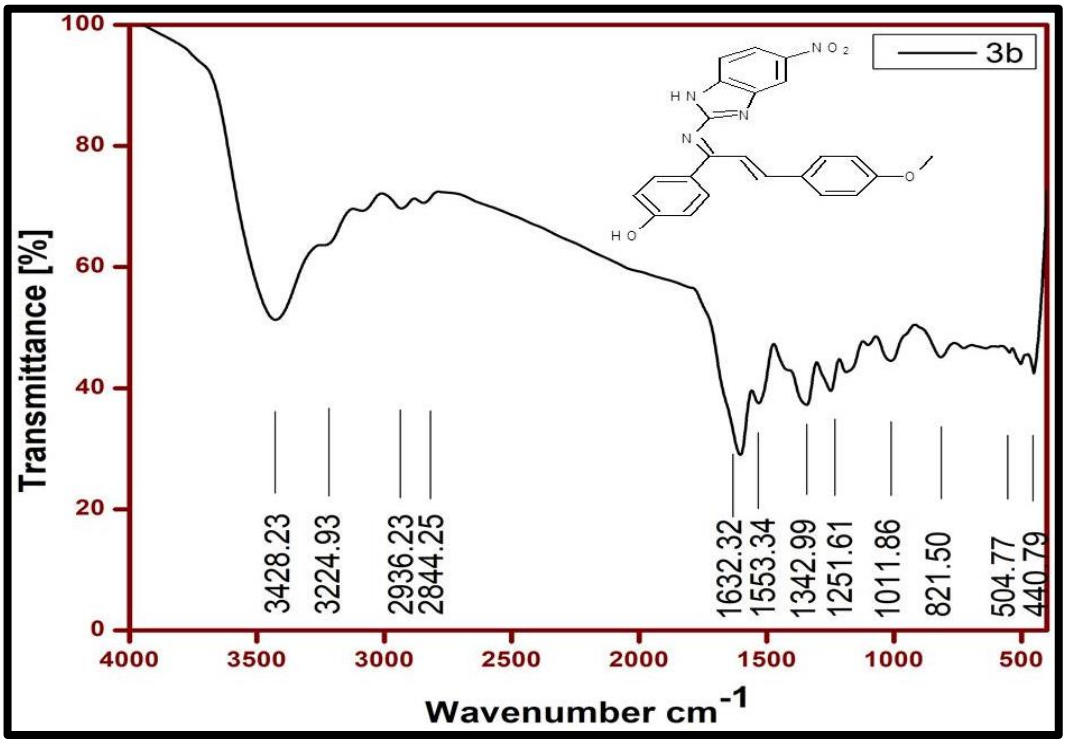

FTIR spectrum of compound 3b

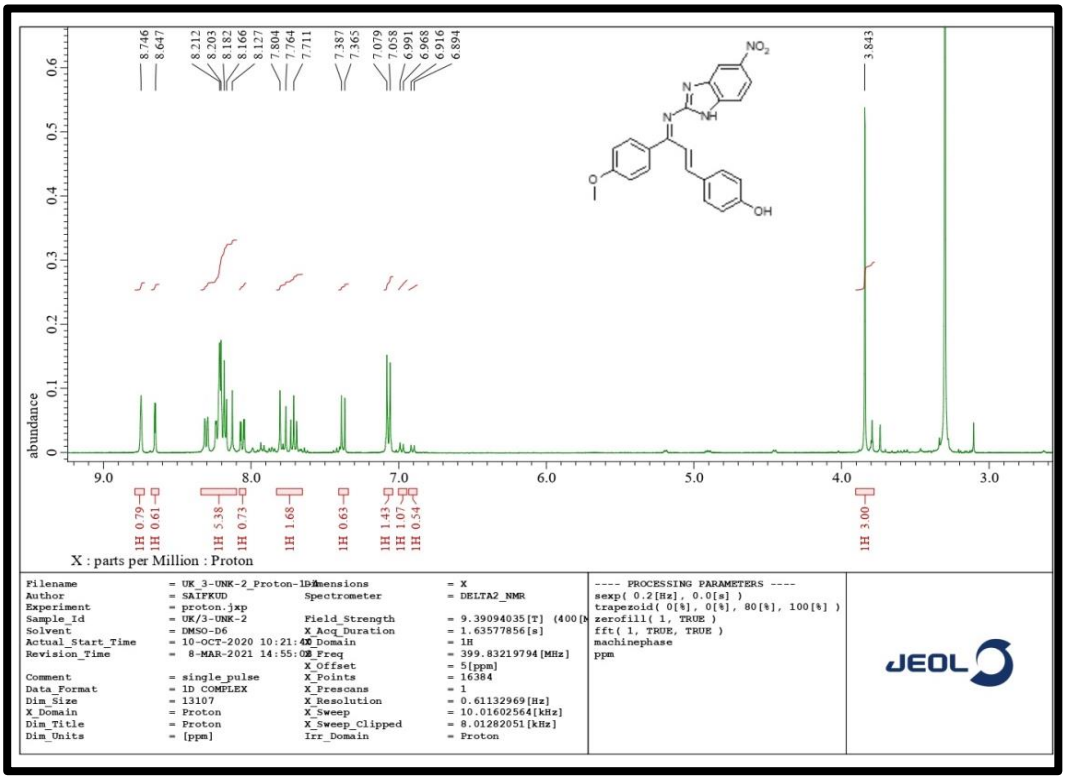

^{1}H-NMR spectrum of compound 3b

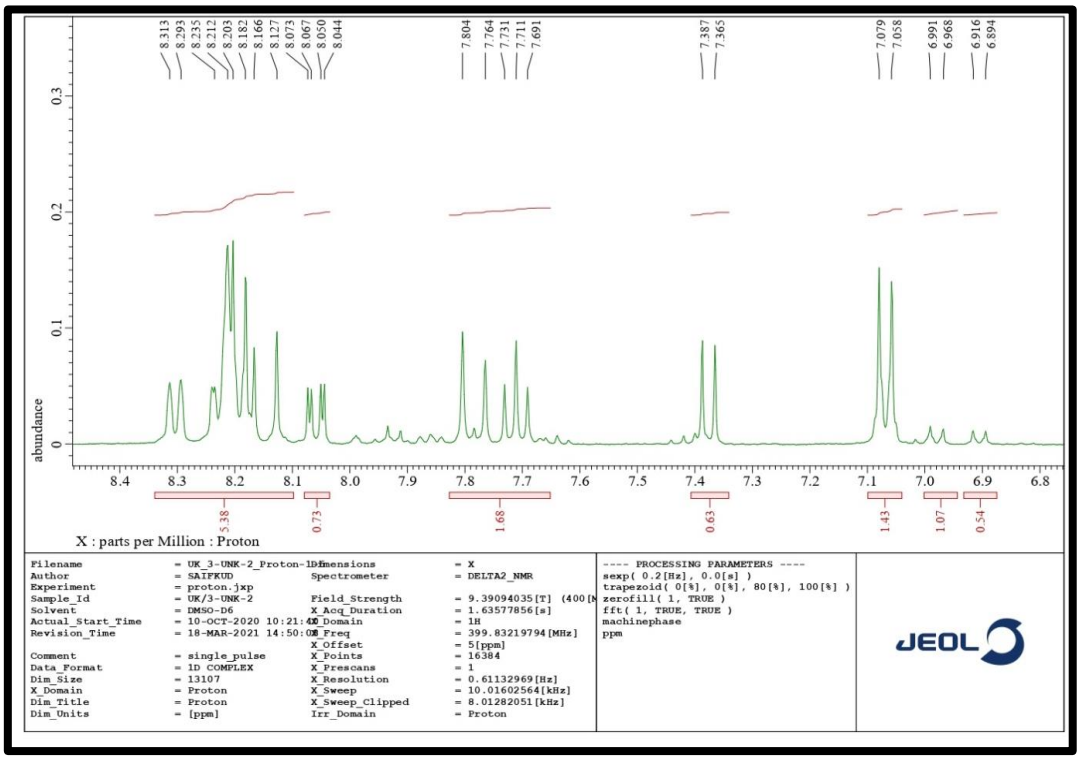

Expansion of ^{1}H-NMR spectrum of compound 3b

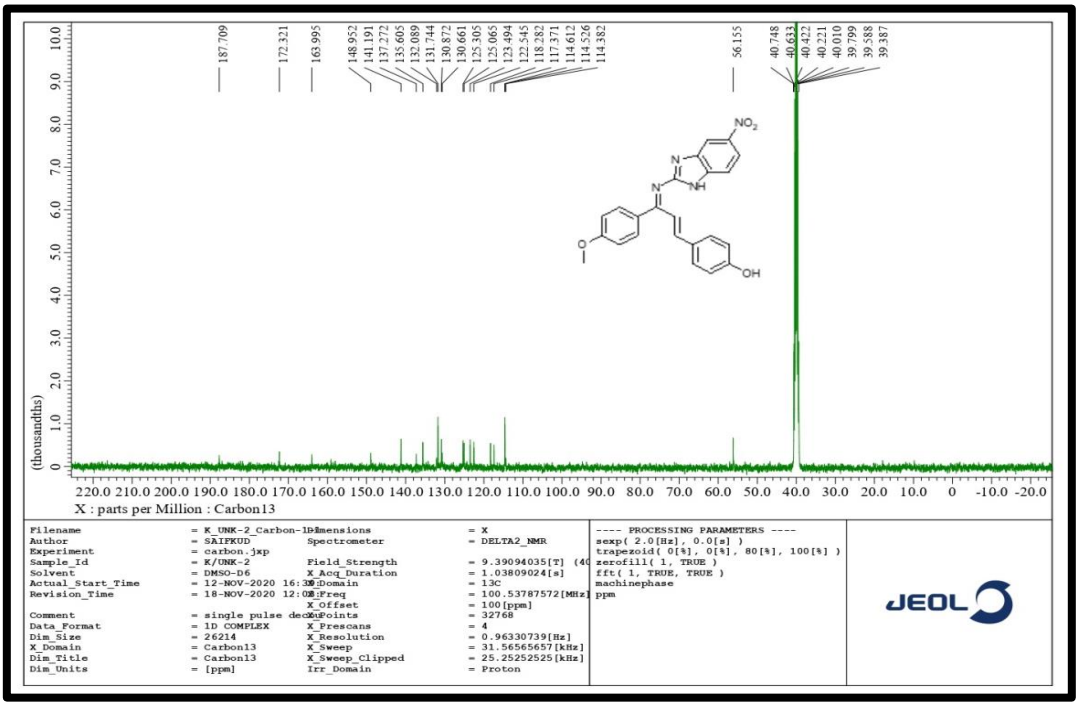

^{13}C-NMR spectrum of compound 3b

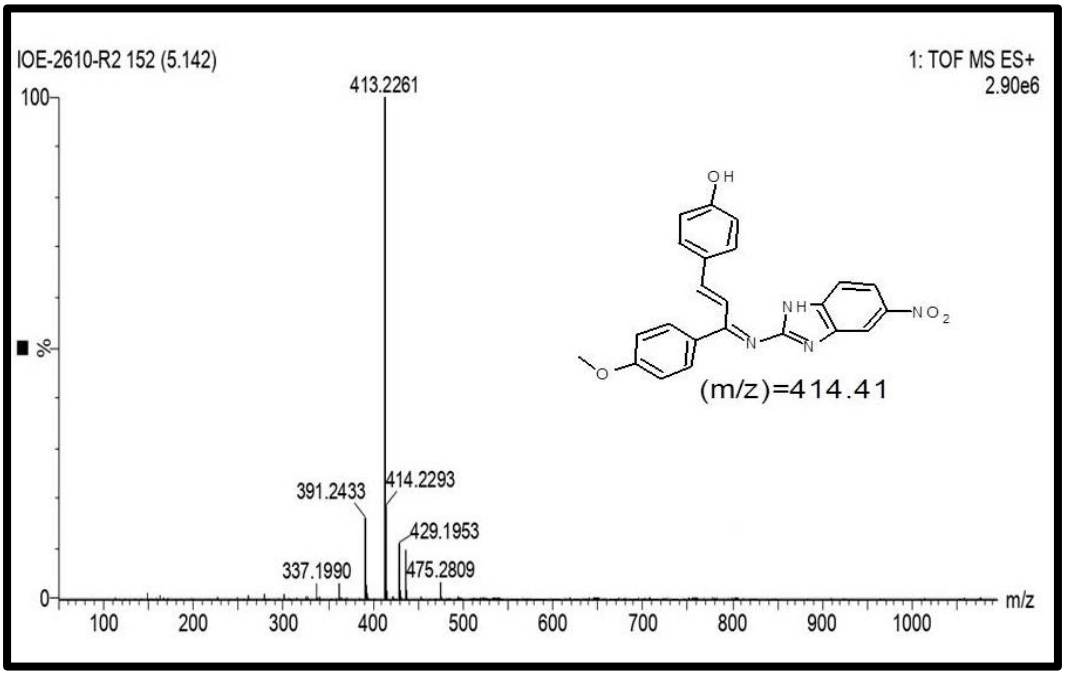

Mass spectrum of compound 3b

4B. 3 Experimental.

4B.3.1 General information.

The used solvents, chemicals, and instruments have been explained in detail in the previous **Chapter 2A**. The detailed of cyclic voltammetry, computational procedure have been discussed in the experimental section **2A.3**.

4B.3.2 General Procedure for the synthesis of substituted chalcone containing 6-nitro-benzimidazole derivatives (3a and 3b).

In a 100 mL round bottom flask, substituted chalcones **1** (**a** and **b**) and 2-amino-6-nitro-benzimidazole (**2**) were taken as equimolar quantity in methanol (10 mL) in presence of AcOH as catalyst and reaction kept under reflux temperature for about 8 h. After the completion of the reaction; the mixture was cooled and poured into 100 mL ice flakes with vigorous stirring to get the solid compound, filtered, washed with water, dried and recrystallized from pure ethanol (**Scheme 4B**).

1-(4-Methoxyphenyl)-3-(3-nitrophenyl)allylidene)-5-nitro-1H-benzo[d]imidazole2-amine (3a):

Yellow solid; Yield: 84%; MP: 235-238 ºC; Mol. Formula: $C_{23}H_{17}N_5O_5$; FTIR (υ, cm^{-1}): 3284 (NH), 2843 (OCH_3), 1638 (C=N), 1556 ($C\text{-}NO_2$); ^{1}H-NMR (δ ppm): 8.74 (s, 1H, NH), 8.65-8.64 (d, *J* = 4 Hz, 1H, Ar-H), 8.31-8.12 (m, 4H, Ar-H), 8.07-8.04 (dd, *J* = 8.8 Hz, 1H), 7.78-7.68 (m, 2H, Ar-H), 7.38-7.36 (d, *J* = 8 Hz,1H, Ar-H), 7.07-7.05 (d, *J* = 8 Hz, 2H, Ar-H), 6.98-6.96 (d, *J* = 8 Hz, 1H, CH), 6.91-6.89 (d, *J* = 8 Hz, 1H, CH), 3.84 (s, 3H, OCH_3); ^{13}C-NMR (δ ppm): 187.70, 172.32, 163.99, 159.14, 148.95, 141.19, 137.27, 135.60, 132.09, 131.74, 130.86, 130.67, 125.29, 125.06, 123.49, 122.54, 118.28, 117.37, 114.61, 56.15; HRMS (m/z): 443.0471 [M^+1]; Anal Cal. For; C 62.36, H 3.86, and N 15.59 %; Found C 61.49, H 3.98, and N 13.65 %.

3-(4-Methoxyphenyl)-3-((5-nitro-1H-benzo[d]imidazol-2-yl)imino)prop-1-en-1-yl)phenol (3b):

Pale yellow solid; Yield: 86%; MP: 230-232 ºC; Mol. Formula: $C_{23}H_{18}N_4O_4$; FTIR (υ, cm^{-1}): 3428 (OH), 3225 (NH), 2936 (CH), 2844 (OCH_3), 1632 (C=N), 1553 ($C-NO_2$); ^{1}H-NMR (δ ppm): 8.74 (s, 1H, OH), 8.64 (s, 1H, NH), 8.31-8.12 (m, 5H, Ar-H), 8.07-8.04 (dd, *J* = 12 Hz, 1H, Ar-H), 7.78-7.68 (m, 2H, Ar-H), 7.38-7.36 (d, *J* = 8 Hz, 1H, Ar-H), 7.07-7.05 (d, *J* = 8 Hz, 1H, Ar-H), 6.99-6.96 (d, *J* = 12 Hz, 1H, CH), 6.91-6.89 (d, *J* = 8 Hz, 1H, CH), 3.84 (s, 3H, OCH_3); ^{13}C-NMR (δ ppm): 187.70, 172.31, 163.99, 148.92, 141.19, 137.27, 135.60, 132.08, 131.74, 130.87, 130.66, 125.30, 125.06, 123.49, 122.54, 118.28, 117.37, 114.61, 114.52, 114.38, 56.15; HRMS (m/z): 414.2261 [M^+1]; Anal Cal. For; C 66.6, H 4.38, and N 13.52 %; Found C 65.39, H 4.28, and N 12.99 %.

4B.3.3. Preparation of Iodine/Triiodide (I^-/I_3) electrolyte.

An equimolar ratio of potassium iodide (1 mM) and iodine crystals (1 mM) was dissolved in 10 mL of ethylene glycol. The mixture was stirred in dark condition for 15 min; due to light sensitivity and obtained a reddish-brown colour solution, then the mixture was stored in a dark room. I^-/I_3 was used as a redox electrolytic solution and poured on a photoanode (dye-coated FTO glass) to measure the *I-V* characteristics [28].

4B.3.4. Fabrication of photoanode.

Initially, a fine FTO (25×25 mm 15 ohm/sqm) conductive glass was cleaned in acetone and ethanol with help of an ultrasonic bath for 10 min and then rinsed with distilled water and ethanol to remove impurities. Measured 0.25 g of nano-TiO_2 into the mortar and grinding by the addition of 0.5 mL of acetic acid for up to 20 min, and

further addition of deionized water and ethanol (1:3) dropwise to afford the clear suspension. Further, to get a clear homogenous paste, Triton-X 100 (binder oil) has been added and grind for another 20 min. Obtained homogenous TiO_2 paste was coated on FTO conductive glass by the doctor blade method on a selected area as a thin film. FTO glass was allowed to dry at room temperature and then sintered at 450 ^oC for 20 min to get a fine mesoporous thin film, further it was immersed in dye solution (0.6 mM dye molecule in 10 mL acetonitrile) for 36 h and kept in a dark room [29].

4B.3.5. Preparation of carbon paste electrode for electrochemical sensor.

Carbon paste electrode was prepared to determine the Dolo drug bin molecule in 1 M NaOH electrolytic solution as a sensor application. The paste was prepared by mixing 75 % of the graphite powder with 15 % of the prepared powder and 10 % of silicone oil was added (20 °C, 0.98-1.0 g/mL and 370-500 mP as viscosity) with a mass ratio of 15:70:15 were manually mixed in a mortar for about 25 minutes to enhance the mechanical strength of the electrode. The well grinded mixture was pasted with the synthesized compounds **3a** and **3b** into a homemade Teflon cavity (0.3 mm of surface area) tube and then the surface was smoothed, pressing gently on weighing paper to ensure better electrical contact [30].

4B.3.6. Current-Voltage studies.

The current-voltage response was studied using two sense Keithley source meter in the presence and absence of light medium using 264 nm mercury lamp as a light source. The fabricated photoanode of a 1cm active area was coated by nano TiO_2 as a mesoporous thin film and immersed in acetonitrile solvent with synthesized compounds for about 36 hours in a dark room [31].

4B.4 Results and discussion

4B.4.1 Absorption properties.

Absorption spectra of synthesized compounds **3a** and **3b** were recorded in different solvents (MeCN, DMSO and EtOH) using a UV-Visible spectrophotometer. **Fig.4B. 1a** shows, dual peaks have appeared at a bathochromic shift at ~333 to 387 nm, for compound **3a**, and compound **3b** has shown~318 nm to 387 nm at the near-visible region. The longer wavelength is due to the aromatic π-conjugation of the compounds and the presence of electron-donating nitro group on benzimidazole and benzene ring and also involves π-π* and n-π* electronic transitions [32, 33]. Further, the experimental optical band was calculated using equation (1).

$$E_g = 1240/\lambda_{onset}\ \text{eV} \qquad \text{— (1)}$$

To study the electronic state, atomic band structures and optical absorption or transmittance window properties of the synthesized compounds by the calculation of energy bandgap. It has been calculated from the Tauc method using Kubelka–Munk theory and the graph was plotted against $(\alpha hv)^2$ *vs* hv [34, 35]. In the solvent system (**Fig. 4B.1b. a-c**), the energy bandgap was obtained at 3.0 eV- 3.9 eV and compound **3a** have been found at 3.03 eV, 3.02 eV, and 3.03 eV, while compound **3b** has been at found 3.18 eV, 3.52 eV and 3.35 eV. Here, **3b** has been found higher energy band gap than compound **3a** due presence of electron-donating (OH) and electron-accepting (OCH_3, NO_2) groups where both groups will be a donor-π-acceptor moiety, while in **3a** compound electron-accepting (OCH_3 and NO_2) groups were acting as acceptor moieties. Obtained absorption values and calculated optical band gap from the equation (1) and Tauc plot results were summarized in **Table 4B.1**. It suggests that synthesized compounds are semiconductors in nature to use in photovoltaic devices [36].

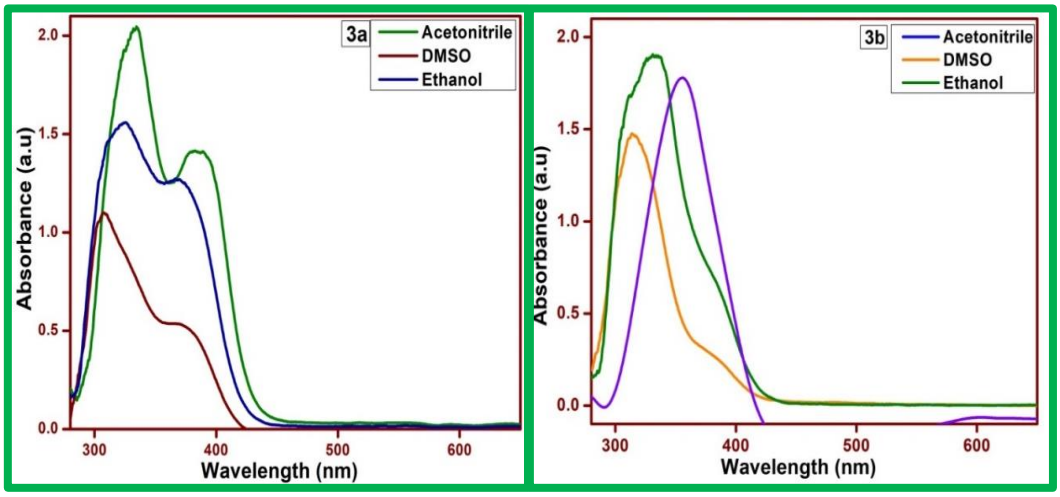

Fig.4B.1a. UV-Visible absorption spectra of compounds **3a** and **3b** in different solvent.

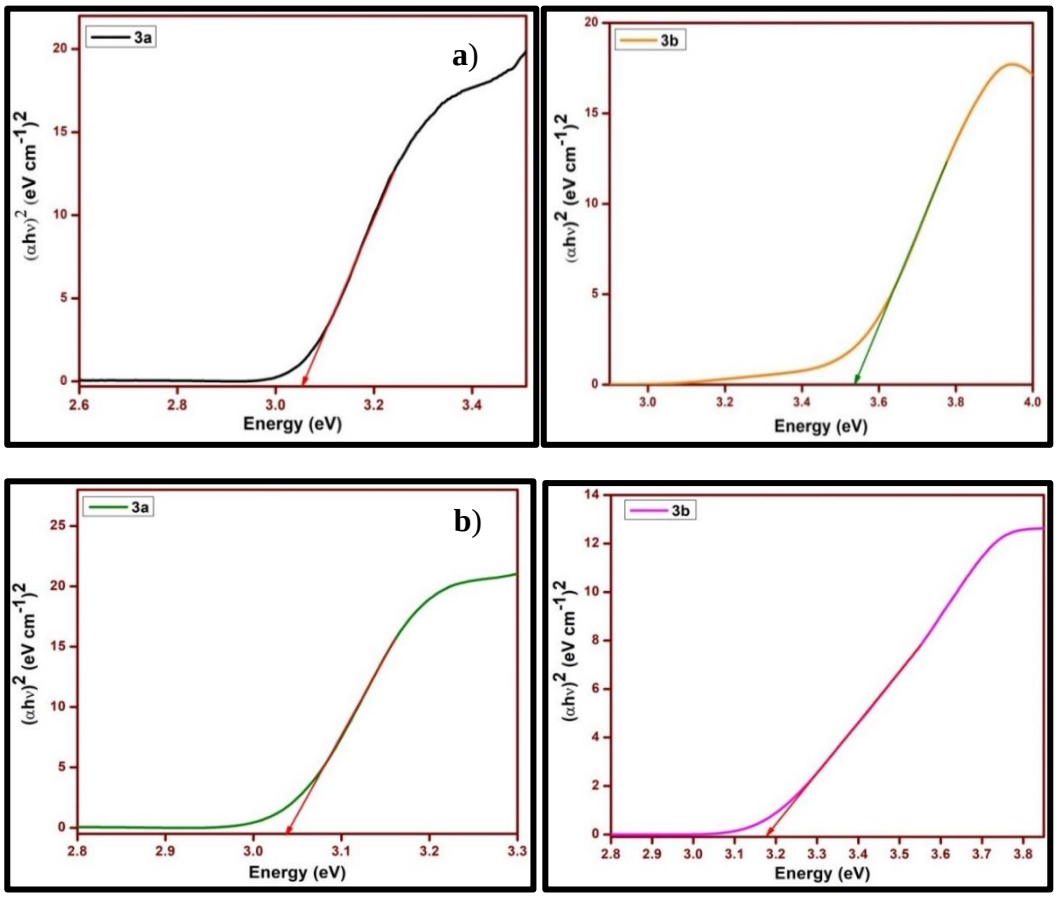

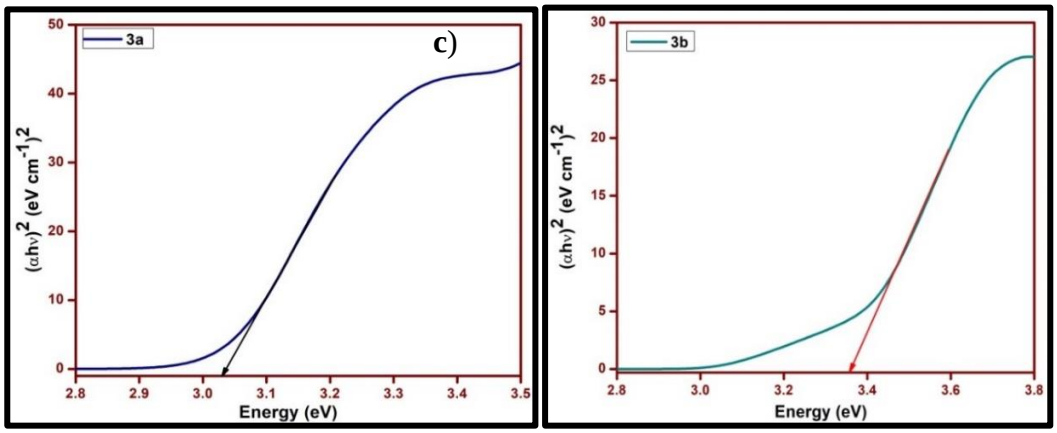

Fig.4B.1b. Tauc plots of synthesized compounds **3a** and **3b** in different solvents **(a)** DMSO, **(b)** MeCN and **(c)** EtOH.

Table 4B.1. Optical properties of dye compounds **3a** and **3b** in solvent system with an optical band gap.

Solvents	Entry	λ_{abs} (*nm*)	Experimental E_g^{OTP} (*eV*)	Tauc Plot E_g^{OTP} (*eV*)
Acetonitrile		333 and 387	3.72 and 3.20	3.03
DMSO	**3a**	325 and 375	3.81 and 3.33	3.02
Ethanol		307 and 377	4.03 and 3.28	3.03
Acetonitrile		355	3.79	3.18
DMSO	**3b**	318 and 387	3.89 and 3.20	3.52
Ethanol		337	3.67	3.35

4B.4.2 Emission Studies.

Emission studies were carried out in Photoluminescence spectrophotometer using DMSO solvent and those were represented in **Fig.4B.2a**. Compounds **3a** and **3b** were emitted at longer wavelength 546 nm and 576 nm with higher intensity due to anchoring groups such as electron-withdrawing NO_2 and OCH_3 group and electron-donating OH group [37, 38]. Further, PL properties also help to understand the efficiency of charge carriers in semiconductors and have been determined using a CIE diagram with calculated chromaticity coordinates as shown in **Fig.4B.2b**. Compounds **3a** and **3b** gives *X*= 0.455; *Y*= 0.5176 and *X*=0.4019; *Y*=0.5601. Position of the color

coordinates represented by star mark in the CIE diagram. The larger the difference is termed as stoke shift and the smaller difference is known as the anti-stokes shift. While **3a** and **3b** compounds have exhibited larger differences at 159 nm and 191 nm respectively, hence compounds have good interaction between solute and solvent. Emission spectral values were summarized in **Table 4B.2**.

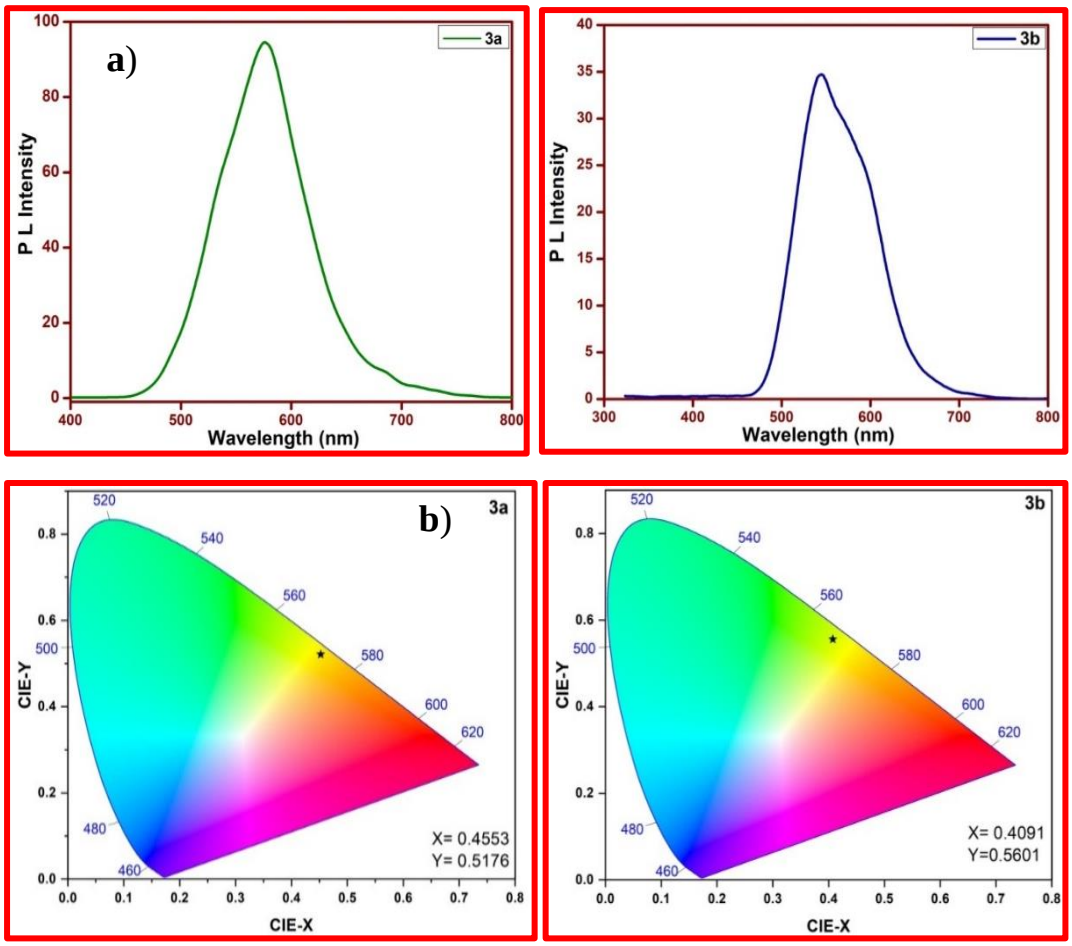

Fig.4B.2. (a) Photoluminescence spectra **(b)** CIE graphs of **3a** and **3b.**

Table 4B.2. Emission spectral results of synthesized dye compounds **3a** and **3b**.

Entry	$\lambda_{ecx\ (nm)}$	$\lambda_{emi\ (nm)}$	Stokes shift
3a	387	546	159
3b	385	576	191

4B.4.3 Electrochemical studies.

The electrochemical properties of compounds **3a** and **3b** were measured by using a cyclic voltammogram at the concentration of 3×10^{-6} M in DMSO solvent and PBS (7-pH) as supporting electrolytes. From the CV measurement, redox onset potential and redox current peaks have been determined, compounds **3a** and **3b** have exhibited two cathodic reduction peak current (E_{pc}) at -0.59 eV, -0.07 eV and -0.58 eV, -0.08 eV and one anodic oxidation peak current (E_{pa}) at 0.03 eV, and 0.05 eV respectively as shown in **Fig.4B.3(a)**. The electron-withdrawing groups (OCH_3 and NO_2) interact strongly through the E_{LUMO} and electron-donating groups (OH) interact through the E_{HOMO}. The compound shows quasi-reversible one-electron transfer and obtained redox onset potential used to calculate the energy levels E_{HOMO} and E_{LUMO} experimentally by using equations (3) and (4) [39]. The experimental calculated E_{LUMO} and E_{HOMO} of synthesized compounds **3a** and **3b** were obtained at -4.43 eV, -5.0 eV, and -4.45 eV, -4.98 eV respectively. The redox peak current and experimental parameters have been tabulated in **Table 4**.

$$E_{(HOMO)} = -\,[E_{(ox\text{-}onset)} + 4.4]\ \text{eV} \qquad \text{— (3)}$$

$$E_{(LUMO)} = -\,[E_{(red\text{-}onset)} + 4.4]\ \text{eV} \qquad \text{— (4)}$$

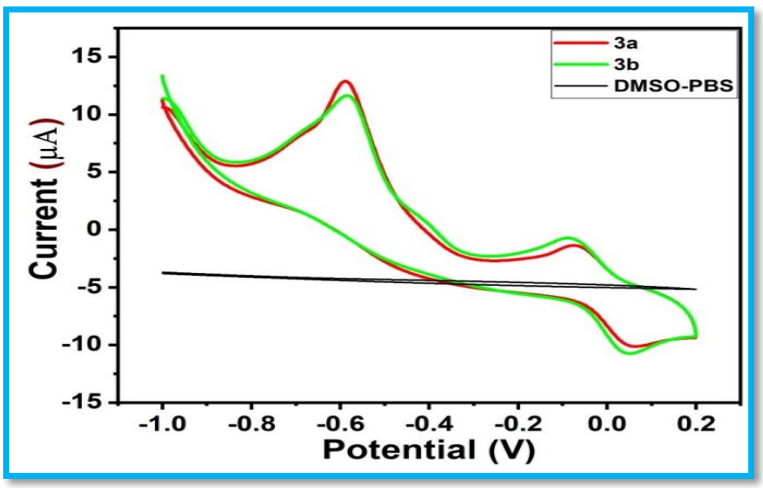

Fig.4B.3. Graph of Cyclic voltammogram (**3a** and **3b)** in DMSO and PBS as electrolyte.

Table 4B.3. Electrochemical parameters of synthesized dye compounds **3a** and **3b.**

Entry	E_{pa} (V)	E_{pc} (V)	E_{HOMO} (eV)	E_{LUMO} (eV)
3a	0.03	-0.59 and -0.07	-4.43 and -5.00	-3.81
3b	0.05	-0.58 and -0.08	-4.45 and -4.98	-3.82

4B.4.4 Electrochemical sensor.

The determination of Dolo bin drug in 1M NaOH solution as sensor application of synthesized compound **3a** and **3b** were assessed by the cyclic voltammogram of CH potentiostat instrument, where the dye compounds were used as a modifier by pasting to carbon electrode as the working electrode. In **Fig. 4B.4**, we found a variation in redox onset potential peaks which confirms the prepared carbon paste electrode using synthesized compounds **3a** and **3b** are the effective materials for sensor application. There was a change between anodic oxidation and cathodic reduction, whereas the cathodic reduction peak occurs at -0.64 eV and -0.71 eV for the compounds **3a** and **3b** and the same as anodic oxidation occurs at two peaks at -0.51 eV, 0.02 eV and -0.46 eV, and 0.04 eV respectively. We observe the two oxidation peaks for the synthesized compounds which may be the oxygen evolution peak that enhances the electrochemical sensor. The estimated electrochemical sensor data have mentioned in **Table 4B.4**.

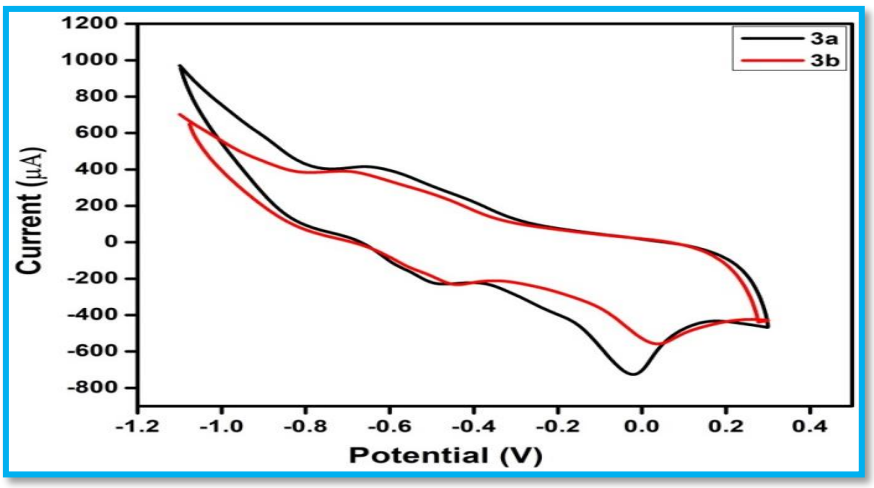

Fig.4B.4 Electrochemical sensing of Dolo bin drug in 1M NaOH solution**.**

Table 4B.4. Electrochemical sensor data of synthesized compounds **3a** and **3b** using Dolo drug molecule.

Entry	Anodic oxidation on set potential (V)	Cathodic Reduction on set potential (V)
3a	-0.51 and -0.02	-0.64
3b	-0.46 and 0.04	-0.71

4B.4.5 Theoretical study.

The geometrical and molecular optimization properties of synthesized compounds **3a** and **3b** were obtained from density functional theory (DFT) in the gaseous phase and solvent phase (DMSO). Both the dye compounds belong to the C_1 point group and optimized molecular structure with atom numbers represented in **Fig. 4B.5**.

4B.4.5.1 FMOs.

Energy molecular orbitals (HOMO and LUMO) are considered as FMOs and their energy bandgap were essential quantum chemical parameters that understand the chemical stability of synthesized compounds. These molecular orbitals were investigated both in the gaseous phase as well as in the solvent (DMSO) phase as shown in **Fig. 4B.6 (a** and **b)**. The highest occupied molecular orbital (HOMO) directly relates to ionization potential (*I*) where, the donation of electron takes place, similarly, the lowest unoccupied molecular orbital (LUMO) is directly related to an electron affinity (*EA*) where the electron can be accepted [40]. FMOs play a major role in understanding the electronic and optical properties of compounds. Compounds **3a** and **3b** are given higher HOMO values of both phases -6.53 eV, -6.52 eV and -6.80 eV, -6.78 eV respectively; lower LUMO values -3.26 eV, -1.08 eV and -3.26 eV, -2.28eV respectively. The HOMO-LUMO gap is the difference between energy molecules and gives 3.27 eV, 5.45 eV and 3.54 eV, 4.50 eV (Eq. 5). Higher the

energy gap informs the electron interaction and ability within the molecules, **3b** compound has found higher value than **3a** compound, hence **3b** compound has a higher chemical reactivity and kinetic energy stability [41, 42]. Estimated HOMO-LUMO with energy gap values has been summarized in **Table 4B.5.**

$$\Delta E = \text{LUMO} - \text{HOMO} \qquad \text{— (5)}$$

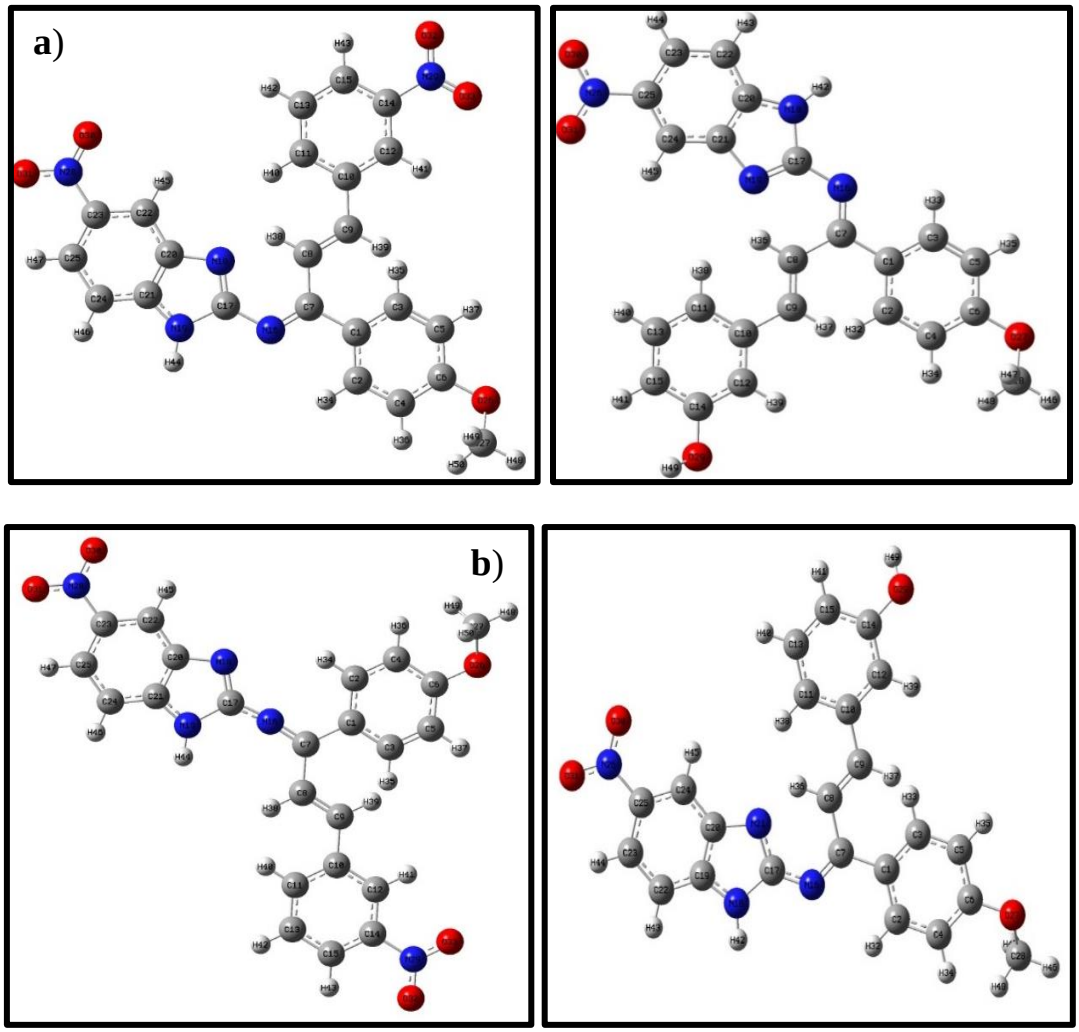

Fig.4B.5. Geometrical optimized structure with their atom numbers of synthesized compounds **3a** and **3b** at **(a)** gaseous phase, **(b)** solvent phase (DMSO).

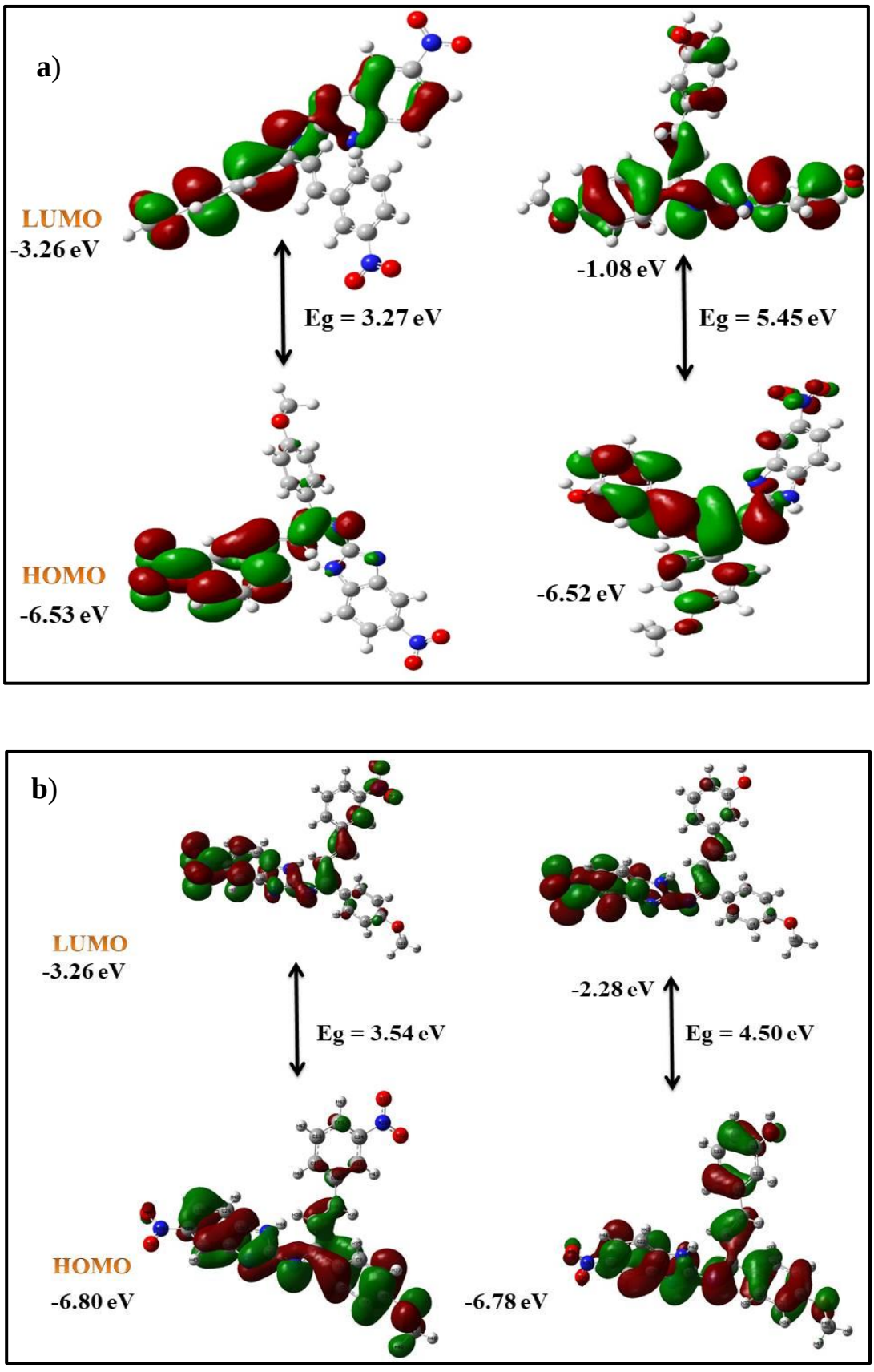

Fig.4B.6. Energy level distribution of HOMO and LUMO of the synthesized compounds **3a** and **3b** at **(a)** gaseous phase (**b**) solvent phase (DMSO).

4B.4.5.2 Quantum chemical parameters.

According to Koopmans theorem, the quantum chemical parameters have been calculated theoretically such as Electron affinity [$A = -E_{LUMO}$)], Ionization potential [$I = -E_{HOMO}$], Chemical hardness [$\eta = ½ (I – A)$], chemical softness [$\sigma = 1/\eta$], Electronegativity [$\chi = ½ (I + A)$], Chemical potential [$\mu = -\chi$] and Electrophilicity index [$\omega = \mu^2/2\eta$] to understand the structural activity like donor-acceptor interaction and charge transport abilities of the synthesized compounds [43].

Chemical hardness and softness stand for the ability of intramolecular charge transfer (ICT), kinetic stability, photostability and chemical reactivity. The larger the energy gap is said to be a hard molecule, while the smaller gap is called a soft molecule. The ΔE value of compounds **3a** and **3b** were found to be 3.27 eV and 5.45 eV at the gaseous phase 3.54 eV and 4.50 eV in the solvent phase. Compounds **3a** and **3b** give higher the energy gap in both phases than it is said to be hard molecules, hence higher in kinetic stability which can make more stable to use in solar cell applications. Theoretically calculated electronegativity of compounds **3a** and **3b** was found higher values in the solvent phase which relates the intrinsic properties. Compounds **3a** and **3b** have the greater electrophilicity index is obtained at 7.23 eV and 2.65 eV and chemical potential is -4.89 eV and -3.80 eV respectively, which confirms the greater photostability. Based on theoretical calculations and results revealed that obtained **3a** and **3b** compounds have greater stability, are higher in intramolecular charge transfer and have good intrinsic properties with photostability [44, 45]. Calculated quantum chemical parameters along with dipole moment as appended in **Table 4B.6.**

Table 4B.5. Frontier molecular orbital's (FMOs) of synthesized compounds **3a** and **3b.**

Entry	Gaseous phase			Solvent phase (DMSO)		
	HOMO (eV)	**LUMO (eV)**	***ΔE***	**HOMO (eV)**	**LUMO (eV)**	***ΔE***
3a	-6.53	-3.26	3.27	-6.80	-3.26	3.54
3b	-6.53	-1.08	5.45	-6.78	-2.28	4.50

Table 4B.6. Theoretical Chemical parameters of synthesized compounds **3a** and **3b.**

Parameters	**Gaseous phase (eV)**		**Solvent phase (DMSO) (eV)**	
	3a	**3b**	**3a**	**3b**
Ionization energy (I)	6.53	6.52	6.80	6.78
Electron affinity (A)	3.26	1.08	3.26	2.28
Global hardness (η)	1.63	2.72	1.77	2.25
Global softness (σ)	0.61	0.36	0.56	0.44
Electronegativity (χ)	4.89	3.80	5.03	4.53
Chemical potential (μ)	-4.89	-3.80	-5.03	-4.53
Electrophilicity index (ω)	7.23	2.65	7.14	4.46
Dipole moment (D)	7.50	9.24		

4B.4.6 Current-Voltage studies

Open circuit voltage and current sweep analysis have been carried out using synthesized dye compounds **3a** and **3b**. A mercury-vapour lamp has been used as a light source and a dye-coated photoanode connected directly to the Keithley source meter with help of crocodile terminals. Open circuit voltage (V_{oc}) and current sweep condition have been measured separately in dark and light-medium with help of iodine/triiodide as an electrolyte at room temperature [46].

From **Fig.4B. 7** and **4B. 8**, we do observe that compounds are having good sensing ability in presence of light and found a variation in the current-voltage measurement. At 1 cm area, under light-medium, compounds **3a** and **3b** have been found 4.88 V and 4.84 V for voltage response and at dark medium give 3.60 V and

3.74 V respectively. Similarly, the current sweep measurement has been found 2.36 A and 3.60 A in the light medium and 1.20 A and 1.19 A in the dark medium respectively. Both compounds **3a** and **3b** have a good response in current-voltage measurement due to the presence of electron-withdrawing and donating groups, where these groups can act as anchoring groups. The drop of current in a dark medium is due to the blocking effect of dye compounds and no moment of electrons absorbed from the light source. Measured values are appended in **Table 4B.7**, based on the above discussion synthesized dye compounds are potential materials for DSSCs applications [47].

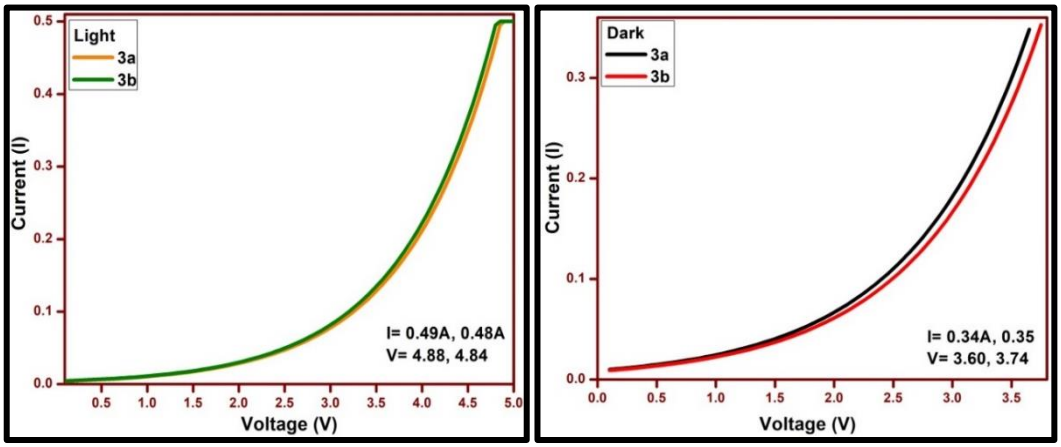

(a) **(b)**

Fig.4B.7. Current-Voltage measurement (open circuit voltage) **(a)** Under light and **(b)** Dark medium.

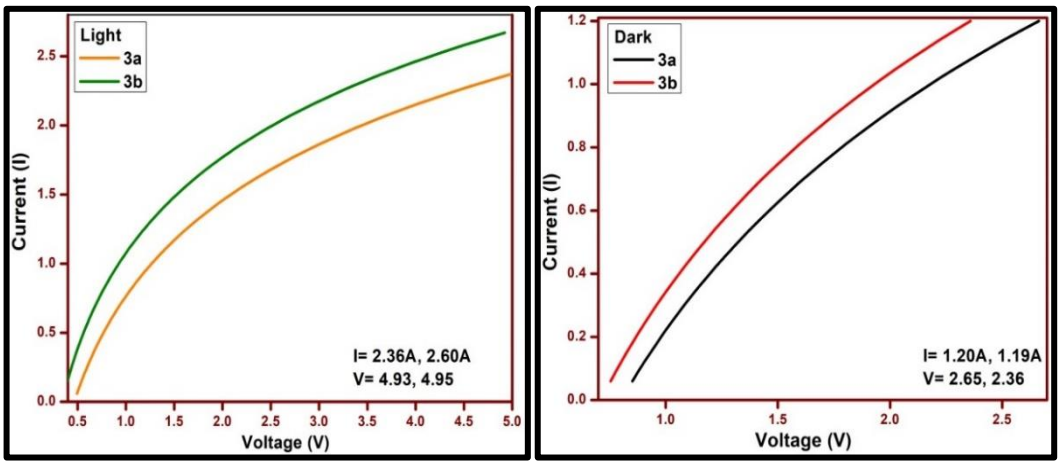

(a) **(b)**

Fig.4B. 8. Current-Voltage measurement (Current sweep) Under light **(a)** and Dark medium **(b).**

Table 4B. 7. *I-V* characteristics of synthesized compounds **3a** and **3b.**

Entry	Open Circuit voltage (V_{oc}) (V)	Current Sweep (A)
3a	4.88	2.36
3b	4.84	2.60

4B.5 Conclusion.

In summary, the synthesized compounds **3a** and **3b** have good absorption properties by absorbing at the visible region and emitting at a blue level emission in the solvent system and absorption as well emission spectrum with CIE diagram suggested dye compounds to be used in LED chips. Redox behaviours were shown quasi-reversible of one wave electron transfer occurs, further, redox onset potentials were estimated to calculate the energy molecules and quantum parameters experimentally. The synthesized compounds have a good sensing ability by sensing the Dolo drug molecule in 1M NaOH solution. In addition, geometry optimization, FMOs and quantum chemical parameters were studied theoretically at the gaseous phase as well as the solvent phase and results suggest that synthesized compounds are higher chemical reactivity, good intramolecular charge transport and higher photostability. Likewise, synthesized compounds (**3a** and **3b**) were used to study *I-V* characteristics under dark and light medium; we found good current and voltage response under light medium, hence synthesized compounds are potential materials for the OLEDs, sensor materials and photosensitizers in third-generation photovoltaic cells (DSSCs).

4B.6 Reference.

1. B.O. Regan, M. Gratzel, *Nature.*, 353 (1991) 737-740.
2. F. Arkan, M. Izadyar, *J. Opt*., 203 (**2020**) 1-31.
3. R. Vakulchuk, I. Overland, D. Scholten, *Energy Rev.*, 122 (**2020**) 109547-109560.
4. S.O. Ganiyu, C.A. Martínez-Huitle, M.A. Rodrigo, *Appl. Catal. B.*, 270 (**2020**) 118857-118893.
5. A. Irfan, A. Kalam, A.R. Chaudhry, A.G. Al-Sehemia, S. Muhammad, *Optik.*, 132 (**2017**) 101-110.
6. M.M. Makhlouf, A.S. Radwan, B. Ghazal, *J. Appl. Surf. Sci.*, 452 (**2018**) 337-351.
7. J.L. Segura, M.J. Manchen˜o, F. Zamora, *Chem. Soc. Rev.*, 45 (**2016**) 5635-5671.
8. D. Coskun, B. Gunduz, M.F. Coskun, *J. Mol. Struct.*, 1178 (**2019**) 261-267.
9. S. Manoharan, S. Anandan, *Dyes and Pigm.*, 105 (**2014**) 223-231.
10. A.A. Babu, T. Shankar, K. Swarnalatha, *J. Phys. Chem. Lett.*, 699 (**2018**) 32-39.
11. Z.J. Zhong, *World Sci. Publ. Co. Pte. Ltd.*, 359 (**2009**) 1-38.
12. X.Y. Wang, C.G. Niu, L.Y. Hu, D.W. Huang, S.Q. Wu, L. Zhang, X.J. Wen, G. *J. Sens. Actuators. B. Chem.*, 243 (**2017**) 1046-1056,
13. A.R. Chaudary, A. Irfan, S. Muhammad, A.G. Al-Sehemi, R. Ahmed, Z. Jingping, *J. Mol. Graph.*, 75 (**2017**) 355-364,
14. Z.S. Wang, Y. Cui, K. Hara, Y. Dan-oh, C. Kasada, A. Shinpo, C, Kasada, A, Shinpo, *Adv. Mater.*, 19 (**2007**) 1138-1141.
15. M. Zeng, A. Rammohan, B.V. Bhaskar, N. Venkateswarlu, W. Gu, G.V. Zyryanov, *J. Bioorg. Chem.*, 95 (**2020**) 103527-103542.
16. Z.S. Wang, Y. Cui, K. Hara, Y. Dan-oh, C. Kasada, A. Shinpo, *Adv. Mate.*, 19 (**2007**) 1138-1141
17. S. Manoharan, S. Anandan, *Dyes and Pigm.*, 105 (**2014**) 223-231.
18. Z. Lei, J.M. Cole, *ACS applied materials & interfaces.*, 7 (**2015**) 3427-3455.
19. T.A. Fayed, *J. Chem. Phys. Lett.*, 324 (**2006**) 631-638.

20. P.C. Rajesh Kumar, V. Ravindrachary, K. Janardhana, B. Poojary, *J. Cryst. Growth.,* 354 (**2012**) 182-187.

21. A.O. Elzupir, K.H. Ibnaouf, H. Idriss, M.A. Ibrahem, S. Prasad, M.A. Alrajhi, M.S. AlSalhi, A.S. Alaamer, *Acta Phys. Pol. A.,* 133 (**2018**) 121-125.

22. M. Shkira, S. Muhammad, S. AlFaifya, A. Irfan, P.S. Patil, M. Arora, H. Algarni, Z. Jingping, *RSC advances.,* 106 (**2015**) 87320-87332.

23. C. Shruthi, V. Ravindrachary, B. Guruswamy, D.J. Prasad, J. Goveas, *Single crystal, AIP Conf. Proc.,* 2244 (**2020**) 1-5.

24. D. Haleshappa, B. Raghavendra, A. Jayarama, Q.C. Kheng, H. C. Kwong, P. Shankaragouda. *J. Mol. Str.,* 1232 (**2021**) 130053-130064.

25. M.N. El-Nahass, T.A. Fayed, S.A. Elazim, M.M. El-Gamil, D.F. Draz, F. Hassan, *J. Mol. Str.,* 1240 (**2021**) 130581-130588.

26. K.Y. Teo, M.H. Tiong, H.Y. Wee, N. Jasin, Z.Q. Liu, M.Y. Shiu, J.Y. Tang, J.K. Tsai, R. Rahamathullah, W.M. Khairul, M.G. Tay, *J. Mol. Str.,* 1143 (**2017**) 42-58.

27. J. Sanja, Y.S. Maryc, Y.S. Mary, S. Pelemišd, S. Armakoviće, *Comput. and Theo. Chem.,* 1197 (**2021**) 113160-113168.

28. G. Lusvardi, C. Barani, F. Giubertoni, G. Paganelli, *Materials (Basel).,* 10 (**2017**) 1-11.

29. B. Hemavathi, J.V. Pradhan, S.C. Gokul, G.J. Kusuma, G.K. Chandrashekar, P.C Ramamurthy, R.K Pai, K.N. Narayanan Unni, T.N. Ahipa, S. Suraj R.G Balakrishna, *Sol. Energy.,* 174 (**2018**) 1085-1096.

30. B. Avinash, C.R. Ravikumar, M.R. Anil Kumar, H.P. Nagaswarup, M.S. Santosh, A.S. Bhatt, D. Kuznetsov, *J. Phys. Chem. Sol.,* 134 (**2019**) 193-200.

31. K.V. Basavarajappa, Y.A. Nayaka, R.O. Yathisha, K.B. Manjunatha, *J. Fluoresc.,* 29 (**2019**) 1201-1211.

32. T. Sutradhar, A. Misra, *J. Phys. Chem. A.,* 122 (**2018**) 4111-4120.

33. M. Mohan, S. Pangannaya, M.N. Satyanarayan, D.R. Trived, *Opt. Mater.,* 77 (**2018**) 211-220.

34. A. Dolgonos, T.O. Mason, K.R. Poeppelmeier, *J. Sol. Sta. Chem.,* 240 (**2016**) 43-48.

35. E. David, K. Thirumoorthy, N. Palanisami, *J. Appl. Org. Meta. Chem.,* 32 (**2018**) 01-12.

36. B. Baroudi, K. Argoub, D. Hadji, A.M. Benkouider, K. Toubal, A. Yahiaoui, A. Djafri, *J. Sulfur Chem.,* 41 (**2020**) 310-325.

37. G. Ceyhan, M. K¨ose, M. Tümer, I. Demirtas¸, A.S. Ya˘glio˘glu, V. McKee, *J. Lumi.,* 143 (**2013**) 623-634.

38. L. Leonat, S. Gabriela, I.V. Branzoi, *U.P.B. Sci. Bull. Series B.,* 75 (**2013**) 111-119.

39. I. Yilmaz, M.B. Kocak, *J. Polyhed.,* 23 (**2004**) 1279-1285.

40. E.M. Espinoza, J.A. Clark, J. Soliman, J.B. Derr, M. Morales, V.I. Vullev, *J. Electrochem. Soc.,* 166 (**2019**) 3175-3187,

41. J. George, J.C. Prasana, S. Muthu, T.K. Kuruvilla, S. Sevanthi, R.S. Saji, *J. Mol. Str.,* 1171 (**2018**) 268-278.

42. D.F.V. Lewis, C. Ioannides, D.V. Parke, *J. Xenobiotica.,* 24 (**1994**) 401-408.

43. R. Parr, G. Donnelly, R.A. Levy, M.W.E. Palke, *J. Chem. Phy.,* 68 (**1977**) 3801-3807.

44. N.A. El-Ghamaz, M.A. Diab, A.A. El-Bindary, A.Z. El-Sonbati, H.A. Seyam, *J. Mat. Sci. Semicond. Processing.,* 27 (**2014**) 521-531.

45. A.Z. El-Sonbati, M.A. Diab, A.A. El-Bindary, S.M. Morgan, *Spectrochim. Acta, Part A.,* 127 (**2014**) 310-328A.

46. T. Venkatesh, K. Upendranath, Y.A. Nayaka, *J. Solid. State. Electrochem.,* 25 (**2021**) 1237-1244.

47. K.V. Basavarajappa, Y.A. Nayaka, H.T. Purushothama, R.O. Yathisha, M.M. Vinay, B.J. Rudresha, K.B. Manjunatha, *J. Mol. Struct.* 1199 (**2020**) 126946-126958.

Chapter -5

Facile synthesis of 7-(4-substitutedphenyl)-5-(4-substitutedphenyl)-1,3-dimethyl-1*H*-pyrimido[4,5-d]thiazolo[3,2-*a*]pyrimidine-2,4(3*H*,5*H*)-dione derivatives and their optoelectronic, DFT and level II & III of LFPs applications

5.1 Introduction.

The multicomponent reaction is one of the synthetic strategies to form new derivatives in a single-step reaction from more than two compounds [1-2]. It is a useful technique nowadays by having many advantages while carrying the reaction such as it avoids unnecessary expensive purification, high atom economy, toxic reagents, and solvents consumption [3-4]. In past decades the multicomponent reaction plays a vital role in synthesizing new derivatives to use in the field of medicinal chemistry and material science applications. Organic compounds with luminous characteristics such as pyrimidine, pyridine carbonitrile, thiazolopyrimidine and other heterocyclic derivatives will majorly be synthesized through multicomponent reactions for OLEDs, electroluminescent indicators, dyes in energy conversion materials [5-6].

Thiazolopyrimidine derivatives are the important groups of heterocyclic compounds and have attracted much more in the field of medicinal chemistry [7]. They have a great deal of interest owing to their biological activities such as antifungal, antibacterial, anti-inflammatory, anti-tubercular etc., [8-16]. These derivatives have been tested for several tumour cells and got accurate results by showing the least IC_{50} values, hence they are potential anti-tumour agents [17]. Moreover, thiazolopyrimidine derivatives, are known as π-deficient compounds, hence they are well-phototonic materials, hence they can be a potential compounds to vislulize the level II and III features of latent fingerprints without background hindrenacne and these derivatives will majorly be synthesized through multicomponent reactions [18-20]. Some of the reported optically important heterocyclic compounds have been discussed as follows.

Youssef *et al.,* reported (2018) a new series of 11-(substituted phenyl)octahydropyrimido[*4",5":4',5'*]thiazolo[*3',2'*-a]pyrimido[*4,5*-d]pyrimidine-2,4, 8,10-tetrathione derivatives (**1**) in microwave. The obtained compounds studied their optical properties, where absorption bands appeared at 320 nm to 335 nm of redshift and emitted at 425 nm to 500 nm of a longer wavelength. Both compounds have exhibited better optical properties by showing absorption and emission bands at redshift [21].

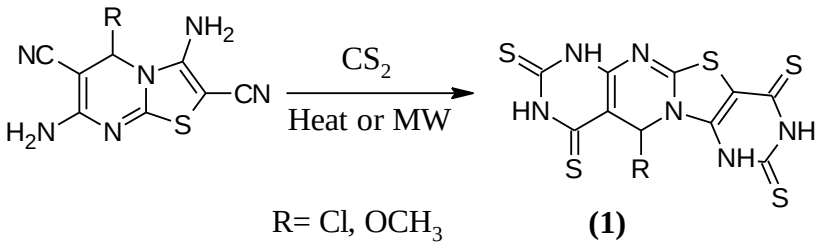

R= Cl, OCH_3 **(1)**

N.H.M. Kareem *et al.,* reported a pyrazole-based tetrahydropyrimidine derivatives (**2**) in ethanol using potassium hydroxide as a catalyst for 4 h reflux condition. The obtained derivatives have been studied theoretically, than these compounds are said to be hard molecules, hence the compounds have better photoactivity. Further compounds have been also screened for biological activity aginst two pathogens (*E. Coli*, *Shigella*) and compounds are proven their better bioactivity for selected bacterial strains by showing a higher zone of inhibition (15 mm and 18 mm) at higher concentration [22].

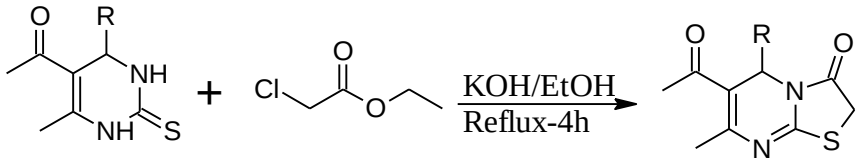

R = C_6H_6, Cl,

(2)

R. Agrawal and co-workers reported a new series of 2- (substituted phenyl) -3-methyl-*6,7*-dihydro-5*H*-thiazolo[3,2-a] pyrimidines derivatives (**3**) in 2021. The obtained derivatives have been analysed for photophysical properties with theoretical studies. Absorption and emission band appeared at longer wavelengths 320 nm to 650 nm and with help of the UV-Visible spectrophotometer, DNA/BSA binding studies have been carried out and synthesized compounds binds efficently at 3.6±0.06 M^{-1} [23].

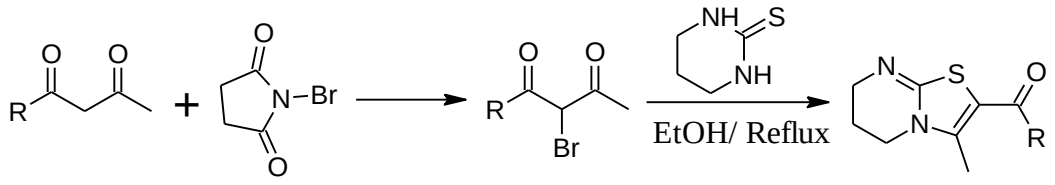

R = Ph, Me, Br, F, OMe, Cl_2, Thienyl **(3)**

In 2019, Houda Serrar *et al.,* reported a new two substituted thiazolopyrimidne compounds as dyes (**4** & **5**) and they have been studied for corrosion inhibitors over mild steel in an acid medium. Obtained compounds found better corrosion inhibitors by decreasing the corrosion rate and increase in temperature. Further, electronic absorption properties were studied under a solvent medium with the least concentration of 2×10^{-3} M, all the compounds had better absorption properties by showing 300 nm to 328 nm [24].

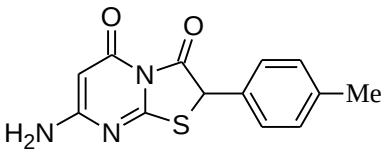

(4)

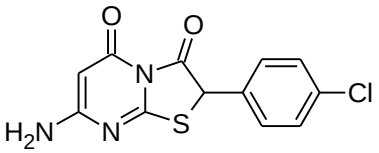

(5)

Zahra Ebrahimpour *et al.,* reported (2019) a novel pyrimido[5,4-e]thiazolo[3,2-a]pyrimidine (**6** & **7**) derivatives. Obtained compounds have been studied for their fluorescence properties and all the derivatives are emitted at a redshift of 410 nm to 425 nm with high extinction coefficients in different solvents [25].

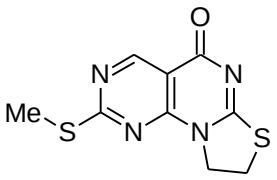

(6)

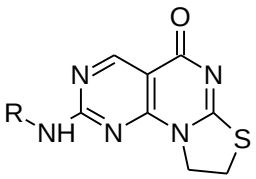

(7)

R = C_5H_4N
C_6H_5N-CH_3
C_6H_5NO

Based on the above findings, we synthesized some new 7-(4-substituted phenyl)-5-(4-substitutedphenyl)-1,3-dimethyl-1,5-dihydro-2*H*-pyrimido[4,5-d][*1,3*]thiazolo[*3,2-a*]pyrimidine-2,4(3*H*)-dione derivatives **4**(**a-d**) and studied for their photophysical, electrochemical, DFT and level II and III features of LFPs.

5.2. Present Work.

In this chapter, we designed and developed some novel *7*-(4-substituted phenyl)-5-(4-substitutedphenyl)-1,3-dimethyl-1,5-dihydro-2*H*-pyrimido[4,5-d][1,3]thiazolo[*3,2-a*]pyrimidine-2,4(3*H*)-dione derivatives **4**(**a-d**) through the multicomponent reaction of 2-(4-substituted phenyl)thiazol-5-amine, 1,3-dimethyl barbituric acid and substituted aldehydes using L-Proline as a catalyst. The synthesized derivatives have been studied for optoelectronic, DFT and Latent fingerprint applications. The mode of reaction pathway has been represented in **Scheme 5**

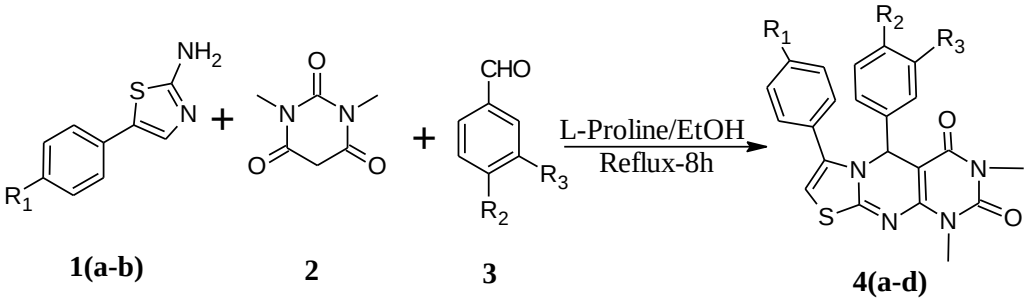

1(a-b) **2** **3** **4(a-d)**

Entry	R_1	R_2	R_3
4a	Br	Br	H
4b	Br	NO_2	H
4c	Cl	OH	OCH_3
4d	Cl	NO_2	H

Scheme 5: Synthesis of 7-(4-Substitutedphenyl)-5-(4-substituted phenyl)-1,3-dimethyl-1,5-dihydro-2*H*-pyrimido[*4,5*-d][1,3]thiazolo[*3,2-a*]pyrimidine-2,4(3*H*)-dione derivatives **4**(**a-d**).

5.2.1 Spectral Characterization.

The synthesized compouds were confirmed by FTIR, ^{1}H-NMR & ^{13}C-NMR and high resulation mass (HRMS) spectroscopic techniques.

The FTIR spectrum of synthesized compound **4a** showed a strong stretching vibration band at 3094.86 cm^{-1} due to the aromatic C-H group and another vibrational band 1670.29 cm^{-1} corresponds to C=O stretching, the band at 1586.75 cm^{-1} corresponds to C=N stretching vibrations. In ^{1}H-NMR spectrum of the compound. **4a,** exhibited singlet band at δ 8.72 ppm due to an CH of thiazole proton, δ 7.68 -7.66 ppm corresponds to the two aromatic protons, and doublet peaks at δ 7.53-7.51 ppm for two aromatic protons. Another doublet peaks at δ 7.34-7.32 ppm corresponds to two aromatic protons, and at δ 7.02-7.00 ppm which is corresponds to two aromatic protons. A singlet peak at δ 5.65 ppm CH junction proton, and a singlet peak at δ 2.49 ppm corresponds two methyl groups. ^{13}C-NMR spectrum of synthesized **4a** appearance of a signal at δ 178.08, 161.81 ppm due to the carbonyl carbon, δ 136.50-105.56 ppm corresponds to C=C carbons and 26.90 ppm for two methyl carbons. High-Resolution mass spectrum showed a molecular ion peak [M^{+}1] at m/z 560.0859 and [M^{+}2] m/z at 562.0541 corresponding to a molecular weight of compound **4a**.

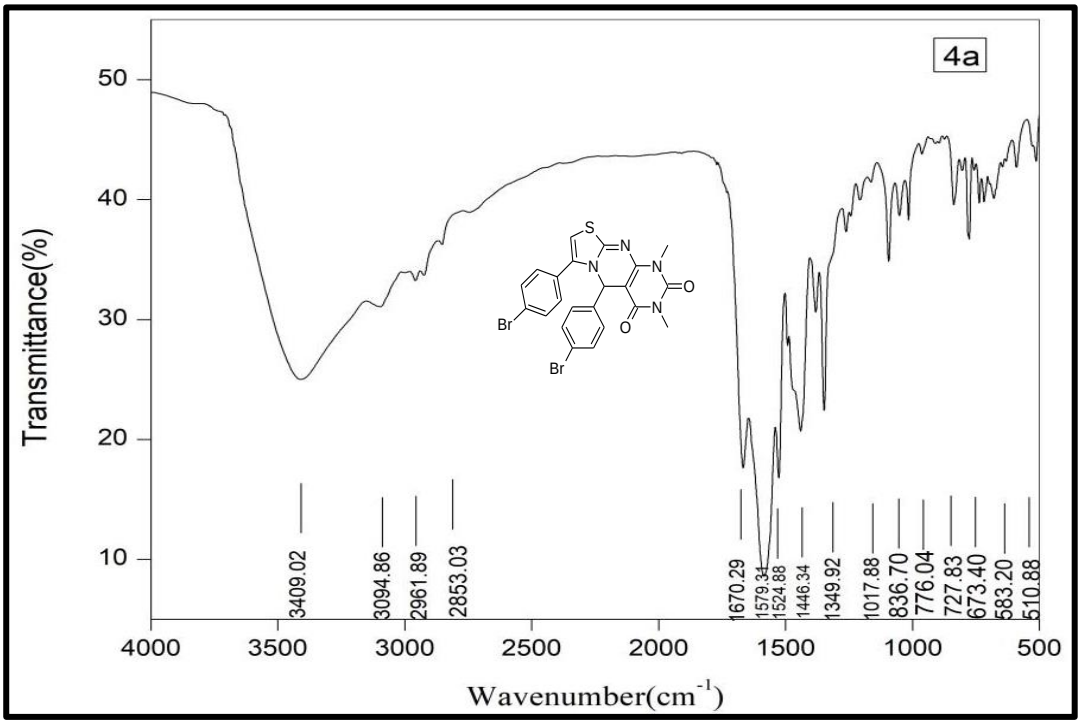

FTIR spectra of compound 4a

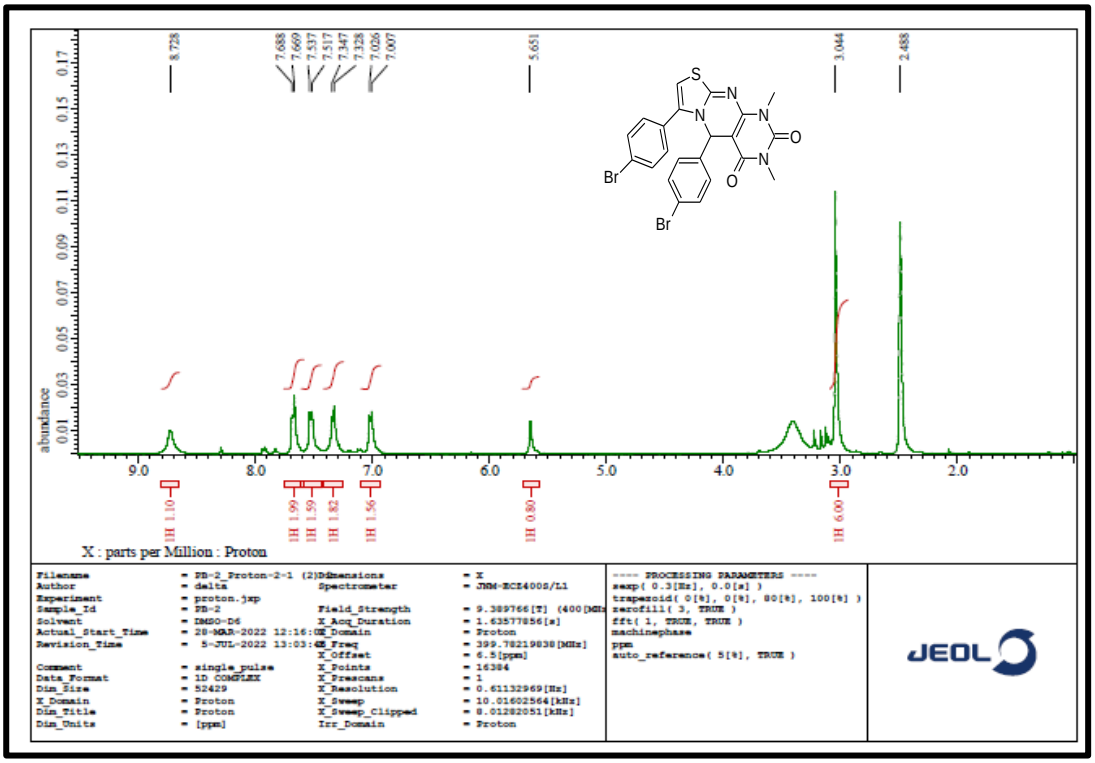

^{1}H-NMR spectrum of compound 4a

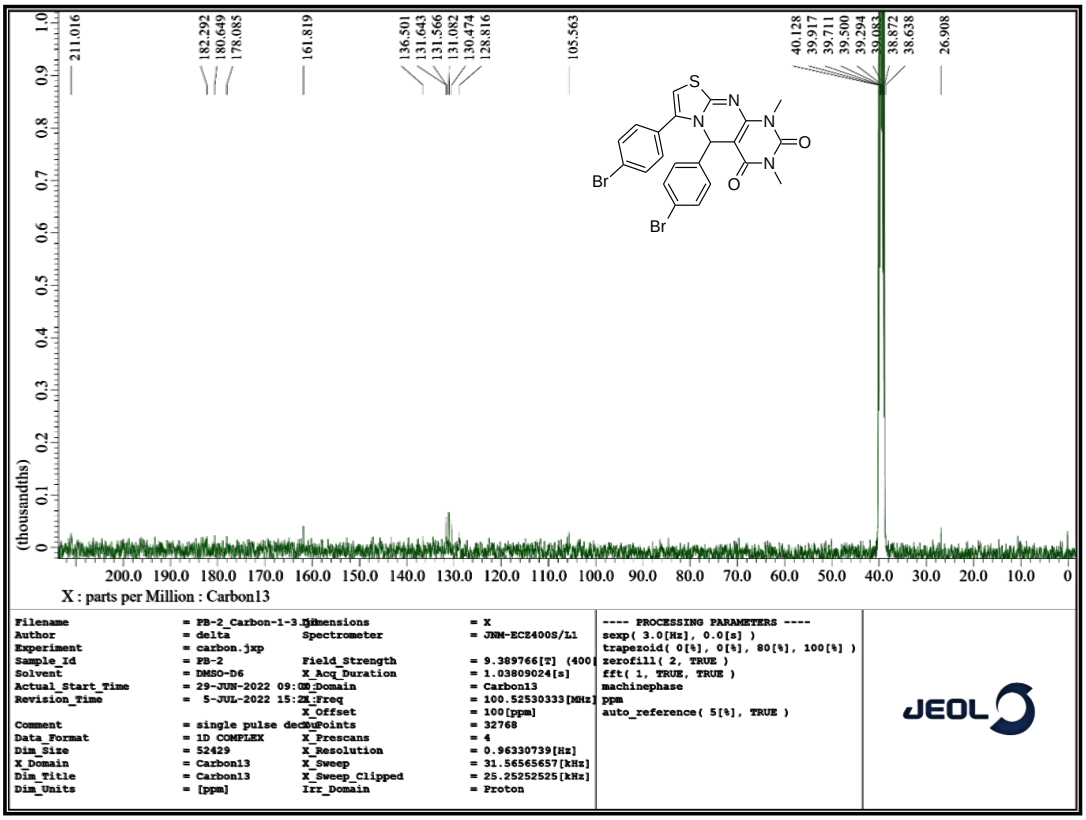

^{13}C-NMR spectrum of compound 4a

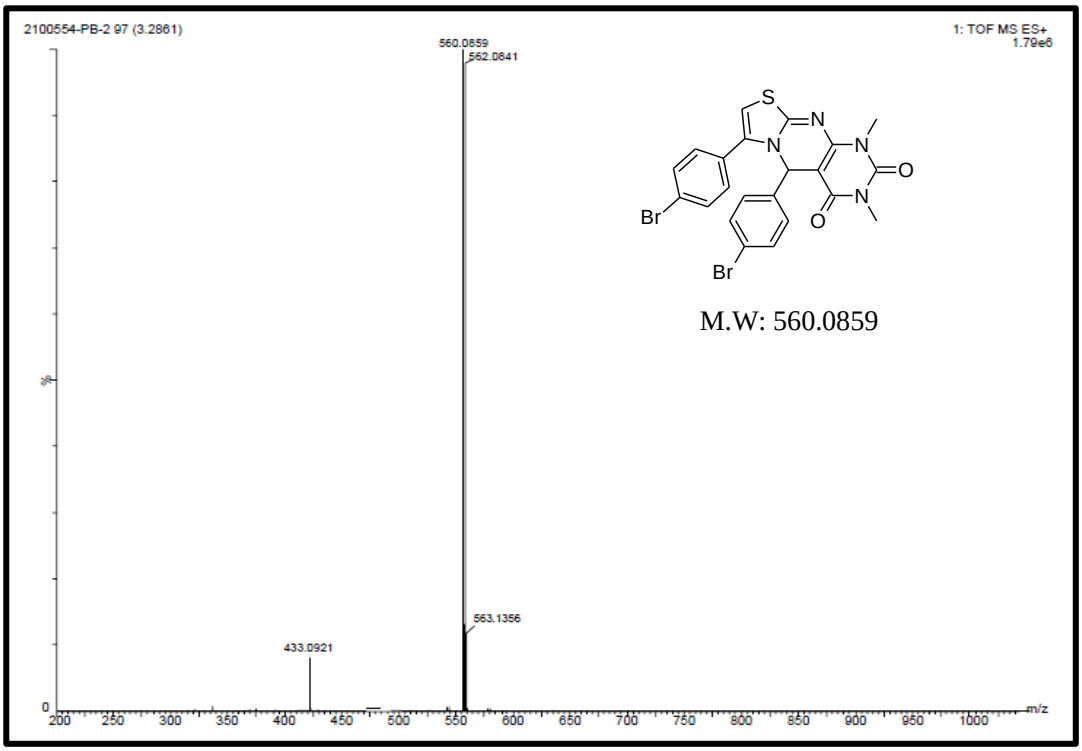

Mass spectrum of compound 4a

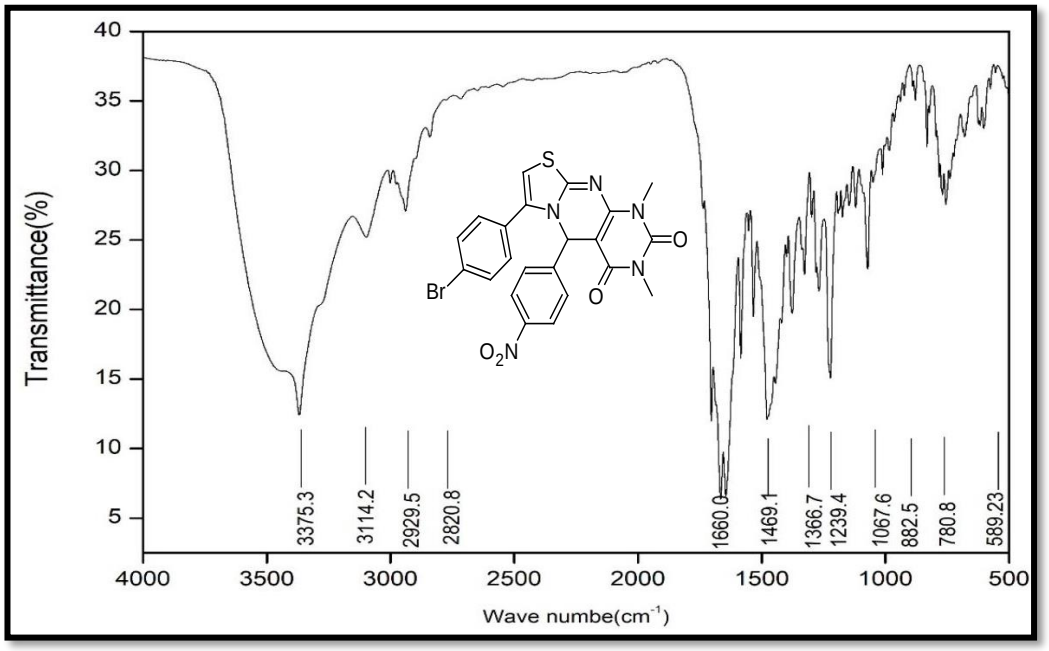

FTIR spectra of compound 4b

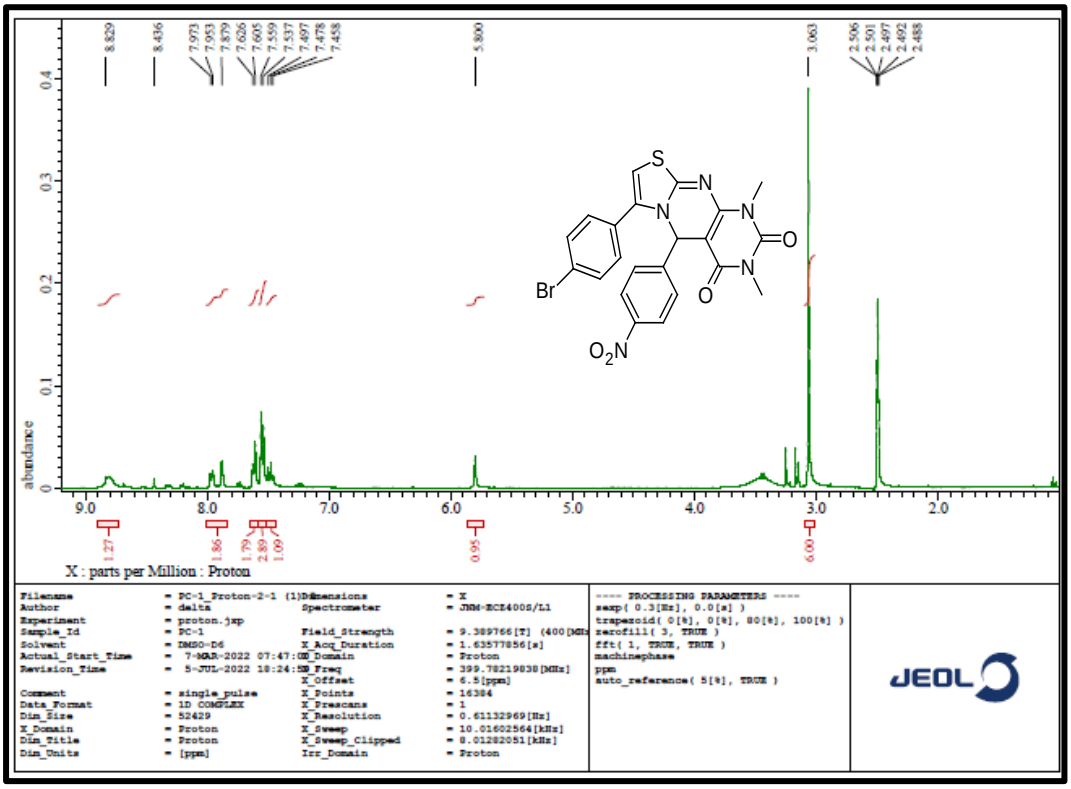

^{1}H-NMR spectrum of compound 4b

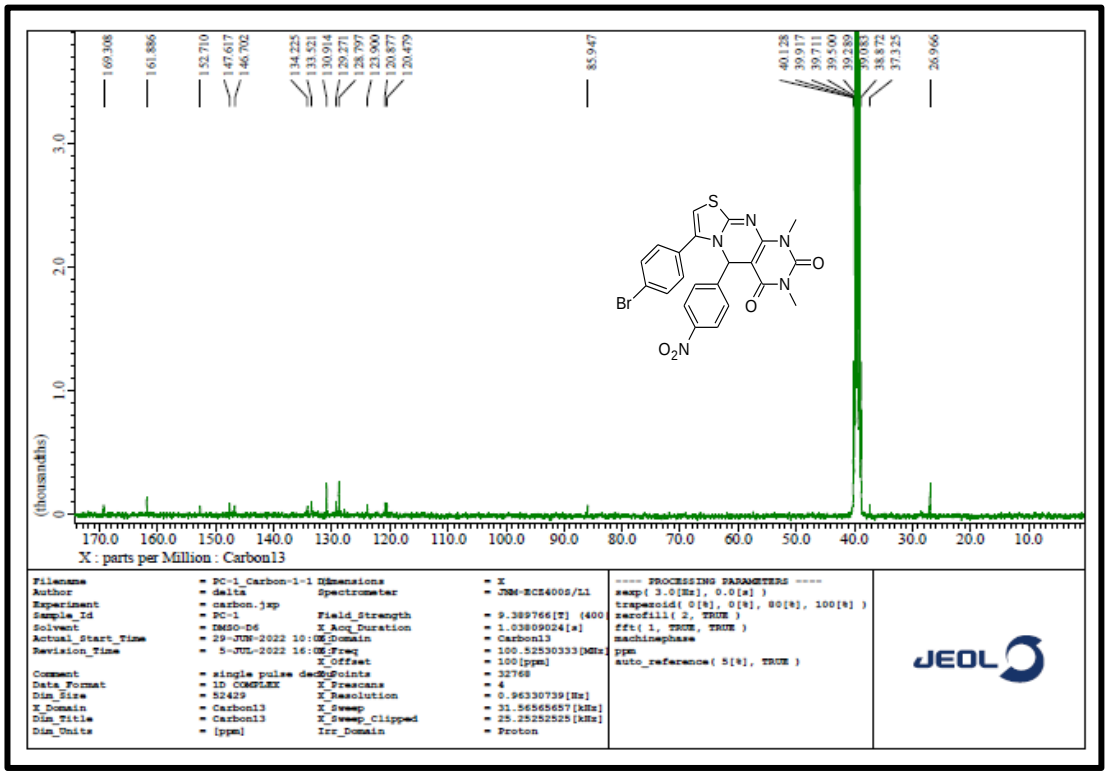

^{13}C-NMR spectrum of compound 4b

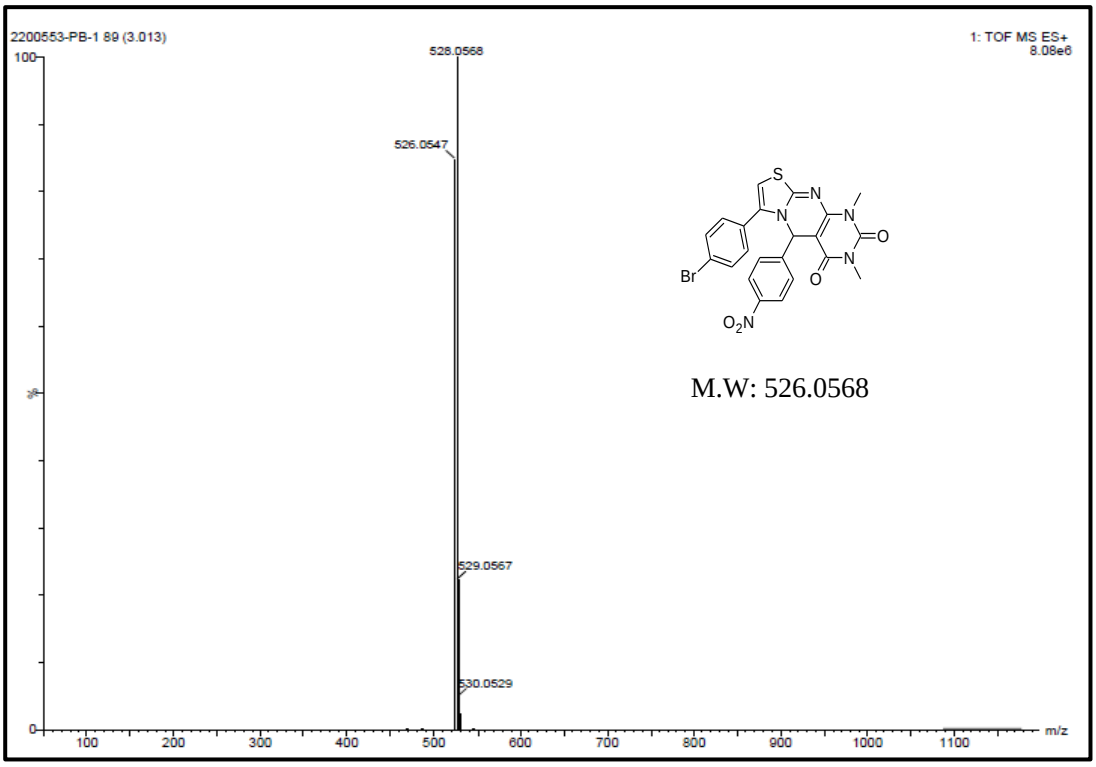

Mass spectrum of compound 4b

5.3 Experimental

5.3.1 General Information

Spectroscopic techniques and purchased chemicals and using of reagents were discussed in previous **Chapter 2A**. Detailed experimental procedure of electrochemical, computational and LFPs were discussed in experimental section **2A.3**.

5.3.2 Procedure for new 7-(4-substituted phenyl)-1,3-dimethyl-5-(4-substitutedphenyl)1,5-dihydro-2*H*-pyrimido[*4,5*-d][*1,3*]thiazolo[*3,2a*]-pyrimidine 2,*4*(3*H*)-dione derivatives 4(a-d).

In a 100 mL round bottom flask, an equimolar quantity (1mM) of 2-(4-substituted phenyl)thiazol-5-amine (**1**) and 1,3-dimethylbarbutaricacid (**2**) with substituted aromatic aldehydes (**3a-d**) were taken in ethanol (20 mL) in presence 10 mol % of L-Proline catalyst. The reaction mixture was kept at reflux temperature for about 8 hours and the progress of the reaction was monitored with the help of TLC (Ethyl acetate and Pet. ether). After the completion of the reaction, the precipitated product was filtered, dried and recrystallized using absolute ethanol.

7-(4-Bromophenyl)-1,3-dimethyl-5-(4-bromophenyl)1,5-dihydro-2H-pyrimido[4,5-d][1,3]thiazolo[3,2a]-pyrimidine2,4(3H)-dione(4a):

Violet solid; Yield; 85 %, MP; 131-135 ^{o}C; Mol. Formula: $C_{22}H_{16}Br_2N_4O_2S$; FTIR (υ, cm^{-1}): 3094 (Ar-CH), 2961 (CH), 1670 (C=O), 1579 (C=N); ^{1}H-NMR (δ ppm): 8.72 (s, 1H, Ar-CH), 7.68 -7.66 (d, *J* = 8 Hz, 2H, Ar-H), 7.53-7.51 (d, *J* = 8 Hz, 2H, Ar-H), 7.34-7.32 (d, *J* = 8 Hz, 2H, Ar-H), 7.02-7.00 (d, *J* = 8 Hz, 2H, Ar-H), 5.65 (s, 1H, CH), 2.49 (s, 6H, 2-CH_3); ^{13}C-NMR (δ ppm): 178.08, 161.81, 136.50, 131.08, 128.81, 105.56, 40.12, 39.50, 39.08, 38.63, 26.90; HRMS (m/z): 560.0859 [M^{+}1] and 562.0541 [M^{+}2]; Anal. Cacld. For C 50.20, H 3.06, N 13.31 %; Found; C 50.02, H 2.99, N 12.79 %.

7-(4-Bromophenyl)-1,3-dimethyl-5-(4-nitrophenyl)1,5-dihydro-2H-pyrimido[4,5-d][1,3]thiazolo[3,2a]-pyrimidine-2,4(3H)-dione (4b):

Yellow solid; Yield; 85%; MP: 138-140 ^{o}C; Mol. Formula: $C_{22}H_{16}BrN_5O_4S$. FTIR: (υ, cm^{-1}) 3114 (Ar-CH), 2945 (CH), 2858 (CH), 1673 (C=O); ^{1}H-NMR (δ ppm): 8.29 (s, 1H, Ar-CH), 7.97-7.95 (d, *J* = 8 Hz, 2H, Ar-H,), 7.62-7.60 (d, *J* = 8 Hz, 2H, Ar-H), 7.49 (s, 1H, Ar-CH), 7.47-7.45 (d, *J* = 8Hz, 2H, Ar-H), 5.80 (s, 1H, CH), 3.06 (s, 6H, 2-CH_3); ^{13}C-NMR (δ ppm): 169.30, 161.88, 152.71, 147.61, 146.70, 134.25, 133.52, 130.12, 129.27, 128.79, 123.90, 120.87, 120.94, 26.96. LCMS; m/z 526.0568 [M^{+}1] and 529.0567 [M^{+}3]; Anal. Cacld. For C 56.30, H 3.78, N 12.31 %; Found: C 54.28, H 3.49, N 11.99 %.

7-(4-Chlorophenyl)-1,3-dimethyl-5-(4-nitrophenyl)-1,5-dihydro-2H-pyrimido[4,5-d][1,3]thiazolo[3,2-a]pyrimidine-2,4(3H)-dione (4c):

Yellow powder; Yield: 88%, MP:130-134 ^{o}C; Mol. Formula: $C_{22}H_{16}ClN_5O_4S$; FT-IR: (υ, cm^{-1}): 3094 (Ar-CH str), 2961 (CH), 1670 (C=O); ^{1}H-NMR (δ ppm): 10.41 (s, 1H, Ar-CH), 8.30-8.28 (d, *J* = 8 Hz, 2H, Ar-H), 7.97-7.95 (d, *J* = 8 Hz, 2H, Ar-H), 7.87 (s, 1H, Ar-H), 7.62-7.60 (d, *J* = 8 Hz, 2H Ar-H), 7.55-7.53 (d, *J* = 8 Hz, 2H, Ar-H), 5.80 (s, 1H, CH), 3.06 (s, 6H, 2-CH_3); ^{13}C-NMR (δ ppm): 169.30, 161.88, 152.71, 147.61, 146.70, 134.22, 133.52, 130.91, 129.27, 128.79, 123.90, 120.87, 120.47, 85.94, 40.12, 39.91, 39.50, 39.28, 39.08, 38.87, 37.32, 26.96. HRMS (m/z): 482.0102 [M^{+}1] and 485.1108 [M^{+}3]; Anal. Cacld. For C 62.38, H 4.68, N 14.72 %; Found: C 60.28, H 4.49, N 13.89 %.

7-(4-Chlorophenyl)-5-(4-bromophenyl)-1,3-dimethyl-1,5-dihydro-2H-pyrimido[4,5-d][1,3]thiazolo[3,2-a]pyrimidine-2,4(3H)-dione (4d):

Yellow powder; Yield: 83%; MP: 126-128 ^{o}C; Mol. Formula: $C_{22}H_{16}BrClN_4O_2S$; FT-IR (υ, cm^{-1}): 3167 (Ar-CH str), 2841 (CH), 1664 (C=O), 758 (C-Cl str), 679 (C-Br); ^{1}H-NMR (δ ppm): 9.89 (s, 1H, Ar-CH), 8.45-8.43 (d, *J* = 8Hz, 2H, Ar-H), 7.99-7.97 (d, *J* = 8 Hz, 1H, Ar-H), 7.89 (s, 1H, Ar-H), 7.54-7.52 (d, *J* = 8 Hz, 2H Ar-H), 7.42-7.40 (d, *J* = 8 Hz, 2H, Ar-H), 4.60 (s,1H, CH), 3.06 (s, 6H, 2-CH_3); ^{13}C-NMR (δ ppm): 165.20, 163.78 (C=O), 159.61, 148.61, 147.70, 138.32, 136.42, 134.91, 133.17, 130.59, 129.90, 127.97, 125.47 (C=C), 116.74, 113.12, 110.81, 55.50, 48.28, 40.45, 38.87, 37.32, 35.96. HRMS (m/z): 516.1079 [M^{+}1] and 518.5287 [M^{+}2]; Anal. Cacld. For C 60.14, H 5.18, N 12.73 %; Found: C 60.00, H 4.99, N 12.08 %.

5.4. Results and discussion

5.4.1 Electronic absorption properties.

Electronic absorption properties of newly synthesized compounds **4**(**a-d**) were recorded from a UV-Visible spectrophotometer in DMSO. We observe in **Fig 5.1**, all the compounds have shown strong absorption bands at near visible region ~250 nm - 500 nm due to the π–π^* and n–π^* electronic transitions with aromatic conjugation. The presence of electron-donating and withdrawing groups on the phenyl ring will act as chromophores which inlfuance to [26, 27] shift of absorption bands at longer wavelength.

Compounds **4**(**a-d)** show the dual absorbption band at the visible region and compound **4a** shows an absorption band at 354 nm and 484 nm, similarly, compound **4b** display an absorption band at 315 nm and 384 nm respectively. While compounds **4c** and **4d** display dual absorption bands at 353 nm and 452 nm and 348 nm and 385 nm respectively. The bathochromic shift of all the compounds is also influenced by the chromophores and better interaction between solvent and compounds. Hence absorption bands have appeared at longer wavelength [28]. Further, the energy band gap was calculated using the equation (1) [29].

$$E_g = 1240/\lambda_{onset}\ \text{eV} \qquad \text{— (1)}$$

Emission properties also have been studied using DMSO in a Photoluminescence spectrophotometer, and all the compounds are emitted at the visible region with respect to the excitation values. **Fig. 5.2.** displays compounds **4**(**a-d**) have emitted at 587 nm, 545 nm, 565 nm and 544 nm respectively, the reason is that all the compounds involve aromatic extended conjugation, electronic transitions by the presence of electron-donating and acceptor groups [30, 31]. Obtained both absorption and emission spectral values are listed in **Table 5.1** with calculated energy band gap.

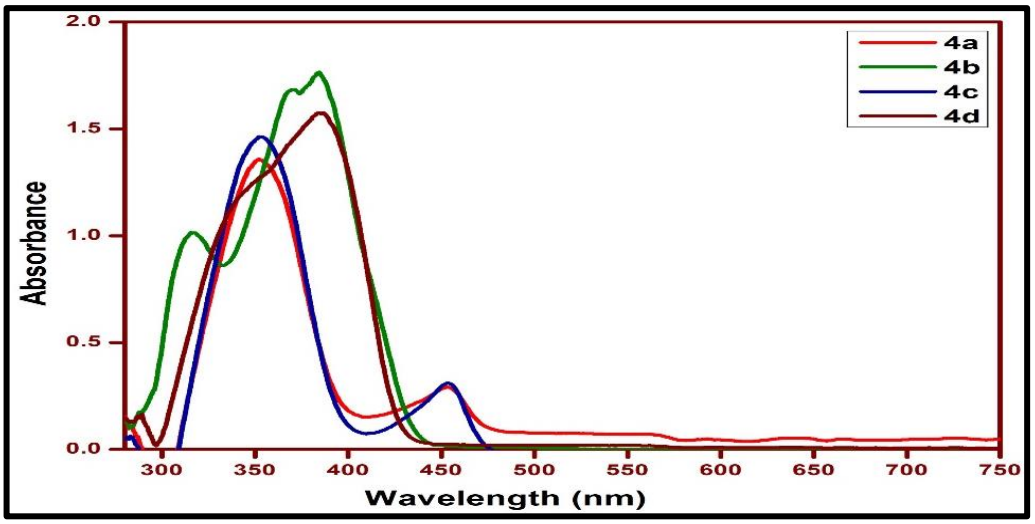

Fig. 5.1. Electronic absorption spectrum in DMSO at 6×10^{-6} M of compounds **4(a-d).**

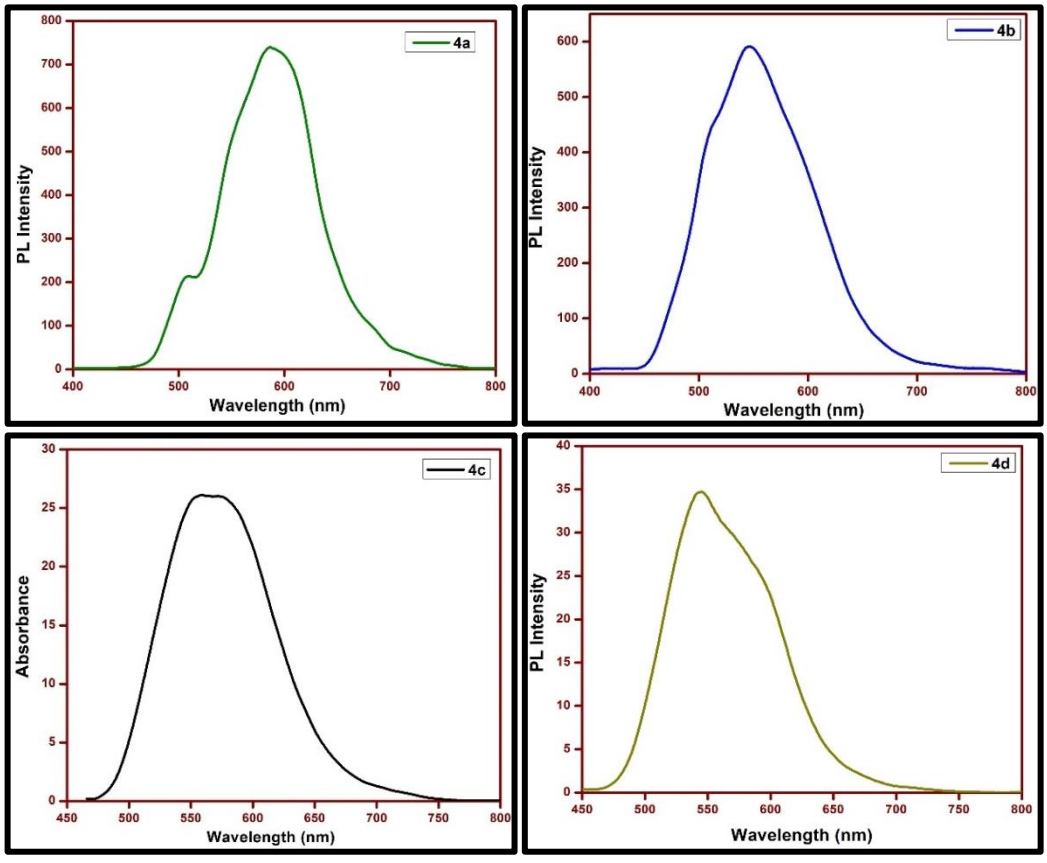

Fig.5.2. Graph of photoluminescence spectras in DMSO at 6×10^{-6} M **4**(**a-d**).

Table 5.1. Absorption and emission spectral values of synthesized compound **4**(**a-d**).

Entry	Solvent	λ_{abs} (nm)	λ_{emi} (nm)	E_g^{OTP}(eV)
4a	DMSO	354 and 484	587	3.50 and 2.56
4b		315 and 384	545	3.94 and 3.23
4c		353 and 452	565	3.51 and 2.74
4d		348 and 385	544	3.24 and 3.22

5.4.2 Electrochemical studies.

The electrochemical behaviour of synthesized compounds **4**(**a-d**) has been studied with help of a three-electrode system by increasing the scan rate from 10 mVs^{-1} to 50 mVs^{-1} in the CH instrument [32, 33]. The redox peak current was observed and noted redox onset potential to calculate experimental (E_{HOMO}-E_{LUMO}) energy molecules. Obtained results are appended in **Table 5.2**.

All the compounds **4**(**a-d**) give the fine redox behaviour by enhancing the quasi-reversible peak current and redox onset potential as shown in **Fig. 5.3**. The compounds **4a**, **4b** and **4c** have shown quasi-reversibility of electron transfer and estimated redox onset potential is -0.52 eV, -0.34 eV, -0.41 eV and 0.05 eV, -0.42 eV, -0.56 eV due to influence of electron-donating and withdrawing group and conjugation of phenyl ring respectively. While compound **4d** has shown quasi-reversibility of electron transfer dual peak of oxidation on set potential at -0.42 eV and 0.24 eV, and reduction on set potential is -0.15 eV.

The energy molecules such as energy E_{HOMO} and E_{LUMO} have been calculated experimentally by substituting the redox onset potentials using equations (2) and (3). In **Table 5.3** we observe that all the compounds have found higher E_{HOMO} values so that, the compounds have better structural properties [34, 35]. Hence, compounds are prosmising materials for photosensitizer.

$$E_{(HOMO)} = -[E_{(ox\text{-}onset)} + 4.4]\ eV \quad \text{— (2)}$$

$$E_{(LUMO)} = -[E_{(red\text{-}onset)} + 4.4]\ eV \quad \text{— (3)}$$

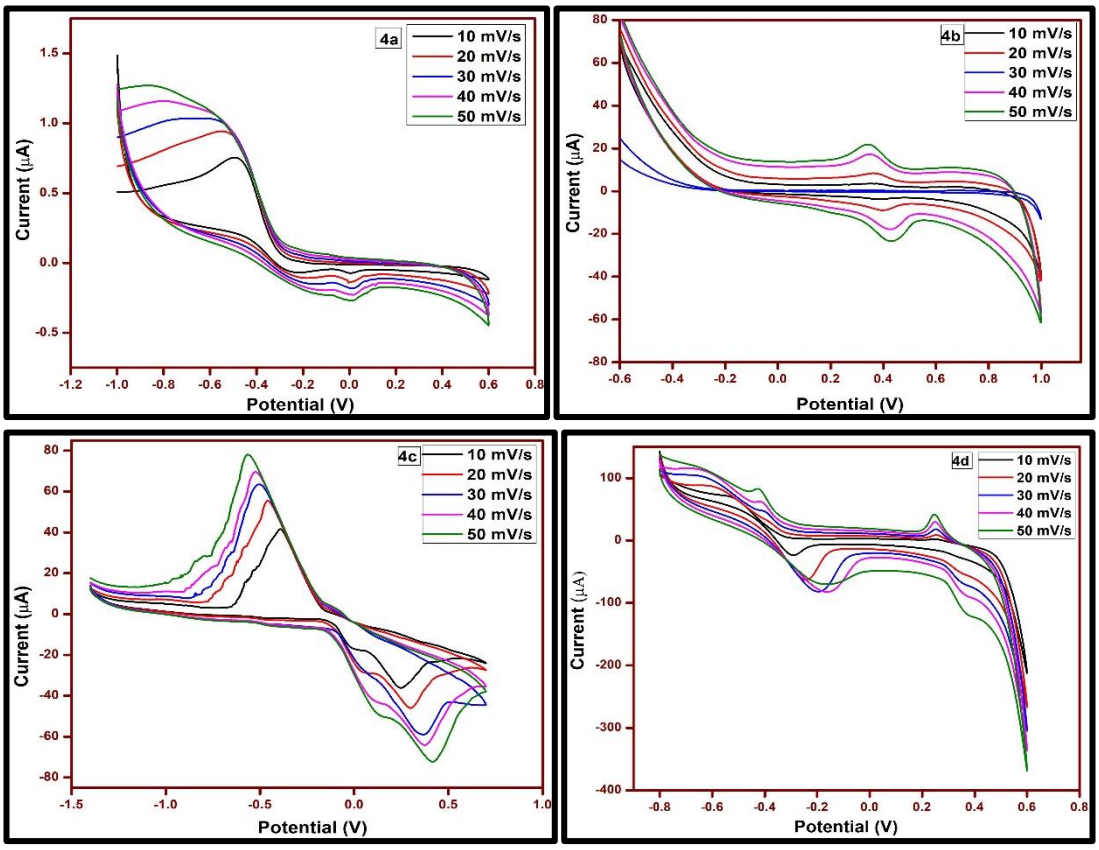

Fig. 5.3 Electrochemical studies of synthesized compounds **4**(**a-d**) at different scan rate in 1M KOH

Table 5.2. Electrochemical parameters of synthesized compounds **4**(**a-d**).

Entry	Oxidation onset potential (V)	Reduction onset Potential (V)	$E_{(HOMO)}$ (eV)	$E_{(LUMO)}$ (eV)
4a	-0.52	0.05	-3.88	-4.45
4b	-0.34	-0.42	-4.06	-4.48
4c	-0.41	-0.56	-3.99	-3.84
4d	-0.42 and 0.24	-0.15	-3.99 and -4.64	-4.25

5.4.3 Theoretical studies.

The geometry optimization, FMOs images and entire quantum chemical calculations were carried out with the help of the DFT/B3LYP method, 6-311++ G (d, p) basis set at the gaseous phase in Gaussian 09 software [36, 37].

5.4.3.1 Optimised structures.

The optimized structures of the synthesized compounds **4**(**a-d**) was subjected to geometry optimization in the ground state and the compounds were belongs to C_1 point group of symmetry as shown in **Fig. 5.4** with atom numbers.

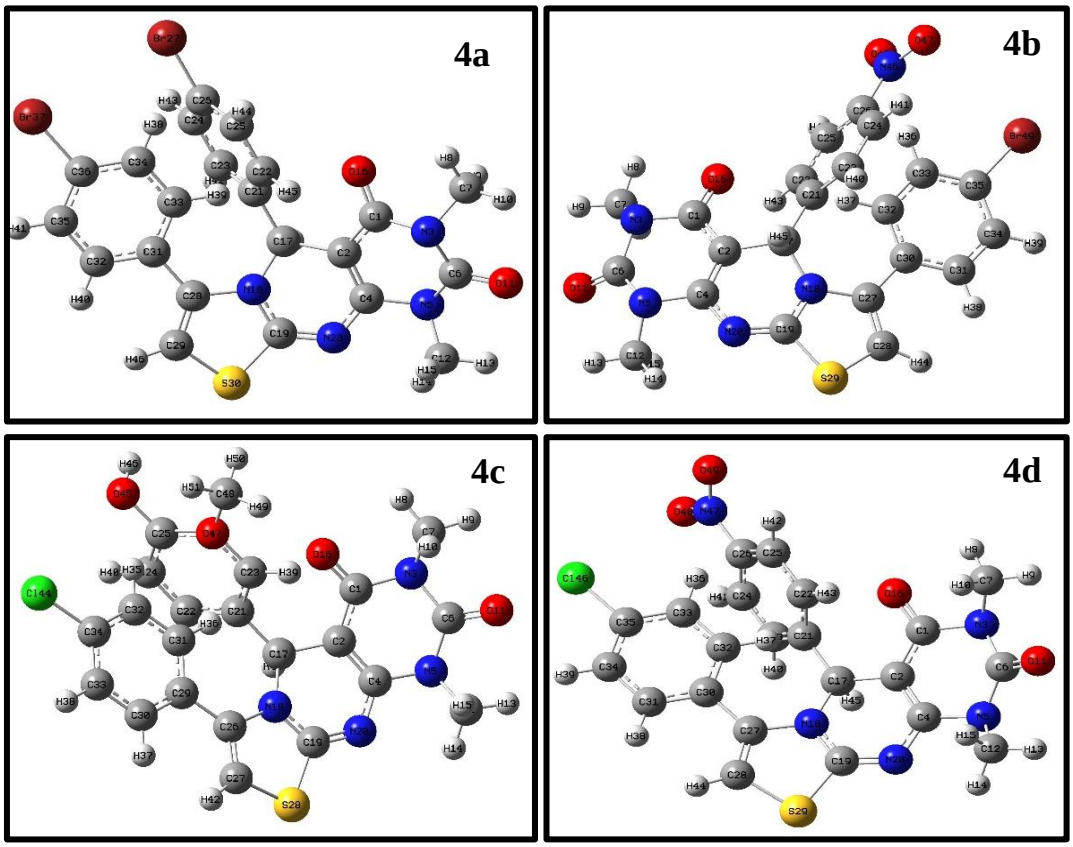

Fig.5.4 Optimised structures of synthesized compounds **4**(**a-d**).

5.4.3.2 Frontier molecular orbitals (FMOs).

Frontier molecular orbitals (FMOs) are E_{HOMO} and E_{LUMO} which is directly proportional to the ionization potential (IP) and the electron affinity (EA). Compounds **4**(**a-d**) have shown higher values in E_{HOMO} -0.22 eV, -0.23 eV, -0.21 eV & -0.23 eV and lower the values -0.10 eV, -0.13 eV, -0.07 eV, and -0.14 eV respectively, and as shown in **Fig. 5.5**. Compounds **4**(**a-d**) are higher energy gap values *i.e* -0.12 eV, -0.10 eV, -0.14 eV, and -0.09 eV respectively, hance compouds are have better kinetic stability and electron conductivity. Obtained values were

tabulated in **Table 5.3.** A higher energy gap indicates kinetic stability and electron conductivity, while a lower energy gap informs higher chemical reactivity and biological stability.

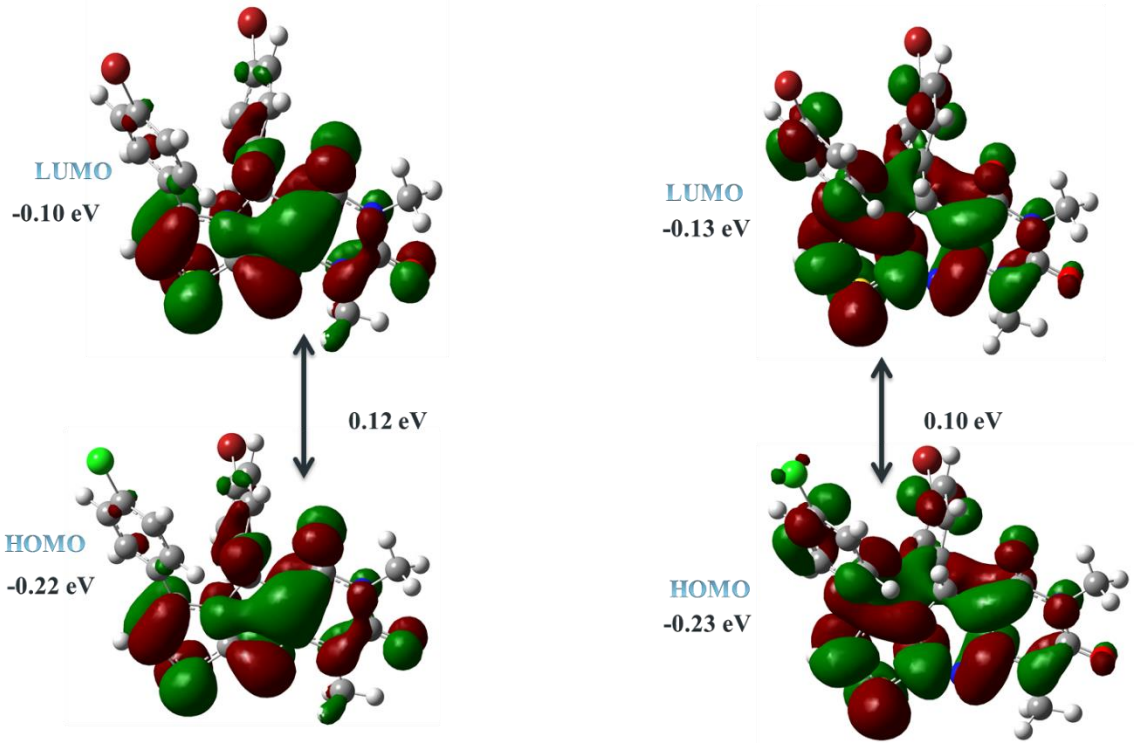

Fig. 5.5 HOMO and LUMO (FMOs) strctures of synthesized compounds **4**(**a-d**).

Table 5.3. Frontier molecular orbitals (FMOs) of synthesized compounds **4**(**a-d**).

Entry	E_{HOMO} (eV)	E_{LUMO} (eV)	ΔE
4a	-0.22	-0.10	0.12
4b	-0.23	-0.13	0.10
4c	-0.21	-0.07	0.14
4d	-0.23	-0.14	0.09

5.4.3.3 Chemical parameters.

According to Koopmans theorems, chemical quantum parameters are calculated using equations (4-8) and results are summarized in **Table 5.4**. Compounds **4**(**a-d**) have shown a higher energy gap, hence these are said to be hard molecules and hence, these molecules are shown greater photostability, higher chemical reactivity and higher intramolecular charge transfer [38, 39].

The intrinsic properties of the compounds will be known by electronegativity. Chemical potential is the negative value of the electronegativity and the global electrophilicity index informs the photostability of compounds. Synthesized compounds show a higher electrophilicity index at 0.274 eV, 0.232 eV, 0.305 eV, & 0.312 eV respectively, which are greater in photostability. Higher the value increases in bonding interaction of compounds obtained by dipole moment, while compounds **4a**, **4b** and **4c** have shown higher values of 12.00 eV, 13.63 eV and 6.871 eV respectively, and compound **4d** has shown a lower value of 4.655 eV due to the presence of highly electron-withdrawing nitro and bromo groups [40, 41].

$$\eta = ½ (I - A) \quad \text{— (4)}$$

$$\sigma = 1/\eta \quad \text{— (5)}$$

$$\chi = ½ (I + A) \quad \text{— (6)}$$

$$\mu = -\chi \quad \text{— (7)}$$

$$\omega = \mu^2/2\eta \quad \text{— (8)}$$

Table 5.4 Quantum chemical parameters of synthesized compounds **4(a-d)**.

Entry	IP (eV)	EA(eV)	η (eV)	σ (eV)	χ (eV)	μ (eV)	ω (eV)
4a	0.21	0.08	0.06	15.38	0.14	-0.14	0.16
4b	0.22	0.11	0.05	20.00	0.16	-0.16	0.25
4c	0.27	0.12	0.07	13.33	0.19	-0.19	0.25
4d	0.23	0.10	0.06	15.38	0.16	-0.16	0.25

5.4.4 Latent Fingerprint studies.

LEPs are one of the advance and promising techniques used as a secondary source in criminal investigation [42]. The chemical method (powder dusting) was used to develop and visualize the latent fingerprints using synthesized compounds **4(a-d)** on different substrates such as mobile, reagent bottle, watch and 500 mL beaker LFPs pictures were photographed under 365 nm UV light,

We observe clear visualization of latent fingerprints under 365 nm UV-light on porous/nonporous substrate as shown in **Fig. 5.6**. Synthesized compounds are effective materials to use in forensic science by showing ridges of fingerprints on all the substrate and clearly on reagent bottle by the compound **4b** as shown in **Fig. 5.7**. Accurate level II and III features of latent fingerprint ridges such as short ridges, whorls and eye ridges on reagent bottle which was photographed under 365 nm UV light. All the compounds have better absorption and emission properties hence that compounds are potent materials for energy conversion devices and electroluminescent materials [43].

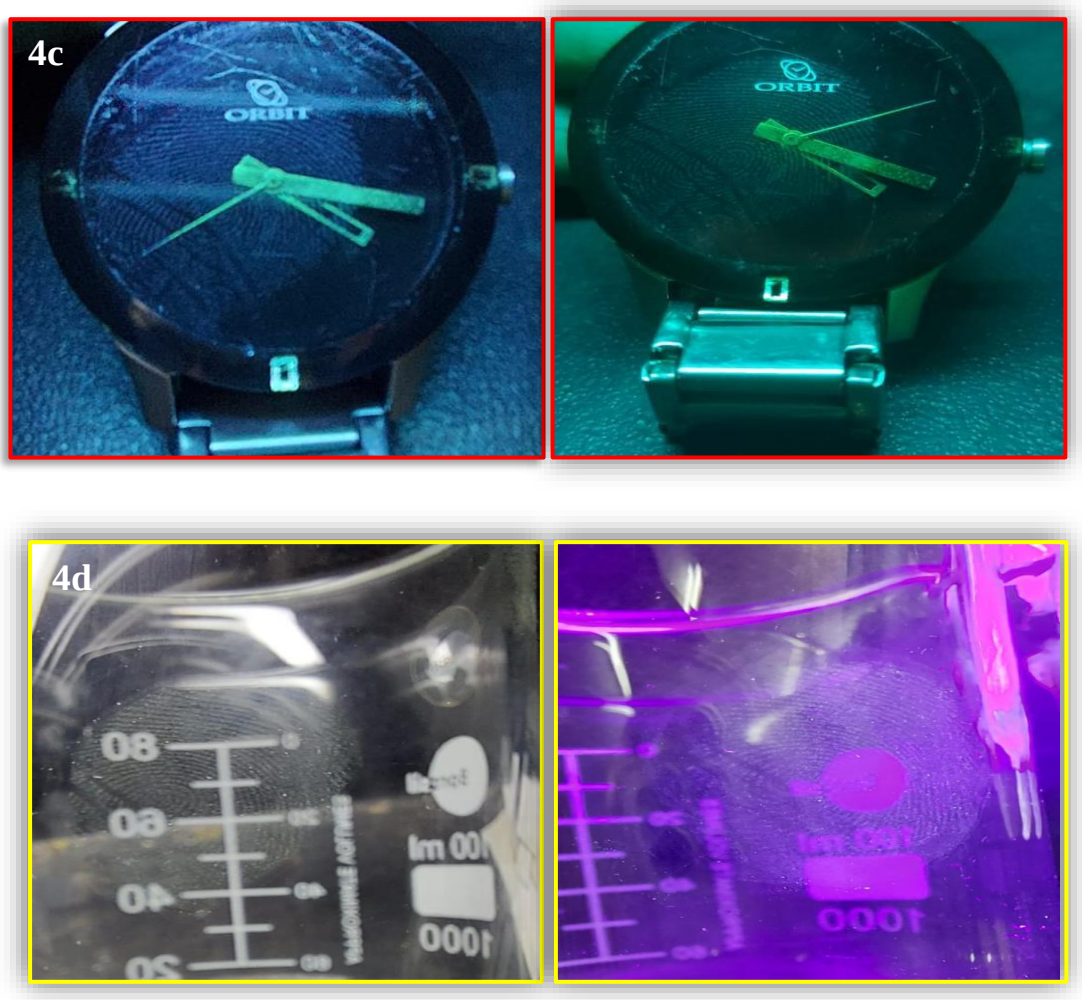

Fig. 5.6 Developed LFPs on reagent bottle, mobile screen, analogue watch and 500 mL beaker using synthesized compounds **4**(**a-d**).

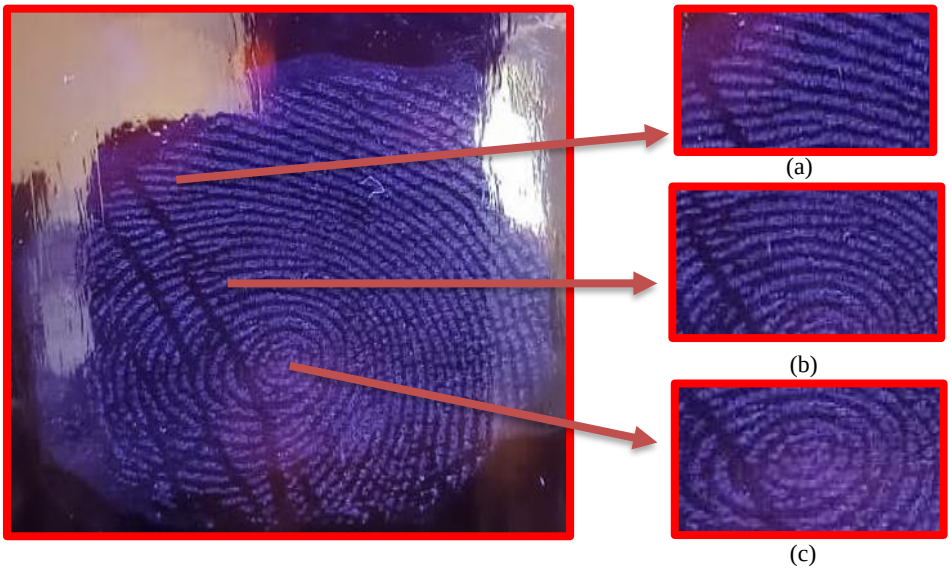

Fig. 5.8 Latent fingerprint ridges on reagent bottle using synthesized compound **4b** in 365 nm, **a)** Short ridges, **b)** Whorls and **c)** Eye ridges.

5.5 Conclusion.

In this chapter, we have synthesized some new substituted thiazolopyrimidne derivatives **4(a-d)** through multicomponent reaction in ethanol and structures were confirmed by FTIR, ^{1}H-NMR & ^{13}C-NMR and mass spectral techniques. All the compounds are well absorbed and emitted at the visible region. Also compounds, **4a** has shown dual absorption bands at 354 nm and 484 nm and emitted at 587 nm. Experimental energy molecules show that all the compounds have good donating and acceptor moieties and have better electrochemical properties by showing fine redox behaviours. Theoretical results suggest that compounds **4(a-d)** are hard molecules by showing higher energy gaps of 0.12 eV, 0.11 eV, 0.15 eV and 0.13 eV. Compound **4c** has a higher energy gap, so that compounds are higher in chemical reactivity and photostability. Further, we observe fine visualization of LFPs on selected porous materials and all the compounds have better adherence between fingerprint ridges and materials. Therefore, we conclude that, all the compounds have better photoactivity and luminescence characteristics and are used as phototonic materials in optoelectronic and forensic science.

5.6 References

1. K.S. Pramod, K.S. Praveen, S.K. Manvendra, M. Mouslim, M.A. Saud, L.S. Puran, D.A. Dau, *ACS Omega.*, 3 (**2018**) 15035-15042.
2. X. Li, L. He, H. Chen, W. Wu, H. Jiang, *J. Org. Chem.,* 78 (**2013**) 3636-3646.
3. C.M.M. Santos, M. Freitas, E. Fernandes, *Eur. J. Med. Chem.,* 157 (**2018**) 1460-1479.
4. P.N. Kalaria, S.C. Karad, D.K. Raval, *Eur. J. Med. Chem.,* 158 (**2018**) 917-936.
5. B.A.A. Rahaman El-Gazzar, H.N. Hafez, *Bioorg. Med. Chem. Lett.,* 19 (**2009**) 3392-3397.
6. A.A.A.R. Mahmoud, O.M. El-Hady, H. Salah, Z. Abo, E.M.M.A.E. Raheem, *J. Het. Chem.,* (**2015**) 1-6.
7. Z. Mario, L. Harald, T. Reinhard, *E. J. Med. Chem.,* 39 (**2004**) 1079-1088.
8. N. Vasu, C. Guochen, S. Qingning, J. Justin, F.S. Donald, *Bioorg. & Med. Chem. Lett.,* 19 (**2009**) 1425-1427.
9. C. Hachem, F. Bocquillon, O. Zahraa, M. Bouchy, *Dyes and Pigm.,* 49 (**2001**) 117-125.
10. C. Christophe, L. Chris, M. Pierre, S. Boca Raton, London, New York, *Washington, DC: CRC Press;* (**2004**) chapter 4.
11. T. Venkatesh, Y.D. Bodke, B. Manjunatha, S.R. Kumar, *Nucleo. and Nucleic. Acids.,* (**2021**) 1-13.
12. B. Sravanthi, L. Kaviarasan, T.K. Praveen, P. Sai Kiran, C. Pavankumar, B. Gowramma, *J. Iran. Chem. Soc.,* 17 (**2020**) 2359-2370.
13. D. Kang, D. Feng, T. Ginex, J. Zou, F. Wei, T. Zhao, B. Huang, Y. Sun, S. Desta, E.D. Clercq, C. Pannecouque, P. Zhan, X. Liu, *Acta Pharm. Sin. B.,* 10 (**2020**) 878-894.
14. P. Prasad, G.K. Anirudhdha, M.P. Patel, *New J. Chem.,* 42 (**2018**) 12666-12676.
15. U.H.K. Zia, U.K. Arif, W. Pingyu, C. Yongmei, K. Dandan, K. Shafiullah, T. Kamran, *Nat. Prod. Res.,* 29 (**2015**) 933-938.
16. S.M. Ghada, Polycycl. *Aromat. Compd.,* 12 (**2021**) 1-17.

17. B.A.A. Rahaman El-Gazzar, H.N. Hafez, *Bioorg. Med. Chem. Lett.*, 19 (**2009**) 3392-3397.

18. A.A.A.R. Mahmoud, O.M. El-Hady, H. Salah, Z. Abo, E.M.M.A.E. Raheem, *J. Heterocycl. Chem.*, 53 (**2015**) 1304-1309.

19. Z. Mario, L. Harald, T. Reinhard, *Eur. J. Med. Chem.*, 39 (**2004**) 1079-1088.

20. N. Vasu, C. Guochen, S. Qingning, J. Justin, F.S. Donald, *Bioorg. Med. Chem. Lett.*, 19 (**2009**) 1425-1427.

21. A.M.S. Youssef, A.M. Fouda, R.M. Faty, *J. Chem. Cent.*, 12 (**2018**) 1-14.

22. K.N.M. Halim, S.K. Ramadan, S.A. Rizk, M.A. El-Hashash, *Synth. Comm.*, 50 (**2020**) 1159-1175.

23. R. Aggarwal, N. Jain, S. Sharma, P. Kumar, G. P. Dubey, H. Chugh, R. Chandra, *Sci. Repo.*, 11 (**2021**) 1-18.

24. H. Serrar, M. Galai, F. Benhiba, M. Ouakki, Z. Benzekri, S. Boukhris, A. Hassikou, A. Souizi, H. Oudda, M.E. Touhami, *J. Chem. Tech and Metta.*, 53 (**2018**) 324-335.

25. Z. Ebrahimpour, M. Bakavoli, A. Shiri, S.M. Seyedi, T. Asghari, J.T. Mague, *J Fluoresc.*, 27 (**2017**) 1183-1190.

26. A.A. Nadia, Elkanzi, A.A.M Farag, N. Roushdy, A.M. Mansour, *Optik.*, 216 (**2020**) 164882-16895.

27. M.M. Duvenhagel, O.M. Ntwaeborwal, H.G. Visser, H.C. Swart, *J. Cond. Matt.*, 439 (**2014**) 46-49.

28. T. Sutradhar, A. Misra, *J. Phy. Chem. A.*, 122 (**2018**) 4111-4120.

29. R.O. Yathisha and Y.A. Nayaka, *SN Appl. Sci.*, 2 (**2020**) 451-467.

30. A. Esvet, L. Abdulkadir, G. Selçuk, R.S. Mehmet, A. İnci, *Bull. Kor. Chem. Soc.*, 31 (**2010**) 3632-3638.

31. D. Stephane, S.H. Garry, W.G Skene, *J. Phys. Chem. B.*, 111 (**2007**) 11407-11418.

32. L. Leonat, S. Gabriela, I.V. Branzoi, *U.P.B. Sci. Bull. Series B.*, 75 (**2013**) 111-119.

33. A.R. Lopes Da Silva, A. Jhones Dos Santos, C.A. Martínez-Huitle, *RSC Adv.*, 8 (**2018**) 3483-3492.

34. A.J.S. Ahammad, S. Sarker, M. Aminur Rahman, J.J. Lee, *Electroanalysis.*, 22 (**2010**) 694-700.

35. I. Fleming, *Wiley.*, (**1977**)

36. R. Parr, G. Donnelly, R.A. Lev, M.W.E Palke, *J. Chem. Phy.*, 68 (**1977**) 3801-3807.

37. P. Udhayakala, T.V. Rajendiran, S. Gunasekaran, *J. Comp. Meth. Mol. Des.*, 2 (**2012**) 1-15.

38. K.V. Basavarajappa, Y.A. Nayaka, R.O. Yathisha, K.B. Manjunatha, *J. Fluor.*, 29 (**2019**) 1201-1211.

39. C.S. Abraham, S. Muthu, J.C. Prasana, S.J. Armaković, S. Armaković, F.B. Rizwana, A. S. B. Geoffrey, *Comput. Biol. Chem.*, 77 (**2018**) 131-145.

40. S. Renuga, S. Muthu, *Spectrochim. Acta Part A.*, 118 (**2014**) 702-715.

41. H.A. Arjun, R.K. Rajan, R. Elancheran, M. Ramanathan, A. Bhattacharjee, S. Kabilan, *Chem. data. Colle.*, 26 (**2020**) 100350-100365.

42. U. Vanitha, R. Elancheran, V. Manikandan, S. Kabilan, K. Krishnasamy, *J. Mol. Str.*, 1246 (**2021**) 131212-131223.

43. J. Janczak, *J. Polyhed.*, 38 (**2012**) 75-87.

List of research articles published

1. **K. Upendranath**, Talavara Venkatesh*, S.H Sukanya, H. Shanavaz, Facile synthesis and in-vitro cytotoxicity study of some 5-(4-substituted phenyl)-7-hydroxy-9-methyl-2-thioxo-2,3-dihydro-1*H*-dipyrimido[*1,2-a:4',5'*-]pyrimidin-4(5*H*)-one derivatives and their Optoelectronic, DFT and LFPs applications.
   Journal: ***Journal of Molecular Structure****,* Year-2021 I.F-3.84

2. **K. Upendranath**, Talavara Venkatesh*, M. Shashank, G. Nagaraju, K.M. Mussuvir Pasha, One-pot. synthesis of some new 7-hydroxy-5-(4-substitutedphenyl)-9-methyl-1,5-dihydro- 2*H*-dipyrimido[1,2-a:4',5'-d]pyrimidine-2,4(3*H*)-dione derivatives and its optoelectronic, DFT, photocatalytic studies and latent fingerprint applications https://doi.org/10.1016/j.molstruc.2021.131930
   Journal: ***Journal of Molecular Structure****,* Year-2021 I.F-3.84

3. **K. Upendranath**, Talavara Venkatesh*, M. Vinuth, Development and visualization of level II, III features of latent fingerprints using some new 4-(4-substitutedphenyl)-6-(4-substitutedphenyl)-2-oxo-1,2-dihydropyridine-3-carbonitrile derivatives: Synthesis, characterization, optoelectronic and DFT studies.
   Journal: ***Journal of Indian Chemical Society****,* Year-2022: I.F-0.24

4. **K. Upendranath**, Talavara Venkatesh*, Y. Arthoba Nayaka, M. Shashank, G. Nagaraju, Optoelectronic, DFT and current-voltage performance of new Schiff base 6-nitro-benzimidazole derivatives, https://doi.org/10.1016/j.inoche.2022.109354.
   Journal: ***Inorganic Chemistry Communication****,* Year: 2022: I.F-3.42

5. **K. Upendranath**, Talavara Venkatesh*, T.N, Lohith, M.A. Sridhar, Synthesis, characterizations of new Schiff base heterocyclic derivatives and their optoelectronic, computational studies with level II & III features of LFPs https://doi.org/10.1016/j.molstruc.2022.133231
   Journal: ***Journal of Molecular Structure****,* Year-2022 I.F-3.84

6. **K. Upendranath**, Talavara Venkatesh*, Facile synthesis of new 7-(4-substitutedphenyl)-5-(4-substitutedphenyl)-1,3-dimethyl-1*H*-pyrimido[4,5-d]thiazolo[3,2-a]pyrimidine-2,4(3*H*,5*H*)-dione derivatives and their optoelectronic and Level II and III features of LFPs applications.
   Journal: ***New Journal of Chemistry*** (Communicated).

List of research papers published as Co-author

1. Priya Rani RS, Talavara Venkatesh, SH Sukanya, **K. Upendranath**, ND Satyanaraya, Synthesis of some new substituted 5-phenyl-3, 4-dihydro-1*H*, 2*H*-3, 4-bipyrazole derivatives and evaluation for their biological activities,
   Journal***: Chemical Data Collection***, Year-2022. I, F-0.60

2. Talavara Venkatesh*, **Kantharaj Upendranath**, Jayappa Manjanna, Optical, Electrochemical and DFT studies of Indol-5,8-pyrimido[4,5-d] pyrimidine Derivatives, https://doi.org/10.1016/j.cdc.2022.100886
   Journal: ***Chemical Data Collections***, Year: 2022.

3. Talavara Venkatesh*, **K. Upendranath** Y. Arthoba Nayaka, Development of electrochemical and optoelectronic performance of new 7-{[1*H*-indol-3-ylmethylidene]amino}-4-methyl-2*H*-chromen-2-one dye, https://doi.org/10.1007/s10008-020-04892-9.
   Journal***: Journal of Solid-State Electrochemistry*** Year-2021. I, F-2.60

List of Papers Presented in National/ International Conference/ Seminars

1. K. Upendranth and Talavara Venkatesh*, One-pot synthesis, characterization of new 1,2-dihydropyridine-3-carbonitrile derivatives for their optoelectronic, DFT studies and LFPs applications. International E-Conference on Sustainable and Futuristic Materials (SFM-2021) held from 29-30th November 2021 organized by International Research Centre and Department of Chemistry, Kalasalingam Academy of Research and Education, Krishnankoil, Department of Chemistry, J. M. Patel Arts, Commerce & Science College, Bhandara. **-Poster Presentation.**
   K. Upendranth and Talavara Venkatesh*

2. Synthesis of 5-Substituted-di-hydro pyrimidines derivatives and evolution of their Anti-cancer and molecular docking studies, International E-Conference on Recent Advances and Innovations in Biological and Applied Sciences (RAIBAS 2022), held during 14th-16th June 2022, at SGT University Gurugram**- Oral Presentation**

   K. Upendranth and Talavara Venkatesh*,

List of Workshop /Conferences Attended:

1. Three days of virtual workshops on **"Computational and Analytical software's**" organized by the Department of Chemistry, Sathyabama Institute of Science and Technology, from 4th August 2021 to 6th August 2021.- **Participated**
2. "Potential Clinical Applications of Plant-Based Natural Antioxidants to Combat COVID-19 Infections", one-day national level webinar conducted by the department of chemistry, Sir MV Science college, Bommankatte, Bhadravathi, Shivamoga on 12th November -2020 - **Attended.**
3. **"**Trends in Science education national seminar" conducted by the Department of PG Studies and Research in Chemistry, Rani Chennamma University, Belagavi, on 01 March-2021- **Attended**.
4. "Role of Chemistry for Sustainable Future", national-level e-conference conducted by the department of chemistry, Shivachhatrpati college, Aurangabad on 23rd May 2021- **Attended.**

Signature of the student **Signature of Research supervisor**

(K. Upendranath.) **(Dr. Talavara Venkatesh)**

Journal of Molecular Structure 1250 (2022) 131930

Contents lists available at ScienceDirect

Journal of Molecular Structure

journal homepage: www.elsevier.com/locate/molstr

One-pot synthesis of some new 7–hydroxy-5-(4-substitutedphenyl)-9-methyl-1,5-dihydro-2*H*-dipyrimido[1,2-*a*:4′,5′-*d*]pyrimidine-2,4(3*H*)–dione derivatives and it's optoelectronic, DFT, photocatalytic studies and latent fingerprint applications

K. Upendranath[a], Talavara Venkatesh[a,*], M. Shashank[b], G. Nagaraju[c], K. M. Mussuvir Pasha[d]

[a] Department of P.G. Studies and Research in Chemistry, Kuvempu University, Jnana Sahyadri, Shankaraghatta, Karnataka 577451, India
[b] Department of P.G. Studies and Research in Industrial Chemistry, Kuvempu University, Jnana Sahyadri, Shankaraghatta, Karnataka 577451, India
[c] Department of Chemistry, Energy Materials Research Laboratory, Siddaganga Institute of Technology, Tumakuru, Karnataka 572103, India
[d] Department of P.G. Studies and Research in Chemistry, Vijayangara Sri Krishnadevaraya University, Ballari, Karnataka 583105, India

ARTICLE INFO

Article history:
Received 20 July 2021
Revised 25 October 2021
Accepted 12 November 2021
Available online 15 November 2021

Keywords:
Pyrimidine
Photoluminescence
Electrochemical
DFT
Photocatalytic
LFPs

ABSTRACT

Metal-free organic dyes are gaining interest and demands in the field of light absorption and light-emitting applications. In this study, we developed efficient one-pot synthesis of 7–hydroxy-5-(4-substitutedphenyl)-9-methyl-1,5-dihydro-2*H*-dipyrimido[1,2-*a*:4′,5′*d*]pyrimidine-2,4(3*H*)–dione derivatives **4**(**a-d**) using L-proline as a catalyst and structures were confirmed by analytical and spectroscopic techniques. Photophysical properties have been studied in a liquid medium; compounds are absorbed in bathochromic shift at ~300–500 nm and blue emission at 530 nm, 560 nm, 401 nm and 614 nm, 622 nm respectively. Electrochemical behavior was studied at different scan rates in CH Potentiostat. CV results revealed that all the compounds shows quasi reversible behavior and experimental HOMO-LUMO have been calculated. FMOs, optimized structure and quantum parameters along with UV, FT-IR and COSMO-RS were investigated theoretically. From the theoretical results, compounds are in good agreement with experimental values with better photostability and chemical reactivity. Further, compounds are excellent photocatalysts towards the dye degradation of malachite green dye by reaching 65%, 83%, 87% and 65% respectively. In addition, LFPs images were developed on porous/nonporous materials and visualized under UV light, compounds are excellent adhesion and sensitivity on the porous/nonporous materials. Hence, the obtained compounds can be used as organic electronics application-oriented materials and in forensic Science.

1. Introduction

Metal-free organic dye compounds containing heterocyclic moieties like coumarin indole, pyridine, pyrimidine, etc., are shows better light absorption and light-emitting properties due to their aromatic conjugations and electronic transitions [1–3]. In general, pyrimidines are well-known drugs in the field of medicinal chemistry as anti-analgesic, anti-microbial, anti-inflammatory and anti-cancer agents [4–7]. As knows of drug molecules, researchers have gained interest to develop and design pyrimidine moieties as photonic materials, as optical chemosensors and as photo-sensitizers due to their better photophysical properties, high electron affinity and act as π-acceptor character. Particularly, pyrimidine was exhibited higher fluorescent properties when having different electron-withdrawing and donating groups [8,9]. Moreover, it acting as an electron-withdrawing character due to its π-deficient nature hence increase color sensitivity, higher molar extinction co-efficient with solvatochromic behavior [10,11]. Photocatalysts play a vital role in purifying the water pollutions caused by the textile, leather, pulp and paper industries. Till now, Nanocomposite metal oxides have been used as photocatalysts under UV-irradiation by dye degradation method. Due to the insolubility of metal oxide nanoparticles and the formation of by-products in the water molecule, researchers interesting to design and develop a simple metal-free organic light-absorbing and emis-

* Corresponding author.
E-mail address: venkateshatalwar@gmail.com (T. Venkatesh).

https://doi.org/10.1016/j.molstruc.2021.131930
0022-2860/

99 (2022) 100388

Contents lists available at ScienceDirect

Journal of the Indian Chemical Society

journal homepage: www.journals.elsevier.com/journal-of-the-indian-chemical-society

Development and visualization of level II, III features of latent fingerprints using some new 4-(4-substitutedphenyl)-6-(4-substitutedphenyl)-2-oxo-1, 2-dihydropyridine-3-carbonitrile derivatives: Synthesis, characterization, optoelectronic and DFT studies

K. Upendranath [a], Talavara Venkatesh [a,*], M. Vinuth [b]

[a] Department of PG Studies and Research in Chemistry, Jnana Sahyadri, Kuvempu University, Shankaraghatta, Shivamogga, Karnataka, 577451, India
[b] Department of Chemistry, NIE- Institute of Technology, Mysore, Karnataka, 570018, India

ARTICLE INFO

Keywords:
Pyridine-3-carbontrile
Optical properties
Electrochemical
DFT
LFPs

ABSTRACT

Organic dye compounds with luminescent properties are in demand to use in visualizing the latent fingerprints (LFPs) at crime spot investigation. Here, we synthesized some new 4-(4-substitutedphenyl)-6-(4-substitutedphenyl)-2-oxo-1,2-dihydropyridine-3-carbonitrile **4(a-d)** and were confirmed using spectroscopic approaches. Optical properties were recorded in solvent media, where peaks were absorbed in ~300–400 nm of longer wavelength and emitted at ~467–574 nm in the blue region. Dual redox peak current was observed in Cyclic voltammetry at different scan rate and estimated redox onset potential, and energy molecules have been experimentally calculated. DFT studies have been carried out using Gaussian 09 software at the gaseous phase. From the results of theoretical investigations, compounds **4(a-d)** showed higher photostability, chemical reactivity and good reactive sites. Also, synthesized compounds were used to determine the latent fingerprints with the help of powder dusting method. Level II and III features of LFPs are observed on porous/non-porous surfaces without optical hindrance and images were taken in normal and 365 nm UV light. From the above results, the synthesized compounds are efficient materials for forensic science applications.

1. Introduction

Multicomponent reactions (MCRs) are one of the easiest methods to synthesis of poly-functional molecules in a single-step reaction with high competence over multistep synthesis [1]. Generally, MCRs are as an efficient tool for synthesis of new and several active drug molecules by having many advantageous such as avoid unnecessary expensive purification, high atom economy, toxic reagents and solvent consumptions. From the past decades, polyfuctional molecules were gain interest to use as organic fluorescent materials in light emitting fields as electroluminescent indicators and forensic science [2].

Now a day's fingerprints are commonly used in personal identifications such as mobile locks, banking sectors and biometric sensors etc., [3]. Fingerprints are considered as primary evidence in the criminal investigation due to their unique identification [4]. Generally, hands and feet are constituted with the natural secretions due to eccrine glands, which produce sweat, mixture of water, salt and other small traces on fingers [5]. Two types of fingerprints were used to visualize in crime spots, *i.e* patent fingerprints and latent fingerprints (LFPs). Among them, LFPs are predominately used in forensic science, because of the difficulty to see through naked eyes and data can be stored for a longer time [6]. LFPs are categorized into three different levels such as levels I, II and III. In level I, consist of whorl, arch and loop which are found more than 60% in the human population and level II consist of a core, delta and bifurcation which are found not more than 30% [7]. Similarly, level III deals with pores, ridge path deviation, edge contour, breaks, creases, scars and found less than 10% [8]. Level III of finger marks gives the accurate quantitative data of each fingerprint and predominantly in fragmentary fingerprint comparison [9].

Many different techniques have been approached to visualize the latent fingerprints through chemical reagents, such as silver nitrate spraying, powder dusting, ninhydrin and iodine fuming etc., [10]. Form these techniques, the powder dusting method is one of the simplest methods and easy to handle, so commonly encourage to use in forensic

* Corresponding author.
E-mail address: venkateshatalwar@gmail.com (T. Venkatesh).

https://doi.org/10.1016/j.jics.2022.100388
Received 30 September 2021; Received in revised form 28 December 2021; Accepted 9 February 2022
Available online 12 February 2022

Inorganic Chemistry Communications 139 (2022) 109354

Contents lists available at ScienceDirect

Inorganic Chemistry Communications

journal homepage: www.elsevier.com/locate/inoche

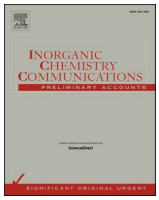

Optoelectronic, DFT and current-voltage performance of new Schiff base 6-nitro-benzimidazole derivatives

K. Upendranath [a], Talavara Venkatesh [a,*], Y. Arthoba Nayaka [a], M. Shashank [b], G. Nagaraju [c]

[a] Department of PG Studies and Research in Chemistry, Jnana Sahyadri, Kuvempu University, Shankaraghatta, Shivamogga, Karnataka 577451, India
[b] Department of P.G. Studies and Research in Industrial Chemistry, Jnana Sahyadri, Kuvempu University, Shankaraghatta 577451, Karnataka, India
[c] Energy Materials Research Laboratory, Department of Chemistry, Siddaganga Institute of Technology, Tumakuru 572103, Karnataka, India

ARTICLE INFO

Keywords:
6-Nitro-benzimidazole
Optical
Electrochemical
DFT
I-V Characteristics

ABSTRACT

In the present work, we have synthesized a new Schiff base 6-nitro-benzimidazole derivative (**3a and 3b**) and were confirmed by analytical and spectroscopic methods. TiO_2 nanoparticle (NP) has been synthesized using a sol–gel method and characterized by using X-ray diffraction, SEM and EDAX techniques. Photophysical properties were analyzed in the liquid state; all the compounds were absorbed in ~300–390 nm at longer wavelength and are emitted at 546 nm and 576 nm in the blue region. In addition, the energy bang gaps have been calculated using Tauc plot in the solvent system. Cyclic voltammetry technique was applied to study the electrochemical properties in DMSO and PBS (7 pH) electrolytic solution. Compounds show quasi-reversible redox peak current and found greater sensing response of DOLO drug molecule by the formation of dual redox peaks and also used to calculate the energy molecules (E_{HOMO}-E_{LUMO}) experimentally. Similarly, DFT studies were investigated at the gaseous and solvent phase to understand intrinsic and extrinsic properties and found higher chemical reactivity and better photostability in both phases. Also, Current-Voltage (*I-V*) studies have been done using synthesized compounds at a 1 cm active area of photoanode in a two-sense Keithley source under light and dark medium. In presence of light-medium, we found a good current (2.36 A and 3.60 A) and voltage (4.88 V and 4.84 V) response. From the above results, the synthesized **3a** and **3b** compounds are efficient photosensitizers to use in DSSCs applications.

1. Introduction

The growth of population and industrial sector leads to greater demands in the use of renewable energy sources such as wind, water and solar [1–4]. To reduce human efforts and to reach the industrial demands, the researchers have been interested in the development of metal-free organic dyes as an organic semiconductor to use in energy conversion devices by absorbing the sunlight. Photovoltaic cells (PV cells) or dye-sensitized solar cells (DSSCs) are considered an energy conversion device that generates electricity using dye compounds under sunlight. DSSCs were known as third-generation photovoltaic cells and nowadays it is much more fascinating than silicon-based solar cells by using organic dyes as semiconductors [5]. The previous reports reveal that many metal complexes as dyes were used in OLEDs, organic-thin-film transistors (OTFTs), and PV cells due to their better optical and intramolecular charge transportation with molar extinction co-efficient properties [6,7]. Metal complexes were found some drawbacks such as lower efficacy, high cost of metals and lengthy step reactions. To overcome these challenges, simple metal-free organic dyes as organic semiconductors are concentrated to increase the efficiency of the DSSCs. Simple metal-free organic dyes consisting of chalcones [8], benzimidazole [9], coumarins [10] having D-π-A groups are known as electro-optical materials are the futures due to their structural characteristics, ease synthesis and fabrication as well as low-cost productions on an industrial scale [11]. Recently, π-conjugated open-chain systems were nominated as electro-optical materials because of their unique structural properties and the presence of carbonyl group act as acceptor group, hence it's attracting towards to energy storage materials such as opto-electronics, OLEDs, super-capacitors and NLO devices etc., [12,13]. Open chain π-conjugated compounds have proved their stability in the pharmaceutical field as anti-fungal, anti-cancer, anti-microbial and as anti-diabetics [14–17]. In addition, chalcones are open-chain π-conjugated organic compounds connected by α, β-unsaturated carbonyl compound, where the molecules belong to one of the most important

* Corresponding author.
E-mail address: venkateshatalwar@gmail.com (T. Venkatesh).

https://doi.org/10.1016/j.inoche.2022.109354
Received 5 November 2021; Received in revised form 2 March 2022; Accepted 3 March 2022
Available online 7 March 2022

Journal of Molecular Structure 1264 (2022) 133231

Contents lists available at ScienceDirect

Journal of Molecular Structure

journal homepage: www.elsevier.com/locate/molstr

Synthesis, characterizations of new Schiff base heterocyclic derivatives and their optoelectronic, computational studies with level II & III features of LFPs

K. Upendranath [a], Talavara Venkatesh [a,*], T.N. Lohith [b], M.A. Sridhar [b]

[a] Department of P.G. Studies and Research in Chemistry, Kuvempu University, Jnanasahyadri, Shankaraghatta, Karnataka 577451, India
[b] Department of Studies in Physics, University of Mysore, Manasagangotri, Mysuru 570006, India

ARTICLE INFO

Article history:
Received 30 November 2021
Revised 18 April 2022
Accepted 4 May 2022
Available online 5 May 2022

Keywords:
Schiff base heterocycles
Optoelectronic
Computational
LFPs

ABSTRACT

Organic Schiff base compounds with luminous characteristics are receiving attention and increasing demand for the imaging of latent fingerprints (LFPs) at crime scenes. **Sb1** and **Sb2** novel Schiff base heterocyclic compounds were synthesized and confirmed by using analytical and spectroscopic methods. The existence of both donating and accepting groups influenced the appearance of absorption bands at longer wavelength and was recorded using UV-absorption and emission spectrum in solvent media. Compounds **Sb1** and **Sb2** emit at 576 nm and 646 nm in bathochromic shift respectively. The electrochemical properties were investigated using cyclic voltammetry. Quantum chemical parameters with vibrational frequency have been estimated in density functional theory (DFT), using TD-DFT/CAM (B3LYP) approach employing 6–311++ G (d, p) basis set in the ground state. Theoretical vibrational frequency values were specifically agreed to obtained experimental values. Furthermore, FMOs, MEPs, RDG analyses and Mulliken atomic charges have been calculated. In addition, LFPs images were developed by powder dusting approach on specified materials using synthetic compounds and visualized under Visible and UV light. The level II and III properties of LFPs on the substrate were observed under light-medium with no background interference, therefore these compounds are potential materials for electroluminescent, OLEDs and forensic science applications.

1. Introduction

Latent fingerprints (LFPs) are used as physical evidence in criminal investigations because each person has different types of fingerprints. Generally, fingerprints are identified based on their level I and they are categorized into three levels. Level I deal with a whorl, arch and loop, level II consists of a core, delta and bifurcation; level III shows the sweat pores [1–3]. Commonly levels II and III occur in every human and are difficult to identify, specific powders required to develop and visualize. There are various chemical powders were carried out to visualize the LFPs such as regular, metallic and luminescent powders [4,5]. Regular powders are resinous polymers and colorant and these powders are not suitable to develop on the challenging surface and then using of metallic powders affect the human health due to the presence of metals such as lead, gold, silver etc., Both regular and metallic powders had some drawbacks like low contrast, background hindrance and low resolution [6,7]. These materials are non-luminescent properties hence low resolution occurrs and in the viewpoint of the user's health metallic powders are not suitable for development. To overcome these difficulties researchers are concentrating on organic luminescent powders to develop and visualization of LFPs and to replace regular and metallic powders [8,9].

The Schiff base is a condensation reaction between primary amine and aldehyde which leads to a formation of imines or azomethine (-HC=N-) [10]. These imines are considered as versatile organic compounds and received considerable attention in the field of pharmacological chemistry, and these are has proven their ability of pharmaceuticals as antifungal, anti-microbial, antiviral, anti-cancer and anti-TB agents [11–15]. Apart from pharmaceutical agents, the researchers have concentrated on metal-free organic Schiff base compounds to prove their ability in electroluminescent, NLO, sensor and organic photovoltaic materials [16–18]. Moreover, the π-conjugated organic compounds mainly exhibit higher luminescence properties, by having an anchoring group such as electron-accepting and electron-donating groups were acting as D-π-A moieties, this reason may help organic compounds to use in

* Corresponding author.
E-mail address: venkateshatalwar@gmail.com (T. Venkatesh).

https://doi.org/10.1016/j.molstruc.2022.133231
0022-2860/

KUVEMPU UNIVERSITY

Department of PG Studies and Research in Chemistry, Jnanasahydri,
Kuvempu University, Shankaraghtta-577451

A Thesis submitted to the Faculty of Science, Kuvempu University

For the award of the degree of

DOCTOR OF PHILOSOPHY
in
CHEMISTRY

"SYNTHESIS, CHARACTERIZATION AND APPLICATIONS OF SOME NOVEL NITROGEN HETEROCYCLIC COMPOUNDS"

-: Submitted By: -

Mr. K. Upendranath M.Sc.
Research Scholar
Dept. of P.G. Studies and Research in Chemistry
Kuvempu University, Jnanasahyadri
Shankaraghatta-577451

-: Research Supervisor: -

Dr. Talavara Venkatesh M.Sc., Ph.D.
Assistant Professor
Dept. of P.G. Studies and Research in Chemistry
Kuvempu University, Jnanasahyadri
Shankaraghatta-577451

2022-23

For summary, kindly refer individual chapters.